EXPERIMENTAL INVESTIGATION OF GASOLINE – DI-METHYL ETHER DUAL FUEL CAI COMBUSTION WITH INTERNAL EGR

A thesis submitted for the degree of Doctor of Philosophy

By

Haofan Zhang

School of Engineering and Design
Brunel University
United Kingdom

December 2011

Brunel University
School of Engineering and Design
United Kingdom

Haofan Zhang

Experimental Investigation of Gasoline -- Di-Methyl Ether Dual Fuel CAI Combustion with Internal EGR

December 2011, Ph.D.

Abstract

A new dual fuel Controlled Auto-Ignition (CAI) combustion concept was proposed and researched for lower exhaust emissions and better fuel economy. The concept takes the advantage of the complementary physical and chemical properties of high octane number gasoline and high cetane number Di-Methyl Ether (DME) to organize the combustion process. Homogeneous gasoline/air mixture is utilized as the main combustible charge, which is realised by a low-cost Port Fuel Injection (PFI) system. Pressurised DME is directly injected into cylinder via a commercial Gasoline Direct Injection (GDI) injector. Flexible DME injection strategies are employed to realise the controlled auto ignition of the premixed charge. The engine is operated at Wide Open Throttle (WOT) in the entire operating region in order to minimize the intake pumping loss. Engine load is controlled by varing the amount of internal Exhaust Gas Recirculation (iEGR) which is achieved and adjusted by Positive Valve Overlap (PVO) and/or exhaust back pressure, and exhaust re-breathing method. The premixed mixture can be of either stoichiometric air/fuel ratio or fuel lean mixture and is heated and diluted by recycled exhaust gases. The use of internal EGR is considered as a very effective method to initiate CAI combustion due to its heating effect and moderation of the heat release rate by its dilution effect. In addition, the new combustion concept is compared to conventional SI combustion. The results indicate that the new combustion concept has potential for high efficiency, low emissions, enlargement of the engine operational region and flexible control of CAI combustion.

Acknowledgements

My deepest gratitude goes first and foremost to Professor Hua Zhao, my supervisor, for his constant encouragement, guidance and trust during this project in the last four years. I am deeply honoured to be one of his students and what I have learned from him, not only the academic knowledge but also the research skills, will be a precious treasure of my life. I also would like to thank Dr. Lionel Ganippa to be my second supervisor.

I would like to express my sincere gratitude to technicians, Kenneth Anstiss and Clive G. Barrett, for their valuable help and advices in setting up experimental facilities. I also thank the other staffs in the lab, Andy Selway, Paul, Les and John Langdon for their technical and substantial support.

I also would like to express my appreciation to my colleagues and friends, Dr. Yan Zhang, Mr. Jun Ma and Dr. Cho-yu Lee, for their encouragement and valuable discussions; Dr. Changho Yang and Dr. Manida Tongroon for their help in the early stage of my research; Mr. Barnaby Coates, Mr. Martin Lawrence and Mr. Ewan Wilson for proof-reading my thesis. I would like to thank all my friends' continuous support and friendship to keep me motivated and give me a wonderful life experience during my PhD study at Brunel University.

My big thanks would go to my beloved parents, Mr. Zuohe Zhang and Ms. Lijun Song. I extremely appreciate them to raise me up and give me mental and financial support throughout my life. I could not have reached where I am today without their selfless love.

Finally, I would sincerely thank my wife, Ms. Chenxi Zhong, for always being on my side for encouraging me to overcome difficult moments, sharing my happiness and keeping me fit. No words can express my love for her.

To my parents and my wife, with love…

Nomenclature

General Abbreviations

AFR	Air/Fuel Ratio
AI	Auto Ignition
ATDC	After Top Dead Centre
BEVs	Battery Electric Vehicles
BMEP	Brake Mean Effective Pressure
BTDC	Before Top Dead Centre
CA	Crank Angle
CAI	Controlled Auto-Ignition
CARB	California Air Resources Board
CCR	Combustion Chamber Recirculation
CFD	Computing Fluid Dynamics
CI	Compression Ignition
CN	Cetane Number
CNC	Computer Numerical Controls
CNG	Compressed Nature Gas
COVimep	Coefficient of Variation in IMEP
CR	Compression Ratio
DAQ	Data Acquisition
DI	Direct Injection
DME	Di-Methyl Ether
DOD	Displacement on Demand
DPF	Diesel Particulate Filter
EGR	Exhaust Gas Recirculation
iEGR	internal Exhaust Gas Recirculation
E/IPR	Exhaust/Intake Port Recirculation
ET	Exhaust Throttling
EU	European Union
EV	Electric Vehicles
EVC	Exhaust Valve Closing
EVO	Exhaust Valve Opening

FCEV	Fuel Cells Electric Vehicles
FID	Flame Ionisation Detection
FPR	Flame Propagation Ratio
FSI	Fuel Stratified Injection
FuelMEP	Fuel Mean Effective Pressure
FVVA	Fully Variable Valve Actuation
GC	Gas Chromatography
GDI	Gasoline Direct Injection
HC	Hydrocarbons
HCCI	Homogeneous Charge Compression Ignition
HEV	Hybrid Electric Vehicle
HRR	Heat Release Rate
IC	Internal Combustion
ICE	Internal Combustion Engine
IMEP	Indicated Mean Effective Pressure
IPCC	Intergovernmental Panel on Climate Change
ISFC	Indicated Specific Fuel Consumption
IVC	Inlet Valve Closing
IVO	Inlet Valve Opening
KERS	Kinetic Energy Recovery System
KOF	Knock Occurrence Frequency
LCV	Light Commercial Vehicles
LES	Large Eddy Simulation
LEV	Low Emissions Vehicle
LHV	Lower Heating Value
LNT	Lean NOx Trap
LPG	Liquid Petroleum Gas
LTC	Low Temperature Combustion
MBT	Minimum Spark Advance for Best Torque
MFB	Mass Fraction Burned
MS	Mass Spectrometry
NASA	National Aeronautics and Space Administration
NDIR	Non-Dispersive Infrared
NVO	Negative Valve Overlap
OECD	Organization for Economic Co-operation and Development

ON	Octane Number
PCCI	Premixed Charge Compression Ignition
PFI	Port Fuel Injection
PID	Proportional + Integral + Differential
PM	Particulate Matter
PMEP	Pumping Mean Effective Pressure
PON	Pumping Octane Number
PPC	Partially Premixed Combustion
ppm	parts per million
PRF	Primary Reference Fuel
PVO	Positive Valve Overlap
RCCI	Fuel Reactivity Controlled Compression Ignition
rpm	revolutions per minute
SCR	Selective Catalytic Reduction
SI	Spark Ignition
SOI1	First Start of Injection
SOI2	Second Start of Injection
SULEV	Super Ultra Low Emissions Vehicle
TDC	Top Dead Centre
TDI	Turbocharged Direct Injection
THC	Total Hydrocarbons
TLEV	Transitional Low Emissions Vehicle
UEGO	Universal Exhaust Gas Oxygen
UK	United Kingdom
ULEV	Ultra Low Emissions Vehicle
US	United States
VCR	Variable Compression Ratio
VVA	Variable Valve Actuation
VVT	Variable Valve Timing
VW	Volkswagen
WOT	Wide Open Throttle
ZEV	Zero Emissions Vehicle

General Notation

λ, lambda	Relative air/fuel ratio
γ	Ratio of specific heats
η_c	Combustion efficiency
η_t	Thermal efficiency
η_g	Gross indicated efficiency
η_n	Net indicated efficiency
η_b	Brake efficiency
η_{ge}	Gas exchange efficiency
η_m	Mechanical efficiency
σ	Standard deviation
θ	Crank angle
AFRg stoi	Stoichiometric AFR gasoline
AFRd stoi	Stoichiometric AFR DME
a	Crank radius,
B	Cylinder bore diameter
c_v	Specific heat at constant volume
Hcv	Atomic ratio of Hydrogen t o Carbon in the fuel
K1	Number of Carbon atoms in each of the HC molecules being measured
Kp	Assumed relation of CO_2, CO, H_2O and H_2 concentrations
l	Connecting rod length
LHV_g	Lower heating value of gasoline
LHV_D	Lower heating value of DME
ma	Air mass flow rate
mg	Gasoline mass flow rate
md	DME mass flow rate
m_g	Mass of gasoline in one cycle
m_D	Mass of DME in one cycle
Ocv	Atomic ratio of Oxygen to Carbon in the fuel
P	Pressure
P_{ave}	Averaged pressure data
Q_{HV}	Lower heating value of the fuel
Q_{net}	Net heat release
Q_{hr}	Heat released during combustion

Q_{ht}	Heat exchange with combustion chamber walls
r	Compression ratio
s	Distance between the crank axis and the piston pin axis
T	Temperature; break torque
dU	Systematic change in internal energy
V	Volume
V_c	Clearance volume
V_d	Displaced volume
W_g	Gross work in one cycle
W_n	Net work in one cycle

Chemical Symbols and Abbreviations

CH_4	Methane
CO	Carbon monoxide
CO_2	Carbon dioxide
DME	Di-methyl ether
H_2O	Water
HCHO	Formaldehyde
HO_2	Hydrogen dioxide
N_2	Nitrogen
N_2O	Nitrous oxide
NO	Nitric oxide
NO_2	Nitrogen dioxide
NO_x	Combined oxides of nitrogen
O	Oxygen radical
O_3	Ozone
OH	Hydroxyl radical
PTFE	Polytetrafluoroethylene
R	Radical
ZrO_2	Zirconia

Contents

Chapter 1

Introduction

Chapter 1 Introduction

1.1 Background

In the history of human development, the requirement of power is kept increasing with the development of technology and science. Since the Internal Combustion (IC) engine was invented over a century ago, they have flourished and propelled industrial production and human activity, especially transportation, and thoroughly changed human life. The invention and development of IC engine technologies have lead to the modern automotive industry which enhances the tempo of modern living and enlarges the living radius. Therefore, it is thought that the IC engine has become one of the 'motive powers' of modern civilization.

The technologies of IC engines have been significantly developed in the past century and Spark Ignition (SI) and Compression Ignition (CI) engines are the most popular and widely used in either heavy duty or light duty vehicles. However, as the oil crisis and serious environmental pollution are increasingly becoming important, the demands of more efficient and cleaner engines are urgently needed through continued researches and technology developments. Although electric vehicles and fuel cell technologies are considered as future alternatives, IC engines are likely to remain dominant for automotive applications for decades to come, until the severe limitations of the electric battery, such as cost, power density, durability, safety and reliability, as well as the source of electricity and charging infra-structure, are solved.

In the last fifty years, a number of technological advantages have been introduced and used in the IC engines in order to increase engine efficiencies and reduce emissions, for example, Gasoline Direct Injection (GDI), Variable Valve Actuation (VVA), 3-way catalyst, the utilization of alternative fuels and so on. These applications either raise the efficiencies and reduce the emissions via improving the combustion process, or increase the conversion rate of the exhaust gas.

Towards the investigation of improving combustion process, an engine which is as clean as a petrol engine and, at the same time, as efficient as a diesel engine is greatly expected. Thus, an alternative combustion technology has recently been introduced to implement the expectation. It is known by a number of names and the most popular two are Controlled

Auto Ignition (CAI) and Homogeneous Charge Compression Ignition (HCCI). Engines with this combustion are able to achieve higher efficiencies and lower emission than conventional SI engines in terms of both theory and practice. However, there are several drawbacks and challenges of CAI combustion, such as the restricted operating range, the difficulty in initiating auto ignition and the difficulty in controlling combustion phasing, which need to be overcome before this technology being widely used in commercial applications.

There has been significant process made in the field of CAI since first implemented in the 1970's [1]. With these investigations, some technologies are introduced in order to overcome the drawbacks and challenges of the CAI combustion. These technologies include the introduction and control of internal or/and external Exhaust Gas Recirculation (EGR), Variable Compression Ratio (VCR), Fully Variable Valve Actuation (FVVA) mechanism, combustion mode transition, variable fuel injection strategies and introducing an ignition promoter.

With the method of introducing an alternative fuel as an ignition promoter in a gasoline CAI engine, Di-Methyl Ether (DME) has been considered as an ideal ignition promoter due to its high cetane number. It can be produced from a range of energy sources such as biomass, coal and natural gas. The DME storage, supply and injection system can be the same as the one designed for Compressed Nature Gas (CNG) or Liquefied Petroleum Gas (LPG).

In order to overcome the limitation of current CAI gasoline engine and to utilise the ultra-low emission characteristics of the low temperature combustion operation, a new concept of CAI combustion is introduced and studied in this thesis.

1.2 Objectives

The objectives of the project are to:

(i) Investigate the CAI combustion of diluted premixed mixture in a gasoline engine with various strategies of DME injection in terms of optimal operation parameters, engine performance, emissions, and heat release analysis.

(ii) Extend both high load boundary and low load boundary of CAI operation region by means of hybrid combustion processes using varied DME DI injection strategies.

(iii) Investigate and compare the effects of internal EGR (iEGR) achieved by either PVO together with exhaust throttling or exhaust re-breathing methods on engine performance, efficiencies and emissions of CAI combustion.

(iv) Compare the new concept CAI combustion with conventional SI combustion in terms of engine performance, efficiencies, heat release analysis and emissions.

1.3 Outline of Thesis

Following the introduction, Chapter 2 contains the literature review. Firstly, a review of emission legislation, global warming and fossible fuel supply is provided as the motivation of continuing research and development of powertrain systems. Secondly, some up to date achievements and applications towards high efficiency and low emissions engines are presented. Next, the fundamentals of the CAI combustion are described and the previous researches are reviewed, which provides a basis for the formulation of the new concept combustion. At the end of Chapter 2, there is a short review of DME property and DME engine applications.

Chapter 3 describes the experimental test facilities and data analysis methods. It contains the introduction to the research engine, detailed description of the development and implementation of a newly designed DME supply and injection system. Then, the engine control and measurement system as well as the data processing and analysis are presented. In addition, the methods of dual fuel air fuel ratio measurement are given and discussed at the end of this chapter.

Chapter 4 presents and discusses the results of experiments carried out to determine the engine variables that can be used to achieve stable CAI combustion. The engine performance, combustion, and emissions characteristics are analysed for different main and pilot DME injection timings, DME split in each injection, and DME/gasoline ratios.

Chapter 5 presents the results of the investigation of the dual fuel CAI concept with internal EGR achieved by positive valve overlap and exhaust throttling. In this chapter, it

firstly describes the operating boundaries by DME split injections. Then the boundaries have been extended and a full engine operation map is presented and comprehensively analysed with various DME injection strategies. Finally, these results are compared with the results of conventional SI combustion achieved in similar conditions on the same engine.

Chapter 6 describes the results of the new concept with iEGR achieved by exhaust re-breathing strategy. A new intake cam lobe is designed and employed to achieve internal EGR without the pumping losses associated with exhaust throttling. Some specific test points are selected to compare with the results in the Chapter 5 to demonstrate the improvements in engine efficiencies and emissions.

Chapter 7 summarises the conclusions from the results obtained in Chapter 4, 5 and 6. The recommendations for the future work are also given in this chapter.

Chapter 2

Literature Review

Chapter 2 Literature Review

2.1 Introduction

Nowadays, the current powertrain developments are concentrated on increasing efficiency and reducing environmental damage. This indicates that vehicles with lower fossil fuel consumption and more environmental-friendly engines will be the trend of technology development. Fossil oils are a non-renewable and limited energy source and so demand for them highly increases. It will become more precious in the next several decades and the prices of petrol and diesel will continue to increase. In the mean time, combustion engine vehicles are considered the cause of one third of the greenhouse gas emission sources in the UK and make up over 20% of total emissions [2]. The principal greenhouse gases associated with combustion engine vehicles are carbon dioxide (CO_2), methane (CH_4) and nitrous oxide (N_2O). What's more, pollutions from vehicle emissions including benzene, 1,3-butadiene, carbon monoxide (CO), nitrogen oxides (NOx) and particulates (PMs) cause some health problems such as the incidence of respiratory and cardio-pulmonary disease and lung cancer, which all threaten human health.

2.1.1 Emission Legislation and Emission Fundamentals

Over the last three decades, with the development of technologies such as after-treatment technology, great reductions of NOx and unburned hydrocarbons have been achieved and continually more stringent legislations have been enforced in the European Union (EU), United States (US) and Japan, which are widely used or followed by other countries. The legislations are constantly being reviewed and updated in line with the technology development such as combustion optimization and after-treatment systems. Table 2.1 shows the emission level legislations for passenger cars in the EU and California Air Resources Board (CARB) [3] [4].

Table 2.1 Legislated Emissions for Passenger Cars: European Union (EU) and California Air Resources Board (CARB) Emission Standard [3] [4]

Euro Standards	Year	Engine Type	CO (g/km)	THC (g/km)	NOx (g/km)	HC+NOx (g/km)	PM (g/km)
Euro III	2000	SI	2.3	0.20	0.15	-	-
		CI	0.64	-	0.50	0.56	0.05
Euro IV	2005	SI	1.00	0.10	0.08	-	-
		CI	0.50	-	0.25	0.30	0.025
Euro V	2009	SI	1.00	0.10	0.06	-	0.005*
		CI	0.50	-	0.18	0.23	0.005
Euro VI (Future)	2014	SI	1.00	0.10	0.06	-	0.005*
		CI	0.50	-	0.08	0.17	0.0025
CARB (LEV II)	2004-2010	Any	2	0.033	0.04	-	-
TLEV			-	-	-	-	-
LEV			4.2	0.056	0.07	-	0.01
ULEV			2.1	0.034	0.07	-	0.01
SULEV			1	0.006	0.02	-	-

*Applies only to vehicles with direct injection engines

The EU emission standard set up a certain date, from which all newly-manufactured vehicles must comply with the acceptable limits for exhaust emissions. Emission levels of CO, uHC, NOx and PM are restricted for most vehicle types such as passenger cars, light commercial vehicles (LCV), lorries and buses. The engine is run at a standardised test cycle and the new vehicle will be determined compliant or non-compliant to the emission standard. Table 2.1 shows the reduction trends are significant in later steps and the proposed Euro VI in 2014 is extremely low compared with the previous standard.

The US CARB legislation is considered as the most stringent vehicle emission limitation in the world. It defines the light duty vehicles as the following categories: Transitional Low Emission Vehicle (TLEV), Low Emission Vehicle (LEV), Ultra-Low Emission Vehicle (ULEV), Super-Ultra Low Emission Vehicle (SULEV) and Zero Emission Vehicle (ZEV). The US applies a ‘fleet-averaged’ emission strategy that forces individual manufacturers to have to meet these average emission levels in its overall sales of vehicles.

These emissions fundamentals, particularly in SI engines, are briefly described as follows:

Unburned hydrocarbons

As summarized by Heywood [5] there are four possible formation mechanisms for HC emission for SI engines.

1) **Flame Quenching at the Walls.** A layer of unburned mixture is adjacent to the chamber wall when combustion flame is quenching at the wall.
2) **Crevice HC Mechanism.** The flame quenches at the crevice entrance during the main combustion process and the unburned mixture fills into crevice volumes.
3) **Absorption and Desorption in Engine Oil.** During intake and compression stoke, some fuel is absorbed by oil layers on the cylinder wall and then released into the cylinder during the expansion and exhaust process.
4) **Poor Combustion Quality.** Partial burn and misfire lead to incomplete combustion in parts of engine's operating cycles.

When SI engine is operated under normal operating conditions, the HC level in the exhaust is around 1000 to 3000 ppm. Air/fuel mixture that is either substantially richer or leaner than stoichiometric can induce incomplete combustion or misfire, where HC emissions can rise rapidly due to the deteriorating combustion quality.

Carbon-monoxide

Carbon-monoxide emissions from internal combustion engines are primarily controlled by air/fuel ratio. The formation mechanism of CO can be summarized as:

$$RH \rightarrow R \rightarrow RO_2 \rightarrow RCHO \rightarrow RCO \rightarrow CO,$$

where R stands for the hydrocarbon radicals. As the SI engine usually operates near stoichiometric at part load and fuel-rich at full load, the CO emissions are significant and must be controlled. In the fuel-rich mixture, the richer the fuel mixture is, the more CO emissions achieved. However, when the engine operates in a lean mixture, CO emissions in the exhaust are too small to be taken as a serious concern.

The trends of reducing CO emissions in the internal combustion engine research community are as follows.

1) Improving mixture uniformity in multi-cylinder engines.
2) Making the intake mixture lean.
3) Controlling of fuel metering during transient engine operation.
4) Applying exhaust after-treatment devices to oxidise CO in the exhaust.

Nitrogen Oxides

Nitric oxide (NO) and Nitrogen dioxide (NO_2) are usually considered and measured together as the combination NOx emissions with a chemiluminescence analyser, in which NO is the main oxide of nitrogen produced inside the engine cylinder. The oxidation of atmospheric nitrogen is the predominant source of NO. Although the combustion of fuel that contains significant nitrogen could be another source of NO, both gasoline and diesel fuels contain negligible amounts of nitrogen.

The fundamental reactions of NO formation in the combustion near-stoichiometric air- fuel mixture are as follows [6]:

$O+N_2$ - NO+N
$N+O_2$ - NO+O
N+OH - NO+H

In SI engines, the NO_2/NO ratio are negligibly small for the burned gas at typical flame temperature. However, in diesel engines NO_2 can take 10 to 30 percent of total NOx. The principle of NO_2 is that NO can be rapidly converted to NO_2 in the flame zone by:

$NO+HO_2$ - NO_2+OH

Subsequently, conversion of this NO_2 to NO via

NO_2+O-NO+O_2,

except the NO_2 formed in the flame is quenched by mixing with cooler fluid [7].

In the typical SI engine, the air fuel ratio, the burned gas fraction of in-cylinder unburned mixture and spark timing are the most important engine variables that affect NOx emissions. With variable air fuel ratio, NOx emissions peak at slightly leaner than a stoichiometric mixture. In rich mixtures, substantial NO decomposition occurs when the cylinder pressure is maximum. While in a lean mixture, NO concentration freezes and little decomposition occurs [8]. The recycled burned gas is used for controlling the NOx emissions. The burned gas dilutes the unburned mixture and reduces flame temperature by increasing the heat capacity of intake charge. It is indicated by previous researches that with 15 to 25% exhaust gas recirculation (EGR), the reductions of NO concentration can be significant. Spark timing also plays a significant role in affecting NO emissions. Advancing the spark timing makes the combustion occur earlier, inducing a higher peak in-cylinder pressure and a higher peak burned gas temperature and hence higher NO formation rates [9].

2.1.2 Global Warming and Carbon Emissions Reduction

Global warming is the climate change which causes the increase of average temperature of the Earth's lower atmosphere. It is confirmed by observation of the temperature rising over a century and this increase is expected to continue into the future. According to a report from United State National Academy of Science [10], the temperature of global surface has increased at about 0.8 °C (1.4 °F) during the 20th century, with most of the warming attributed in the last 30 years, as shown in Figure 2.1 [11]. It is predicted that the potential temperature increase until year 2100 would be around 2.0-5.4 °C (3.6-9.7 °F) based on a computer model of climate systems introduced by the Intergovernmental Panel on Climate Change (IPCC) [12] and National Aeronautics and Space Administration (NASA) [11] as partly presented in Figure 2.2.

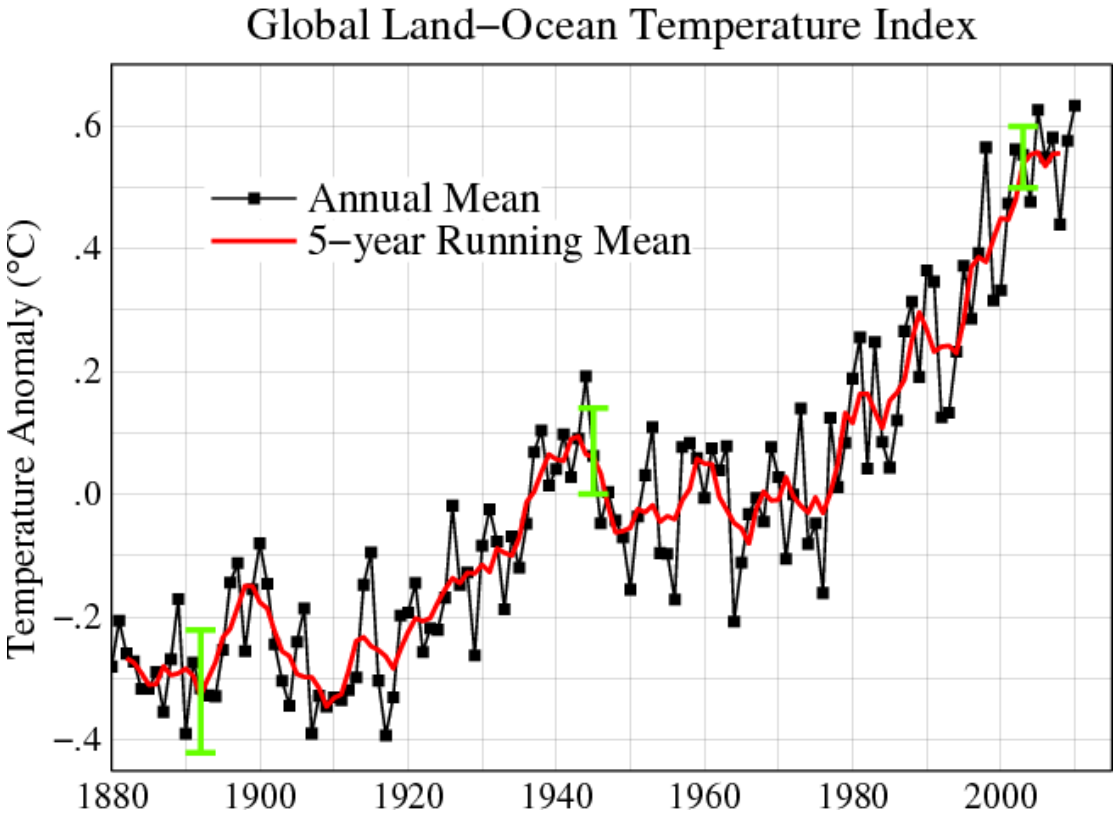

Figure 2.1 Global Temperature Anomalies 1880-2010 (Base Period=1951-1980) [11]

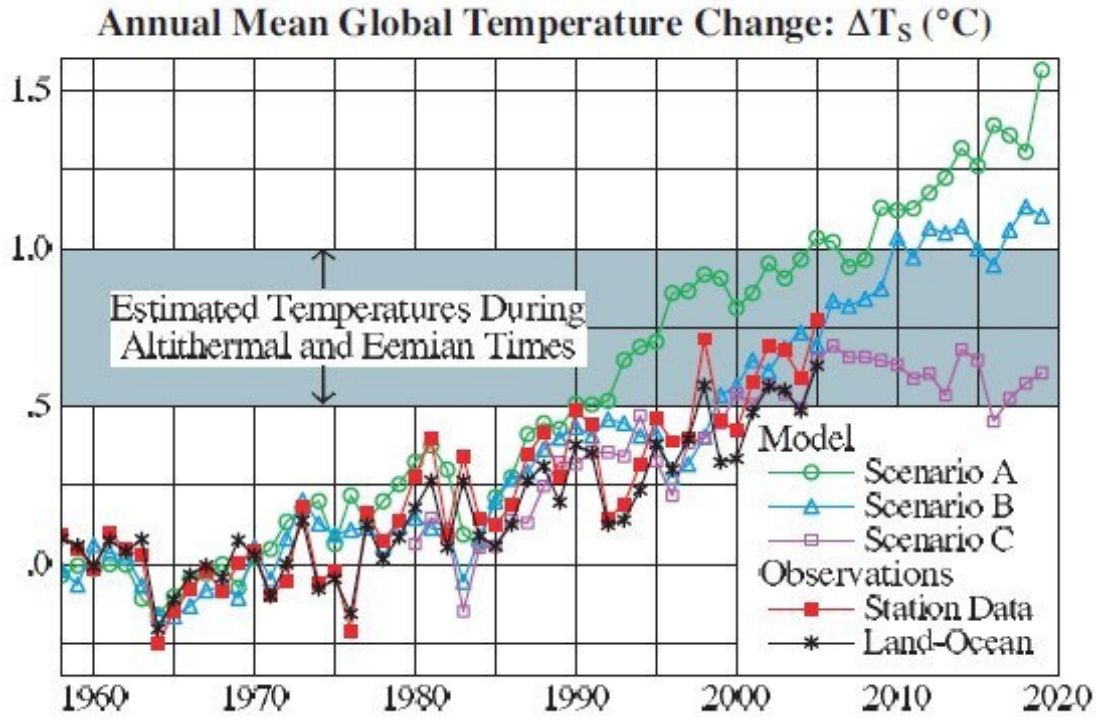

Figure 2.2 Global Surface Temperature Computed for Scenarios A, B, and C, Compared with Two Analyses of Observational Data [11]

Hansen, et al. [11] concluded that global warming of more than around 1 °C can be considered as "dangerous" climate change that may result in the rise of sea levels and the extermination of species.

Global warming is considered as the results of the effect of greenhouse gas emission, which is the process of absorption and emissions of infrared radiation by gases in the atmosphere. The greenhouse gas effect, which is attributed by water vapour (36-70% effect), CO_2 (9-26% effect), CH_4 (4-9% effect) and ozone (O_3) (3-7% effect), keeps the mean temperature of the Earth at 15 °C (59 °F), which is crucial for existing lives [13]. The increase in concentrations of greenhouse gas has been initiated by human activity, especially since the industrial revolution and humanity's massive use of fossil fuel. CO_2 is considered as the major greenhouse gas because CH_4 can still be captured and burned as a fuel and CO_2 is the product of fossil fuel burning. It could be said that the CO_2 absorbed by plants over millions of years is released through human activity within several decades.

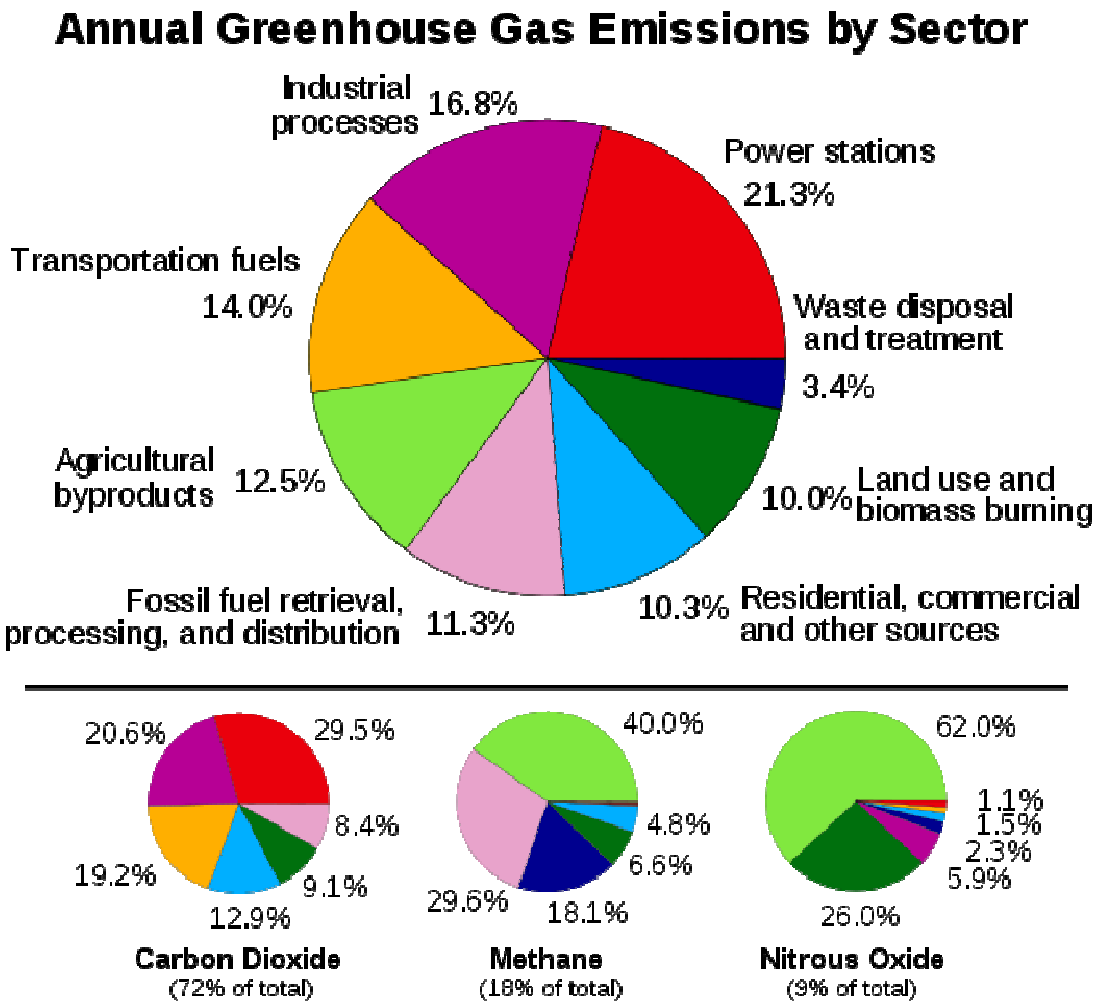

Figure 2.3 Global Man-made Greenhouse Gas Emissions in Year 2000 [14]

Figure 2.3 illustrates the global contribution of greenhouse gas generated by human actions in 2000. It can be concluded that CO_2, initiated by human activities, are mainly from the burning of fossil fuels such as coal, gasoline, diesel, natural gas etc. to provide power for transportation, industrial, commercial and residential purpose.

In Figure 2.3, transportation contributes about 14% of the overall greenhouse gas emissions and 20% of the total CO_2 emissions in year 2000, and according to the International Transport Forum, total transport makes up 23% of the carbon emissions globally and 30% in Organization for Economic Co-operation and Development (OECD) countries in 2010 [15]. It is expected to continue to grow by about 40% from 2007 to 2030.

Therefore, a comprehensive policy and strategy is set out by the European Commission to reduce the CO_2 emissions from the sale of passenger cars and light duty vehicles in order

to implement its greenhouse gas emission consents under the Kyoto Protocol and beyond. In July 2007 (when this study started), the European Commission set a public hearing that the new passenger cars are supposed to reach the EU objective of 120 g/km average CO_2 emissions by 2012. The reduction should come from two sources: down to 130 g/km by engine technology improvement and the rest through other approaches. The LCV (light commercial vehicle) should reach 175 g CO_2/ km emissions by 2012 [16]. Later in October 2007, the European Parliament adopted a resolution that the average new car fleet should reach 125 g CO_2 /km in 2015 and 95 g CO_2/km by 2020, and possibly achieve 70 g CO_2/km by 2025 if possible, subject to a review before 2016 [17]. At the end of 2010 (when this study almost finished), a progress report of implementation of 2007 strategy from European Commission concluded that the 130 g CO_2/km target had been achieved for passenger cars in 2009 by the improvement in engine technology and would turn into full force in 2015, but it was not possible to reach 120 g/km in 2012 [18]. In February 2011, the 175 g/km target for LCV is extended to be achieved by 2017 according to an updated standard. As a result, the automotive industry is still under pressure to reduce CO_2 emissions especially in LCV to meet mid and long term targets.

2.1.3 Oil Crisis

Besides the concern of emission threat and global warming, the increasing cost of conventional liquid gasoline and diesel fuel is also a challenge of the automotive industry.

Gasoline and diesel come from petroleum which is considered as a non-renewable energy source. Figure 2.4 [19] shows the Brent barrel petroleum spot price in the US which is expected to continually increase in the future as the demand of oil increases as well.

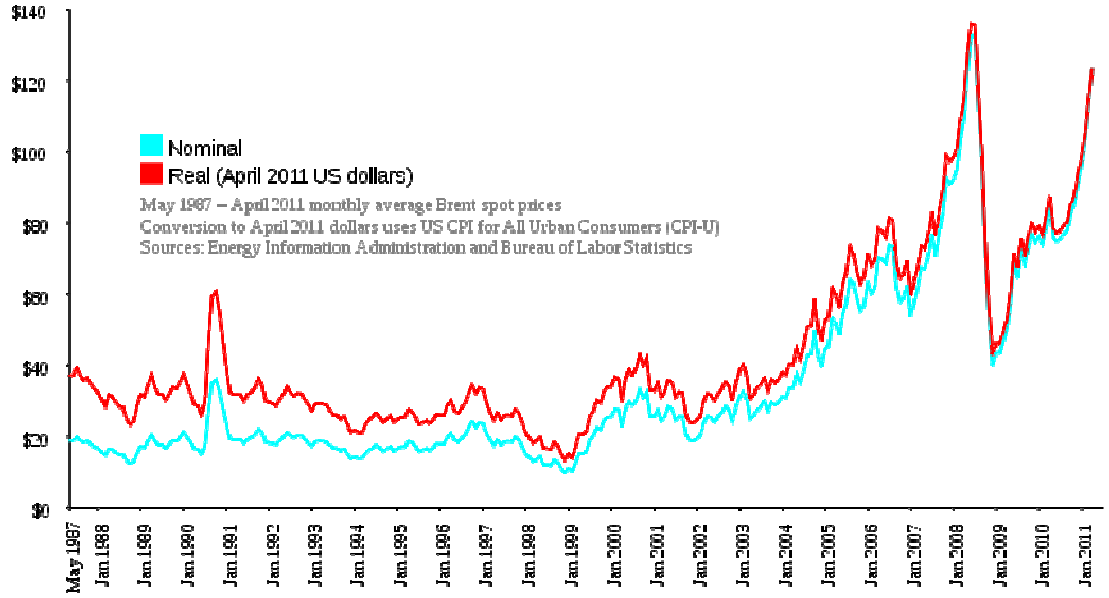

Figure 2.4 Brent Barrel Petroleum from 1987 to 2011 [19]

BP, who publishes its Statistical Review of World Energy every year, indicates that there is still at least 40 years of proven reserves to provide sufficient oil consumption at its current rate all over the world [20]. Scientists like John H. Wood, et al. [21] pointed out that the world will never physically run out of crude oil unless the oil eventually becomes as expensive as the increasing demands without any lower-cost alternatives.

2.2 Achievements and Applications toward High Efficiency and Low Emission Engines

In order to meet the emission legislations and respond to the oil price increase as well as demands, some technologies are introduced and developed by automotive industries to improve engines with higher efficiency and lower emissions.

2.2.1 Hybrid and Electric Vehicles

Disregarding the source for generating electricity, the electric vehicle (EV) itself can actualize zero emissions. The electric energy of the vehicle can be produced from either charging a battery from a charging station named Battery Electric Vehicles (BEVs) or from fuel cells called Fuel Cells Electric Vehicles (FCEVs). The BEVs have an on-board efficiency of about 80% [22] and FCEVs offer around 48% efficiency [23].

However, if the electricity generating process is taken into account, also known as well-to-wheel efficiency and emissions, the electric vehicles will lose their advantages unless either electricity or hydrogen for fuel cells is from a renewable energy source such as solar energy or nuclear energy. What's more, the entry of electric vehicles into the main stream of the automotive market is, at the moment, restrained by some factors, such as the range, the charging time requirement of the battery, battery endurance, initiate cost, hydrogen storage safety concerns, electric vehicle safety and reliability concerns, and the requirements of battery recharging stations.

Hybrid vehicle technology is a transition between pure conventional internal combustion engine (ICE) vehicle and pure EV. The Hybrid Electric Vehicle (HEV) combines an internal combustion engine with one or more electric motors. The HEV shuts down the engine at idle speed, reducing the idle emissions and fuel consumption and restarts it when needed. The engine runs at the maximum efficiency if the vehicle is driven by electric motor only, further increasing fuel economy. ICE-Electric hybrid automotives are widely available by main auto manufacturers such as Toyota (Prius), Honda (Insight), Ford (Fusion), Volkswagen (Touareg), Mercedes-Benz (S400 BlueHybrid) and BMW (Active Hybrid X6). The efficiency advantage of the hybrid is from 30% in 1995 to 25% in 2005 and is expected to be below 23% in 2015 due to the advanced conventional vehicle [24].

However, the extra cost and system stability and the reliability of HEVs are still the challenges of their popularization.

A Kinetic Energy Recovery System (KERS) is another hybrid technology, which has been used by Formula 1 in seasons 2009 and 2011, and is being developed for automotive applications [25]. The system recovers the kinetic energy under the vehicles' braking process and store the energy by a high speed flywheel in a sealed vacuum chamber. The recovered energy is converted to power which can be called upon to boost acceleration. The kinetic energy of the vehicle during braking can also be absorbed and stored by pressurized fluid, named as hydraulic hybrid, which is primarily used for commercial vehicles because it is of less weight and cost compared to the flywheel one. The hydraulic hybrid vehicle systems contain four main components: the working fluid, reservoir, pump/motor and accumulator. The braking kinetic energy drives the pump and pumps the working fluid from the reservoir to the accumulator, and pressurises the fluid. The pressurised working fluid will power the vehicle while it is under accelerations [26]. It is said that the large SUV or pickup truck with a parallel hydraulic system have better acceleration and, meanwhile, a significant 40% improvement in fuel economy [27].

In 2009, a cost effective air hybrid concept is introduced by Brunel University, which is proposed to achieve around 15% regenerative efficiency, but with little cost by capturing, storing and reusing the break energy with an air tank [28]. This concept will be implemented in the near future and expected to be applied in LCVs and Heavy Duty Vehicles soon. Some other hybrid concepts such as using engine inertia energy [29-30] or solar energy [31] are still in the concept stage.

2.2.2 Emission After-treatment

The reduction of toxic emissions from current vehicles requires much development and improvement of emission after-treatment technologies.

Catalysts are used in the exhaust pipe to stimulate the chemical reaction of converting toxic CO, uHC and NOx to less-toxic or inert substances such as CO_2, H_2, N_2 and O_2. The 3-way catalytic converter is widely used in the case of a gasoline engine that runs a stoichiometric charge and the oxidation catalyst is generally used in engines which burns an overall lean mixture. The catalysis technology requires unleaded and low sulphur gasoline, avoiding

catalyst poisoning. The developments of after-treatment systems to clean up lean-burned exhaust are sorely required [32] when the Diesel and stratified GDI technologies, which allow lean combustion, are widely used and developed in the modern automotive industry.

Diesel particulate filter (DPF) is employed to remove diesel particulate matter or soot from the exhaust of the diesel engine. With current technologies, a wall-flow DPF could remove over 85% of the soot. Under certain condition, the attainable soot removal efficiencies could be closed to 100% [33]. In addition, the Lean NOx Trap (LNT) and Selective Catalytic Reduction (SCR) technologies are developed and applied, particularly in diesel applications, in order to reduce NOx emissions. The LNT is designed to absorb the NOx emitted in the exhaust gas of lean burn engines and the SCR is a means of converting NOx and NH_3 with the aid of a catalyst into innocuous N_2 and H_2O. The configuration of multiple alternating zones of LNT and SCR catalyst can be one potential solution for the alternative lean/rich operation cycles [34].

2.2.3 Engine Operation Technology Developments

Since the internal combustion engine was invented and used in transportation, scientists and engineers have kept trying to improve it. Various technologies have been introduced and developed to improve engine performance and emissions. In the first decade of the 21st century, the following applications were considered as the leading edge and trend in this area.

Direct Fuel Injection

With direct fuel injection technology, fuel is directly injected into the cylinder in order to precisely control the injection timing, spray shape and amount. It is applied in both conventional diesel and gasoline engines.

One of the most famous diesel direct injection engines is developed and produced by the Volkswagen (VW) Group. Coupled with a turbo charging technique, it is widely known as a marque of TDI (Turbocharged Direct Injection) in its passenger car and LCV products. These TDI engines achieve higher efficiency by reducing heat losses as well as having greater power outputs by increasing the induction of fresh air and fuel, while they also reduce emissions and provide more torque compared with indirect injection and non-turbo

engines. The latest VW Golf with BlueMotion 1.6 TDI 105PS engine could offer 105 horse power with combined fuel consumption 3.8 litres per 100 km and 99 g CO_2 /km emission, which has easily met Euro V emission legislation [35].

Gasoline Direct Injection (GDI) system, opposed to conventional port fuel injection (PFI) system, is an application that pressurises and injects gasoline directly into the cylinder. A more advanced version of GDI is stratified charge operation which forms the stratified charge inside the cylinder. The conventional PFI engine load control is normally achieved by airflow throttling in the intake manifold, which increases the pumping loss and has the effect of 20% efficiency reduction under idle conditions. However, stratified charge enables the engine to be operated at wide open throttle (WOT) with much less throttling loss. In the condition of low load, small amounts of fuel are injected near the top dead centre (TDC) of compression. Thus the stratified charge is formed and an optimal air-fuel mixture is placed around the spark plug so that ultra lean combustion is achieved to improve fuel economy and emission. In moderate and full load conditions, fuel is injected during the intake stroke, producing a homogenous and stochiometric fuel-air mixture in the cylinder and inducing clean exhaust emission. Audi announces that with its FSI (Fuel Stratified Injection) technology, it is possible to improve efficiency by 15% with reduced exhaust emissions and increase the power output and torque of gasoline engines [36]. However, due to the requirement of expensive and less efficient lean NOx aftertreatment, the robustness of GDI engine and the high cost of GDI injector, the stratified charged operation is not featured in the most modern GDI engines. Instead, the downsized GDI gasoline engines are introduced.

Engine Downsizing with Air Boosting

Engine downsizing is the process that shifts the engine operating point to a more efficient region by downsizing the engine capacity as well as maintaining the high load performance by means of intake boosting either by the supercharger or the turbocharger. The downsized engine has high specific power output ensuring that engine works in high speed thus minimising throttling pumping loss which improves the fuel economy. Atkins et al. [37] concluded that, with a well-to-wheel analysis, the gasoline engine downsizing coupled with intake boost charging and variable valve timing (VVT) technologies is the most effective method for immediate implementation to improve overall efficiency and CO_2 emissions. MAHLE powertrain Ltd [38-39] introduced a 3 cylinder 1.2 L high specific

output gasoline downsize engine with the purpose of replacing a typical 2.4 L V6 PFI engine which is used in a C or D class European vehicle platform. This engine is proposed to achieve 30% fuel consumption reduction and is compliant with Euro V and ULEV2 emission legislations. Vehicle manufacturers like VW are also promoting their 1.2 TSI and 1.4 TSI engines into commercial markets.

Variable Valve Actuation (VVA)

In the conventional SI engines, the pumping losses are inversely proportional with the engine load. Without a throttle valve, control of the air-fuel mixture can be realized by variation of the intake vale-opening period. Variable valve actuation (VVA) is used to control the opening timing, opening duration and the lift of both intake valve and exhaust valve while the engine is in operation which has great potential for reducing pumping losses. The variable valves control the flow of intake charge into the cylinders as well as the exhaust going out of them. Optimum valve timing and lift settings are different due to the change of engine speed, load and other operation conditions, which affect engine efficiency and emissions. VVA system is mature and widely used in mass production, such as BMW Double VANOS, Ford Ti-VCT. Mechanical variable lift devices include, Honda Advanced VTEC, Nissan CTVCS and Toyota VVTL-I etc. Hong et al. [40] concluded that VVA can improve the engine efficiency by the range of 7% to 16% after reviewing and analysing 8 ways of VVA strategies.

Cylinder Deactivation

Cylinder deactivation, also called variable displacement or displacement on demand (DOD), is the technology that allows an engine to change its displacement by means of the disabling some of the cylinders. The cylinder deactivation technology shifts the lower loads operation of a large engine to the higher loads operation of a small one. It is used in the low load operation of large and multi-cylinder engines which originally induces large pumping loss. It is said that with this method, the fuel consumption can be reduced by 8% to 25 % in high way conditions [41].

2.2.4 Combustion Technology

Towards the target of producing a high efficiency and low emission engine, combustion technologies have been significantly developed and become the main research interest since the internal combustion engine was invented and played such a key role in human life. There are four combustion processes introduced in time sequence:

1 **Spark Ignition (SI) Combustion** such as conventional gasoline engines are homogeneous premix air-fuel mixture charge and flame propagation with around 10-30% efficiency varying with speed and load.

2 **Compression Ignition (CI) Combustion** such as conventional diesel engine which are characterised by inhomogeneous charge and diffusion flames with over 40% efficiency in modern DI diesel engines.

3 **Stratified Charge Lean-burn Combustion** such as some modern GDI engines whose operations include stratified lean charge and flame propagation, achieving up to 15% efficiency improvement compared with a modern PFI engine.

4 **Controlled Auto Ignition (CAI) Combustion** which are characterised by diluted or premixed air-fuel mixture charge and auto ignition combustion, which could achieve roughly 50% brake indicated efficiency in lab results [42].

In some recent researches, the combustion process can not be clearly distinguished from one of the above, which induces hybrid combustion inside the cylinder. CAI combustion will be further discussed in the next section.

2.3 Controlled Auto Ignition (CAI) Combustion

2.3.1 Introduction

Scientists and engineers are striving to produce an engine which is as clean as a petrol engine and, at the same time, as efficient as a diesel engine. Although GDI technology has closed the gap between gasoline and diesel engines to a significant extent, the CAI engine makes the difference very small and insignificant even [43].

CAI is short for Controlled Auto Ignition. It is also widely recognized as HCCI which refers to Homogeneous Charge Compression Ignition in numerous related researches. However, the author believes that HCCI is a kind of CAI with a homogeneous air/fuel mixture where combustion occurs in every part of the cylinder without flame front. As diversiform as 'this' kind of combustion mode is, the air fuel mixture charge may be not homogeneous. The term 'CAI' is more comprehensive to describe this kind of combustion as distinguished from SI or CI combustion.

Among the numerous research papers, CAI engines have a lot of advantages compared with conventional SI and CI engines, both in fuel economy and exhaust gas emissions. It is considered as the ideal way to achieve new emission legislations in the near future. The engine is working at high levels of dilution. The dilution is so high that the engine can be operated unthrottled, which results in significant low pumping work during the intake stroke. It leads to high improvement of fuel economy. What's more, the peak temperature of burned gas in the cylinder is low, which in turn reduces the heat loss and increases the thermal efficiency. What attracts the researchers most is that the PMs are at near zero level and the NOx emission is much lower than either conventional SI or CI engines. Najt et al. [44] indicate that a CAI engine is expected to offer 15% to 20% improvement in fuel economy with significant reduction in NOx emission compared with a conventional SI engine.

However, although the optional benefits of HCCI/CAI are great, there are some unique disadvantages, such as higher HC emission levels, limit of operating region and difficulty in controlling the combustion phasing, due to its principles.

2.3.2 Fundamentals and Applications of CAI Combustion to Achieve Potential High Efficiency and Low Emissions

2.3.2.1 Fundamentals of High Efficiency

The characteristics of heat release rate of SI and CAI combustion can be presented by Figure 2.5 [45].

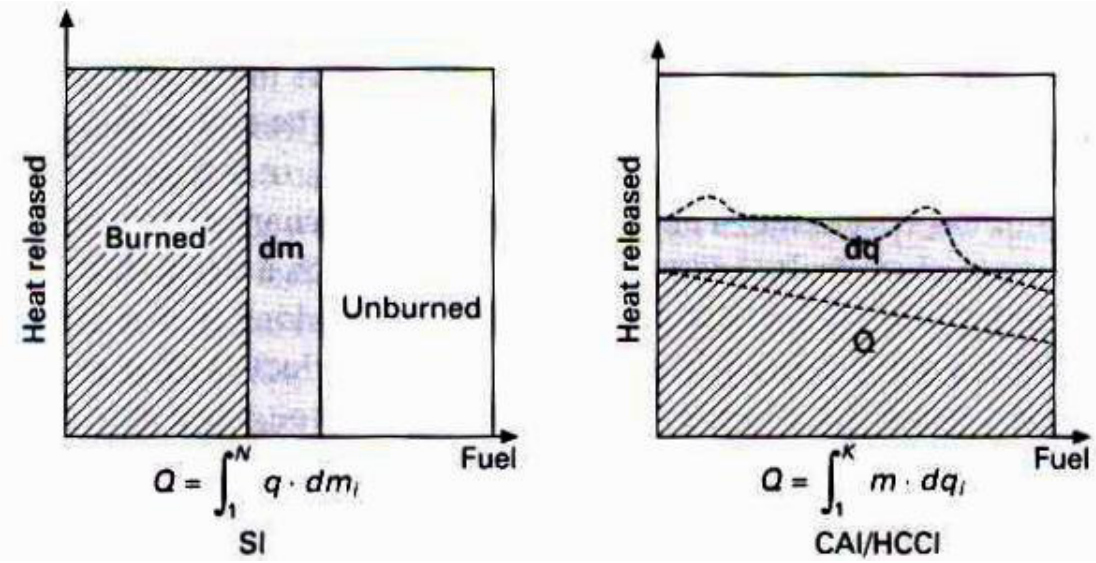

Figure 2.5 Heat Release Rate of SI and CAI Combustion [45]

In SI combustion, the burned and unburned mixture is separated by a thin chemic reaction zone which is also considered as flame front. The heat of the fuel that is involved in the reaction is ideally fully released and then the unburned mixture takes into account the reaction with the flame propagation. Therefore, the cumulative heat release rate in SI case is the sum of the heat release by the certain fuel mass, dm_i in the flame front as follows:

$$Q = \int_1^N q * dm_i \qquad \text{Equation 2.1}$$

Where q is indicated as the heating value per unit mass of fuel and air mixture, N is the number of reaction zones.

However, the combustion takes place simultaneously in an idealised CAI process. All the fuel air mixture is involved in the chemical reaction and releases its heat instantly in the combustion process. It can be expressed as

$$Q = \int_1^K m * dq_i \qquad \text{Equation 2.1}$$

Where K indicates the total number of heat release reactions, m is the complete mixture and q_i is the ith heat release value of per unit mass of air and fuel mixture.

The dash line indicates the heat release rate in the practical combustion process as the heat release process will not be completely uniform due to the intake of air and fuel mixture and temperature distribution can not be homogeneous.

Heywood [46] presented the three ideal engine cycles including constant-volume cycle, constant-pressure cycle and limited-pressure cycle. It is concluded that the constant-volume cycle has the highest efficiency. CAI is characterized by a rapid and high peak heat release rate which has shorter combustion duration than conventional SI combustion due to its simultaneous chemical reaction of air fuel mixture taking place without flame front. It is much closer to ideal constant-volume cycle than any other combustion process. In addition, as it is well known that the indicated fuel conversion efficiency increases with increasing compression ratio [46], CAI engine can be operated in a lean mixture which is able to employ higher compression ratios (CR) (>15) like CI engines, and thus achieves better performance, fuel economy and low hydrocarbon emissions compared to SI engines. CAI engines are also able to operate in wide open throttle during the whole working range, omitting the pumping losses and further increase the efficiency.

2.3.2.2 Fundamentals of Low Emissions

To understand the advantages of the exhaust emission of CAI, Figure 2.6 [47-48] was made to explain the pollutant formation processes of different combustion mode.

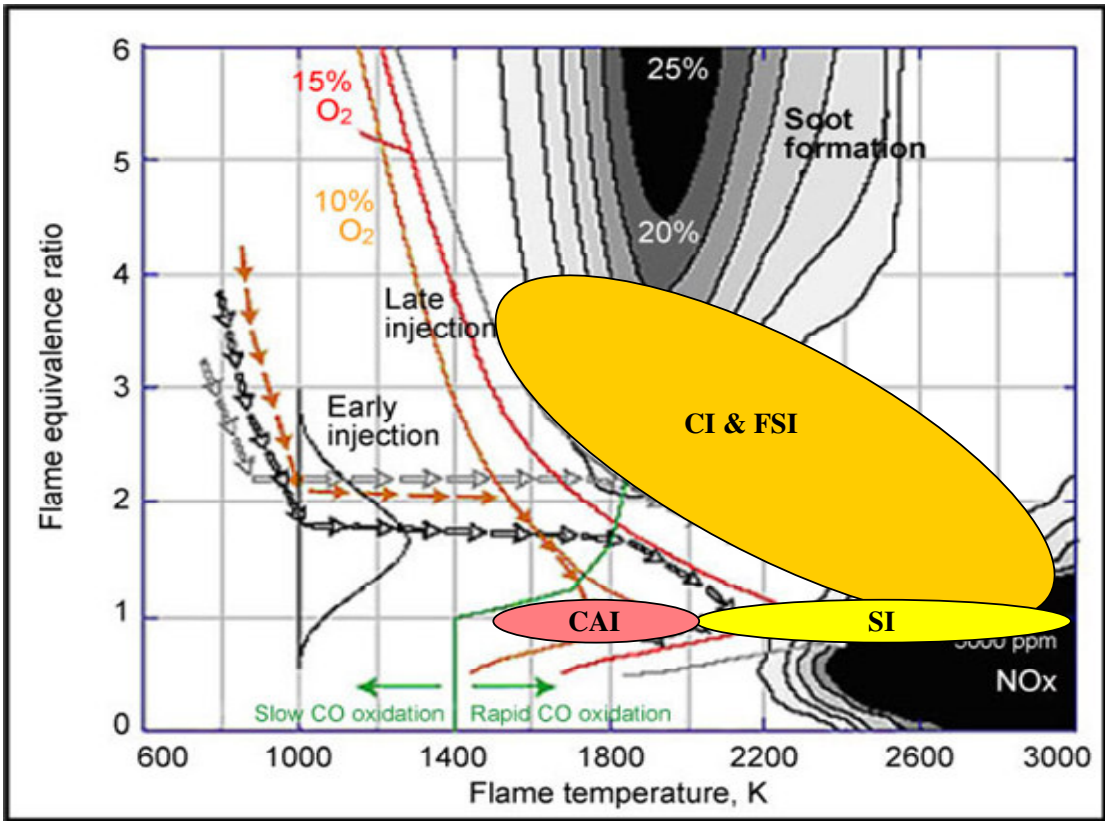

Figure 2.6 Regimes of Soot and NOx Formation In Terms of Equivalence Ratio (Fuel Air Ratio) and Flame Temperature [47-48]

In CI and stratified GDI engines, the fuel is directly injected into the cylinder. The ignition core of either diffusion flames or propagation flames starts with a partial relative rich mixture. The combustion process passes both soot formation and NOx production zones in the figure. SI engines are operated in a homogeneous stoichiometric mixture. The temperature of partial regions inside the cylinder suffers a jump when flame front arrives and then stays in a high temperature, forming high NOx emissions. Some technologies such as late fuel injection, EGR, premix fuel/air mixture with early injection and combined spilt fuel injections are introduced to shift the operating region to the left, which is recognized as low temperature combustion (LTC) region. CAI process is part of LTC region whose NOx and soot emissions are extremely low in the whole operation range.

2.3.2.3 Previous Research

In early CAI research, Noguchi, et al. [49] firstly indicated in their Toyota-Soken process research that a 2-stroke horizontally opposed piston engine could achieve 40% improvement in fuel economy as well as 1/3 uHC emission reduction compared with SI

engines because the heat release rate reaches a maximum immediately after TDC and the combustion could start at lower temperature and pressure. Thring [50] applied 370 °C intake air heating and 20-30% EGR in a single cylinder engine indicating that the HCCI gasoline engines have fuel economy as good as DI diesel ones, whose, specifically, the best indicated specific fuel consumptions (ISFCs) are from 180-200 g/kWh.

Lavy, et al. [51] applied internal EGR using VVT to enhance CAI and low NOx emissions in the 4-stroke powered gasoline auto-ignition controlled combustion engine (4-SPACE) and concluded that ISFC values were 3-4% lower in the range 3-4 bar IMEP and 7-8% lower when using lean mixtures at 2.9 bar IMEP at 1500 rpm, with drastic NOx emission reduction by 40 times in all load ranges. However, HC emissions are similar to SI combustion and even higher for the range lower than 3 bar IMEP, and CO emission reduces mainly in lean mixtures. In [52], Oakley studied the gasoline CAI range with regard to EGR and air fuel ratio, and concludes that the fuel consumption at the highest load is best at around 200 g/KWh, which shows that 20% reduction of total CO_2 emissions is possible compared with SI operation as well as 97% NOx emission reduction. But HC emissions and CO emissions at lower loads are high and that can potentially be a problem. Hyvonen, et al. [53] announced that HCCI can reach 40% to 45% net indicated efficiency with three multi-cylinder HCCI engines with different displacements as shown in Figure 2.7.

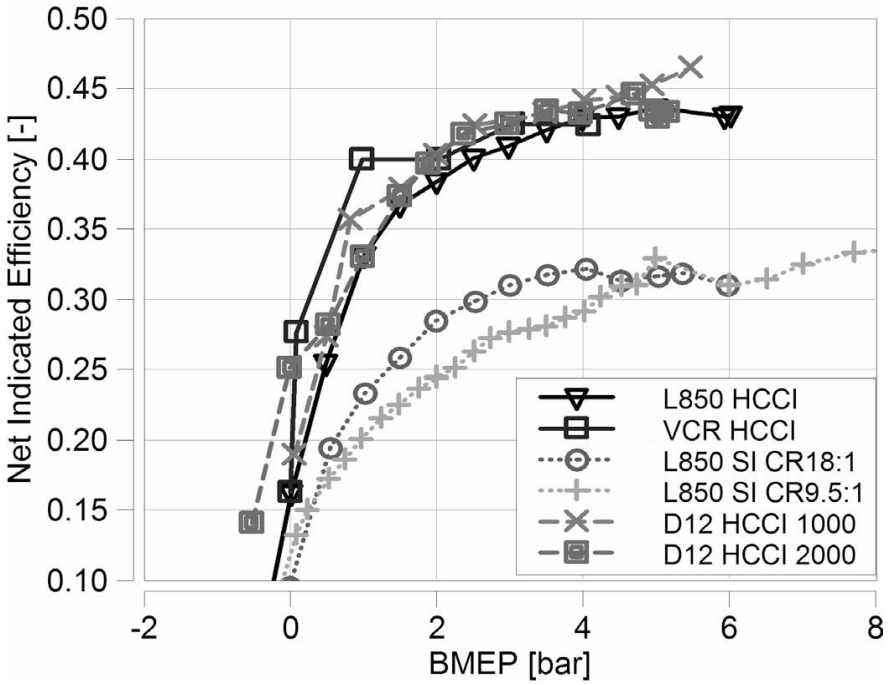

Figure 2.7 Net Indicated Efficiency of Three HCCI engines comparing with SI Combustion [53]

Lang, et al. [54] presented possible mechanical valve train concepts to realize the CAI combustion including Combustion Chamber Recirculation (CCR), which is implemented by Negative Valve Overlap (NVO), and Exhaust/Intake Port Recirculation (E/IPR) realised by exhaust re-breathing. It is concluded that the CCR by NVO leads to a maximum stratification and high temperature of residual gas and fresh air in the cylinder, performing a significantly earlier inflammation and faster combustion, which can be used to realize low loads operation, but with significantly high gas exchange losses. However, the E/IPR by exhaust re-breathing induces the most homogeneous air and residual gas mixture with lower temperature in the cylinder and minimum gas exchange loses. It is obvious that the E/IPR features the lower gas exchange losses resulting in relatively better fuel economy. What's more, the maximum possible load for E/IPR is higher than that of CCR extending the possibly higher operation boundary of the CAI combustion.

2.3.2.4 Partially Premixed Combustion (PPC)

A new combustion solution of CAI combustion, Partially Premixed Combustion (PPC), which is outside the HCCI field, has been introduced since 2006 in order to achieve high engine efficiency as well as low NOx and soot emissions. Diesel PPC was first

investigated by Kalghatgi in 2006 [55]. With PPC, fuel is injected during the compression stroke and partially mixed with air before combustion occurs. In diesel PPC, the compression ratio needs to be kept high and the maximum load will be limited by this. If the load range needs to be extended, the compression ratio should be reduced, or extremely high EGR should be introduced, to avoid a violent combustion process, which results in efficiency reduction. It requires more resistant fuel than diesel. Therefore, gasoline PPC is now being developed and investigated by KTH Royal Institute of Technology [55-56], Lund University [57] and University of Wisconsin- Madison [58].

In the KTH concept, the combustion is controlled to start after the end of injection, as they believe that if the combustion phasing (CA50) and ignition delay are matched, the emission will be the same regardless of the fuel volatility and composition differences, as it is the ignitibility property of gasoline that plays a substantial role rather than its volatility [59]. With a heavy duty diesel engine, they apply single injection at the condition of CR=14, 1200 rpm, 25% EGR and achieve 46% indicated efficiency at 14.86 bar IMEP with 1.21 g/KWh NOx emission. Furthermore, 23% pilot gasoline injection is applied under the same condition and the maximum load border is extended to 15.95 bar IMEP with similar efficiency (47%) but significantly reduced NOx (0.39 g/KWh) emissions [57-58].

However, the Lund concept indicates that the combustion starting during the fuel injection with appropriate λ and EGR can achieve better performance and emissions. That means it is better to burn the fuel while it is in mixing or partially mixing controlled mode [60]. In their research, an amazing 52-53% gross indicated efficiency at 5-26 bar IMEP is achieved with a Scania D13 engine and NOx emission is below 0.65 g/KWh, which is lower than Euro VI regulations in most of the load points.

Hanson, et al. [58] in University of Wisconsin investigated two load points of 11.5 bar IMEP and 6.5 bar IMEP in a HD CI engine with 91 PON (Pumping Octane Number = $\frac{RON + MON}{2}$) gasoline. They apply a split injection strategy in which one is an early pilot injection to get air fuel mixture partially premixed and the other one is near TDC to keep combustion phasing (CA50) at 373±1 °CA (13 °CA ATDC ±1). This combustion phasing is selected as the best operation character and of the highest engine output and most stable combustion in all his previous researches. The mixing extent of air/fuel mixture is higher than conventional diesel combustion and lower than HCCI combustion, which is believed

to achieve HCCI emission level and avoid the difficulty of HCCI combustion phasing control at the same time. External EGR is used to obtain longer ignition delay and it is up to 45% EGR, over which the unstable combustion happens due to the loss of combustion control. They also investigated the effects of dual injection timing and pilot/main fuel percentage splits. The results show 1st injection timing has no effect on HC and CO emissions and 2nd injection timing can successfully control CA50. However, HC and CO will significantly increase if combustion starts excessively late. Furthermore, when 1st injection fuel percentage increases, the mixture is more pre-mixed inside the cylinder, resulting in the reduction of NOx but an increase in HC emissions. Furthermore, as EGR increases, ignition delay becomes longer, allowing more time for air fuel mixing. The combustion becomes more pre-mixed with shorter combustion duration and a higher heat release rate. As a result, ISFC slightly decreases down to 173 g/KWh with maximum 45% EGR. Last but not least, the single injection strategy is also implemented and found to achieve similar emissions but better ISFC compared with split injection strategy. Although the quarter-load condition (6.5 bar IMEP) of this engine is operated successfully, the lower load combustion also needs to be investigated, which is not mentioned in their researches. The methods to extend the lower load border and maintain high efficiency and low emission are part of the research work in this thesis.

2.3.3 Dual Fuel CAI Combustion

Most previous CAI research has been strictly focused on single fuel - either high octane number (ON) fuel such as conventional gasoline or high cetane number (CN) fuel like conventional diesel. The advantages of high ON fuel (gasoline) for CAI combustion are its high volatility resulting in rapid fuel vaporization speed, and that the premixed or homogeneous fuel air mixture is easy to be obtained by Port Fuel Injection (PFI). But it lacks an auto-ignition quality, thus the low load operation is difficult to be controlled or even achieved. In contrast, high CN fuel (diesel) has a significant auto-ignition quality. However, it is difficult to get the fuel fully evaporated or partially premixed when the PPC strategy is applied. What's more, not only will the survived liquid fuel droplets burn as diffusion flames, resulting in high NOx and soot emissions [61], but the combustion phasing is difficult to control when engine load increases.

Bessionette et al. [62] suggested that the ideal fuel for CAI combustion is CN~27 at high load (up to 16 bar BMEP) and CN~45 at low load (down to 2 bar BMEP). Therefore, dual fuel CAI combustion is introduced and developed in recent research works.

Dual fuel CAI, also known as dual fuel PCCI (Premixed Charge Compression Ignition) or fuel RCCI (Reactivity Controlled Compression Ignition), applies in-cylinder fuel blending with PFI or early GDI of high ON fuel (such as gasoline) and utilizing various direct injection strategies of high CN fuel (such as diesel) to control combustion phasing in whole CAI operation regime, which could achieve high engine efficiencies and low emissions at the same time.

University of Wisconsin-Madison performed comprehensive research on the gasoline-diesel dual fuel CAI combustion in a heavy duty engine.

In the research work by Kokjohn, et al. [63], simulations and experiments were implemented at 6 bar IMEP and 11 bar IMEP. Single diesel pilot injection is firstly applied with EGR sweeping. The effect of fuel reactivity indicates that at 6 bar IMEP, minimum ISFC is achieved at PRF (Primary Reference Fuel which equals to the gasoline percentage of combined fuel) 62- 70 with CA50 at 4-6 °CA ATDC (364-366 °CA). At 11 bar IMEP, the best ISFC is achieved at PRF 60-90, depending on EGR with CA50 at 6 °CA ATDC (366 °CA). It is concluded that PRF is the key issue to control the combustion phasing and the level of fuel stratification, which is defined by the start of the diesel injection, controls the rate of heat release as load increases. In this paper, a split injection strategy is also performed with SOI1 (start of injection) near 60 °CA BTDC (300 °CA) with 60% of diesel, and SOI2 near 33 °CA BTDC (327 °CA). Under both 6 bar and 11bar IMEP load conditions, the stage heat release process is observed due to the stratified combustion behaviour of fuel reactions. The heat release process starts with low temperature reaction of diesel, followed by a high temperature heat release, and then the gasoline starts to be ignited due to the thermal ignition of diesel. Two peak hot flames are detected at 11 bar IMEP in this combustion process because of high temperature oxidation of CO formed by diesel and oxidation of CO formed by gasoline respectively.

Presented by Hanson, et al. [64], the effects of operation characters such as the first and second SOI timing and amount, and dual fuel component concentration, are investigated at a medium engine load of 9 bar net IMEP, as shown in Table 2.2. It is concluded that most

dual fuel CAI operations have NOx and soot levels well below the US EPA 2010 heavy duty limits and, at the same time, have around 50% thermal efficiency and acceptable pressure rise rates.

Table 2.2 The Effects of Operation Characters of Duel Fuel CAI from [64]

	Change	CA50	PPRR	ISFC	NOx	CO	uHC
SOI 1 timing	Advanced	Delay	↓	↔	↓	↑	↔ A
SOI 2 timing	Advanced	Same	↓ B	↔ C	↓	↔	↔
SOI 1 % D	Increase	Delay	↓	↓	↓ E	↔	↔
Gasoline %	Increase	Delay	↓	↓ F	↓	↑ G	↑ G

↓: Decrease ↑: Increase ↔: No obvious change

A: As SOI1 is advanced, the amount of spray liner impingement does not increase. HC is from the piston liner crevice region

B: More homogeneous mixture, longer ignition delay.

C: Because CA50 is the same.

D: Two-stage high temperature heat release is detected for the 39% case.

E: Because the mixture is less stratified reducing the reaction extent.

F: Because CA50 is delayed due to less direct injection diesel and lower rates of heat transfer and reduced soot radiation.

G: Because the oxidation rate of emission is reduced due to cooler in-cylinder temperature.

The dual fuel CAI (RCCI) combustion is compared with conventional diesel combustion in a single cylinder heavy-duty diesel engine by Kokjohn, et al. [65]. It is stated that compared with diesel combustion without EGR, RCCI combustion achieves 3 orders reduction of NOx emissions, reducing 6 times the soot emissions and achieving 18% gross indicated efficiency improvement. Comparing RCCI with diesel combustion with high EGR, 2 orders of the NOx emission reduction and 10 times of soot reduction are achieved with 13% gross indicated efficiency increase. The increase of efficiency of RCCI combustion is because of low temperature combustion due to a lean mixture, where the heat transfer loss is 42% less than its diesel mode. It can be concluded that there are two factors to explain the thermal efficiency improvement of RCCI combustion over diesel combustion. One is that the temperature of the piston bowl in diesel mode is too high, but RCCI could avoid this high temperature region. The other is the short combustion duration of RCCI combustion which could improve control ability over the start and end of

combustion, resulting in minimum compression work and maximum expansion work. In summary, taking out the heat transfer, the RCCI combustion process is able to transfer 10% more energy to useful work compared to conventional diesel under similar operation conditions.

Besides University of Wisconsin-Madison, Yeom et al. [66] researched on a HCCI gasoline engine with the combination of variable valve timing (VVT) technology to utilize internal EGR and a direct injection DME strategy in order to extend higher load boundary and control combustion phasing. It looks similar to the work performed in this thesis. However, there are several differences between this research and Yeom's. Firstly, Yeom only uses internal EGR to control the combustion phasing and does not value the EGR rate and the effect of EGR rate on performance and emissions which in this thesis' research, internal EGR rate is measured and the effect of EGR is deeply investigated. The combustion phasing is mainly controlled by DME injection timing in this research. Secondly, in Yeom's research, the engine load is adjusted by the injection of dual fuel quantity whilst in this thesis' research engine load is mainly adjusted by the internal EGR amount. Thirdly, Yeom aims to extend the high load border of the HCCI regime, but in this thesis' research, the author is mostly interested in the low load CAI operation and extends both low and high load boundary by applying various DME injection strategies.

2.3.4 EGR in CAI Researches

In order to achieve CAI combustion, the engine requires a high intake charge temperature and appropriate charge dilution so that the homogeneous or partially premixed mixture can reach the auto ignition conditions. High in-cylinder temperature can initiate and maintain the chemical reactions, inducing auto-ignition, and adequate charge dilution limits the peak heat release rate, both of which can be implemented by introducing exhaust gas recirculation (EGR).

Zhao [67] performed a comprehensive research on the effects of EGR on CAI combustion and presents five kinds of effects, which are: charge heating effect, dilution effect, heat capacity effect, chemical effect and stratification effects. Each of the effects is isolated and studied over its effect on auto ignition (AI) timing, combustion duration, heat release rate (HRR) and NOx emissions. It is concluded that the charge heating effect of hot burned gas is in charge of AI timing, which increases HRR and shortens combustion duration. The

dilution effect has no effect on AI timing, but it extends combustion duration and reduces HRR only when large EGR is introduced. Heat capacity effects on AI timing becomes the main factor on AI timing if more than 40% EGR is present and it extends the combustion duration as well as dilution effects. The chemical effect does not affect the AI timing and HRR, but shortens the combustion duration when large amounts of burned gas are present.

Based on Zhao's theory, the external EGR could mainly provide dilution effect rather than heating effect on CAI combustion, because of the low temperature burned gas recirculation due to heat transfer loss outside the cylinder. Inagaki et al. [68] discussed the possibility to induce external EGR to control the combustion phasing and conclude that the engine maximum power output will be limited, and the delay of external EGR delivery timing to the cylinder would cause unstable transient operation. On contrast, internal EGR could make the most use of both heating effect and dilution effect to initiate CAI. In other words, internal EGR can provide a large amount of hot residual gas into the cylinder, where 'large' and 'hot' are considered as two key factors when EGR is used to initiate CAI combustion [51]. Internal EGR can be realised as either the residual gas trapping by the negative valve overlap (NVO) method or the residual gas re-breathing by the positive valve overlap (PVO) method. With NVO, the burned gas from a previous cycle is trapped inside the cylinder by both the early closure of exhaust valves and late opening of intake valves. Li et al. [69] stated that the NVO is an effective and feasible way to achieve CAI combustion, but it could limit the CAI upper limit due to the restriction of gas exchange. With PVO, the exhaust valve is closed later than normal and intake valve is opened earlier than normal. Thus, the burned gas is re-breathed back into the cylinder during the overlap. Yang [70] has successfully overcome the gas exchange limit associated with NVO and achieved CAI combustion with PVO together with variable compression ratio and intake charge heating. PVO strategy is used in this research.

2.3.5 CAI Operation Range

It is always a big challenge of CAI research to extend the operating load range while maintaining most of the CAI combustion benefits.

Oakley et al. [52] presented an attainable CAI region with three main boundaries showed by Figure 2.8:

1. Knocking limit at high load, where the peak pressure rise rate is so large that knocking combustion and unacceptable noise take place, inducing in-cylinder pressure oscillation and potential engine damage.
2. Partial burn limit at low load, where combustion temperature is too low to complete the combustion.
3. Misfire limit at high EGR rates, where CO_2 and H_2O concentrations in the intake charge are so high that the mixture fails to be auto ignited.

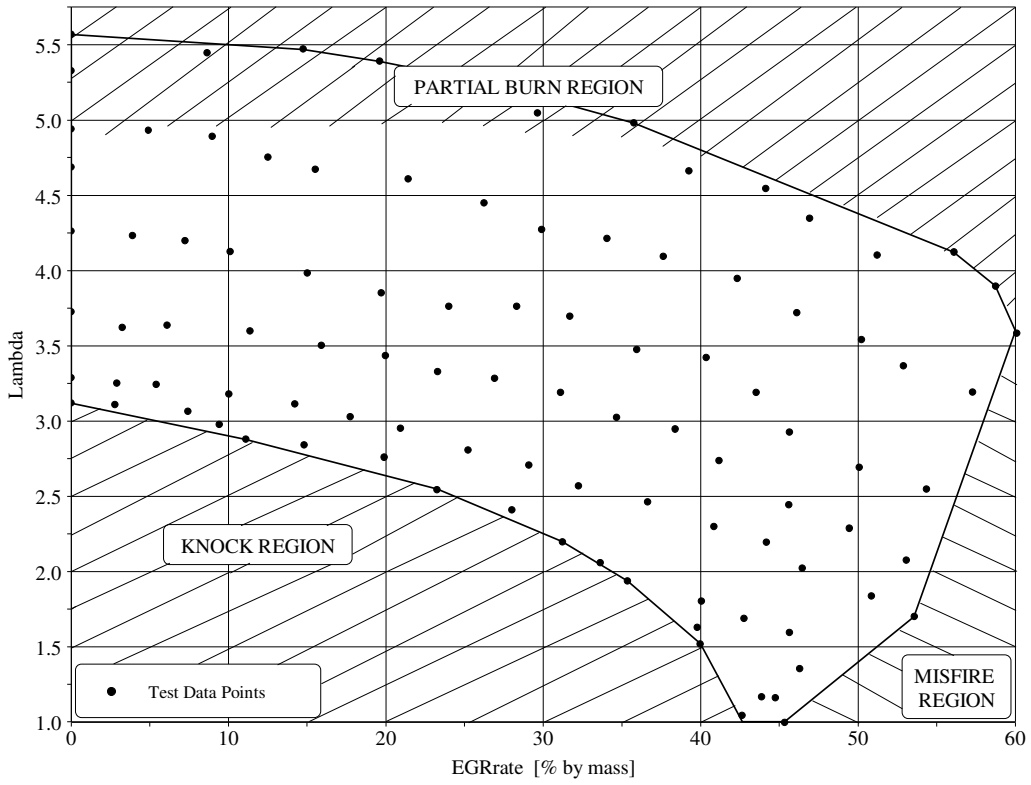

Figure 2.8 CAI Operation Regions for Standard Gasoline [52]

Li et al. [69] stated that the CAI operating range was achieved at engine speed 1000 rpm to 3500 rpm and load range from 0.5 bar to 4 bar BMEP in a gasoline engine with NVO, and indicate two main limits of the CAI region. One is the gas exchange limit at high engine load due to lower valve lift and shorter valve duration. The other is misfire limit at low engine load caused by the lower exhaust gas temperature which is not able to initiate CAI combustion. They also announce that it is more difficult to extend the lower limit and suggest finding some other ways to raise in-cylinder temperature. Achieving low load CAI combustion is one of the proposed works by this thesis' research.

2.3.6 Flame Propagation and Auto-Ignition Hybrid Combustion Process

There is another combustion process between pure SI and CAI combustion, named SI-CAI hybrid combustion. The applications of SI-CAI hybrid combustion mostly refer to spark assisted CAI research, which utilizes a spark to flexibly control the ignition timing and take benefit of conventional SI combustion in high load operation.

Since other ignition sources other than spark are introduced, the term 'flame propagation and auto-ignition hybrid combustion' describes this combustion process more extensively than SI-CAI hybrid combustion. Nevertheless, the principles are the same. The first part of this hybrid combustion is similar to the SI combustion process. The ignition source ignites the nearby combustible mixture (e.g. spark) or is compressed ignited (e.g. diesel, DME) and generates a flame front. The flame propagates from the ignition core to other parts of the cylinder and initiates auto-ignition for the rest of the unburned charge mixture.

It is said that the hybrid combustion can take place either at the low load boundary [71] or at the high load boundary of CAI operating range [72-73]. At the low load boundary, the in-cylinder temperature is too low to initiate auto ignition, resulting in a miss fire cycle. The propagating flame from the ignition source will promote fuel and air mixture into auto-ignition. At the high load boundary, rapid heat release happens because of early combustion. In order to avoid the combustion noise or even damage to the engine associated with the rapid heat release rate, external cooled EGR is introduced to delay auto ignition. In this case, spark ignition can be used to partially control the start of combustion.

2.4 Di-methyl Ether (DME) and DME Engine Applications

DME (Di-methyl Ether) is considered as an alternative fuel for transport, power production and household use. DME can be manufactured from various abundant hydrocarbons, such as natural gas, bio-mass and coal. Due to its low boiling point and vapour pressure, DME is easily vaporized and its combustion is smokeless as the result of no C-C combustions and no sulphur. It is said that DME is a superior fuel in ignition characteristics because of its high cetane number (>55) and the ignition delay is much shorter than the other gaseous fuels. What's more, because of its high combustion velocity and low ignition temperature, DME also has superior combustion characteristics.

The key properties of DME and diesel fuel are shown in Table 2.3 [74]. The attractive characteristics of DME used as CAI ignition promoter in this study are summarised as follows:

1 There are no C-C bonds but only C-O and C-H bonds in DME molecule with large fraction of Oxygen atom, which leads to few unburned hydrocarbon and PM emissions.

2 The cetane number of DME is higher than diesel and the auto-ignition temperature is lower than diesel. As a result, DME is of better auto-ignition quality and the ignition delay will be shorter than diesel.

3 The enthalpy of vapourization of DME is 467 kJ/kg, which is 1.56 time of that of diesel (300 kJ/kg). The high heat of vaporization will significantly reduce the peak in-cylinder temperature resulting in low NOx emissions.

4 The low boiling point of DME (248.1K) ensures that the DME will vaporise immediately after being injected into the cylinder.

Therefore, DME is sufficient to satisfy the requirement of the 'high cetane number fuel' in this dual fuel CAI combustion concept.

Table 2.3 Properties of DME and Diesel Fuel [74]

Property (unit/condition)	Unit	DME	Diesel Fuel
Chemical structure		CH_3-O-CH_3	C_xH_y
Molar mass	g/mol	46	170
Carbon content	mass%	52.2	86
Hydrogen content	mass%	1313	14
Oxygen content	mass%	34.834.8	0
Carbon-to-hydrogen ratio (H/C)		0.3377	0.516
Critical temperature	K	400	708
Critical pressure	MPa	5.37	3.00
Critical density	kg/m^3	259	-
Liquid density	kg/m^3	667	831
Relative gas density (air = 1)		1.59	-
Cetane number		>55	40-50
Auto-ignition temperature	K	508	523
Stoichiometric air/fuel mass ratio		9.0	14.6
Boiling point at 1 atm	K	248.1	450-643
Enthalpy of vapourization	kJ/kg	467.13	300
Lower heating value	MJ/kg	27.6	42.5
Gaseous specific heat capacity	kJ/kg K	2.99	1.7
Ignition limits	vol% in air	3.4/18.6	0.6/6.5
Modulus of elasticity	N/m^2	6.37E+08	14.86E+08
Kinematic viscosity of liquid	cSt	<0.1	3
Surface tension (at 298 K)	N/m	0.012	0.027
Vapour pressure (at 298 K)	kPa	530	<<10

Several automotive industries and research labs are developing engines and technologies to demonstrate the feasibility of DME as a fuel, most of them utilized DME as an alternative fuel in diesel engines. AVL, for example, has demonstrated the use of DME on a diesel truck or bus. They concluded that the DME engine could achieve ULEV without EGR and after-treatment process. And Elana M. Chapman et al. [75] have successfully converted a campus shuttle bus to operate on DME. They blended DME with diesel fuel to avoid bad

lubricity of DME. In their conclusions, they stated that significant reductions in particular emissions were observed when the bus was operated on a DME-Diesel blend. In 2005, the Volvo group announced its first truck equipped with a DME engine. According to their report, the emissions from the engine are lower than the future Euro V standards and the fuel consumption is almost similar to a diesel truck in energy equivalents [76]. In other research, Teng and McCandless discuss the compression ignition delay of DME and conclude that the ignition delay of DME is shorter than diesel because its higher vaporization and shorter heated time [77]. A research from Xi'an Jiaotong University investigated the effect of NOx emission and engine performance by EGR. They declare that the NOx is 40% lower when the EGR rates are 17%-22% and there is no evidence of thermal efficiency decrease for the engine [78].

Chapter 3

Experimental Test Facility

Chapter 3 Experimental Test Facility

3.1 Introduction

In this chapter, the experimental test facilities and measurement systems will be presented as well as data analysis methodology. A Ricardo E6 engine has been adapted for the experimental work in this thesis, whose key features are variable compression ratio, variable cam timing to achieve positive valve overlap and port gasoline fuel injection. For the proposed research, a DME supply and direct injection system was designed, manufactured and assembled. In addition, the methods for determining air fuel ratio and internal exhaust gas recirculation (iEGR) rate are also discussed.

3.2 Experimental Set up and Control Facilities

3.2.1 Single Cylinder Engine

3.2.1.1 General Description

A Ricardo E6 engine (Figure 3.1) was adapted for the current research. It is a single-cylinder, two-poppet-valve and four-stroke type engine, which has a stroke of 111.1 mm and a bore of 76.2 mm with a capacity of 507 cc. The normal speed range is 1000-3000 rev/min. Its compression ratio can be continuously adjusted from 4.5:1 to 20:1.

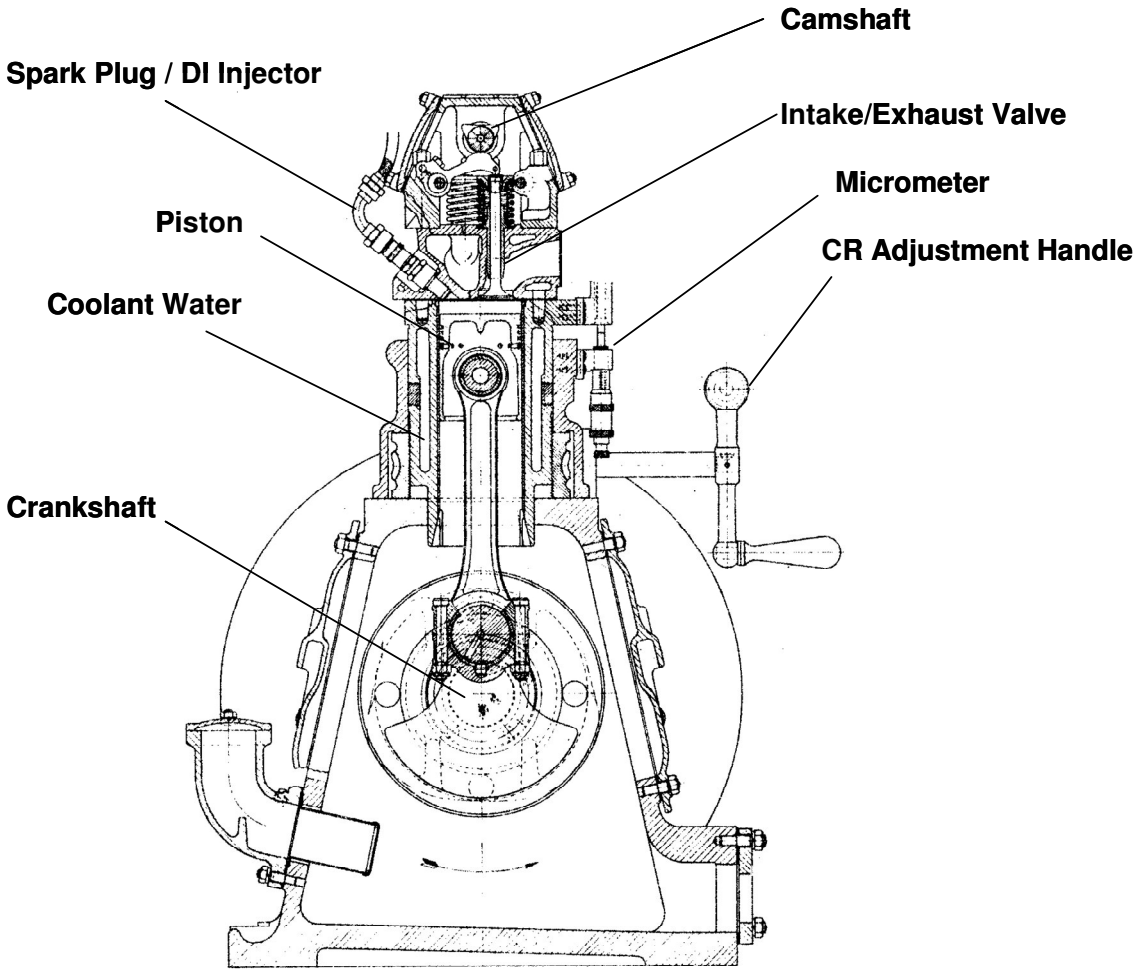

Figure 3.1 Ricardo E6 Single Cylinder Research Engine

The lubricating system is of the wet sump type. The oil pump is gear driven by the crankshaft and the oil is delivered directly to the crankshaft and camshaft so that the cam surface can be lubricated by means of radial feeds as well as big-end bearings. A relief valve is utilized to control the pressure. An electrical heater of 0.5 KW rating is immersed in the crankcase for the purpose of reducing the cold start period.

The coolant water is circulated around the engine by an electrical motor. The coolant temperature is controlled by a closed loop controlled heated coolant system in order to keep the temperature constant and independent of engine operating conditions (Figure 3.2). A thermocouple is employed and set up at the coolant exit from the engine, which gives the feedback temperature to a PID controller. The controller adjusts the flow rate of the mains water through a heat exchanger by an on-off valve. The heater is heating the coolant water continuously as the cooling ability of the heat exchanger is greater than that of the

heater. This method of controlling temperature with the heat exchanger is more effective than controlling engine temperature with the heater.

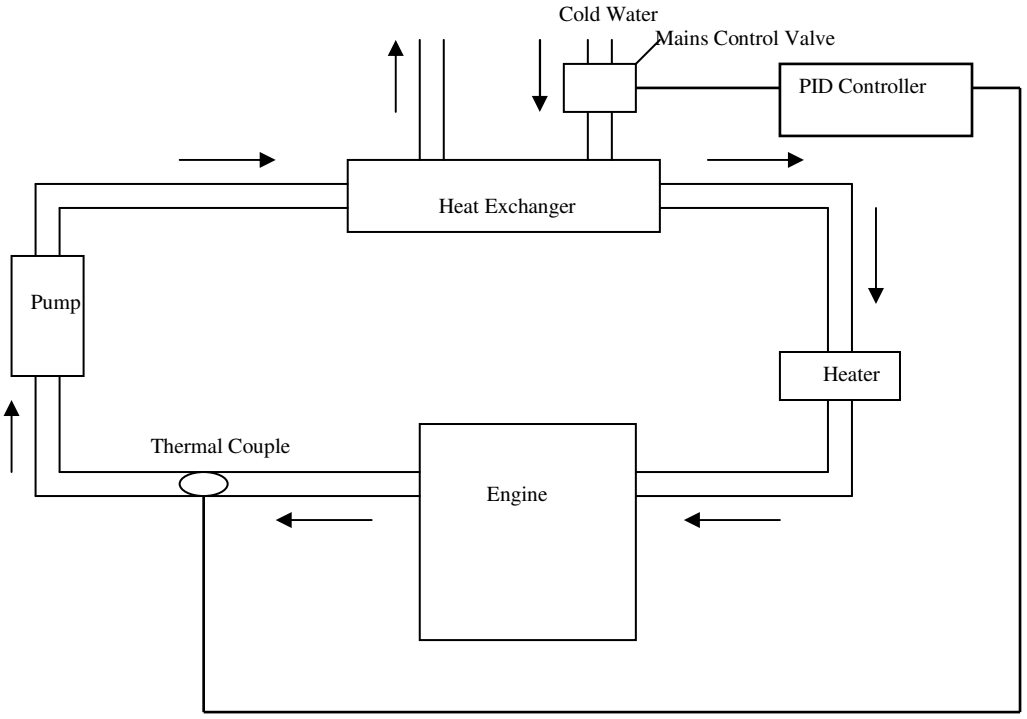

Figure 3.2 Coolant System

3.2.1.2 Intake and Exhaust Systems

Figure 3.3 shows the intake and exhaust systems used for these tests. The proposed work for this research is focused on advanced combustion operation. In addition, some conventional port fuel injection spark ignition (SI) tests have also been carried out to compare engine performance.

In the controlled autoignition (CAI) mode, the engine is operated at wide open throttle (WOT) all the time in order to minimize the intake pumping loss. In the SI mode, the throttle is used to control the engine load, which is calibrated so that it can be set anywhere manually between 0° closing and 60° fully opening corresponding to WOT with 0.5° accuracy. Both CAI and SI tests are carried out at naturally aspirated intake condition.

Several fittings have been applied to the exhaust pipe to allow exhaust gas analysis. These include the connection point with a Horiba MEXA-554JE emission analyser, Signal

3000HM HC analyser and 4000VM NOx analyser, a Bosch LSU lambda sensor, and a connection point with a Cambustion NDIR Fast CO_2 analyser. The exhaust then passes through a silencer and is exhausted to atmosphere.

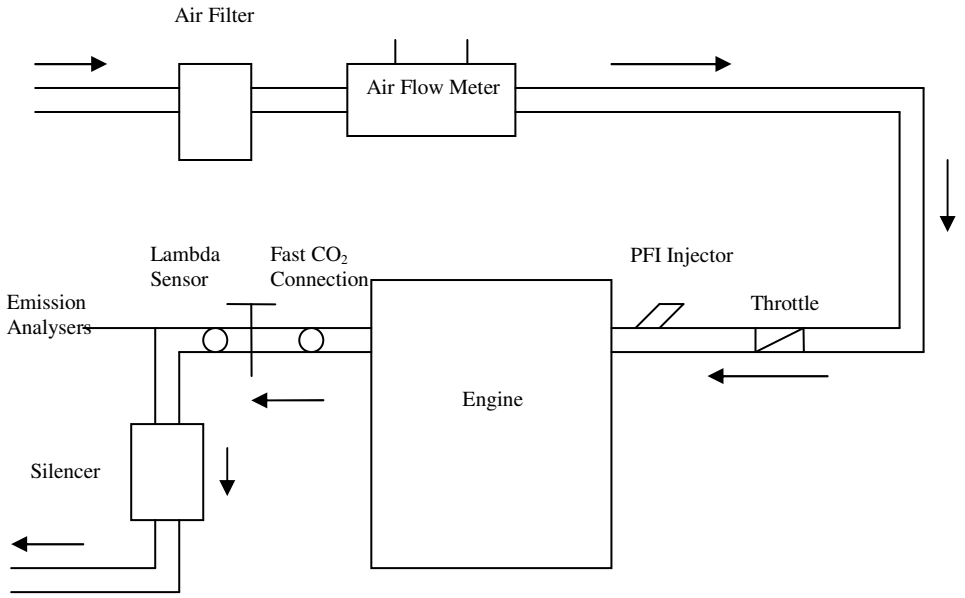

Figure 3.3 Schematic Diagram of Intake and Exhaust Systems

3.2.1.3 Variable Compression Ratio

The most attractive feature of this engine base is the variable compression ratio. It is ideal for exploring some unknown research fields with different fuel features and operation strategies. The compression ratio can be continuously adjusted from 4.5:1 to 20:1 by means of a worm gear. The distance between cylinder head and crankshaft can be changed manually with a handle either under inactive condition or during normal engine operation. A calibrated micrometer is set up at the side of the cylinder and a diagram as provided by the manufacturer indicates the relationship between the meter reading and the geometric compression ratio.

3.2.1.4 Variable Valve Timing Camshaft

A camshaft was designed and implemented by a previous researcher [70] so that the cam phasing can be changed manually. Appendix A shows the drawing of this modified camshaft. The valve lift is 8 mm and the intake valve duration and exhaust valve duration

are fixed at 224 °CA and 229 °CA respectively. The start of the valve opening duration is defined as the actual start of the movement of the intake valve measured by the dial test indicator. So does the end of valve duration. It should be noted that in this thesis the 0° crank angle refers to the gas exchange top dead centre (TDC). The whole engine cycle is divided to 720 degrees and thus the top dead centre of compression here is 360 °CA. The cam shaft is specially designed with two smooth-surface parts and two screw parts instead of the original ones. The intake and exhaust cams lobes are assembled on the smooth part of the shaft and two nuts are screwed tightly next to each cam lobe. Each of the lobes can be rotated freely and independently and fixed by the screw nuts. Therefore, in each valve, either opening timing or close timing can be fixed, and with fixed valve duration. By adjusting the exhaust valve close timing and intake valve open timing, variable positive valve overlap can be implemented to obtain different iEGR rate.

However, there could be interference between piston head and valves near TDC at higher compression ratios, which can cause serious damage to the valves and/or piston head. Therefore, there is a maximum compression ratio, below which it can tolerate the intake and exhaust timing being changed to any position without damage (See Figure 3.4). This maximum compression ratio is calculated as 14.9. If the compression ratio is greater than 14.9, the valve timing must be carefully selected to avoid the clash. This limited the degree of valve overlap at higher compression ratios.

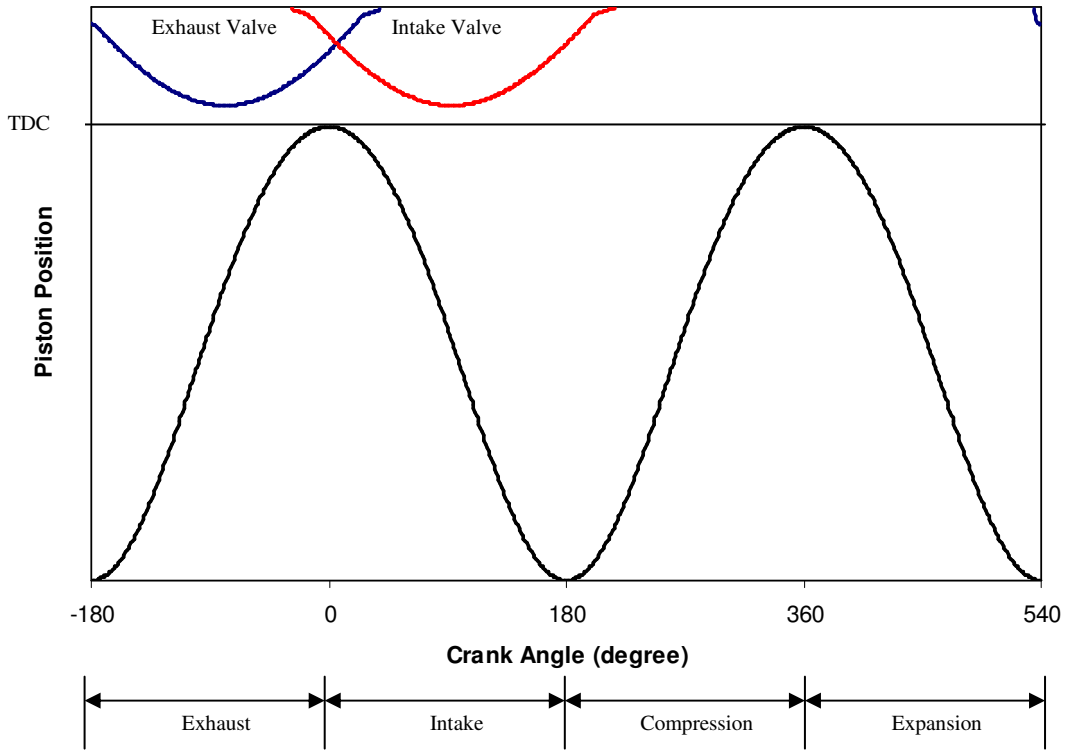

Figure 3.4 Intake and Exhaust Valves against Piston Position

In this study, as the maximum compression ratio is 14.5, the valve overlap of this research work is not affected by this limitation.

A dial test indicator is applied to measure the opening time of the intake valve and exhaust valve as shown in Figure 3.5. The indicator is set appropriately with its head contacting the end of valve stem. There are two ways to ensure the valve timing. One is to find the crank angle of both valve opening time and closing time. The other is to find out the crank angles of symmetric positions of the cam lobe which have the same indicator meter readings and then find out the crank angle of the middle line which is considered as the centre of valve opening time. Thus, after several repeated measurements, the valve timing can be determined with its known duration.

The aim of positive valve overlap is to achieve iEGR. Thus, the internal EGR rate is more important than the overlap duration value. The method of iEGR rate measurement will be presented in 3.3.3.

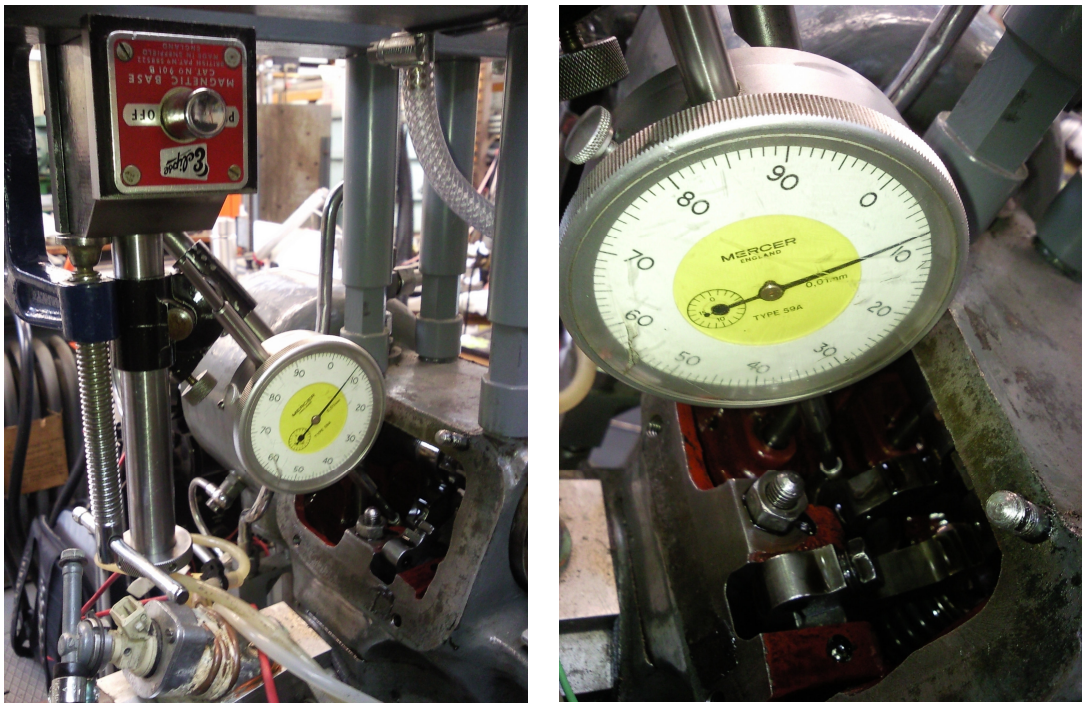

Figure 3.5 Measure Valve timing with Dial Test Indicator

3.2.1.5 Dynamometer

A Laurence Scott 'NS' type Swing field AC Dynamometer is connected to the engine flywheel. This is used for measuring the engine output, motoring the engine and keeping constant engine speed. The engine speed is controlled by an oil-cooled regulator with a hand wheel. Although there is a revolution meter indicating the speed from the dynamometer, the accurate speed reading comes from the clock output of a crankshaft encoder.

3.2.1.6 Gasoline Supply and Port Injection System

Figure 3.6 shows the gasoline fuel supply and port injection system. A single Bosch gasoline injector is installed in the intake port. The fuel tank can be either isolated from the main fuel line by closing the main valve and measuring the gasoline fuel consumption with a graduated scale or connected to the main fuel line by opening the valve for continuous operation. A pressure regulator together with a pressure damping chamber is used to maintain the fuel injection pressure constant at 2.5 bar gauge pressure. A steel fuel tank is joined to the gasoline supply system to improve the fuel cooling, which avoids the vapour gasoline existed in the fuel line.

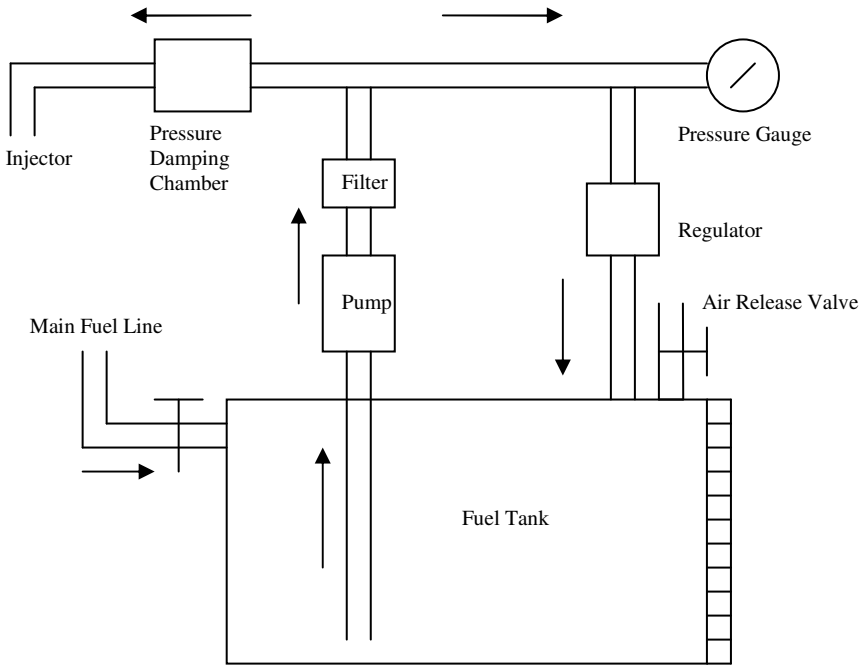

Figure 3.6 Gasoline Supply and Port Injection System

3.2.2 DME Supply and Direct Injection System

Due to its ease of vaporisation and flammable character, the DME injection system was carefully implemented. A two stage pressure raising strategy is applied to supply DME as shown in Figure 3.7.

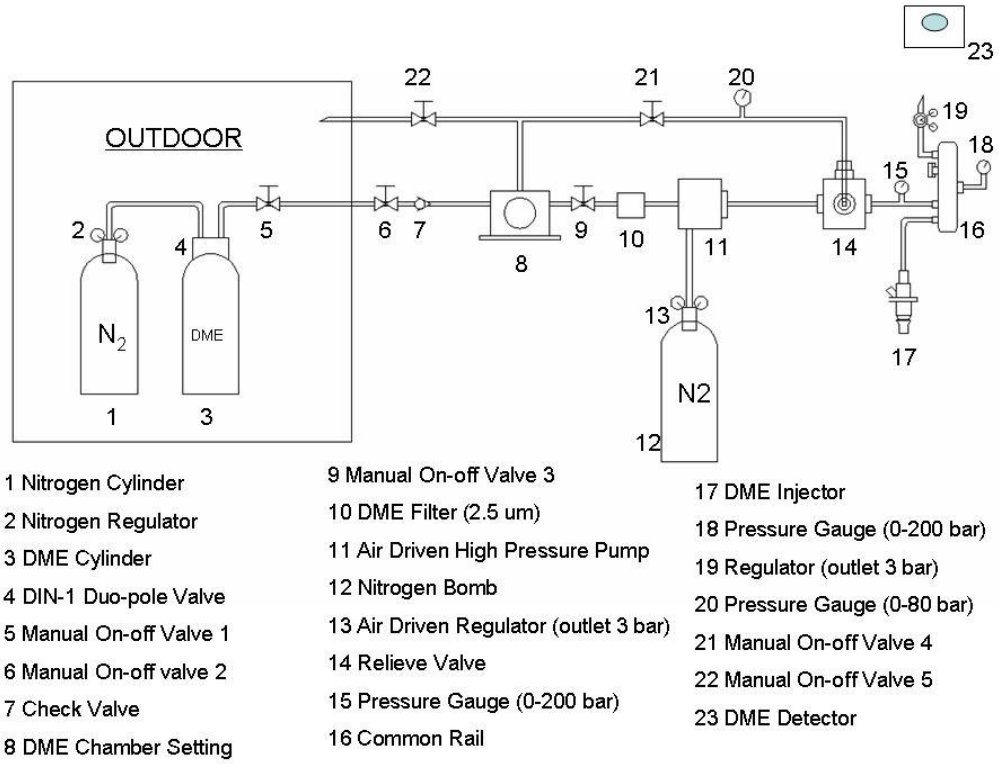

Figure 3.7 DME Supply and Injection System

The DME is bottled as 5kg with 200 psi (13.8 bar) pressure. A DIN dual port full length dip valve is fitted on the top. The valve has one inlet for connecting nitrogen gas and pressurizing the DME and the other outlet is for outputting liquid fuel. The DME bottle is located outdoor for safety concern and 15 bar nitrogen gas is connected to the inlet valve of DME cylinder, which pressurizes DME to 15 bar, keeping it liquid in the entire supply pipe. A check valve is applied to prevent backflow of DME. Then the low pressure DME goes through a setting chamber. The view window of the chamber is for watching whether the DME is liquid all the time. What's more, although 15 bar pressure can keep DME liquid all the time, there might be some tiny gas bubbles in the supply pipe. The chamber can also keep the gas bubbles on the top so that all DME supplied to the filter will be liquid. The chamber window is graduated in order to roughly measure and calibrate DME

flow rate after closing the main front on-off valve. Following the filter, a Haskel air driven liquid pump is used to raise low pressure DME to high pressure. The pump is driven by nitrogen gas in order to avoid accidental ignition by an electrical pump. The outlet pressure of DME depends on the nitrogen gas pressure. The outlet pressure can be raised up to 150 bar. A diesel common rail injection system has been used for DME direct injection as it can keep the injection pressure constant and offer high pressure injections. The high injection pressure can be determined either by air pump driven pressure or by a direct-acting relief valve. Together with the common rail, the DME injection pressure can be accurately adjusted and kept constant. Two pressure gauges are employed on the common rail and setting chamber respectively to watch the injection pressure.

There are two holes in the cylinder head. One is occupied by a Kistler 7061B piezoelectric pressure transducer for measuring in-cylinder pressure. The other one can be used for a spark plug or a DME direct injector. A Bosch 036 gasoline direct injection injector is mounted here to inject DME into the cylinder directly. As the hole is originally designed for spark plug, an injector sleeve adapter has been designed and manufactured with the same thread as the spark plug and same length of the head so that the compression ratio is not affected (Figure 3.8). The injector should be well sealed on the adapter avoiding any leakage because its head is placed inside the cylinder and the in-cylinder pressure is high when combustion occurs.

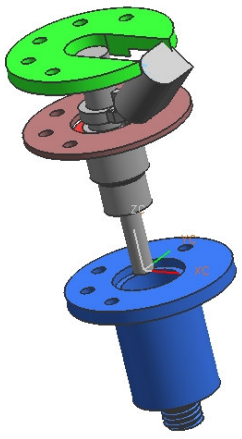

Figure 3.8 DME Direct Injector and Injector Sleeve

3.2.3 Engine Control and Operation System

3.2.3.1 Crankshaft Encoder and Camshaft Encoder

A crankshaft encoder is fitted to the end of the crankshaft and used to send reference signals to the port fuel injector control box, spark control box and DAQ system. An optical sensor of this encoder sends two signals to each of these control or measurement systems. One is considered as a reference signal, which is sent once per crankshaft revolution. The other is clock signal and is sent 360 times per crankshaft revolution. Each of the control boxes detects the reference signal and then relates to any specific crank angle with clock signal. The control accuracy is 1 °CA.

The camshaft encoder is fitted to the camshaft and it sends signals to two separate DME direct injection control boxes. It operates on the same principle as a crankshaft encoder. The camshaft encoder selected generates 720 clocks per camshaft revolution because within one engine working cycle, the camshaft rotates one revolution. Therefore, the control accuracy is also 1 °CA.

3.2.3.2 Spark Timing Control

As a baseline, conventional SI combustion process has been tested as well. The spark is controlled by a modified 'Dial-a-Time' control unit which is originally made by Lucas Engineering Ltd.. The trigger signal and clock signal are from the crankshaft encoder and the spark timing can be adjusted from 79 °CA BTDC to 45 °CA ATDC to within 0.5 °CA.

3.2.3.3 Gasoline Port Injection Control

The gasoline injector is controlled by a control box whose trigger signal comes from the crankshaft encoder. In the beginning of the tests, as the crankshaft encoder generated one signal every revolution, the injector injects twice during one working cycle (two revolutions). The injection timing was set at 45 °CA ATDC. The results of these tests showed an average higher cycle by cycle variation happening among all the test points. It may be because as soon as intake valve opened, the fuel injected during the intake stroke was sucked into the cylinder together with the injected fuel from the last revolution and the fuel was not well vaporized and was affected by residual gas. In order to avoid this

problem, a half-moon plate was applied on the camshaft in order to generate a blocked signal, which can block one of the two trigger signals. Thus, the injection happens once per engine working cycle as in the production engines and the fuel flow rate is adjusted by changing injection duration. The port injection timing is still kept at 45 °CA ATDC of compression so that the fuel evaporation could take place before the induction process. With this single port injection modification, the cycle by cycle variation is significantly reduced.

The port injector is calibrated to get accurate flow rate by two methods. One is to let the injector inject gasoline into a graduated flask and measure the fuel quantity with fixed injection times (1000 times for example) under a specific injection pulse width. The other is to run the engine under normal SI operation and calculate the fuel consumption by air fuel ratio reading from emission analyser (or lambda sensor) and intake air quantity from air flow manometer. After the calibration, a diagram is drawn with input pulse width versus air flow rate. Therefore, the gasoline flow rate can be determined by the pulse width of input signal for all test work.

3.2.3.4 DME Direct Injection Timing and Amount Control

The proposed work includes DME split injection, early single injection and late single injection strategies. Thus, it requires two separate and independent control systems for each of the split injections. Each of the controllers can adjust injection timing and duration over a wide range.

The trigger signals come from the camshaft encoder. Each of the controllers can generate a TTL signal starting at any point of the whole engine working cycle, and the injection start timing can reach 1 °CA accuracy.

The pulse width can be varied from 0.6 ms to 3.6 ms which is beyond the injector minimum start-up pulse width limit and over maximum DME quantity requirement. The injection timing can be set to any crank angle of the entire engine cycle though the injection timing is always set during the compression stroke. These two TTL signals are inserted to an ‘AND gate’ with two on-off switches respectively. When both of the switches are turned on, split injection can be achieved. If only one switch is turned on, single injection can be achieved. The combined or single TTL signal then enters a Gasoline

Direct Injector (GDI) control driver which is specifically designed by Tianjin University. This unit needs a 12 volt external DC power supply. After the TTL signal is triggered, a solenoid current is generated to drive the GDI injector (See Appendix B).

In Figure 3.9, a general DME injector calibration method is shown to estimate DME flow rate against injection pulse width. A rubber balloon is located inside a sealed container which is filled with water. A tube is inserted to the bottom of the container and the other end is connected to a measuring cup. The balloon is connected to a 3 way 'T' shape tube and the other two connections are linked to DME injector and a U-tube manometer respectively. A manual ball valve is applied in the middle of U-tube connection. When the unit is being calibrated, the valve before the U-tube is closed. The injection duration is set and DME starts to be injected into the balloon. As the balloon expands, water goes into the graduated measuring cup. After it is stable, the volume of water is recorded. Then the valve is turned on and the pressure in the balloon is recorded. Finally, all DME is released and the next test starts. A thermocouple is inserted into the balloon to measure the temperature of injected DME. The injected mass of DME can be calculated either by DME density at a specific temperature or by the ideal gas law, PV=nRT where the DME pressure P, injection volume V and injection temperature T are all known, and R is constant.

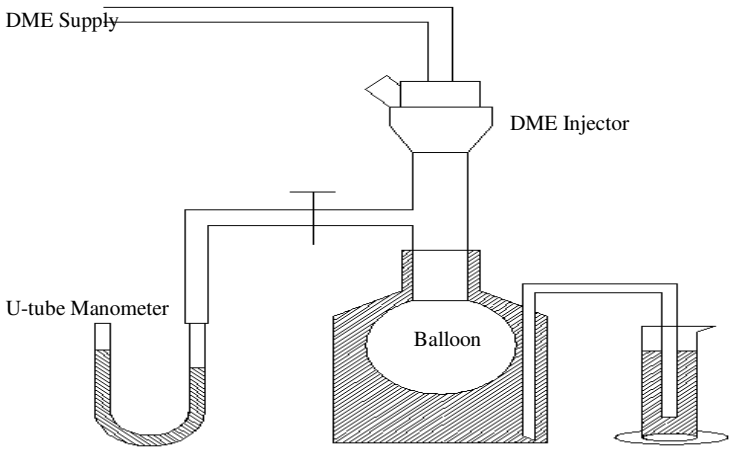

Figure 3.9 Estimate DME Flow Rate with Various Injection Pulse Width

However, DME injection amount can be affected by injection pressure, TTL pulse width and in-cylinder back pressure when injection happens. Although the injection pressure can be easily kept constant and the TTL pulse width can also be fixed, the in-cylinder pressure during DME injection will be variable due to the change of injection timing. Thus, the

DME injector calibrations are precisely applied in the injection timing of 290 °CA, 320 °CA, 330 °CA, 340 °CA and 350 °CA whose in-cylinder back pressures are around 3 bar, 7 bar, 10 bar, 15 bar and 21 bar respectively. These calibrations are achieved by running the engine with pure DME injections and calculating the DME flow rate with air fuel ratio and intake air flow rate.

In this study, DME injection pressure is set to 40 bar because a very small quantity of DME is needed as the ignition promoter. The above calibrations are only applied when DME has to be isolated and calculated independently, for example, the researches on effects of DME concentration of total fuel and the efficiency calculations. It should be clarified that the DME injection quantity is only estimated using the method described above for all test work. This research work is mostly focussed on the effects of total air fuel ratio (λ overall) rather than the effects of DME quantity or DME concentration of total injected fuel. The DME injection calibration graph is not of sufficient accuracy to be used to determine air fuel ratio. The method to determine total air fuel ratio (λ overall) is presented in Section 3.4 and the effects of DME quantity is described in the next chapter.

3.3 Experimental Measurement Systems

3.3.1 In-cylinder Pressure Measurement and Data Acquisition System

The work output of an internal combustion engine comes from the chemical reaction of the fuel converting to mechanical work by high pressure burning and burned gas forcing the movement of the piston. Therefore, the in-cylinder pressure can directly indicate the performance of the engine. The in-cylinder measurement can be used for heat release analysis which gives information such as ignition and instantaneous burning rate, engine load, cycle by cycle variation and so on.

The real-time in-cylinder pressure measurement system is used in all experiment works. It provides information of the engine in real-time to identify the normal SI/CAI combustion and abnormal misfire or knocking combustion. What's more, together with exhaust analysers, this information can also be considered as a feedback to engine controlling parameters. The appropriate control parameters are adjusted and developed due to this 'feedback' information.

A Kistler 7061B piezoelectric pressure transducer is mounted in the cylinder head. The transducer is water-cooled in order to maximize the sensitivity and minimize the temperature effect (also known as thermal shock). The charge output from the pressure transducer is amplified by a Kistler type 5001 charge amplifier. The capable range of this transducer is 0-100 bar gauge pressure. A dead weight testing device is used for calibration. The charge amplifier output is adjusted as 10 bar/V with known pressure applied on the transducer. The voltage of the output signal is analogue and is converted to a digital one via an analog-to-digital (A/D) converter, which is built into a National Instruments^{TM} computer-based Data Acquisition System (DAQ).

A National Instruments^{TM} type PCIMIO16-1 DAQ card is used to receive the voltage signal from the pressure transducer system as well as clock signal and trigger signal from the crankshaft encoder. The software is programmed via NI Labview^{TM} for real-time data analysis which displays on the monitor and records in-cylinder pressure data corresponding to crank angle. The real-time program window displays the heat release, IMEP and COVimep, and knocking combustion etc.. The fundamentals of these analytical procedure and calculations are presented in 3.5.

3.3.2 Exhaust Emission Measurements

3.3.2.1 CO, CO_2 and O_2 Measurements

A Horiba MEXA-554JE automotive emission gas analyser is used to measure CO, CO_2 and O_2 with the measuring range of 0-10%, 0-20% and 0-25% respectively. The exhaust gas is taken from the middle of the exhaust pipe, delivered by coiled copper tube and connected to the analyser via a short silicon rubber line. The copper tube ensures the exhaust gas sample to be cooled, and a water trap, a combined condensate and particulate removal filter are passed through before the exhaust gas extracted by an integral vacuum pump. The cold dry gas enters the analyser and is split to an infrared absorption cell and a galvanic cell for analysis.

The combined non-dispersive infrared (NDIR) technology is applied to measure CO and CO_2 in this analyser. The key components are an infrared light source, a sample chamber, a wavelength filter and an infrared detector. Dried exhaust gas is passed through the sample chamber. The chamber has two optical accesses at both ends. A broad band infrared source, which can be absorbed by a wide range of molecules, passes through the chamber. An optical filter is applied in front of the sample chamber to eliminate all light except the wavelength that CO (4.6 μm) and CO_2 (4.2 μm) can absorb. A reference beam is passed through a non-absorbing gas (nitrogen) to provide a base line signal. The absorbed light is detected by a solid-state infrared detector. The quantity of absorbed infrared radiation is proportional to the component concentration while the reference theoretically never changes. The NDIR detectors are regularly calibrated with known concentration calibration gas, such as 3.18% CO and 14.04% CO_2.

O_2 concentration is measured via a galvanic cell in this unit. The cell can be considered as a diffusion-limited metal/air battery with a gold plated anode and a silver plated cathode immersed in electrolyte. The oxygen in the exhaust sample diffuses through a PTFE membrane and reaches the anode. A current is generated when the circuit is completed, which is proportional to the oxygen concentration. It is calibrated with a known O_2 concentration zero grade air which is considered as 20.9%.

3.3.2.2 Unburned Hydrocarbon Measurements

A 'Signal 3000HM' total hydrocarbon analyser is applied to measure the exhaust hydrocarbon emissions. The analyser applies the well established principle of Flame Ionisation Detection (FID) technology to detect volatile organic compounds of the sampled emissions.

In the analyser, the hydrocarbons are burned and carbon atoms are ionised. An electric field is applied to the detector, and the formed electrons and positive ions generate electric current. The current is proportional to the number of carbon atoms contained in the sample, which can be accurately measured using an internal galvanometer. Hydrogen is used as the fuel because its burned flame is non-ionised, which ensures the accuracy of measurement. The detector responds to carbon ions and a mixture of hydrocarbon compounds is converted to an output proportional to the carbon count. The methane (CH_4) equivalent in part per million (ppm) is used as the simplest expression of quantity. For example, 100 ppm CH_4 and 100 ppm C_3H_8 mixture results in an output of 400 ppm CH_4.

The exhaust sample is drawn from the exhaust pipe with a heated sample line and then heated to 191°C in an oven before entering the analyser avoiding any condensation of hydrocarbon species. An internal dual headed pump provides sample flow and bypass air. A part of bypass air is passed through a catalytic purifier to provide zero grade air and FID combustion air. The unit requires two gas bottles for normal operation. One cylinder containing 40% hydrogen and 60% helium mixture is connected to the fuel inlet. The other cylinder is a 500 ppm propane mixture with nitrogen balance. Together with an internal loop of zero grade air, calibration of the analyser can be performed and adjusted to the correct range.

The FID detector can only be used to measure total unburned hydrocarbon in engine emissions. It has the limitation of determining the individual hydrocarbon species concentrations due to the unknown hydrogen/carbon ratio of the sample. More intelligent techniques such as Gas Chromatography (GC) combined with Mass Spectrometry (MS) can be used to identify the volume concentration of specific hydrocarbon species in the emissions measurement.

3.3.2.3 NO_x Measurement

As mentioned in the last chapter, Nitric oxide (NO) and nitrogen dioxide (NO_2) are usually grouped together as NO_x emissions in engine research. A 'Signal 4000VM' NO_x analyser is employed to quantify the oxides of nitrogen in the exhaust gas using the Chemiluminescent method. The system contains a heated sample lines which is directly connected to the rear panel sample inlet connections, the remote vacuum and bypass pumps which provide instant sample flow at correct temperature and the main analyser unit. The principle of this chemiluminescent analyser is to quantify the NO_x concentration by detecting the emission of light from excited nitrogen dioxide (NO_2).

The exhausted oxides of nitrogen are composed of nitric oxide (NO) and nitrogen dioxide (NO_2). Firstly, all NO_2 in the sample is converted to NO by passing it through a catalyst. Some ozone is generated by an electric discharge with oxygen, which is drawn from the 'Zero Grade Air' gas bottle. The chemiluminescent gas phase reaction between Ozone and Nitric oxide to give Nitrogen dioxide and Oxygen. Around 10% of the produced Nitrogen dioxide is in an excited state. The transition from this electronically active state to normal state, as the molecules lose energy, promotes light emission, varying in wavelength between 0.6 and 0.3 micrometers according to the user manual [79].The intensity of this emission is comparable to the mass flow rate of NO, which enters the reaction chamber. The emission is measured using a photomultiplier tube and associated electronics

$$NO + O_3 \dashrightarrow NO_2^* + O_2 \qquad \text{Equation 3.1}$$

$$NO_2^* \rightarrow NO_2 + \text{Light} \qquad \text{Equation 3.2}$$

Only a small percentage of excited NO_2 loses energy by emitting light while majority of energy is lost by collision with other molecules. The reaction chamber is operated at a low pressure in order to maximise the light output from the chemiluminescent reaction of NO_2 and minimise interference from other gases, such as carbon dioxide (CO_2) and water (H_2O) vapour. The low pressure can limit the significant deactivating effect of CO_2 and H_2O vapour on nitrogen dioxide and reduce the quenching effect to negligible levels. In addition, the photomultiplier detector is located in a special housing which is fitted with a thermo electric Peltier cooler in order to eliminate the effect of ambient temperature changes on the 4000VM.

3.3.2.4 Temperature Measurement

Several type K thermocouples are employed to measure appropriate temperatures. One is located in the exhaust port to measure exhaust gas temperature. Another one is located at the inlet of the oil cooler to detect oil temperature. The other two thermocouples are placed at the inlet and exit points of the engine block respectively to get coolant temperature readings. There is also a thermocouple applied to record intake air temperature although this is not used in this study.

All thermocouples are connected to a Pico TC-08 thermocouple Data Logger and its output connects to the USB port of a Windows based PC. The temperatures can be read simultaneously with PicoLog software and, in addition, the variation of each temperature can be traced and recorded.

3.3.3 Internal Exhaust Gas Recirculation (iEGR) Rate Measurement

Internal EGR is achieved by applying positive valve overlap (PVO) and increasing exhaust back pressure if the EGR rate achieved by PVO is not sufficient.

With PVO, as the exhaust valve closes late and intake valve opens early, there is a period of valve overlap when both intake and exhaust valves are open at the same time. At the end of the exhaust stroke, the burned gas is blown into the intake port by early opening of the intake valve. In the coming intake stroke, as both intake and exhaust valves are open, the burned gas in the exhaust port is re-breathed directly into the cylinder, while in the intake port the small amount of trapped gas mixed with fresh air is sucked into the cylinder. The quantity of residual gas mainly depends on the combustion from previous cycle and valve overlap durations.

The maximum overlap is chosen as 63 °CA degrees and provides around 12% residual gas at 1500 rpm engine speed and Wide Open Throttle (WOT).

However, as the trapped EGR is used as the principal means to control the engine load, the exhaust pressure is applied as a tool to provide extra residual gas in mid and low load operation if EGR rate is not sufficient. The exhaust pipe is throttled by a manual valve increasing the exhaust back pressure, which significantly increases the amount of trapped

residual gases. A pressure tank is connected to the exhaust pipe before the manual valve in order to damp out the instantaneous pressure wave. A pressure gauge is installed on the pressure tank to measure the exhaust back pressure.

There are three reasons to throttling the exhaust pipe rather than further extending the overlap. Firstly, because of the fixed duration of either intake valve or exhaust valve, further increase the PVO will increase the negative work. The valve timings at the maximum overlap are shown in Figure 3.10. The valve timing is EVO=187 °CA BTDC, EVC=30 °CA ATDC IVO=33 °CA BTDC and IVC=191 °CA ATDC. In order to increase the valve overlap, either the exhaust valve is closed later or intake valve is opened earlier, or both. However, with the fixed valve duration, if the EVC is retarded, the EVO will be also retarded. The exhaust valve could be opened after the Bottom Dead Centre (BDC). On the other hand, if IVO is advanced, the IVC could be implemented before BDC. Both of above conditions will significantly increase the negative work. Although throttling the exhaust pipe will also increase the negative work as well as retarding the EVO, the author prefers to keep the negative work by PVO method minimum. This is because in this way, nearly all the pumping work comes from the exhaust throttling and it is easy to control and compare with other residual-gas-trapping methods. What's more, the engine test points by PVO methods only will implement its best performance in term of 'NET' value, such as net IMEP and net indicated efficiency. Secondly, adjusting the exhaust pressure enables the EGR rate to change continuously during engine combustion. Due to the limitation of the facility, the valve timing can not be changed during combustion. The EGR rate is mainly affected by engine speed, inlet pressure, valve overlap and exhaust pressure [80]. In this case, the engine speed is fixed and intake throttle is fully opened. Thus, without throttling the exhaust pressure, the EGR rate can be considered as determined by valve timing. Each valve overlap needs to be adjusted manually after stopping the engine. However, the exhaust pressure can be used as a tool to control the internal EGR rate continuously during engine combustion. Thirdly, the continuous change of EGR rate can achieve some operation points which can not be reached by step change of EGR. With the PVO strategy only, the engine can not be ignited under some test conditions, especially with either lower or higher EGR rate. The use of exhaust pressure to control residual gas rate can cover these gaps. It is because the auto ignition of the air fuel mixture could be significantly affected by the combustion process history of the previous cycle. With the change of exhaust back pressure, the in-cylinder conditions, such as pressure, temperature

and mixture dilution etc. before ignition happening, vary smoothly inducing different combustion processes.

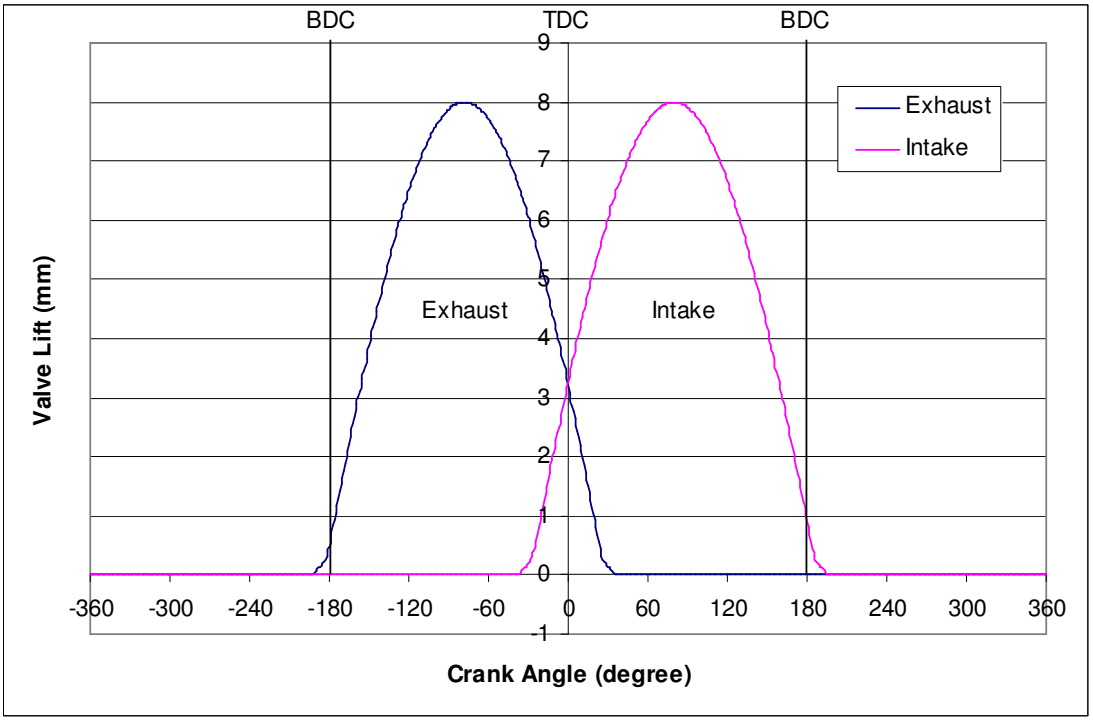

Figure 3.10 Valve Timings at 63 °CA Overlap

Since it is difficult to calculate the internal EGR rate, the in-cylinder sampling technique coupled with exhaust CO_2 measurement can be used to determine the trapped EGR rate.

The concentrations of carbon dioxide (CO_2) in the exhaust pipe and inside cylinder during compression are used to calculate the trapped residual rate. There are three reasons to choose CO_2. Firstly, the facility of measuring CO_2 is mature and widely used. Secondly, CO_2 is stable and hardly converted to other components. Thirdly, the CO_2 concentration in ambient air is 0.039%, which is negligible in the calculation. As a result, all CO_2 can be considered as coming from the previous cycle of combustion. A portion of CO_2 is discharged through exhaust pipe and the rest is re-breathed into the cylinder which is diluted by the fresh charge. The internal EGR rate can be defined and calculated as:

$$\text{iEGR rate (by volume)} = \frac{CO_2\% \text{ inside cylinder}}{CO_2\% \text{ in exhaust}} \qquad \text{Equation 3.3}$$

The iEGR rate presented in this study is on a volumetric basis. It should be clear that, although many CAI researches have used volumetric EGR rate as presented here, the representation of volumetric EGR value is not sufficient to indicate the actual EGR rate when the trapped residual gas is employed to be a key factor that promotes CAI combustion and controls the combustion events. It is because for a known volume, the mass of trapped residual gas depends on its temperature and pressure whose value may not be known well. Thus, the volumetric EGR rate may be somehow different from the actual EGR rate by mass. Nevertheless, in this study, the volumetric EGR rate is still considered as being numerically equal to the EGR rate by mass due to homogeneous charge and the usage of DME as ignition control source.

A high speed intermittent sampling valve is employed to extract in-cylinder gas samples during the compression stroke (Figure 3.11). The sampling valve system is designed and manufactured at Brunel University, which has been used by several researchers [81-83]. The sampling valve is made from high-strength steel. In order to minimize the leakage when operating under high-pressure and high-temperature in-cylinder sampling process, the valve head is designed as a poppet shape with a copper seal and outward opening. The valve closes firmly after opening due to the force from the high-pressure gas and return spring. Electromagnet and percussion principles are applied to increase response time. There is a gap between the stem and armature that provides a distance for the plunger to accelerate and impact the anvil after the electromagnet is switched on. The opening time, duration and extent are defined by the armature momentum, which is controlled by the driven pulse of the electromagnet switch from the sampling valve control system. After an impact, the plunger fast returns to the original position waiting for another driven signal. The design of this sampling valve has limited opening period under the condition of high pressure and high temperature during the combustion process. In this research, the sampling valve can be kept open for sufficiently long period of time to obtain stable results.

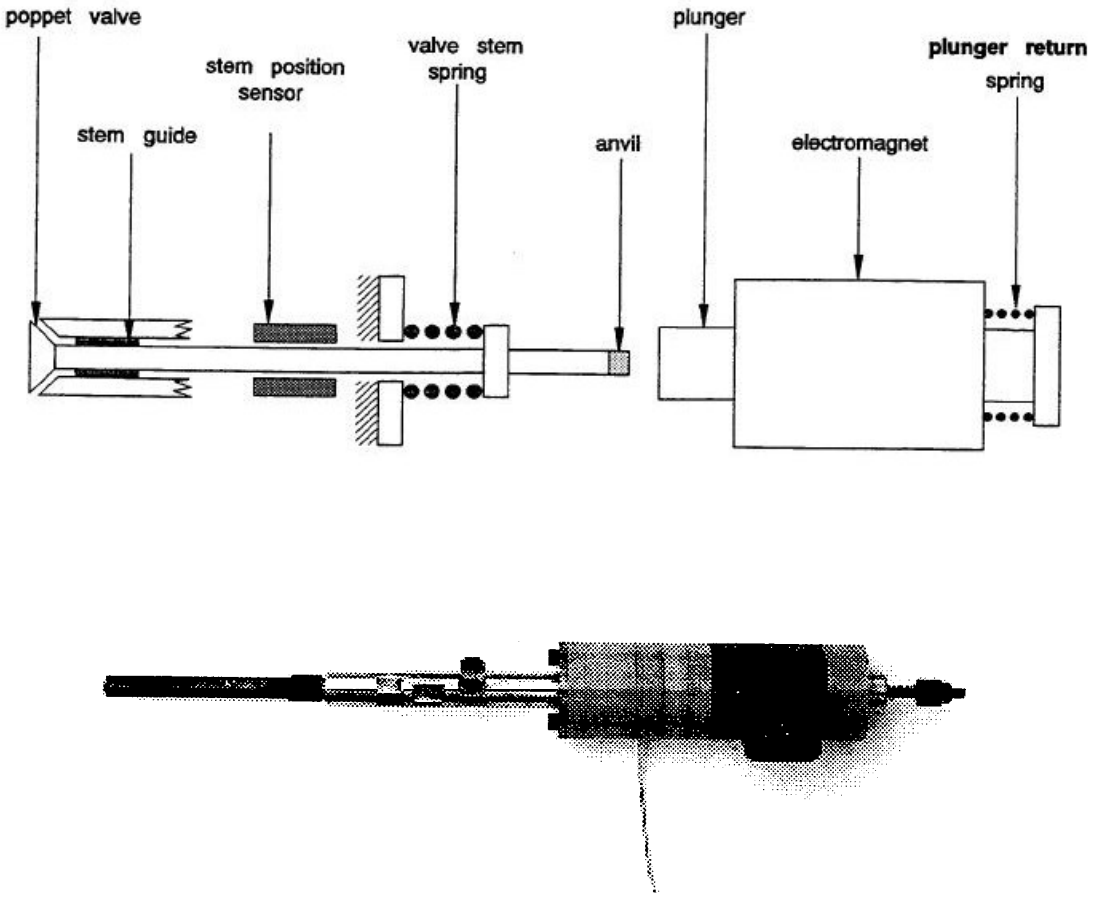

Figure 3.11 Electromagnetic Gas Sampling Valve

The sampling valve is controlled by a drive unit supplied by a 24 Volt dc power unit as shown in Figure 3.12. A reference signal comes from crank shaft encoder and the timing and duration of the drive pulse are controlled by a signal delay unit which receives a reference signal from crank shaft encoder. The actual sampling valve opening time and duration are precisely measured by a co-axial displacement sensor which detects the movement of the stem. The signal is monitored with an oscilloscope. One of the other injector drive signal, such as 2nd DME injection pulse, whose timing and duration are both known and adjustable, is applied to measure and indicate the actual opening time and duration of the sampling valve. Once this opening time and duration are set, the setting of delay unit is fixed and the injector pulse is adjusted for engine operating conditions. The sampling valve opening time is 200 °CA ATDC and lasts 3.16ms which closes at around 240 °CA ATDC at 1500 rpm engine speed.

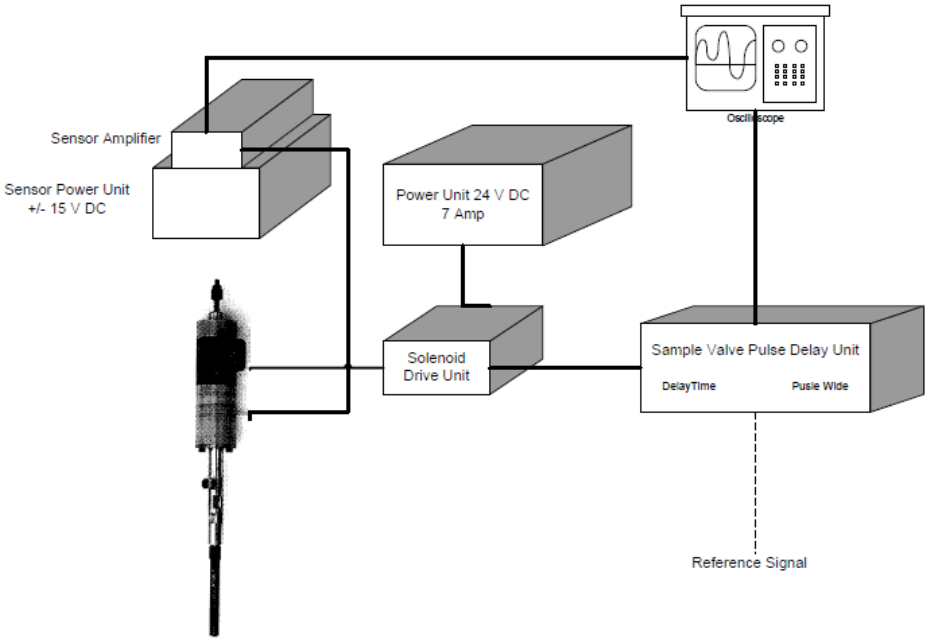

Figure 3.12 Sampling Valve Drive and Control Unit

A Cambustion NDIR500 Fast CO&CO_2 measurement system is employed to measure in-cylinder CO_2 concentration during the compression stroke coupled with in-cylinder sampling technology. With the measured average CO_2 concentration in exhaust by Horiba analyser (presented in 3.3.2.1), the EGR rate can be calculated. The fast CO_2 analyser achieves fast response time with 10-90% in 7 ms by minimizing the NDIR detector and locating it as close as possible to the sampling point.

The system contains two remote sampling heads which houses the NDIR detector, a services control unit, a PC using interface and three calibration gas supplies. The calibration gases include a bottle of oxygen free nitrogen for zero calibration, a bottle of 5% CO_2 balanced by nitrogen for low concentration calibration and a bottle of 12% CO_2 balanced by nitrogen for high concentration calibration. The sampling head receives daily cleaning before the tests with the purpose of removing the residual soot on the sapphire window. Calibration is applied regularly every hour during the tests in order to maintain maximum accuracy.

The sampling head is directly connected to the exit of sampling valve with a T-shape three-way connector. The NDIR analyser draws the sample gas continuously. When the sampling valve closes, all drawn gas is from ambience and the CO_2 concentration reading is the atmosphere CO_2 concentration (0.039% that is near zero). As soon as the engine

works with EGR and the sampling valve opens, the in-cylinder gas sucked by NDIR analyser increases while the drawn ambience air decreases. Thus, the CO_2% rises to peak when all sucked gas is from sampling valve. After the sampling valve closes, the ambient air is drawn by the analyser again resulting in decreased CO_2 concentration. The short delay between sample valve opening and CO_2% starting to increase is due to the distance between the valve poppet head and sampling vale exit point. In order to identify whether the drawn gas by NDIR is diluted by air, the point of the T connector which links to the air is drowned into the water. The bubbles come out when sampling valve works. That means the sample valve provides more gas than what the NDIR analyser requires. Therefore, the peak value of the CO_2% during this measuring cycle indicates the CO_2% inside the cylinder. Then coupled with the measured average CO_2 concentration in exhaust either by Horiba analyser or by the other NDIR analyser channel, the EGR rate can be calculated. Figure 3.13 shows an example of measuring internal EGR rate by two channels of fast CO_2 analyser. The left photo is the interface of fast CO_2 analyser software and the right figure is the result obtained by oscilloscope.

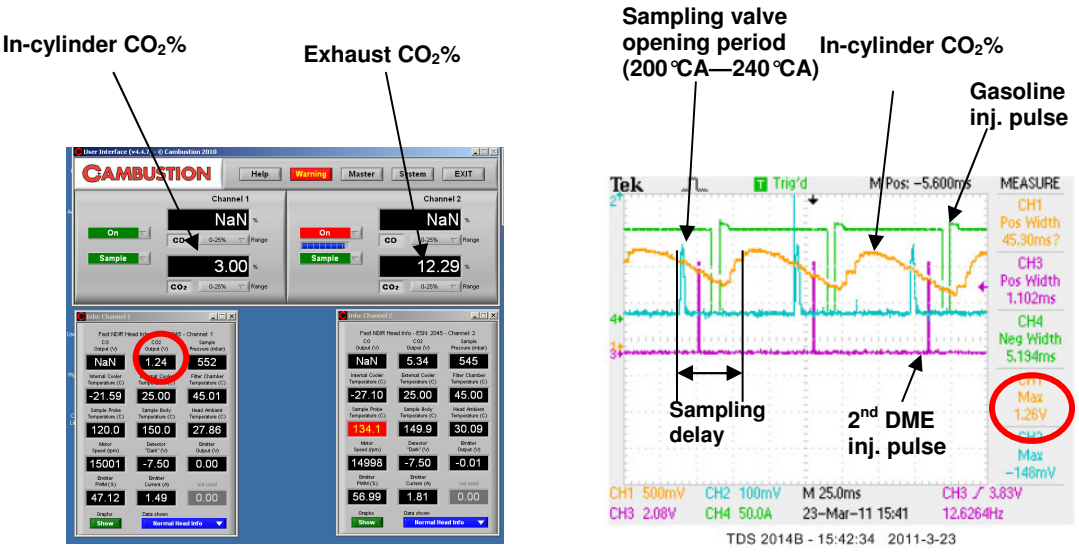

iEGR rate% = 3.15%/12.29%*100%= 26%

Figure 3.13 Measurement of Internal EGR Rate by NDIR Fast CO_2 Analyser

3.4 Air Flow Rate and Dual Fuel Air Fuel Ratio (AFR) Measurement

3.4.1 Air Flow Rate Measurement

An Alcock Viscous Flow Air Meter coupled with a manometer was used to measure the intake air flow rate. The flow meter was installed in the middle of the intake pipe. The multi-range manometer type NO.2690 is a differential pressure (Orifice plate) unit, which was made specially to the requirements of Ricardo by Airflow Developments Ltd.. Measurement is based on the volumetric unit on a meter reading. The reading will be converted to the mass unit by a calibration factor of paraffin. The detailed technical information can be found in Appendix C.

Although this flow meter could give an air flow rate, it is not adequate to show the slight change of intake air flow rate when EGR rate varies. It should be avoided to use this value only to identify air fuel ratio.

3.4.2 Overall Air Fuel Ratio Measurement

In general, gasoline is easy to be measured by a fuel flow meter. However, the DME flow rate and subsequently the overall air fuel ratio in this case are difficult to be identified. In some previous studies [84-88], the researchers apply an electric balance under the DME fuel tank and measure the mass consumption of DME within a particular time. In others [89-91], the researchers state that a mass flow meter can be used to measure the DME flow rate directly. In most of these studies, DME is treated as the main fuel so that the fuel flow rate is sufficient to apply these methods.

Theoretically, the above two methods can both provide good results. However, if these methods are applied, the electric balance and flow meter should be carefully selected, because a tiny quantity of DME is injected in this study which will increase the cost of the facilities. As a result, the electric balance should have over 5 kg measuring range and at least 0.1 g accuracy at the same time. The flow meter should contain special seal material avoiding collision by DME and work under the condition of high pressure (40 bar) and low flow rate (2 g/min).

Although an alternative method is introduced and discussed to measure dual fuel air fuel ratio (AFR) in the next section, the author still believes the electric balance with appropriate design is the best way to determine the DME flow rate.

3.4.2.1 Determination of Overall AFR by Injector Calibrations

The gasoline injector calibration is presented in 3.2.3.3. With this calibration method, the injected gasoline amount can be precisely identified by a known injection pulse width. The DME injection quantity could also be measured by the same method presented in 3.2.3.4. The calibration graphs are shown in Appendix D.

Theoretically, together with measured air flow rate, the relative overall AFR (overall λ) can be defined and calculated as:

$$\text{AFRact overall} = \frac{ma}{mg + md} \qquad \text{Equation 3.4}$$

$$\text{AFRstoi overall} = 14.7 * \frac{mg}{mg + md} + 9 * \frac{md}{mg + md} \qquad \text{Equation 3.5}$$

$$\lambda \text{ overall} = \frac{AFRact}{AFRstoi} = \frac{\frac{ma}{mg + md}}{\frac{14.7 * mg}{mg + md} + \frac{9 * md}{mg + md}} = \frac{ma}{14.7mg + 9md} \qquad \text{Equation 3.6}$$

Where ma: air mass flow rate (g/min)
mg: gasoline mass flow rate (g/min)
md: DME mass flow rate (g/min)
AFRg stoi: stoichiometric AFR gasoline = 14.7
AFRd stoi: stoichiometric AFR DME = 9

λoverall is used for investigating the effect of air fuel ratio on engine performance and emissions. In order to examine the effect of gasoline quantity and DME quantity respectively, the λ' gasoline and λ'DME are introduced and defined as follows:

$$\lambda\text{' gasoline} = \frac{ma}{14.7 * mg} \qquad \text{Equation 3.7}$$

$$\lambda\text{' DME} = \frac{ma}{9 * md} \qquad \text{Equation 3.8}$$

It should be noted that the λ' gasoline and λ' DME is not the actual air fuel ratio of each fuel. As the dual fuel combustion process is mixed, complicated and corresponsive, there is no significance to consider the definition of each air fuel ratio respectively.

The results could give a rough value of AFR. Although it is a straightforward way to indicate the relative AFR, as explained in Section 3.4.1, the air flow rate can not be precisely measured with EGR changes, which significantly affects the AFR. In addition, as mentioned in Section 3.2.3.4, the DME injection calibration graph is not sufficient to identify the air fuel ratio.

3.4.2.2 Overall AFR Measurement by a Wideband Lambda Sensor

Lambda sensors are also known as universal exhaust gas oxygen sensors (UEGO). A Bosch LSU 4.2 lambda sensor is mounted appropriately in the exhaust pipe. It is a wide band lambda sensor with a planar ZrO_2 dual cell limiting current sensor and an integrated heater. Its application range is from λ=0.65 to λ=20, which is the lean limit of what the monitor can indicate.

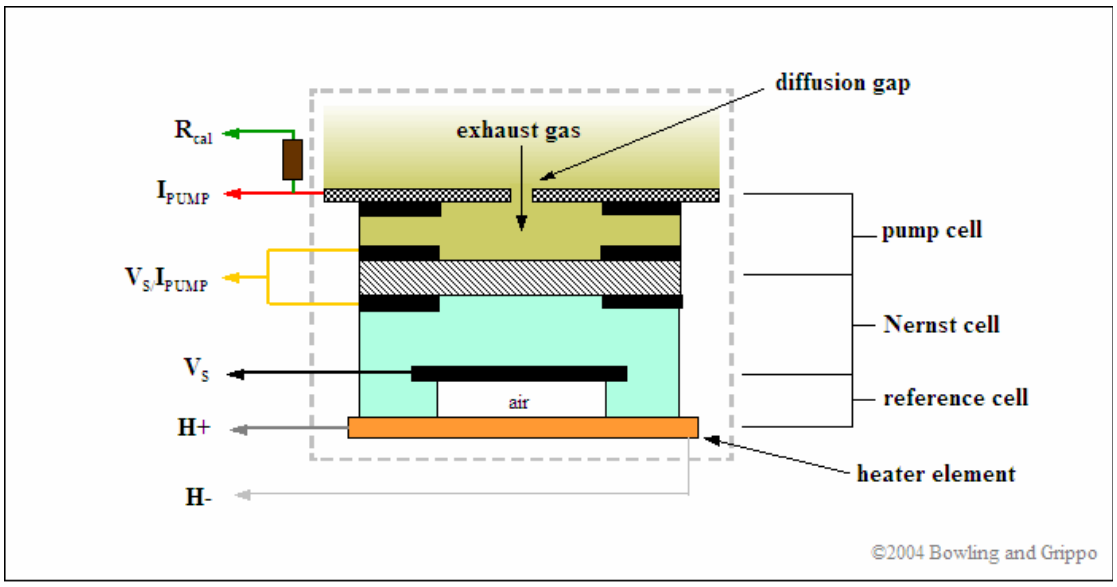

Figure 3.14 Principle of Wide Band Lambda Sensor [92]

Figure 3.14 shows the configuration of a wide band λ oxygen sensor. The sensor contains a Nernst cell unit as a narrow band sensor and an oxygen pump cell together with a reference cell and heater unit. The heater ensures the operating temperature of Nernst and pump cell of over 600 °C. Voltage is adjusted by an electronic circuitry maintaining the composition of the gas in the monitoring chamber at stoichiometric air/fuel ratio. When the mixture is rich, the reference cell produces a high voltage and the controller produces a current that pumps oxygen from the exhaust gas via the diffusion gap and consuming the extra fuel. When the mixture is lean, the current is reversed and the unit discharges the oxygen from the diffusion gap to the surroundings, consuming the free oxygen. When the mixture is stoichiometric, no current is required. The pumping current is proportional to the concentration of oxygen as well as the λ value, which is widely used in engine control system. Based on a formula for calculating the λ from oxygen concentration (in lean region and H/C ratio=2.0) by Bosch. Tech Edge Pty. Ltd [93] produced the graphs showing the relationship between the pump current and O_2 concentration, together with O_2 concentration vs. Lambda, as shown in Figure 3.15.

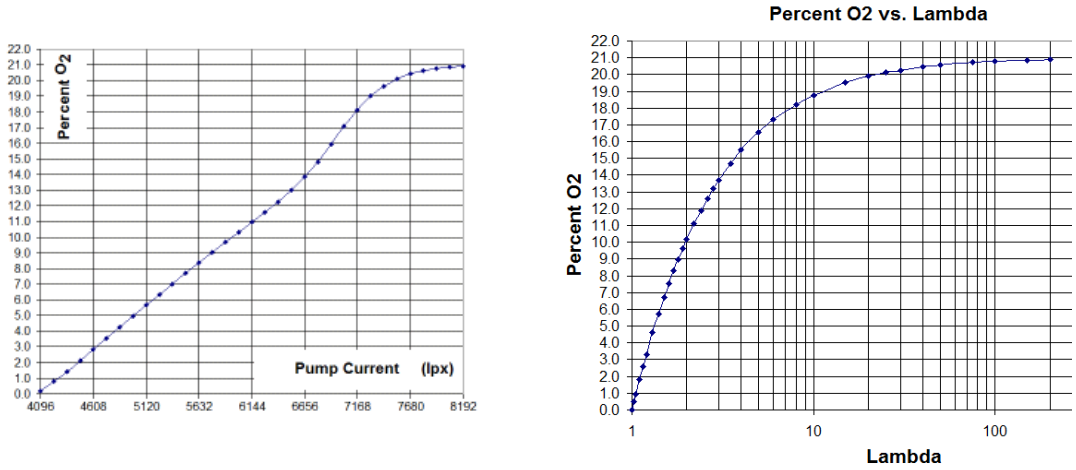

Figure 3.15 The Calculation of λ from Oxygen Concentration [93]

The lambda sensor based on above principle is demonstrated and widely used in studies when the engine operates on a single fuel (gasoline, diesel etc.). However, if the fuel is blended with more than one kind of fuel, as for this study, the lambda sensor cannot indicate the correct value except lambda=1. Bowling and Grippo [92] stated that it is better to use mathematical approach to determine lambda if the fuel component changes or the lambda sensor needs to be recalibrated and a mixture controller is necessary to fit the specific blended fuel mixture. Snyder et al. [94] provided a method to estimate one fuel

content in any lean combustion application with two fuels that have different stoichiometric air fuel ratios. They demonstrate the offset of the curve which indicates the relationship between the O_2 concentration measured by lambda sensor and different biodiesel concentration when engine operated in lean.

In this study, the same phenomenon is discovered as well after almost all possible false effects (such as effects of pressure, temperature, power supply, location, life time etc.) are eliminated. Lambda sensor indicates λ=1 right, but it generates false values when mixture operates lean (the actual lambda value is identified by exhaust components). Another possibility is that some special products exist by the combination combustion of DME and gasoline, which affects the lambda sensor working conditions. This needs further research. However, the lambda sensor reading is very sensitive with varying combustion conditions and has been useful for keeping EGR rate constant despite its wrong value in lean combustion.

3.4.2.3 Determination of Overall AFR with Measurement of Exhaust Components

There are various papers and equations for calculating the air fuel ratio from engine exhaust emissions. Eltinge [95], Spindt [96], Brettschneider, [97], Silvis [98], Heywood [99] and others presented their research and equations in this field. Oakley [100] also stated a way to combine EGR into the chemical equations to determine the air fuel ratio in his PhD thesis. Some of these developments are used to design and produce analysers with AFR output. The Horiba multi-gas exhaust analyser employs 72 different equations for its AFR output.

However, there is only one basic principle for calculating air fuel ratio that is based on chemical reaction balances due to combustion. Thus, in this study, the overall lambda (λ) is determined by all of the exhaust emission components in simplistic relations which is also known as the Brettschneider Equation:

$$\lambda = \frac{[CO_2] + [\frac{CO}{2}] + [O_2] + [\frac{NO}{2}] + (\frac{H_{cv}}{4} * \frac{K_p}{K_p + \frac{[CO]}{[CO_2]}} - \frac{Ocv}{2}) * ([CO_2] + [CO])}{(1 + \frac{H_{cv}}{4} - \frac{O_{cv}}{2}) * ([CO_2] + [CO] + K1 * [HC])} \quad \text{Equation 3.9}$$

Where:

[XX] = Gas Concentration in Volume

Hcv = Atomic ratio of Hydrogen t o Carbon in the fuel

Ocv = Atomic ratio of Oxygen to Carbon in the fuel

K1 = Number of Carbon atoms in each of the HC molecules being measured (Here all uHC is considered as Methane so that K1 = 1)

Kp = Assumed relation of CO_2, CO, H_2O and H_2 concentrations

$$\left(Kp = \frac{[CO]*[H_2O]}{[CO_2]*[H_2]} = 3.5 \right) \quad [96] \qquad \text{Equation 3.10}$$

To specify Hcv and Ocv, the total intake fuel mixture including gasoline and DME is considered as a single hydrocarbon with balanced subscripts chemical formula $C_aH_bO_c$. The value a, b and c vary with different fuel contents. Thus, the H/C ratio and O/C ratio of 0% (by mass) DME and 100% gasoline is 1.87 and 0 respectively. The 1% DME and 99% gasoline have the H/C and O/C ratio 1.88 and 0.003 etc. until 100% DME and 0% gasoline refer to 3 and 0.5. The stoichiometric AFR varies from 14.6 for a pure gasoline limit to 9 for a pure DME limit. Therefore, all 100 possible λ values are calculated with 100 possible H/C and O/C input by spreadsheet. The λ varies within a narrow range. For example,

Exhaust	CO2	CO	uHC	NOx	O2
Concentration	10.38%	0.24%	2257ppm	49.1ppm	5.84%
λ Range	1.336 — 1.327				

The chemical formula of DME is C_2H_6O. If this one oxygen atom is assumed as being consumed by two hydrogen atoms, the H/C ratio of the hydrocarbon left is 2, which is similar as the H/C ratio of gasoline (1.876). In this example, the λ value is determined as 1.3.

Therefore, the final lambda value is identified by this method.

3.5 Data Processing and Analysis

As mentioned in 3.3.1, the in-cylinder pressure data is recorded by the DAQ card and processed by Labview program. This section states the fundamentals of combustion analysis based on this in-cylinder pressure data and engine profiles, which are both used in real-time Labview program and the subsequent data processing and analysing (Figure 3.16).

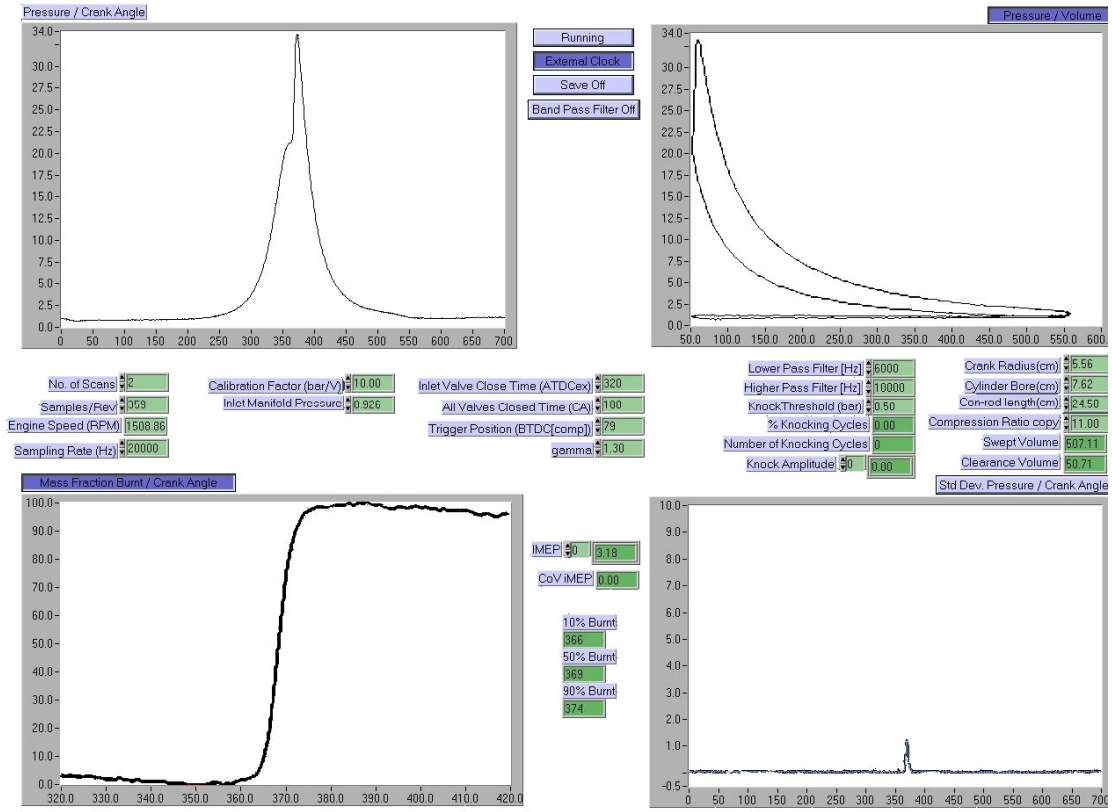

Figure 3.16 Main Interface of DAQ Software

3.5.1 Cylinder Volume and P-θ, P-V, logP-logV Charts

Cylinder volume is directly calculated by the following equations from the crank signal.

$$V = V_c + \frac{\pi B^2}{4}(l + a - s) \qquad \text{Equation 3.11}$$

$$V_c = \frac{V_d}{r - 1} \qquad \text{Equation 3.12}$$

$$s = a\cos\theta + \sqrt{(l^2 - a^2\sin^2\theta)}$$ Equation 3.13

Where:

V_c: clearance volume

V_d: total displacement volume

r: compression ratio

B: cylinder bore diameter

l: connecting rod length

a: crank radius

s: distance between the crank axis and the piston pin axis

θ: crank angle to the vertical

By these means, P-θ (pressure vs crank angle), P-V (pressure vs volume) and logP-logV charts can be plotted. It should be noted that in real engine cycle, logP – logV is a very useful way of calculating the polytropic coefficients of compression and expansion. In addition, the start and the end of combustion are identified by the logP-logV curve leaving from the straight line and returning back to the straight line respectively as shown in Figure 3.17 [101]. What's more, a motoring logP-logV diagram can verify the correction of top dead centre position before tests, which increases the accuracy of tests result [102].

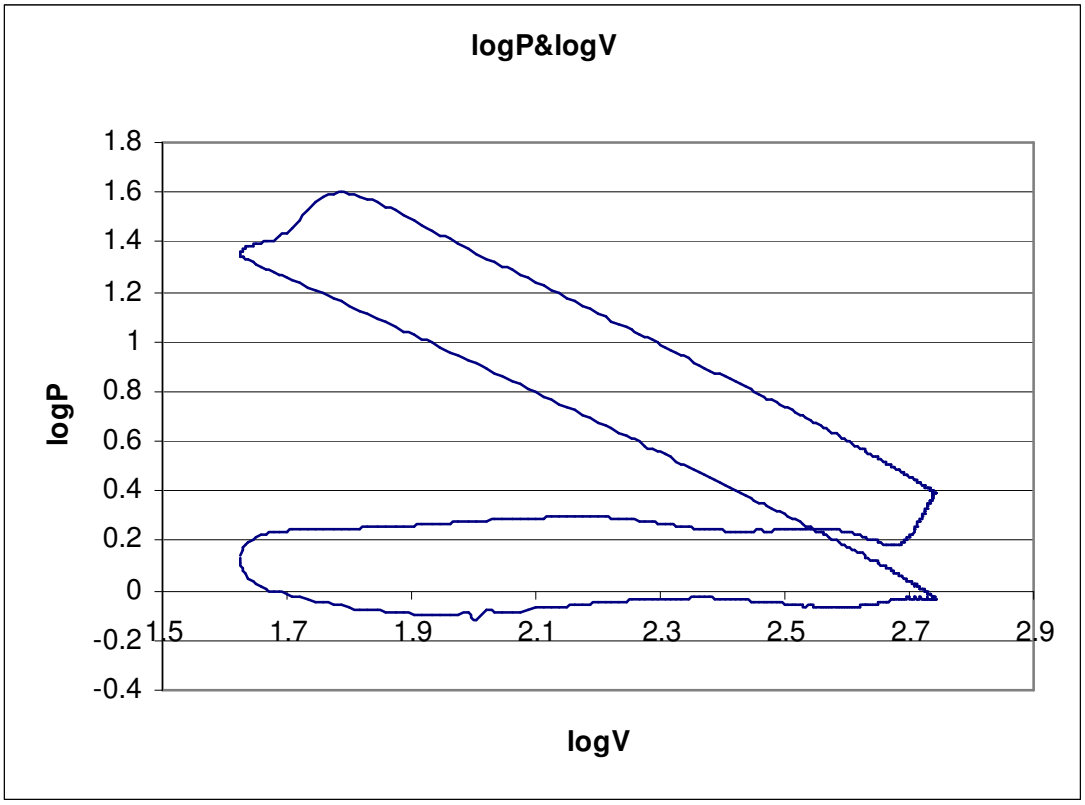

Figure 3.17 logP – logV Diagram

3.5.2 Engine Load, Combustion Variability and Efficiencies Calculations

Indicated Mean Effective Pressure (IMEP) is considered as the best sign of engine load. It indicates the work output per cycle per unit displacement volume. It is calculated as the following equation:

$$IMEP = \frac{1}{V_d} \oint p.dV \qquad \text{Equation 3.14}$$

The Labview program shows the net IMEP, which includes the positive work during compression and expansion stroke and negative work during intake and exhaust stroke. Gross IMEP is also calculated in the after-test analysis, which only includes the positive work. In each test point, 100 consecutive cycles of in-cylinder pressure data are recorded and COVimep is applied to determine combustion variability,

$$COV_{imep} = \frac{100 * \sigma_{IMEP}}{\sum_{1}^{100} IMEP_i}$$ Equation 3.15

Where σ_{IMEP} is the standard deviation in IMEP.

The efficiencies are defined in Figure 3.18. In order to compare the performance of engines with different sizes, all parameters are converted to mean effective values by being divided by displacement volume. The definitions are as follows:

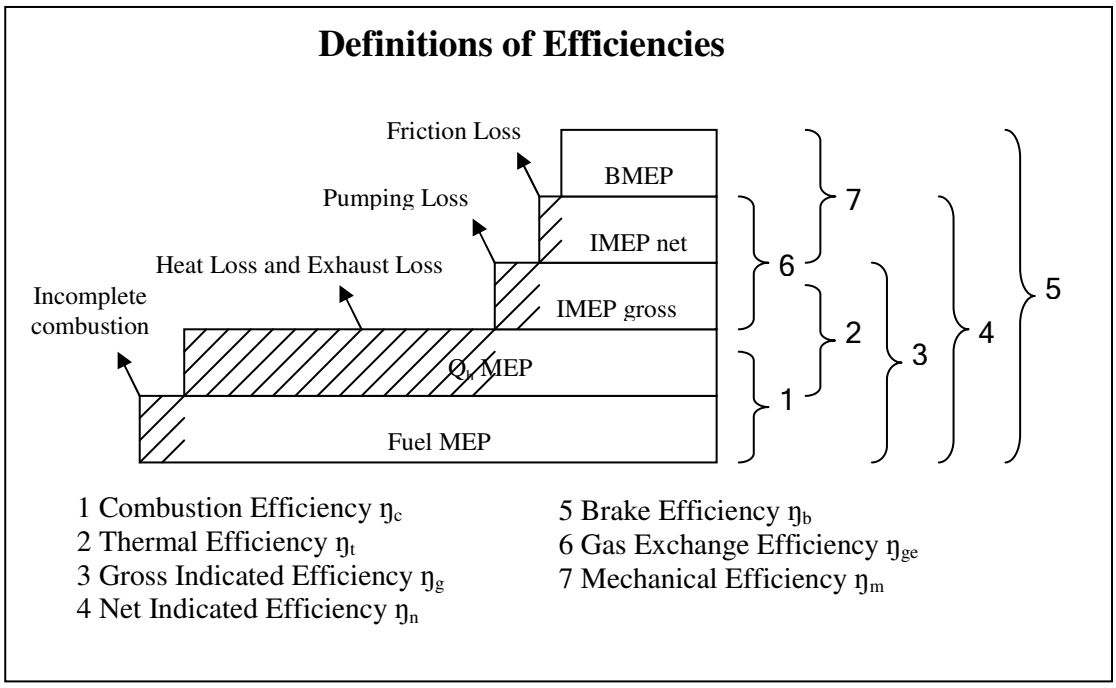

Figure 3.18 Definitions of Efficiencies

$$FuelMEP = \frac{(m_g \cdot LHV_g + m_D \cdot LHV_D)}{V_d}$$ Equation 3.16

$$Q_h MEP = \eta_c \cdot FuelMEP$$ Equation 3.17

$$IMEP_{gross} = \frac{W_g}{V_d} = \frac{1}{V_d} \int_{compression}^{\exp antion} P \cdot dV$$ Equation 3.18

$$IMEP_{net} = \frac{W_n}{V_d} = \frac{1}{V_d}\oint p.dV$$ Equation 3.19

$$BMEP = \frac{4 \cdot \pi \cdot T}{V_d}$$ Equation 3.20

$$\eta_t = \frac{IMEP_{gross}}{Q_h MEP};$$ Equation 3.21

$$\eta_c = 1 - \frac{\sum_i x_i \cdot LHV_i \cdot (m_g + m_D + m_a)}{m_g \cdot LHV_g + m_D \cdot LHV_D}$$ Equation 3.22

$$\eta_g = \frac{IMEP_{gross}}{FuelMEP}; \eta_n = \frac{IMEP_{net}}{FuelIMEP};\ \eta_b = \frac{BMEP}{FuelMEP};\ \eta_{ge} = \frac{IMEP_{net}}{IMEP_{gross}};\ \eta_m = \frac{BMEP}{IMEP_{net}}$$

Equation 3.23

Where:

m_g: mass of gasoline in one cycle

m_D: mass of DME in one cycle

m_a: mass of intake air in one cycle

W_g: gross work in one cycle

W_n: net work in one cycle

T: break torque

x_i: the mass frictions of CO and HC respectively (H_2 and PM are not considered)

LHV_i: lower heating values for CO (10.1 MJ/kg) and HC (44 MJ/kg) respectively.

3.5.3 Heat Release Rate (HRR) and Mass Friction Burned (MFB) Analysis

Heat release analysis is widely used in engine studies and considered as the most useful method of characterising the combustion events. The first law of thermodynamics is used as the basic principle and a closed system is applied to the whole cylinder contents during the combustion event.

$$\delta Q_h = dU + \delta W + \delta Q_{ht}$$ Equation 3.24

Where δQ_h is heat released by combustion, dU is the internal energy raised, δW is the piston work and δQ_{ht} is heat transfer to the chamber wall.

A single zone combustion chamber is assumed that means the reactions and products are fully mixed and have the same properties.

Each of the terms is calculated as:

$$\delta W = pdV$$ Equation 3.25

$$dU = mc_v dT$$ Equation 3.26

Th ideal gas law pV=mRT is reformed as:

$$mdT = \frac{1}{R}\left[pdV + Vdp\right]$$ Equation 3.27

From Equations 3.25, 3.26, 3.27 and 3.28 the net heat release rate (HRR) presents as follow:

$$\frac{dQ_{net}}{d\theta} = \frac{dQ_h}{d\theta} - \frac{dQ_{ht}}{d\theta} = \frac{\gamma}{\gamma - 1} p \frac{dV}{d\theta} + \frac{1}{\gamma - 1} V \frac{dp}{d\theta}$$ Equation 3.28

Where $\gamma = c_p/c_v$, the ratio of specific heats and θ is the crank angle.

Two major assumptions are made for the heat release analysis. One is that the heat release process is irreversible and the other is that the ratio of specific heats γ is considered constant during combustion.

The mass fraction burned (MFB) is obtained by integrating the net HRR with respect to crank angle. The MFB curve can be used to quantify the combustion start timing (CA of

10% MFB), combustion phasing (CA of 50% MFB) and combustion duration (CA 10%-90% MFB).

Zhang [103] develops the utilization of MFB curve in SI-CAI hybrid combustion. In their research, the maximum of second order derivative of heat release rate is considered as a T point, whose horizon position represents the start of CAI and vertical position represents the proportion of flame propagation and CAI in hybrid combustion as shown in Figure 3.19.

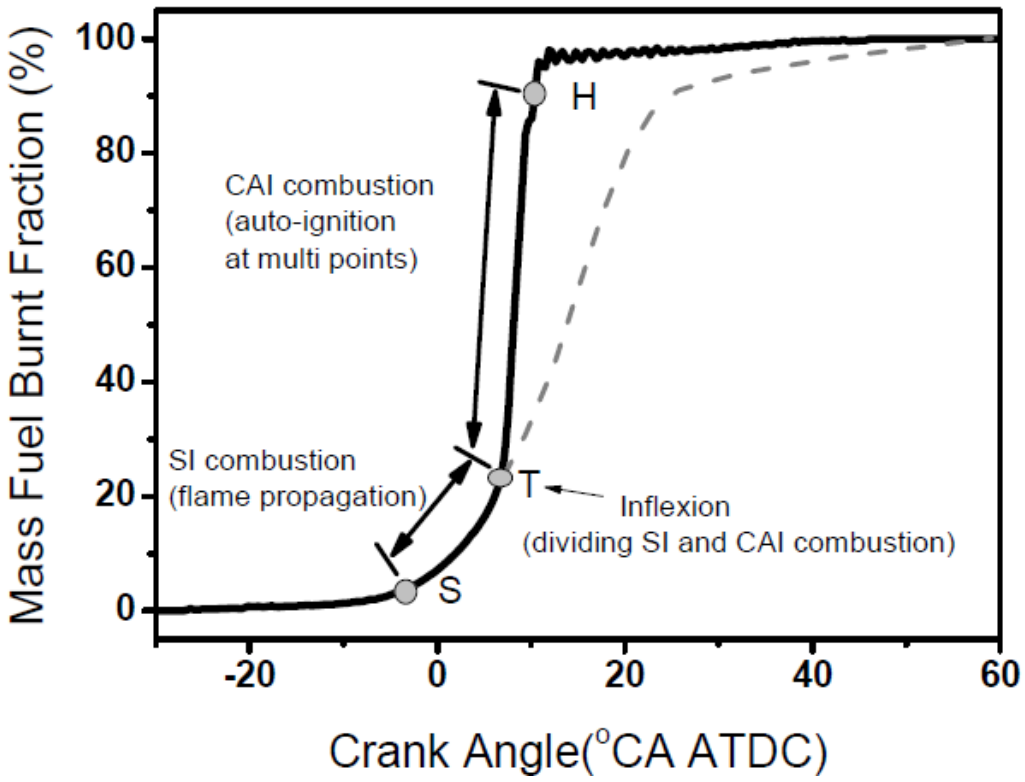

Figure 3.19 SI-CAI Hybrid Heat Release Process [25]

In this study, this method has been used as a tool to identify and quantify flame propagation (like SI) and auto ignition (CAI) combustion during the heat release process.

3.5.4 Knocking Combustion Analysis

The high load operating region of CAI combustion is limited by knocking combustion. Since the CAI combustion is characterised as simultaneous heat release inside the cylinder

during combustion process, the pressure oscillations and audible noise can often be detected.

Although many methods are applied to define the knocking combustion in CAI research, such as Knocking Occurrence Frequency (KOF) in [52], ringing index in [104] and Peak Knocking Pressure (PKMax) in [105], the maximum pressure rise rate based on crank angle, dP/dCA, is used as a criteria to identify knock in this study [106,107]. In [108], a simple practical knock threshold is set and applied at the averaged pressure data $(dP_{ave}/dt)_{max}$ =5 MPa/ms. It is of equivalent to about $(dP/dCA)_{max}$=5.5 bar/deg when the engine is operated at 1500 rpm in this study.

Therefore, in this study, any individual cycle with $(dP/dCA)_{max}$>5 bar/deg is considered as a knocking combustion cycle and the percentage of $(dP/dCA)_{max}$>5 bar/deg cycles of 100 continuous cycles is used as a criterion to evaluate the extent of knocking combustion. If over 50% of 100 cycles with max dP/dCA > 5bar, the test point is identified as unacceptable knocking combustion, which should be avoided.

Chapter 4

Dual Fuel CAI with iEGR Achieved by Positive Valve Overlap and Exhaust Back Pressure

Chapter 4 Dual Fuel CAI with iEGR Achieved by Positive Valve Overlap and Exhaust Back Pressure

4.1 Introduction

This chapter presents the DME-Gasoline dual fuel CAI combustion concept through the utilization of internal EGR to implement engine load control. Internal EGR is achieved by positive valve overlap coupled with exhaust back pressure in this chapter. Split DME Injection Strategy is applied to control CAI combustion, and the effects of DME injection (defined as Start of Injection, SOI) timings and quantity, and DME/gasoline ratio are also investigated. Finally, the results of the Split Injection Strategy are compared to those of a single DME injection strategy.

4.2 Determination of Initial Test Conditions

As the dual fuel CAI combustion had not been researched, it was necessary to carry out some preliminary experiments to determine the appropriate engine operating conditions for such a combustion process to take place. In addition, such experiments were employed to identify most important parameters affecting the new combustion process so that they could be studied in detail. There are many variable parameters during the engine operating process. Table 4.1 shows the engine test conditions employed in this study.

Table 4.1 Engine Test Conditions

Parameters		Value	Parameters	Value
Compression Ratio		13	Valve Lift	8 mm
Engine Speed		1500 rpm	Intake Temperature	20~25 °C
Coolant Temperature		80 °C	Gasoline	Unleaded 95 RON
Oil Temperature		55 °C	Gasoline inj. Pressure	2.5 bar
Valve Timing (63 °CA overlap)	IVO	33 BTDC of intake	DME	Provided by BOC
	IVC	191 ATDC of intake	DME inj. Pressure	40 bar
	EVO	187 BTDC of intake	Intake Pressure	Naturally Aspirated
	EVC	30 ATDC of intake	Wide Open Throttle	

The single cylinder E6 engine has a limited range of engine speed up to 2500rpm. As the main purpose of this study is to demonstrate the feasibility and potential of the dual fuel CAI combustion, the engine speed was fixed at 1500rpm. The engine runs at natural aspired conditions with wide open throttle with the purpose of minimising the intake pumping loss. DME injection pressure was initially chosen at 80 bar similar to the other studies using pure DME engines. However, the minimum DME injection quantity is limited by the minimum start-up drive pulse width of the GDI injector. The minimum amount of DME within the adjustable range was still too large to be used as an ignition promoter. In order to further reduce the injection quantity, the DME injection pressure was reduced and kept at 40 bar in the following tests.

The valve lift is 8mm and the valve timing is EVO=187 °CA BTDC, EVC=30 °CA ATDC IVO=33 °CA BTDC and IVC=191 °CA ATDC, which results in 63 °CA degree positive overlap duration as shown in Figure 4.1. With this valve timing, 13% of internal EGR is achieved by the measuring method which is presented in Chapter 3.

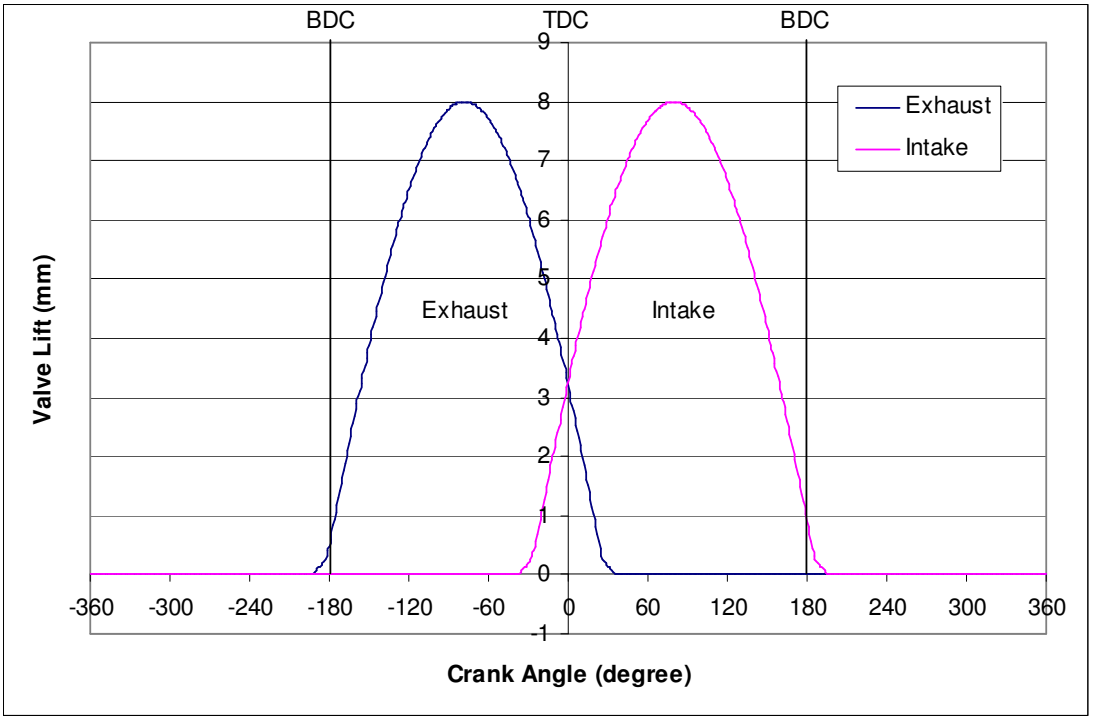

Figure 4.1 Intake and Exhaust Valve Lifts and Timings

To identify the optimal compression ratio (CR), the CR was varied from 14.5 to 13 under the above test conditions. The DME Split Injection Strategy was applied here. The first and

main DME injection (SOI1) started at 100 °CA with a quantity of 2.5 mg/cycle. The start of second DME injection (SOI2) timing was varied around TDC and its quantity was fixed at 1.8 mg/cycle. The total lambda (λ) was kept at 1.2 by the port fuel injected gasoline.

Figure 4.2 shows how net IMEP values vary with SOI2 timing and the compression ratio. At each compression ratio, IMEP initially rises to a region of maximum values when the SOI2 timing is retarded. Retarded injection beyond 25 °CA BTDC causes lower net IMEP due to the reduction of expansion work. Further retarding the SOI2 timing results in unstable combustion and eventually misfire in some engine cycles. In contrast, too advanced SOI2 causes serious knocking combustion which is detected from CR 14.5 to 13.3, where the obtainable maximum obtained net IMEP is limited. However, under CR 13, knocking combustion is avoided and the maximum net IMEP is obtained at 25°CA BTDC under this condition. At CR 13, the SOI2 timing can be considered as an appropriate way to control combustion phasing. In addition, for a fixed SOI2 timing, the increasing compression ratio has the effect of increasing net IMEP due to the higher thermal efficiency of the cycle. Thus, the engine with CR 13 will achieve higher efficiency than it would with CR<13 at the same SOI2 timing. Therefore, CR 13 is considered as the optimal compression ratio for this investigation. It should be clear that CR 13 is the geometric compression ratio. With the above valve timing, the effective compression ratio is 12.92.

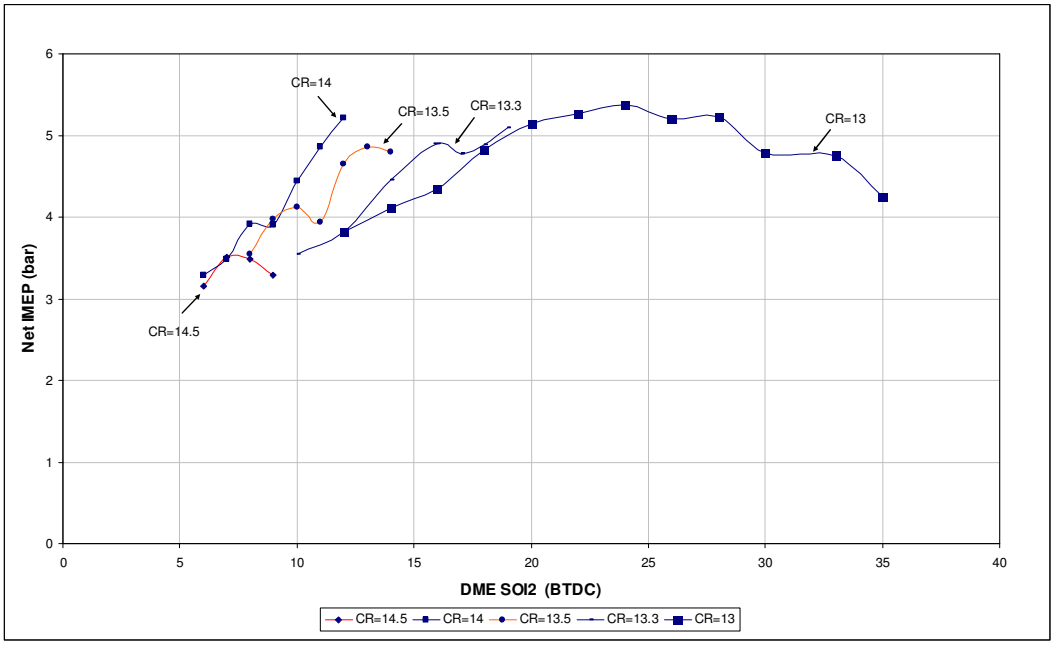

Figure 4.2 Net IMEP as a Function of the Second DME Injection Timing at Different Compression Ratios

4.3 Split DME Injection Strategy

4.3.1 Effect of First DME Injection (SOI1) Timing

In order to investigate the effect of SOI1 timing, the engine tests were conducted at mid-load conditions. The operating conditions are given in Table 4.2 and Figure 4.3. The exhaust pipe was throttled and adjusted to keep the back pressure fixed at 0.448 bar (6.5 psi) gauge pressure, achieving around 23% of trapped residual gases. The gasoline mass fraction of the total fuel was 73.6% with the remaining 26.4% of DME. The DME was injected by two injections with 65% in the first and 35% second. DME SOI2 timing was fixed at 322 °CA and the only variable parameter was the SOI1 timing. Thus, all the effects on combustion phasing and emissions came from the change of SOI1 timing. Two excessive early SOI1 timings were applied so that the SOI1s were implemented during the intake stroke. The other SOI1 timings were applied during the compression stroke in steps of 10 °CA.

Table 4.2 Operation Conditions of DME SOI1 Timing Sweep

Parameter	Value
Injection Strategy	Split Injection
Back Pressure (psi of gauge pressure)	6.5
iEGR Rate (%)	≈ 23
λtotal	1
Gasoline % by mass (%)	73.6
Gasoline inj. duration (ms)	5.279
Mass of Gasoline (mg/cycle)	18
DME SOI1 Timing (°CA)	**120,150,250,260,270,280,290,300,310**
DME SOI1 Duration (ms/°CA)	1.58 / 14.2
Mass of DME SOI1 (mg/cycle)	4.2
Fraction of DME SOI1 (% by mass)	65
DME SOI2 Timing (°CA)	322
DME SOI2 Duration (ms/°CA)	1.04 / 9.4
Mass of DME SOI2 (mg/cycle)	2.26

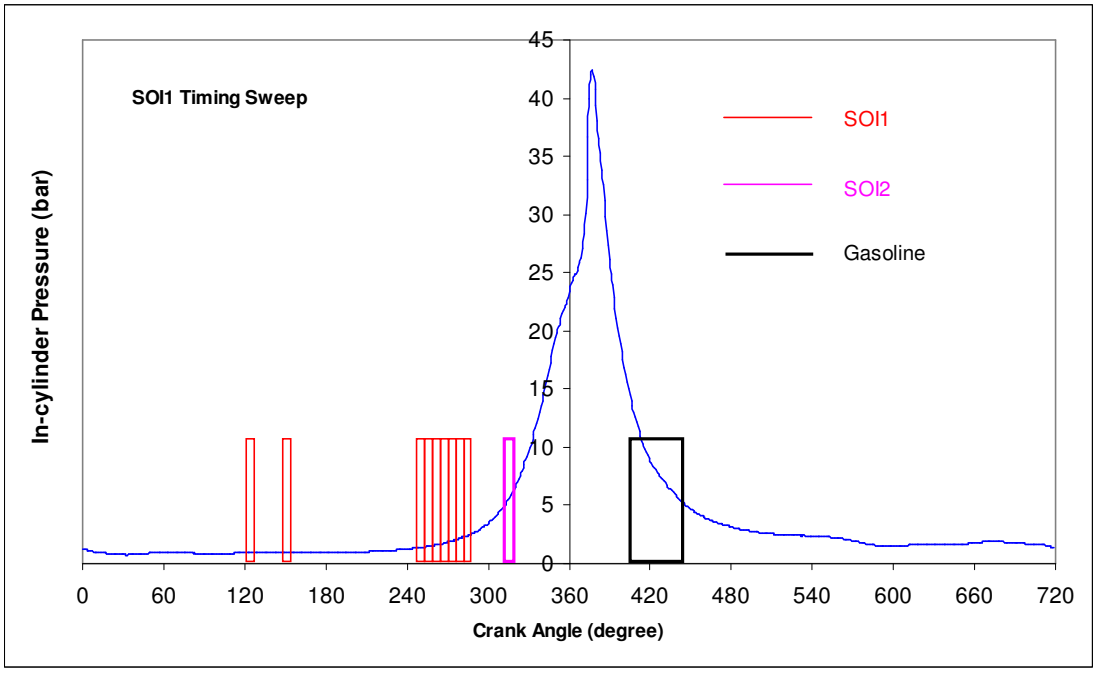

Figure 4.3 Injection Strategy of SOI1 Timing Sweep

Figure 4.4 shows the measured net IMEP and combustion phasing over a SOI1 timing sweep. Figure 4.5 shows the in-cylinder pressure and heat release rate, and Figure 4.6 shows the emissions for the SOI1 timing sweep. Figure 4.4a indicates that the SOI1 DME injected during the compression stroke can achieve higher IMEP than if it is injected during the intake stroke. The SOI1 timing for the best IMEP is between 280 °CA and 290 °CA with combustion phasing at 365 °CA, Figure 4.4b. The combustion starts at TDC and ends quickly after about 10 °CA (as measured by CA10-90), characteristics of simultaneous auto-ignition combustion throughout the cylinder charge.

In two cases of SOI1 in the intake stroke, the combustion starts earlier than TDC (359 °CA) resulting in lower IMEP. The ignition delay is short and independent of the SOI1 timing. This is because the DME from the 1st injection is highly mixed with gasoline/air mixture and is subject to the same in-cylinder conditions during the compression process. The combustion characteristics are determined by SOI2 DME. However, auto-ignition of the homogeneous DME/gasoline/air mixture can easily be auto-ignited resulting in fast combustion, shown in Figure 4.5 by the higher peak HRR and shorter combustion duration of SOI1 at 150 °CA than those of SOI1 timing at 270 °CA and 290 °CA. The increased NOx emission shown in Figure 4.6c at SOI1 at 150 °CA can be explained by the increased in-cylinder temperature and long resident time at higher temperature due to advanced

combustion phasing. In addition, earlier DME injection causes less intake flow rate and thus higher EGR is trapped, which can reduce the IMEP.

When SOI1 injections occur during the compression stroke, it is seen that as SOI1 timing is advanced, the combustion phasing is retarded (Figure 4.4b) and the NOx emissions (Figure 4.6c) and peak HRR (Figure 4.5) are reduced. It is because as SOI2 is retarded, the time between SOI2 and ignition is shorter resulting in a partial higher concentration of DME near the injector nozzle, which is also recognized as stratified DME distribution. In comparison, the earlier injected DME forms a more homogeneous but over diluted DME/gasoline/air mixture. Hence, the stratified mixture is more likely to auto-ignite and leads to earlier combustion. Violent knocking combustion is detected when SOI1 timing is further retarded. As a result, the uHC emissions are slightly reduced with SOI1 timing being retarded, while the NOx emissions are slightly increased, due to increased burned gas temperature of the stratified charge. The same phenomenon is observed by Hanson al etc [62] in their RCCI research work. CO emissions (Figure 4.6a) are found to be reduced as SOI1 is advanced because the later DME is injected, the more stratified the mixture is, where more CO are produced in the rich DME zones. This is different to Hanson's results [62]. The difference between this study and Hanson's may be because the different properties between diesel (used in Hanson's research) and DME as DME is an oxygen-contained fuel and the combustion reactants would be more oxidised when better quality of combustion is applied.

Therefore, the SOI1 timing has been set at 290 °CA in the following research in order to achieve the highest IMEP and optimal emissions.

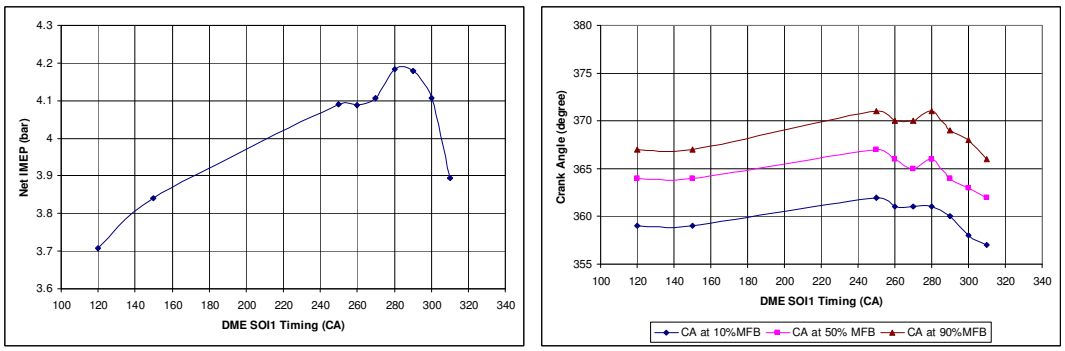

a) Net IMEP b) Combustion Phasing

Figure 4.4 Net IMEP and Combustion Phasing as a Function of DME SOI1 Timing

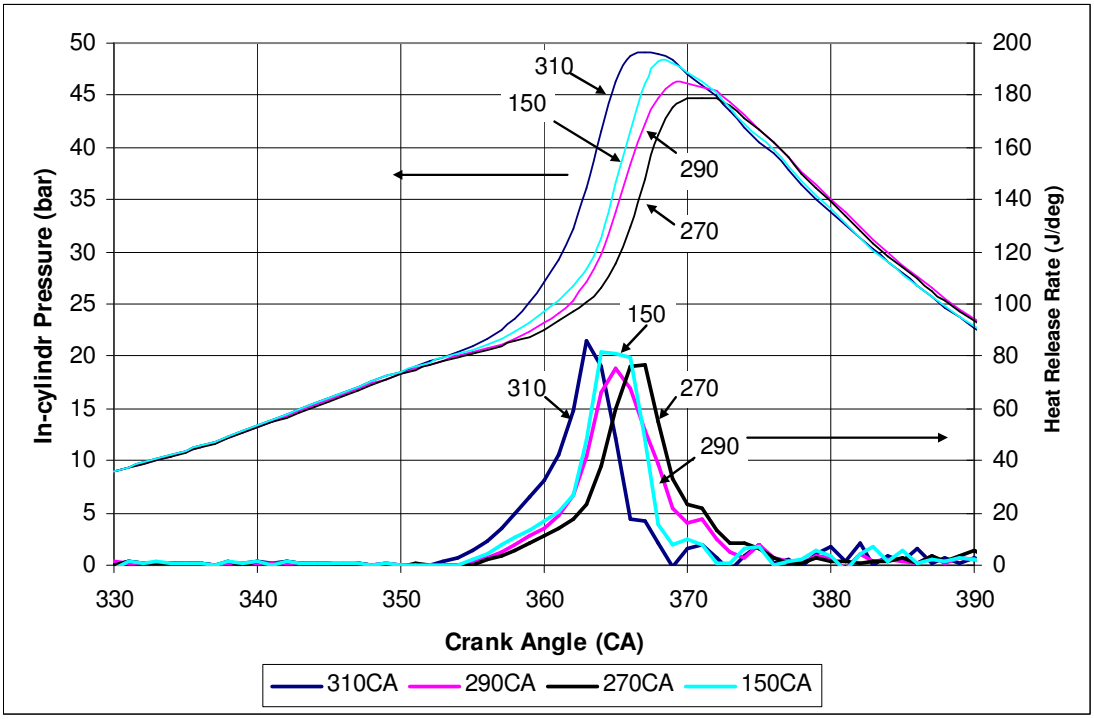

Figure 4.5 In-cylinder Pressure and Heat Release Rate at Various SOI1 Timing

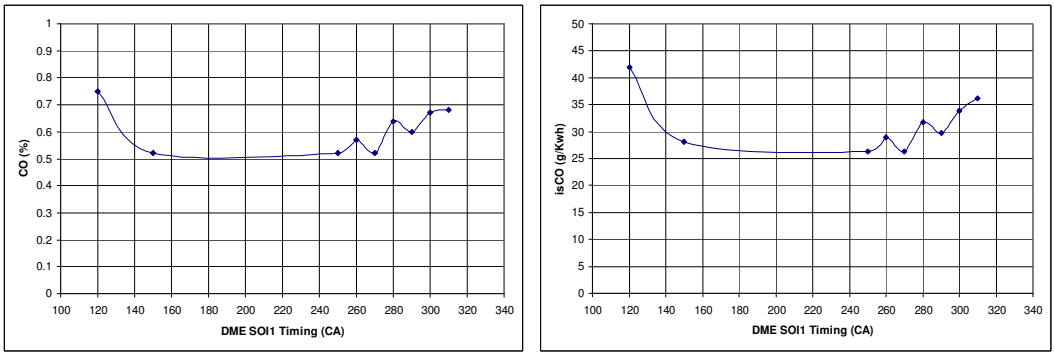

a) CO emissions

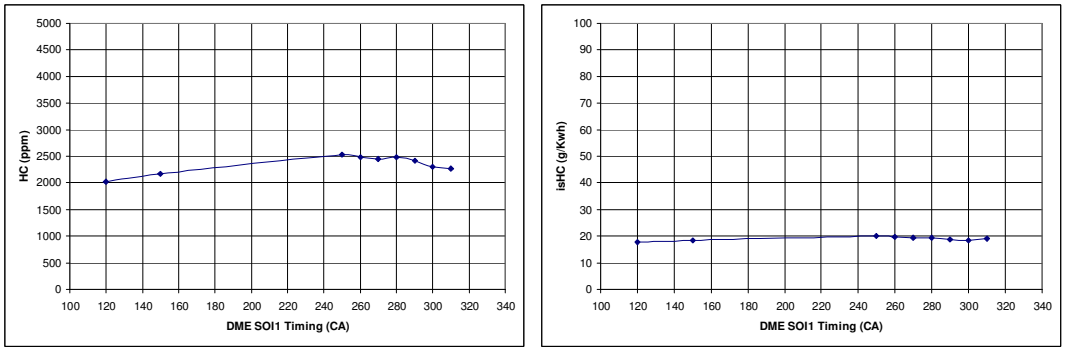

b) HC emissions

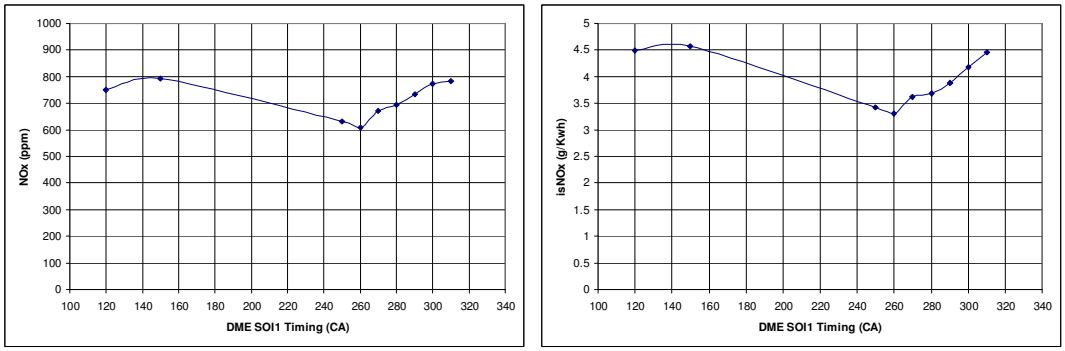

c) NOx emissions

Figure 4.6 Emissions as a Function of DME SOI1 Timing

4.3.2 Effect of Second DME Injection (SOI2) Timing

The operating conditions for the SOI2 timing sweep are given in Table 4.3 and Figure 4.7. Figure 4.8 and Figure 4.9 show the effects of SOI2 timing on engine performance and emissions respectively.

Table 4.3 Operation Conditions of DME SOI2 Timing Sweep

Parameter	Value
Injection Strategy	Split Injection
Back Pressure (psi of gauge pressure)	8.5
iEGR Rate (%)	≈ 31
λ_{total}	1
Gasoline % by mass (%)	73.5
Gasoline inj. duration (ms)	5.0
Mass of Gasoline (mg/cycle)	17.46
DME SOI1 Timing (°CA)	290
DME SOI1 Duration (ms/°CA)	1.58 / 14.2
Mass of DME SOI1 (mg/cycle)	4.2
Fraction of DME SOI1 (% by mass)	65
DME SOI2 Timing (°CA)	**315-337**
DME SOI2 Duration (ms/°CA)	1.04 / 9.4
Mass of DME SOI2 (mg/cycle)	2.26

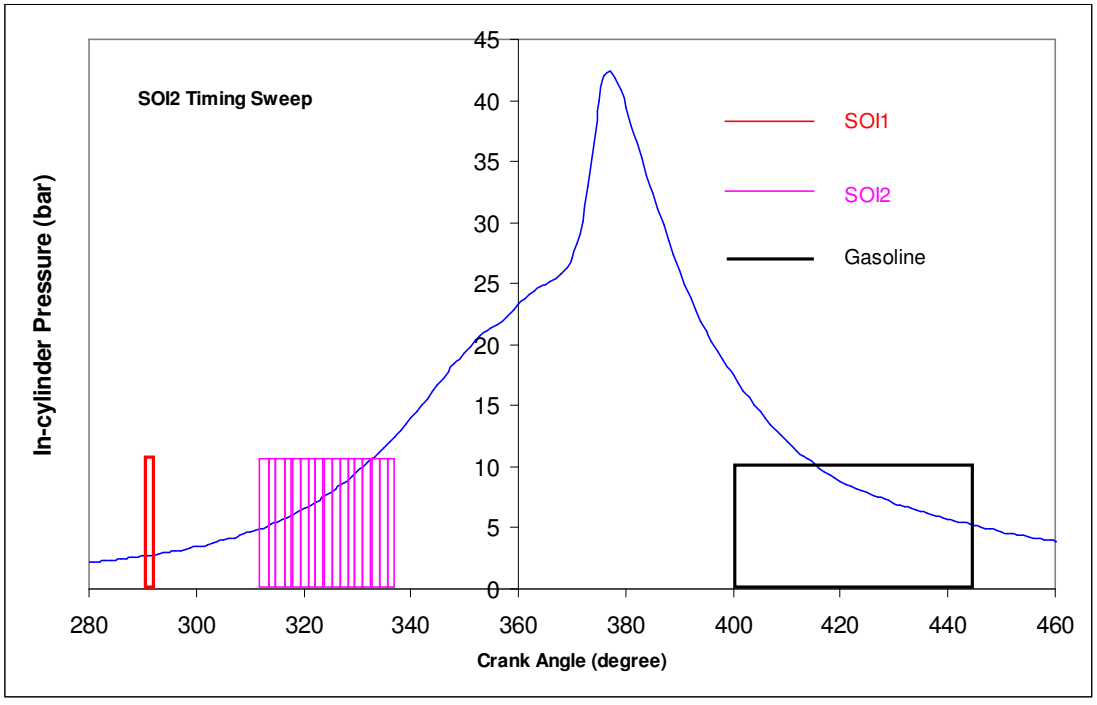

Figure 4.7 Injection Strategy of SOI2 Timing Sweep

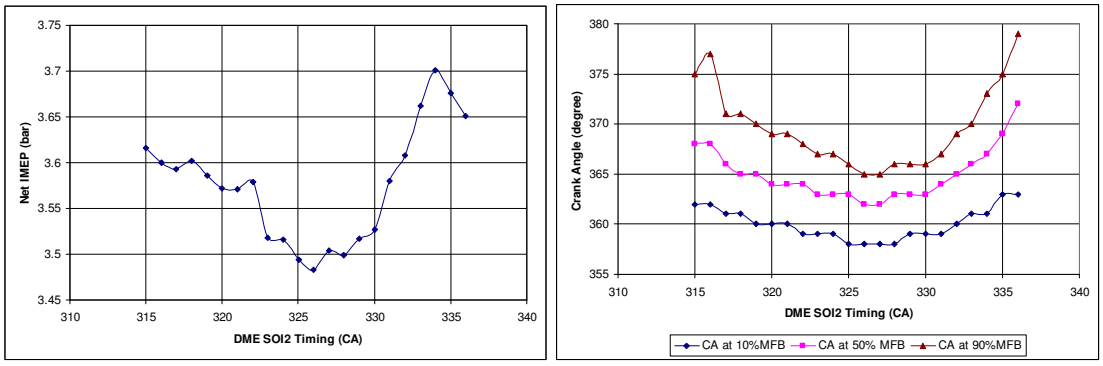

a) Net IMEP b) Combustion Phasing

Figure 4.8 Net IMEP and Combustion Phasing as a Function of DME SOI2 Timing

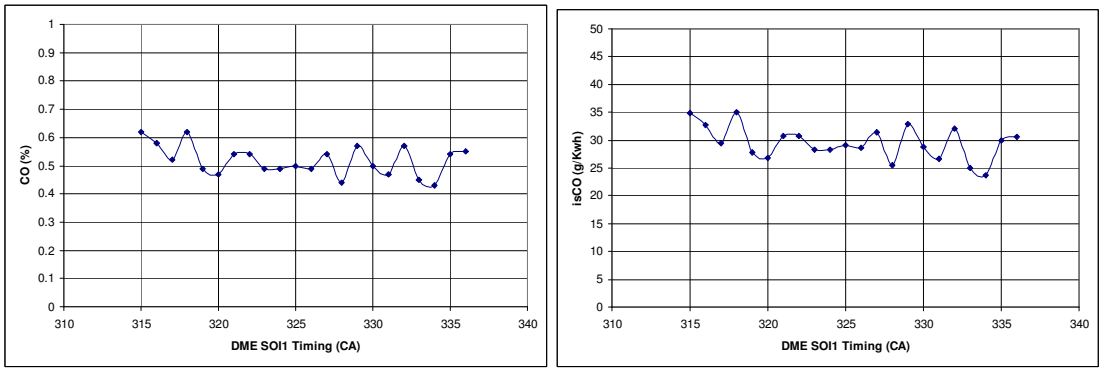

a) CO emissions

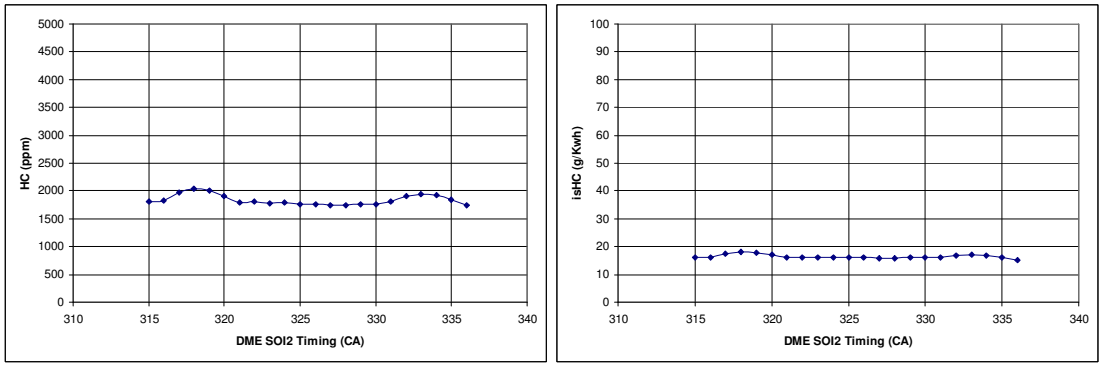

b) HC emissions

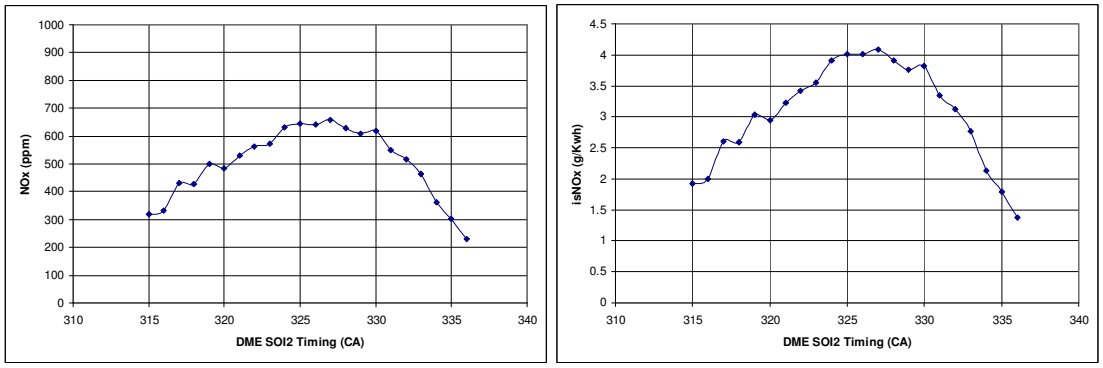

c) NOx emissions

Figure 4.9 Emissions as a Function of DME SOI2 Timing

The operating range of the SOI2 timing sweep under this condition is limited by misfire or unstable combustion when SOI2 timing is either before 315 °CA or after 337 °CA. This is because if SOI2 starts too early, the DME injected would be highly premixed with the in-cylinder charge at a temperature below its auto-ignition temperature. The trapped residual gas under this condition (iEGR = 23%) can not provide adequate thermal energy to initiate auto ignition of the total mixture at such early injection timing. Whereas if SOI2 timing is further retarded after 337 °CA, the combustion starts too late resulting in incomplete combustion. When SOI2 timing is between 315 °CA and 337 °CA, the COVimep is below 4% which indicates good stability of combustion.

The net IMEP slightly varies from 3.5 bar to 3.7 bar with the SOI2 timing sweep. However, the combustion phasing is significantly affected by the SOI2 timing. As SOI2 is retarded from 315 °CA, the IMEP firstly decreases with earlier and quicker combustion, and then increases after SOI2 goes beyond a certain point (327 °CA) and combustion starts later with a longer combustion duration. The MBT timing of this SOI2 sweep is 334 °CA, at which combustion starts 1 °CA after TDC (361 °CA) with 12 °CA duration. CO and HC emissions are independent of SOI2 timing. The early start of combustion results in higher local temperatures and violent combustion, which increase NOx formation. It can be concluded that the IMEP value would mainly be determined by other parameters such as the air/fuel ratio and iEGR rate rather than SOI2 timing. However, the SOI2 timing can be used as an effective tool to control the combustion phasing in order to achieve low NOx emissions.

The in-cylinder pressure and heat release data for SOI2 timing of 317 °CA, 324 °CA and 334 °CA are selected and presented in Figure 4.9 and Figure 4.10 to describe three different combustion processes.

1) **SOI2 (Flame Propagation) →SOI1 (Auto-ignition) →Gasoline (Auto-ignition)**

It can be seen that the HRR of SOI2 at 334 °CA has an obvious two-step heat release process. The first part of the heat release is characterised with a slow heat release rate associated with a propagation flame by the ignition of SOI2 DME. The expansion of the flame front compresses the unburned mixture to reach the auto-ignition temperature of DME from the first injection. The DME is well mixed with gasoline/air mixture and its ignition generates numerous auto ignition sites in the unburned mixture, which is

responsible for the rapid second stage heat release rate. The presence of iEGR helps avoid the presence of violent combustion.

2) **SOI2 (Flame Propagation) → Gasoline + SOI1 (Auto-ignition)**

As the SOI2 is advanced to 324 °CA, less heat is released from flame propagation and more rapid heat release takes place earlier. In this case, the DME SOI2 ignition starts earlier and the in-cylinder pressure and temperature are drastically higher near TDC. Both gasoline and premixed DME reach the auto-ignition conditions. Thus, the whole air/fuel mixture is auto-ignited resulting in significantly faster combustion and high peak heat release rate. This combustion process is similar to the knocking combustion in an SI engine as the results of the spontaneous reaction of the unburned mixture, except that the rate of heat release is modulated by the dilution and heat capacity effects of the dilution (CO_2 and H_2O) via the iEGR. However, there were occasions that heat release rate could be high enough to cause knocking combustion.

3) **SOI1+SOI2 (Auto-ignition) → Gasoline (Auto-ignition)**

When SOI2 timing is further advanced to 317 °CA, only one type of heat release process is observed. The SOI2 timing is so early that the charge temperature is below its auto-ignition temperature. During the ignition delay period, SOI2 DME becomes well mixed. Both SOI1 and SOI2 DME are auto-ignited and then initiate the auto-ignition of gasoline.

This phenomenon is found in the whole mid-load engine operation with a split injection strategy. There is a short range of SOI2 timings that induces violent combustion, which must be avoided. This short range is in the middle of the SOI2 operation. The SOI2 timing is preferred to be selected after this range (near TDC) because of relatively higher IMEP and lower NOx emissions.

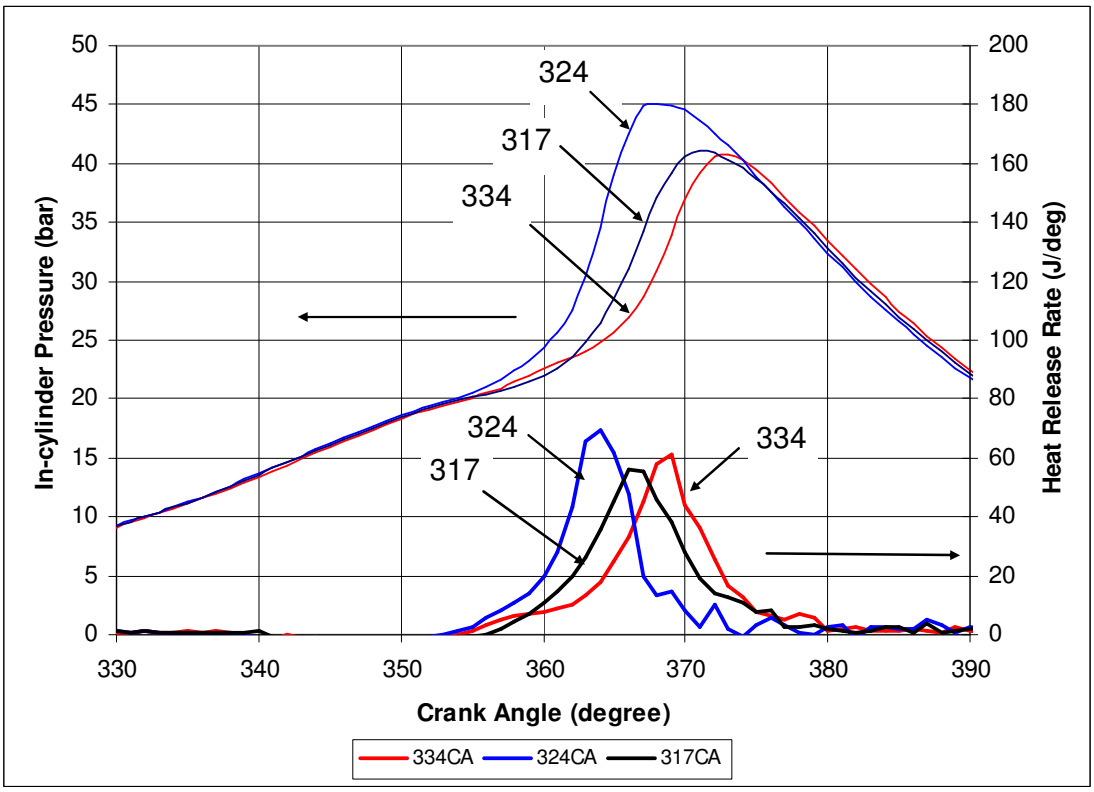

Figure 4.9 In-cylinder Pressure and Heat Release Rate at Various SOI2 Timing

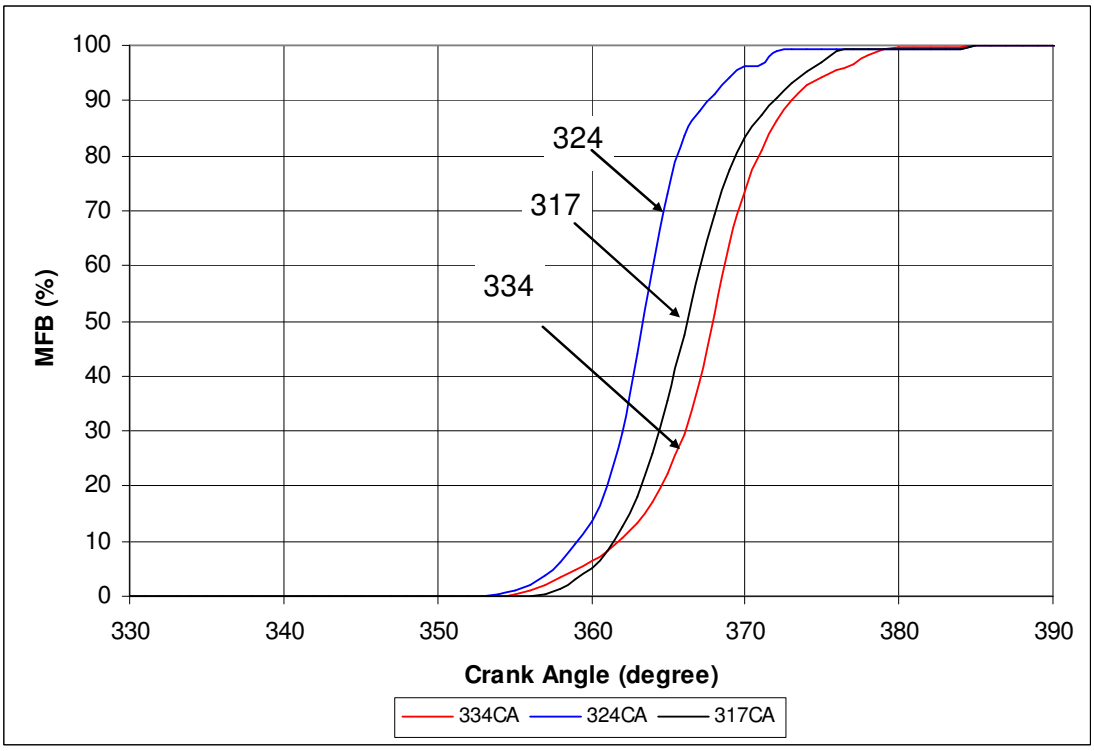

Figure 4.10 Mass Fraction Burned at Various SOI2 Timing

4.3.3 Effect of Ratio of DME Quantity in Split Injections

Table 4.4 Operation Conditions of DME SOI1 Ratio Sweep

Parameter	Value
Injection Strategy	Split Injection
Back Pressure (bar of gauge pressure)	0.517
iEGR Rate (%)	≈ 27
λ_{total}	1
Gasoline % by mass (%)	≈74
Gasoline inj. duration (ms)	5.2
Mass of Gasoline (mg/cycle)	17.46
DME SOI1 Timing (°CA)	290
DME SOI1 Duration (ms/°CA)	0/0 - 1.58 / 14.2
Mass of DME SOI1 (mg/cycle)	0 – 3.99
Fraction of DME SOI1 (% by mass)	**0 - 64**
DME SOI2 Timing (°CA)	327 - 330
DME SOI2 Duration (ms/°CA)	1.8 / 16.2 - 1.04 / 9.4
Mass of DME SOI2 (mg/cycle)	6.14 – 2.42

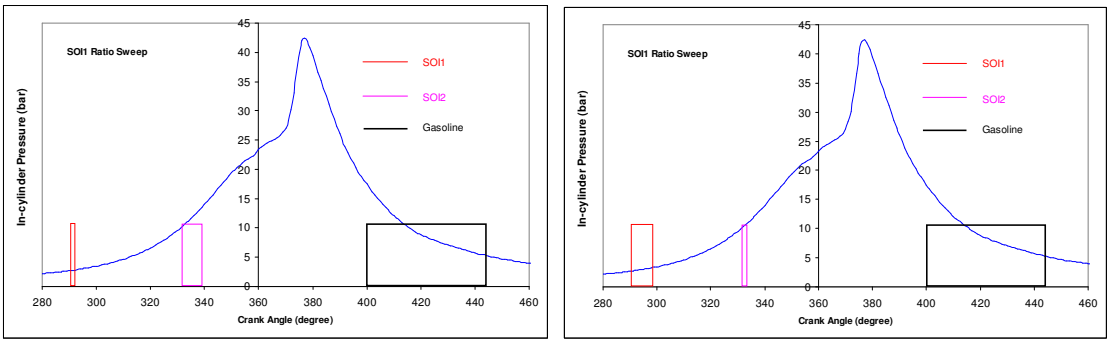

Figure 4.11 Injection Strategy of SOI1 Ratio Sweep

Table 4.4 and Figure 4.11 shows the test conditions of the DME split ratio effect between the two DME injections. The percentage of the first injected DME quantity is used as the parameter to investigate this effect. The total DME quantity is kept constant as well as the overall λ (λ_{total}). The DME SOI1 ratio varies from 0% by mass, which means single SOI2 injection, to 64% by mass which is the misfire limit of the minimum SOI2 quantity.

Figure 4.12 shows the IMEP and combustion phasing of DME SOI1 ratio sweep. As DME SOI1 ratio increases, the ignition delay becomes slightly longer resulting in late start of combustion and higher IMEP. However, the combustion duration remains constant (12 °CA).

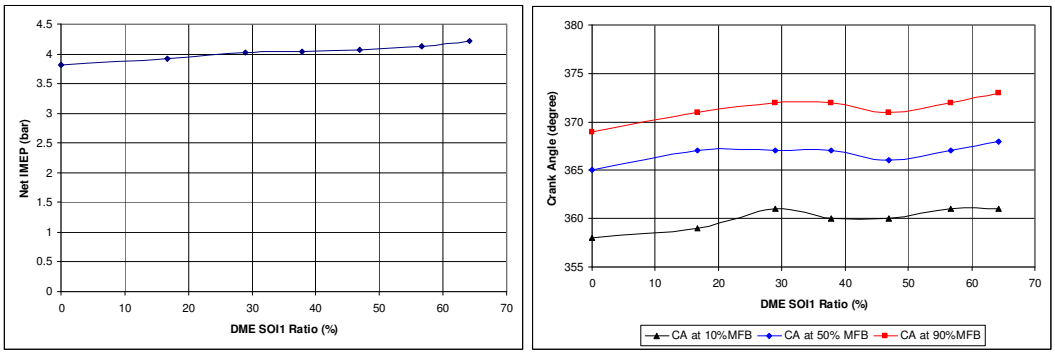

a) Net IMEP b) Combustion Phasing

Figure 4.12 Net IMEP and Combustion Phasing as a Function of DME SOI1 Ratio

Figure 4.13 shows the emission trends for the DME SOI1 quantity sweep. The CO emissions remain at a relatively high level during the whole sweep. This is because under λ =1 conditions, there is a core consisting of a fuel rich zone (λ<1) near the DI injector and the ignition of SOI2 DME starts from it. The HC and NOx emissions are seen to be unaffected by the DME SOI1 ratio and both of them remain at low levels.

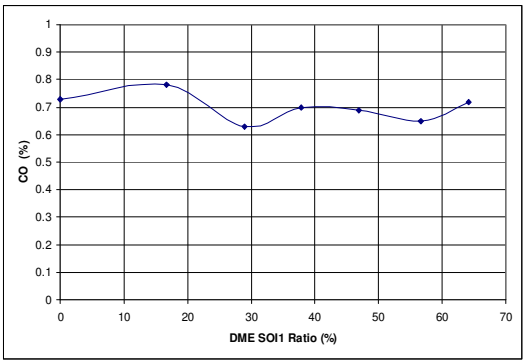

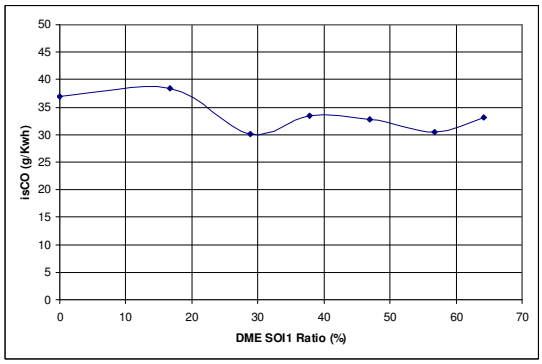

a) CO emissions

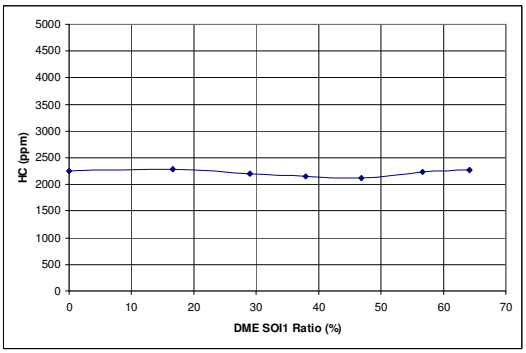

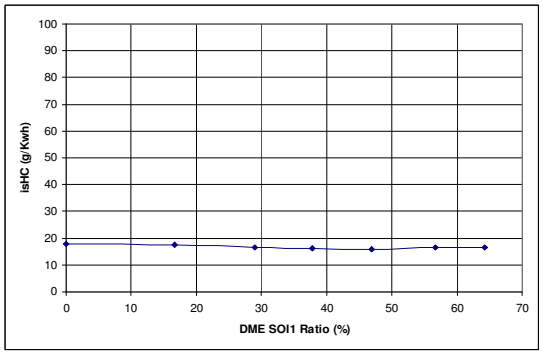

b) HC emissions

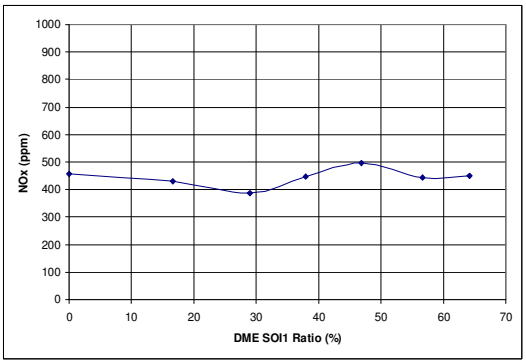

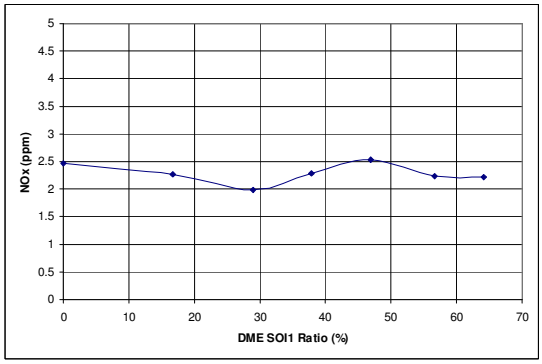

c) NOx emissions

Figure 4.13 Emissions as a Function of DME SOI1 Ratio

Figure 4.14 shows the value of the transition point (T point) between the slow flame propagation heat release and the rapid auto-ignition combustion. As discussed in Section 3.5.3, the T point is determined from the MFB curves in Figure 4.15 when hybrid flame/auto-ignition combustion is present. The crank angle at the T point indicates the start of fast auto-ignition combustion and the vertical position represents the proportion of the heat released from flame propagation combustion to auto-ignition combustion. The results in Figure 4.14 show that the T point position is little changed with different split injection ratios. However, as the quantity of the first injection increases, the flame propagation ratio

(FPR) is decreased. This indicates that the greater the DME is injected near TDC the more heat is released from flame propagation as more near stoichiometric mixture is formed.

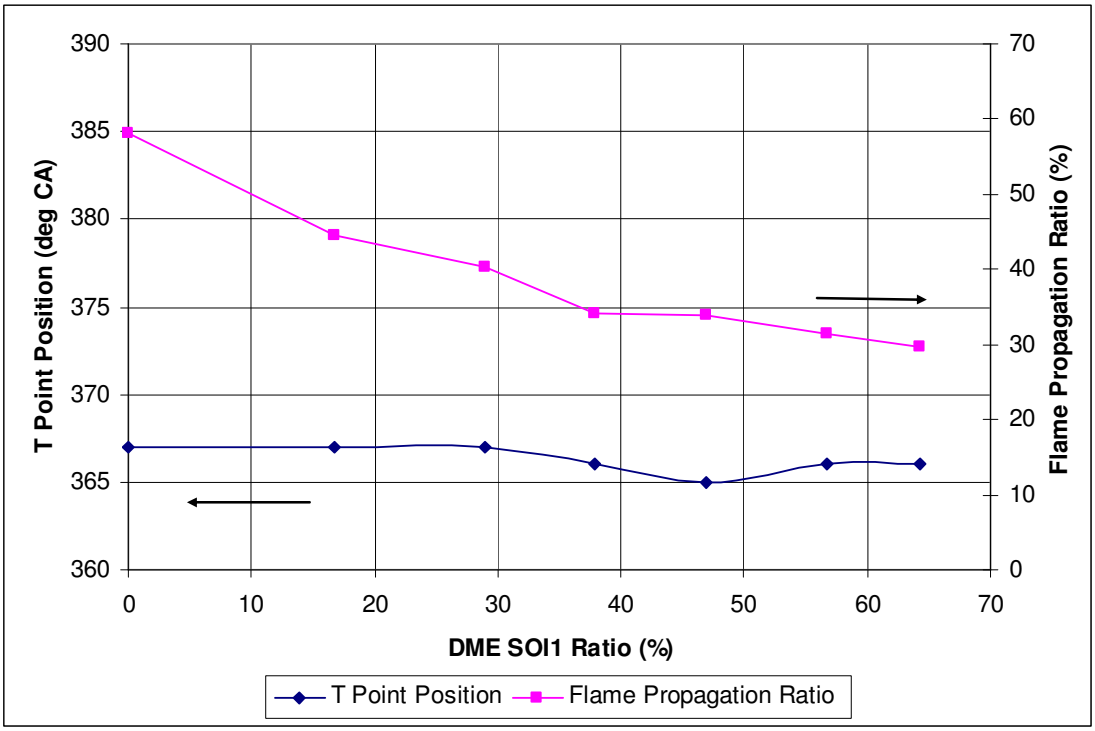

Figure 4.14 Effects of SOI1 Ratio on T Point Position and Flame Propagation Ratio (FPR)

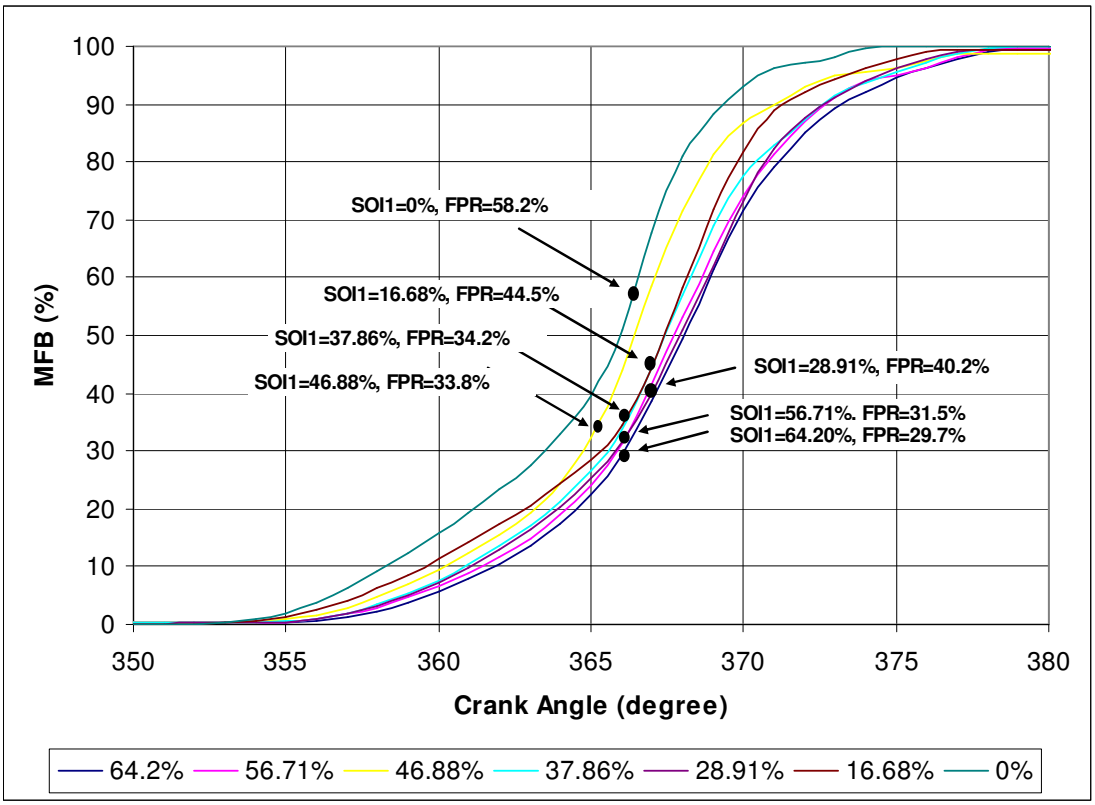

Figure 4.15 Effect of SOI1 Ratio on MFB Curve

Since auto-ignition combustion is likely to achieve better engine performance and emissions than flame propagation combustion, the DME SOI2 quantity is kept as little as it could be to achieve stable combustion in order to get a higher fraction of auto ignition combustion during the mid-load split-injection operations.

4.3.4 Effect of DME/Gasoline Ratio

The effect of the DME/Gasoline ratio with the DME split injection strategy was also investigated. Table 4.5 and Figure 4.16 show the operating conditions and their injection timings for the DME/Gasoline ratio sweep. The quantity of DME in the second injection is kept constant and set to the minimum, while the DME in the first injection increases from 0.8 to 4 mg per cycle. Thus the total DME% by mass varies from 13% - 25% of the total injected fuel.

Table 4.5 Operation Conditions of DME/Gasoline Ratio Sweep

Parameter	Value
Injection Strategy	Split Injection
Back Pressure (psi of gauge pressure)	7.5
iEGR Rate (%)	≈ 27
λ_{total}	1
Gasoline % by mass (%)	87 - 75
Gasoline inj. duration (ms)	5.7 – 5.2
Mass of Gasoline (mg/cycle)	20 - 17
Total DME % by mass (%)	**13 - 25**
DME SOI1 Timing (°CA)	290
DME SOI1 Duration (ms/°CA)	0.64/5.8 - 1.58 / 14.2
Mass of DME SOI1 (mg/cycle)	0.8 – 4
DME SOI2 Timing (°CA)	327 - 330
DME SOI2 Duration (ms/°CA)	0.98 / 9
Mass of DME SOI2 (mg/cycle)	2

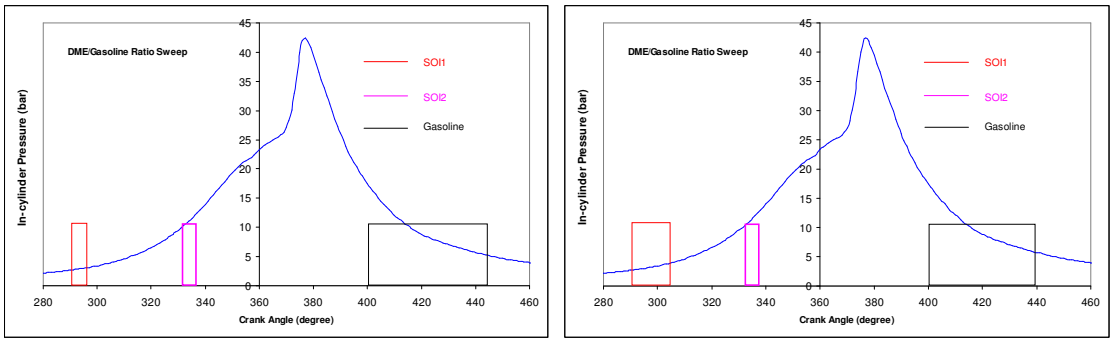

Figure 4.16 Injection Strategy of DME/Gasoline Ratio Sweep

Figures 4.17 - 4.19 show the engine performance, emissions and heat release analysis for the DME/Gasoline ratio sweep respectively.

Generally, quick and stable combustions are achieved when DME Split Injection Strategy is applied as shown in Figure 4.17b and Figure 4.17c. The combustion durations are less than 20 °CA and the COVimep is less than 4%. The engine emissions stay at a low level. From the heat release analysis shown in Figure 4.19b, the hybrid combustion process composed of flame propagation and auto ignition is realised.

As DME fraction is increased, IMEP is seen to be unaffected (Figure 4.17a) as well as the start timing of combustion (CA10 shown in Figure 4.17b). The dip of IMEP value at the condition of 23% DME fraction is possibly because of the deterioration of combustion which can be indicated by the high CO emissions shown in Figure 4.18a. However, the combustion duration has a tendency to be reduced when the DME fraction increases. What's more, the combustion phasing is advanced as the DME fraction increases. The earlier combustion phasing and faster combustion should have increased the IMEP value, which is found constant here. This is because the increased DME direct injection quantity can reduce the intake flow rate and then increase the EGR rate. The benefits on IMEP by faster and earlier combustion balance the drawbacks by increased EGR, resulting in constant engine output.

The heat release analysis is shown in Figure 4.19. As DME fraction increases, the fraction of auto-ignition of the hybrid combustion process increases resulting in quicker combustion. The T point position advances and the flame propagation ratio is reduced. The effects on HC and NOx emissions are negligible as they are kept at a significantly low level. However, CO emissions are seen to increase slightly shown in 4.18a, which is different to Hanson's research [62]. Hanson stated that with the increase of high cetane fuel (diesel fuel in their research), the oxidation rates of the products are faster as the local temperature becomes higher. However, in this study, one of the possibilities of the increased CO emission is that, when DME fraction increases, the injected DME absorbs more heat to vaporise so that the local temperature is reduced resulting in higher CO emissions. This hypothesis needs to be validated by the simulation of the combustion process or the in-cylinder optical investigations. With the increased CO emissions, the gross indicated efficiency is reduced due to the decrease of combustion efficiency as shown in Figure 4.17d.

Therefore, the best pilot DME fraction is 13% for this engine load (4.2 bar Net IMEP). Based on Bessionette's [60] theory, this optimal fraction could be changed with the engine load. In the following studies, the DME fuelling rate is fixed at 4.55 mg/cycle injected by SOI1 and/or SOI2 depends on the injection strategy, regardless of the total air fuel ratio and load. The author believes that if the DME fraction is appropriately adjusted with the lambda and load, the engine performance results would be better than the results presented in the following sections.

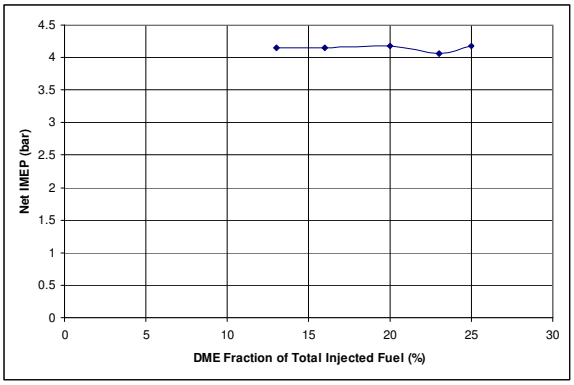

a) Net IMEP

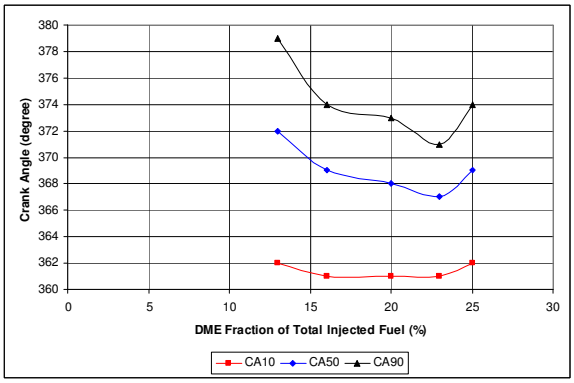

b) Combustion Phasing

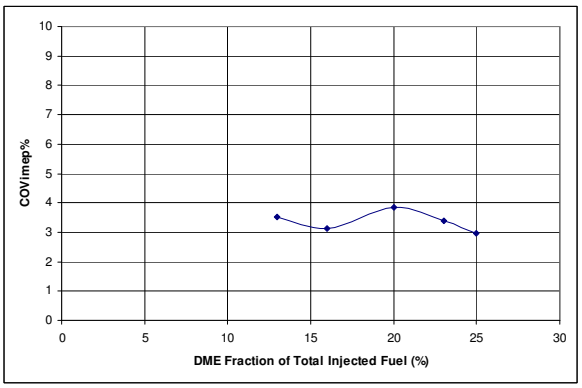

c) COVimep

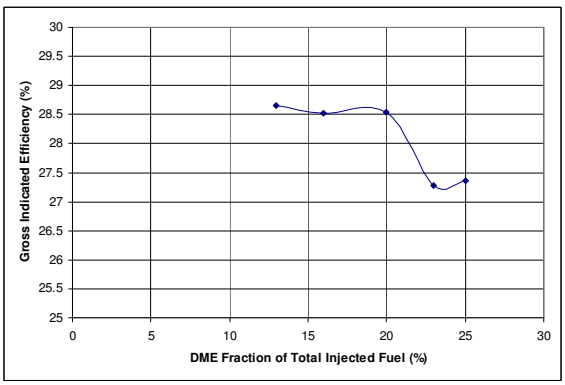

d) Gross Indicated Efficiency

Figure 4.17 Engine Performance as a Function of DME Fraction of Total Injected Fuel

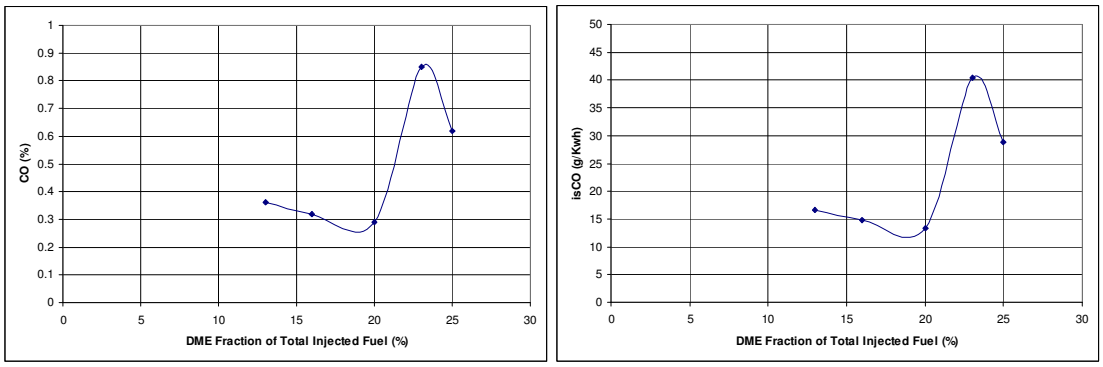

a) CO emissions

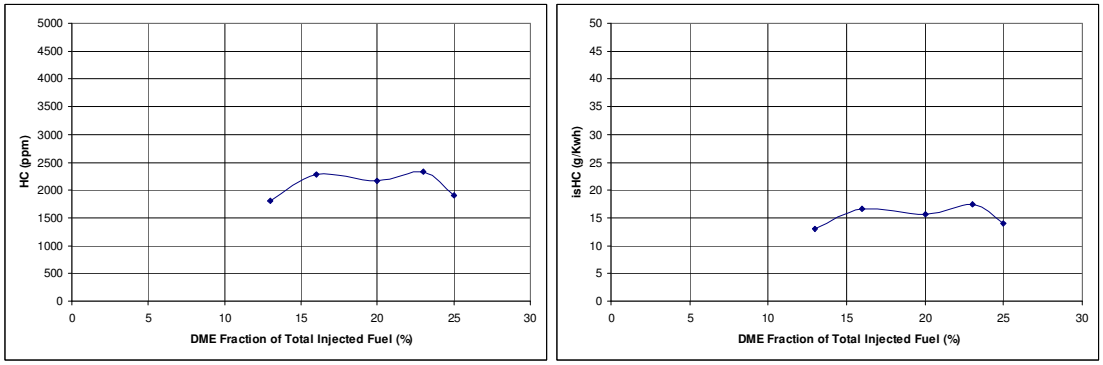

b) HC emissions

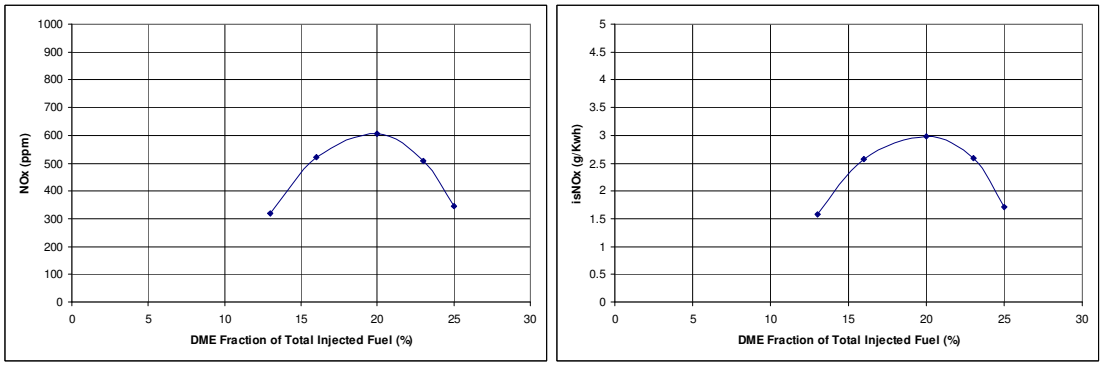

c) NOx emissions

Figure 4.18 Emissions as a Function of DME/Gasoline Ratio

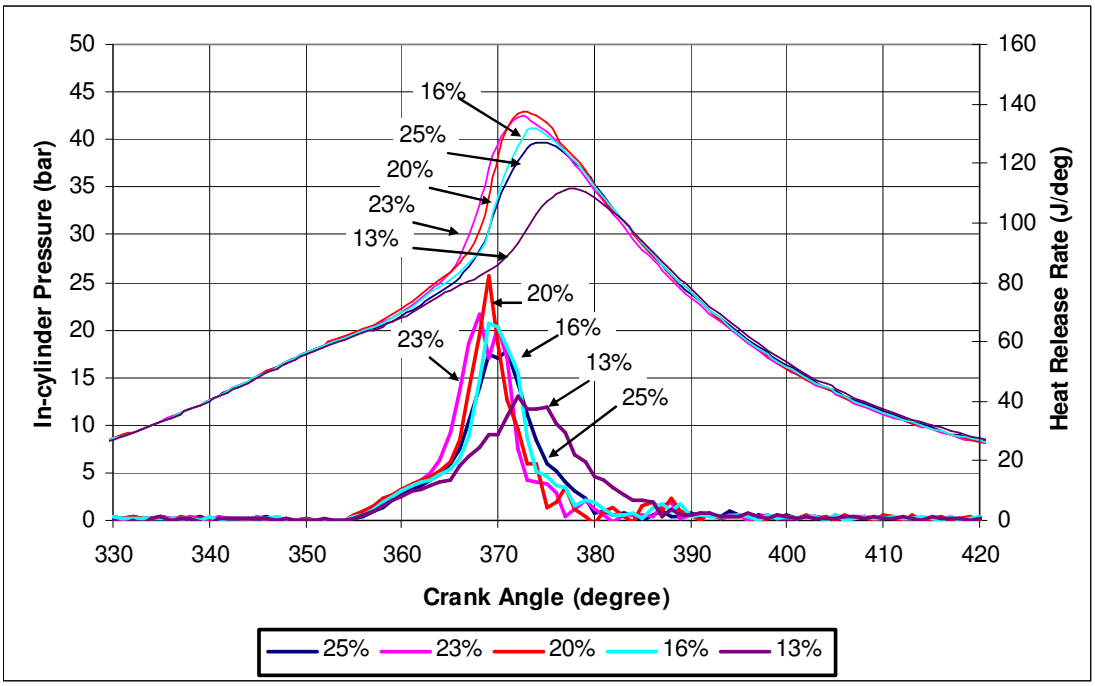

a) In-cylinder Pressure and Heat Release Rate

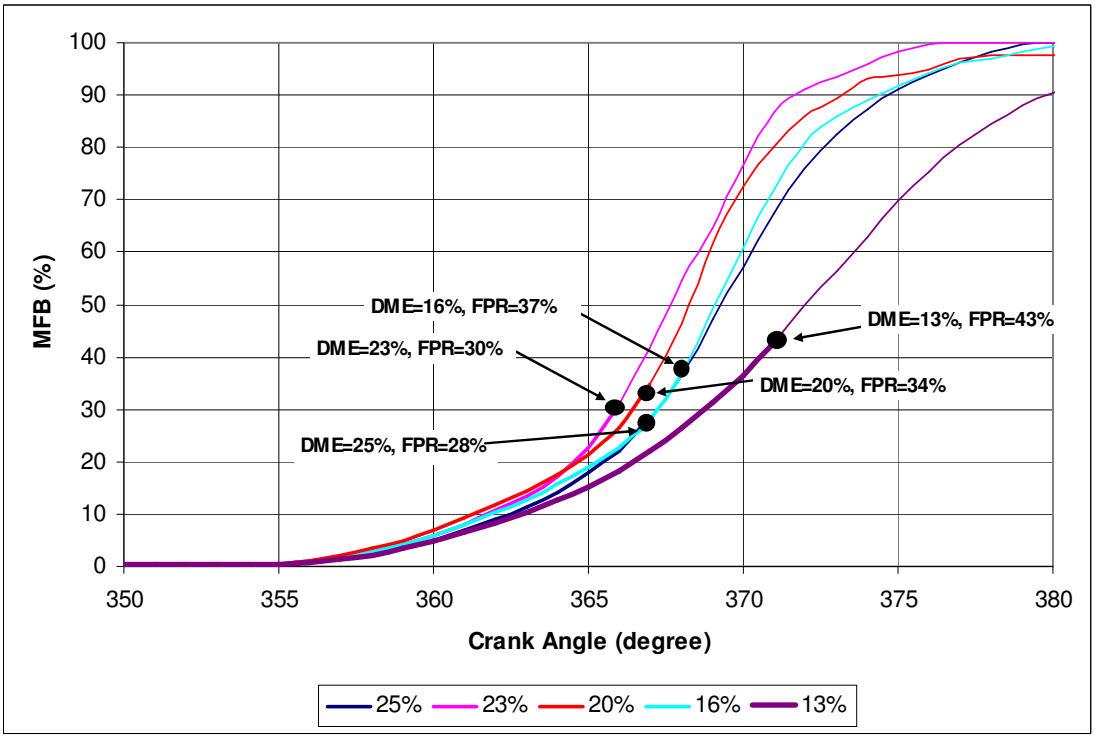

b) MFB Curve

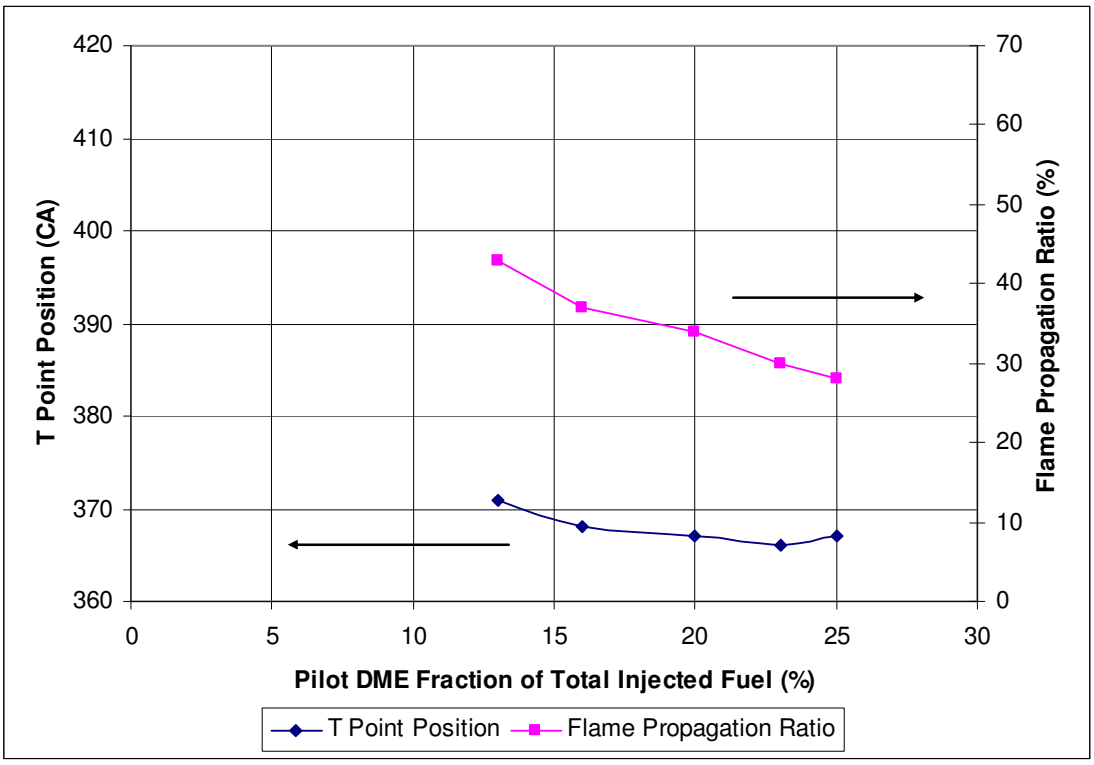

c) T Point Position and Flame Propagation Ratio

Figure 4.19 Heat Release Analyses as a Function of DME/Gasoline Ratio

4.4 Comparison of Single DME Injection Strategy and Split DME Injection Strategy

In order to compare the effect of a single DME injection strategy and split DME injection strategy, some additional tests were performed based on the studies presented in Section 4.3.4.

To apply the single injection strategy, the second DME injection was firstly removed from the split injection strategy and only the early DME injection was performed, which is recognized as Early Single Injection. In this case, it is found that the mixture could not be ignited because the trapped residual gas (iEGR=27%) did not provide enough thermal energy to initiate the ignition of the mixture. Then the first injection was removed so that the second DME injection was employed, which is considered as Late Single Injection Strategy. With the Late Single Injection Strategy, stable combustion was successfully achieved. In this case, the fraction of DME accounted for 9% of the total fuel supplied to the cylinder. The engine performance, emissions and heat release analysis for Late Single Injection Strategy are presented by Figures 4.20, 4.21 and 4.22 respectively together with the results obtained with 12% and 16% DME using split injections from the previous section.

When a single late injection strategy is applied, combustion is initialised by DME, which is characterized by a long-period of flame propagation combustion (Figure 4.20b). Compared to the split injection, the pressure rise rates are reduced and so is the heat release rate because of the slow flame propagation combustion. As a result, NOx emissions are extremely low due to the low in-cylinder temperature. In addition, CO and HC emissions are also low because of the longer heat release process, resulting in more thorough oxidation of products during the expansion stroke. However, combustion is less stable than the split injection case and the gross indicated efficiency is lower because of the lower IMEP value.

When split injection is applied, combustion starts earlier because of the shorter ignition delay due to the low temperature heat release of DME in the first injection. After the flame propagation process has started, the increasing in-cylinder pressure and temperature initiate the auto ignition combustion throughout the rest of air fuel mixture, hence the faster combustion than the single injection.

In conclusion, at this load, the hybrid combustion process realised by a split injection strategy achieves much better engine performance but slightly higher emissions than the flame propagation combustion process with a single injection strategy.

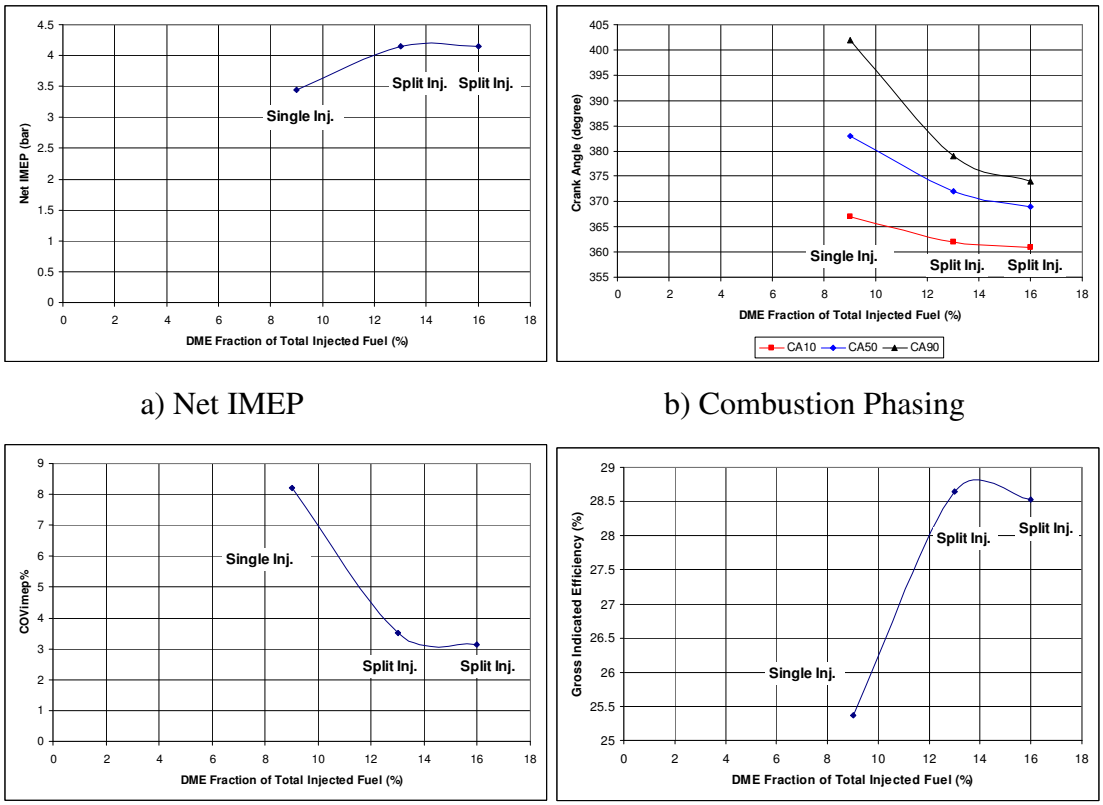

a) Net IMEP

b) Combustion Phasing

c) COVimep

d) Gross Indicated Efficiency

Figure 4.20 Engine Performances of Single and Split Injection Strategies

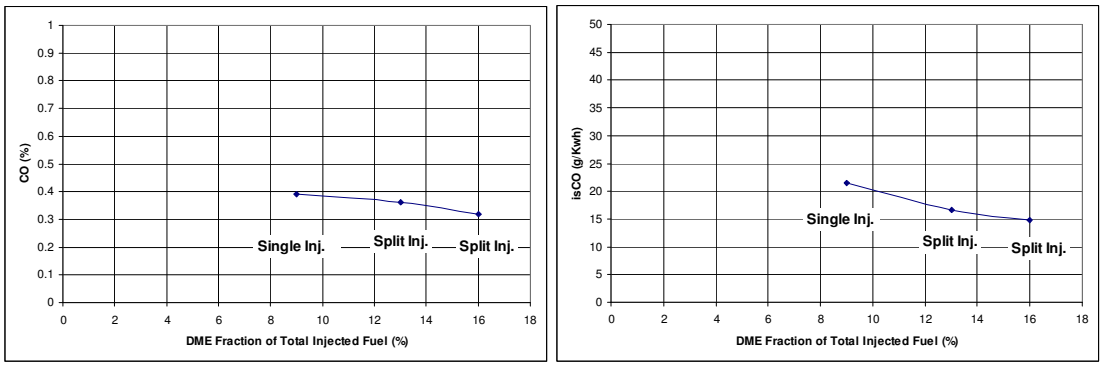

a) CO emissions

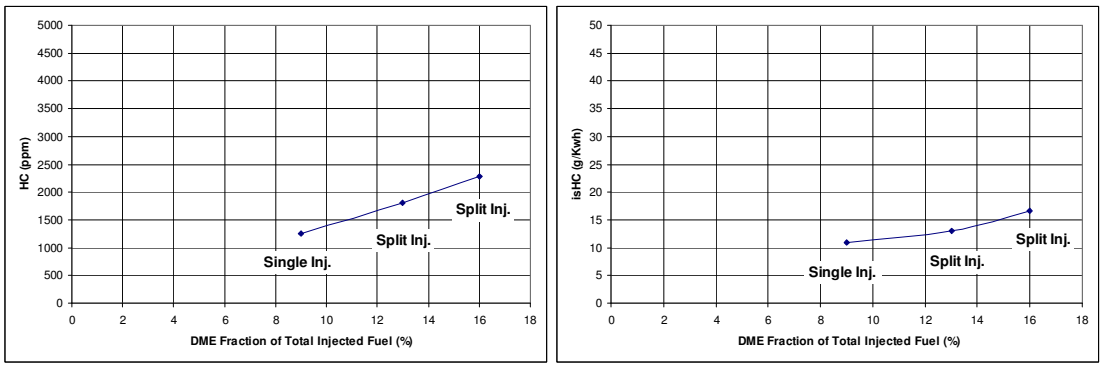

b) HC emissions

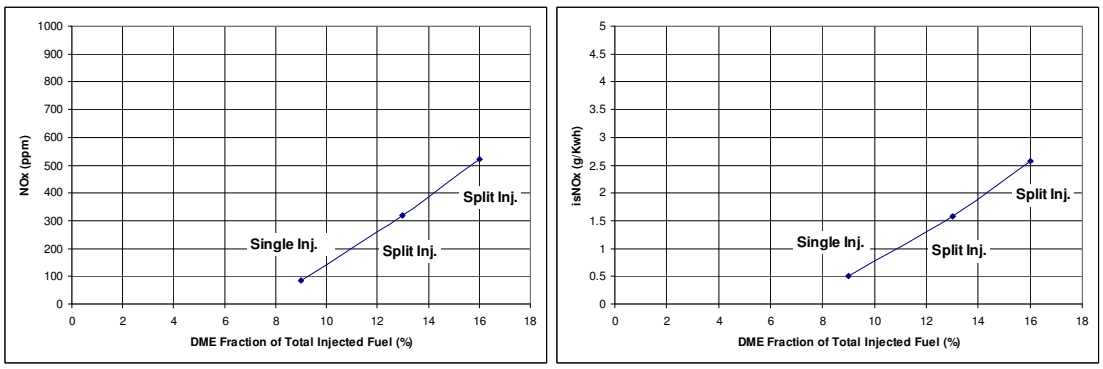

c) NOx emissions

Figure 4.21 Emissions of Single and Split Injection Strategies

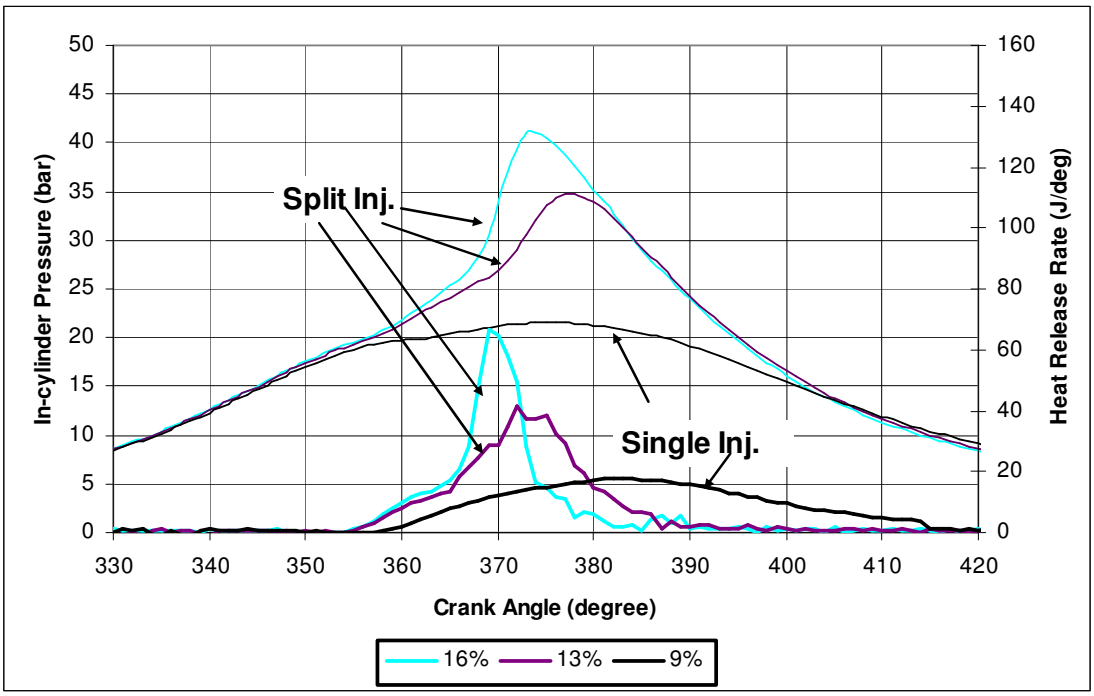

a) In-cylinder Pressure and Heat Release Rate

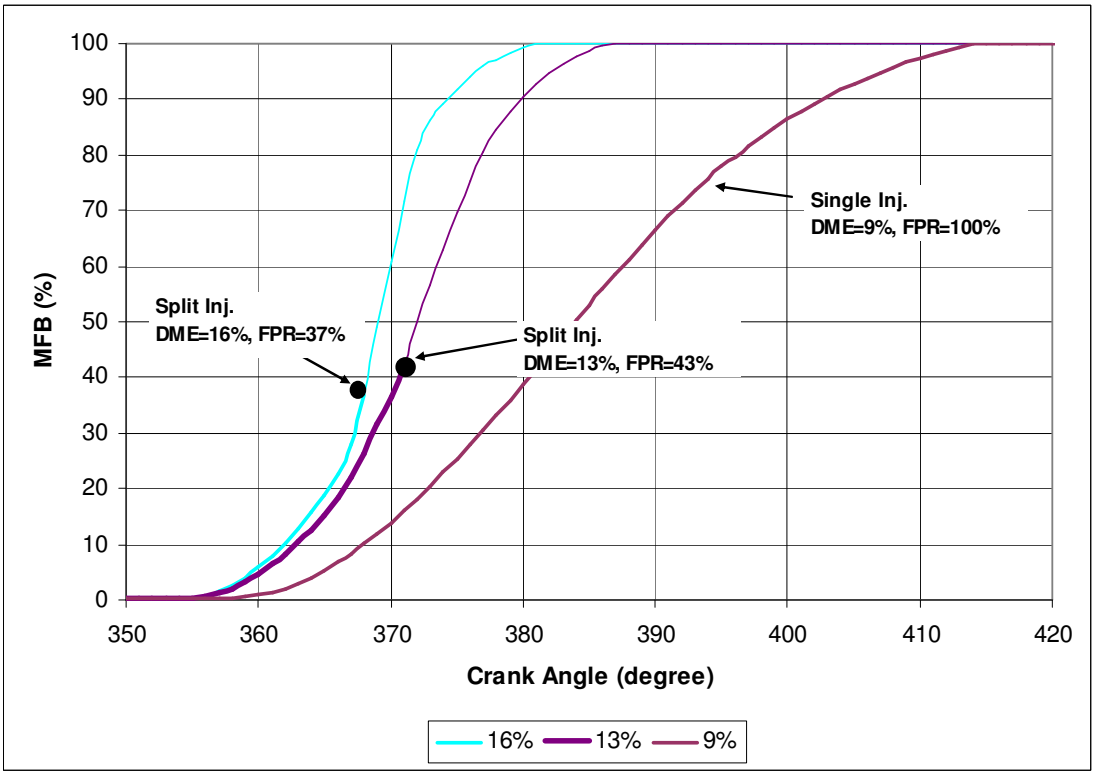

b) MFB Curve

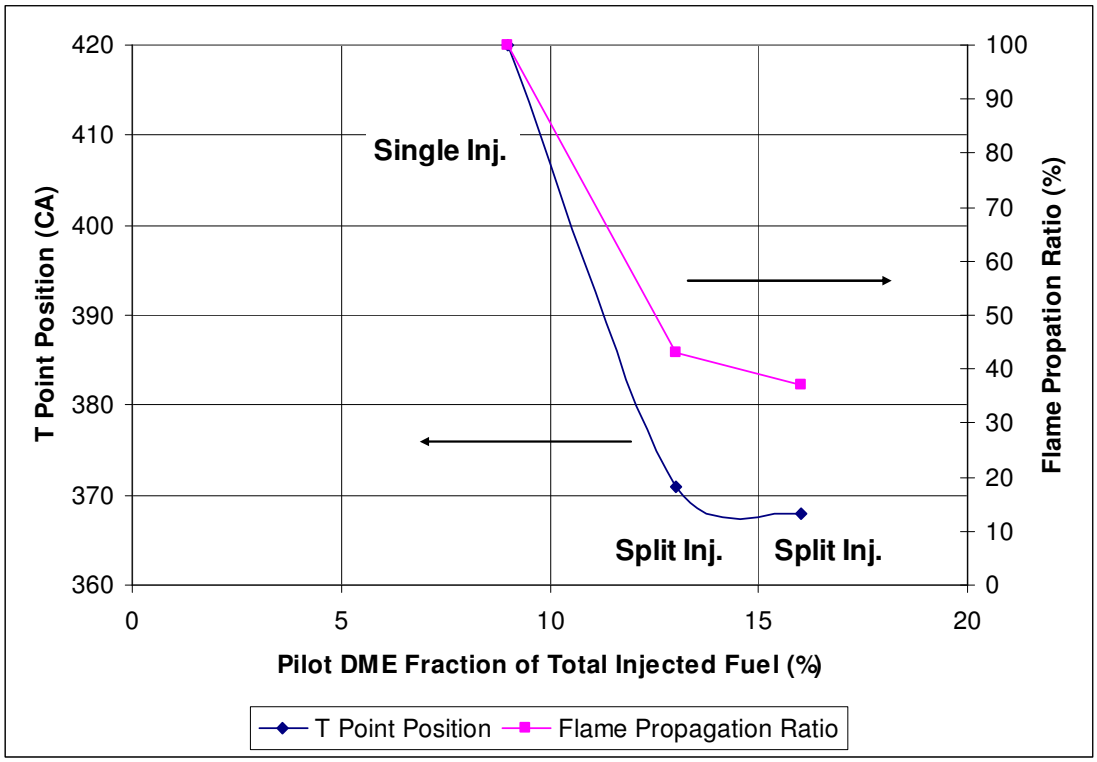

c) T Point Position and Flame Propagation Ratio

Figure 4.22 Heat Release Analyses as a Function of DME/Gasoline Ratio

Chapter 5

Characterisation of Controlled Auto-ignition Combustion by Positive Valve Overlap and Exhaust Back Pressure

Chapter 5 Characterisation of Controlled Auto-ignition Combustion by Positive Valve Overlap and Exhaust Back Pressure

5.1 Introduction

In Chapter 4, results of the effects of injection timing and DME injection strategies were presented on combustion performance and emissions in order to determine the appropriate DME injection strategies and engine operating parameters for CAI combustion. In this chapter, the first section will present the limits and range of CAI operation using a Split DME Injection strategy. Then the work to extend the operation range is discussed by applying a Late Single DME Injection and an Early Single DME Injection in a high load boundary and a low load boundary respectively. The engine performance, emissions and heat release analysis are then presented and analysed throughout the complete CAI operation map. Finally, conventional SI combustion under a specific condition is presented and compared with this new concept.

5.2 Knocking, Partial Burn and Misfire Boundaries of Split DME Injection Strategy

The operation parameters utilised are shown in Table 5.1.

Table 5.1 Engine Operation Conditions for the Split DME Injection Strategy

Parameter	Value
Injection Strategy	Split Injection
DME SOI1 Timing (°CA)	290
DME SOI1 Duration (ms/°CA)	1.12/10.8
Mass of DME SOI1 (mg/cycle)	2.55
DME SOI2 Timing (°CA)	MBT
DME SOI2 Duration (ms/°CA)	0.98 / 9
Mass of DME SOI2 (mg/cycle)	2

The injection timing and the amount of DME in the first injection were fixed. So was the amount of the second DME injection. However, the timing of the second DME injection was varied and then set to the MBT timing at each condition in order to achieve maximum power output.

Firstly, the tests started at mid load with iEGR= 27%. In order to determine the high load boundary, the iEGR rate was reduced by lowering the exhaust back pressure and the load increased until knocking combustion occurred. In contrast, for the low load boundary, the iEGR rate was raised by increasing exhaust back pressure so that the load decreased until the mixture failed to ignite, i.e. misfire. At each selected iEGR rate, the tests began with stoichiometric total air/fuel mixture and then the mixture was made lean by reducing the quantity of PFI gasoline.

The maximum load using a Split Injection Strategy is limited by the appearance of knocking combustion as shown in Figure 5.1. As mentioned in Section 3.5.4, the percentage of $(dP/dCA)_{max}$>5 bar/deg cycles for 100 cycles is used as a criterion to evaluate the extent of knocking combustion. If over 50% of 100 cycles have $(dP/dCA)_{max}$>5 bar/deg, the test point is identified as unacceptable knocking combustion, which should be avoided. When the iEGR rate is less than 20% and total λ<1.2, knocking combustion can not be avoided even though the DME SOI2 timing is retarded. If the SOI2 timing is further retarded, the engine will misfire. It also can be seen that within the knocking combustion region, the extent of knocking increases as the total air/fuel ratio is nearer stoichiometry as well as reducing the iEGR. At any point of the knocking boundary, either increasing iEGR rate or reducing total λ are likely to slow combustion so that knocking combustion is avoided. The knocking boundary defines the highest load that the engine can possible achieve.

The fundamental of presence of knocking combustion is similar to the knocking combustion in SI combustion. When the second quantity of DME is injected near TDC, it auto-ignited to form a flame kernel from which the flame front expands to the rest of the cylinder. This process will compress the unburned gas mixture ahead of the flame front and significantly raise the pressure as well as temperature in the combustion chamber. Since the iEGR rate is low at high load, there is not sufficient residual gas to slow down the heat released rate associated with the spontaneous reactions of the unburned mixture. As a result, a pressure wave forms and traverses from the end gas region to the rest of the

chamber and reflects off the chamber wall travelling back to the end gas region. Therefore, the pressure wave leads to engine vibration that manifests as the combustion noise. However, outside the knocking region, although similar combustion processes take place, the heat release rate of the auto-ignition is modulated by the greater amount of burned gas present.

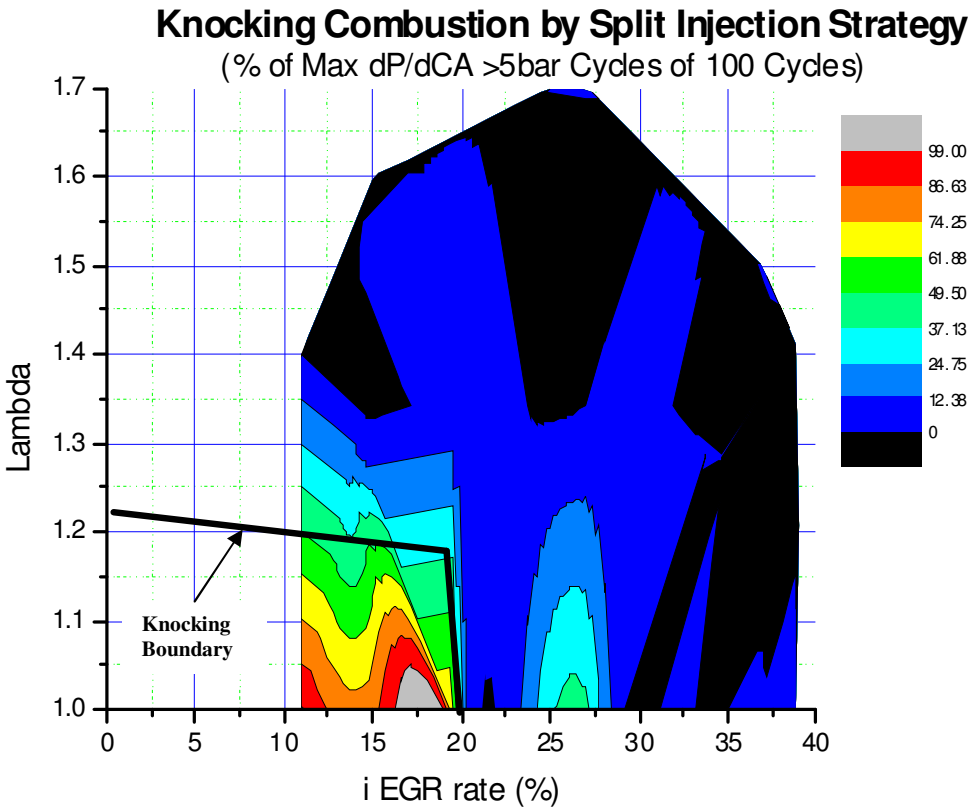

Figure 5.1 Knocking Combustion Determination by Split Injection Strategy

COVimep as a function of iEGR rate and lambda is shown in Figure 5.2 and is used to indicate the combustion stability. Unstable combustion is recognized when COVimep is over 10% as shown in the upper and right region. The upper boundary and the right boundary are distinguished as partial burn boundary and misfire boundary respectively in previous research [98].

The misfire boundary is approached when iEGR rate rises beyond 37% with either rich or lean mixture. At higher EGR rates, the ignition timing is retarded with the increased amount of trapped CO_2 and H_2O, which causes the mixture fail to be ignited in a small proportion of cycles. The unburned charge from the misfire cycle is recycled internally due

to internal EGR strategy and burned with the fresh charge in the next cycle. Thus, the trapped residual gas is made up by either fully burned or unburned gases during the engine operation resulting in a cyclically variable air fuel mixture when mixed with fresh charge. As a result, the engine performance exhibits large oscillations under these conditions. In addition, if the iEGR rate further increases, the engine is unlikely to be ignited because the concentration of residual gas is so high that the flame initiated by the DME from the second injection is unable to sustain and propagate. Thus, the premixed DME from the early injection can not reach the ignition conditions and is unable to activate auto ignition of the gasoline. The engine is totally unfired under these conditions.

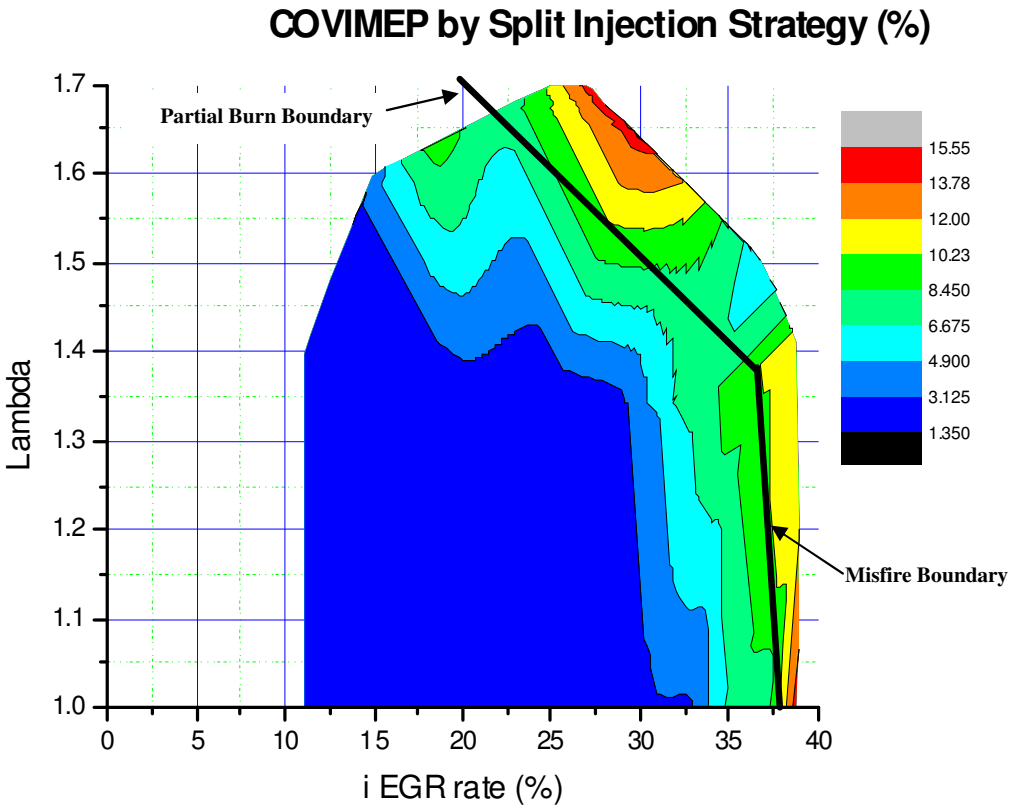

Figure 5.2 COVimep as a Function of iEGR Rate and Lambda

The reduced fuelling rate with increased lambda induces the presence of partial burn boundary when iEGR rate is between 23%-37%. The less residual gas is trapped, the leaner mixture can be for a given amount of fuel. Although unstable combustion is also detected, the differences in principles between the partial burn region and the misfire region are significant. Firstly, in the partial burn region, misfire never occurs. This is because DME is so flammable that the engine can be operated in an extremely lean mixture and the

combustion initiation is not greatly affected when more fresh air is induced. Secondly, in the partial burn region, unburned HC emissions are higher than they are in the misfire region as shown in Figure 5.3. As the mixture goes lean, less fuel is injected and used to heat up the same amount of the air during the combustion process. Therefore, it is difficult to fully complete the fuel oxidation due to the low combustion temperature. As a result, some partially burned products would present in the exhaust stream which exhibits higher uHC emission levels. Oakley [3] defined this boundary when the volumetric concentration of uHC rises to more than 5000 ppm. However, differing to his research with external EGR, the EGR is cycled internally in this study and the average uHC level in the partial burn region is extensively lower than Oakley's results. The external EGR gas is cooled when it is cycled outside the engine. Its heat capacity effect and dilution effect are the major effects on the combustion process to prevent engine from knocking according to Zhao [65]. However, if iEGR is applied, high temperature exhaust gas is recycled due to less heat loss and its charge heating effect becomes dominant amongst all the effects mentioned in Chapter 2. Therefore, the oxidation of the products is more completed resulting in relatively lower uHC emissions.

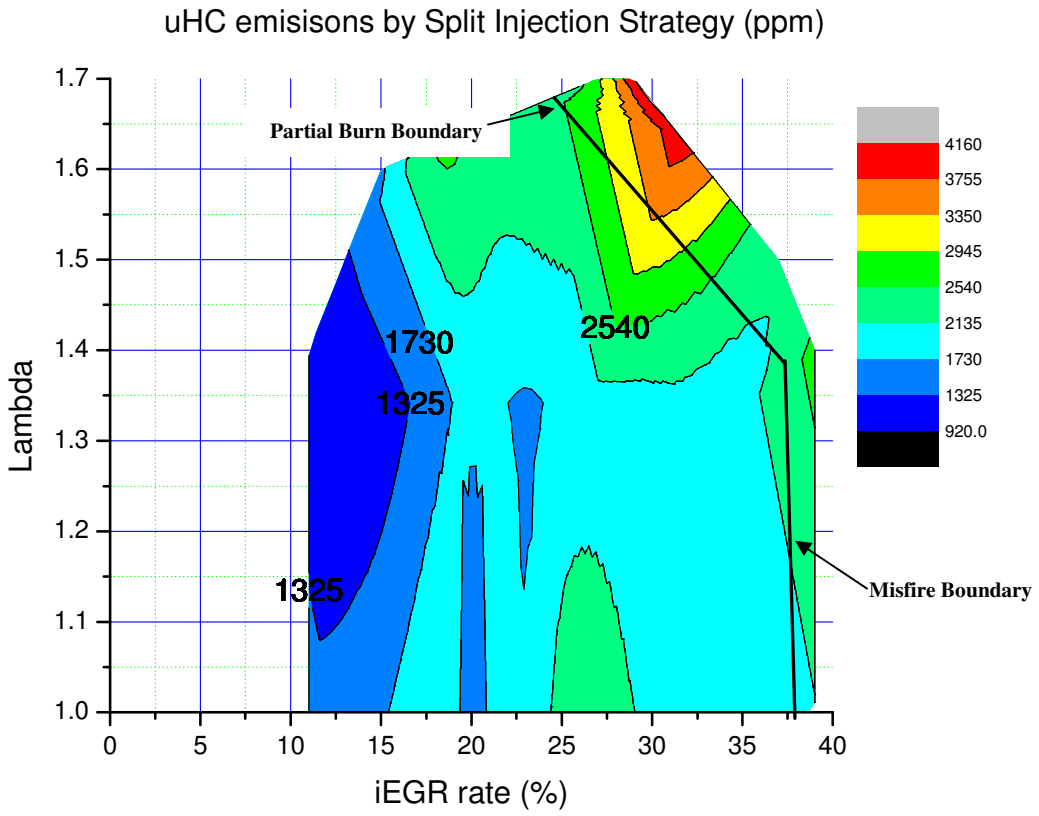

Figure 5.3 uHC Emission as a Function of iEGR Rate and Lambda

Therefore, limited by knocking boundary, misfire boundary and partial burn boundary, the working range map by Split Injection Strategy is presented in Figure 5.4.

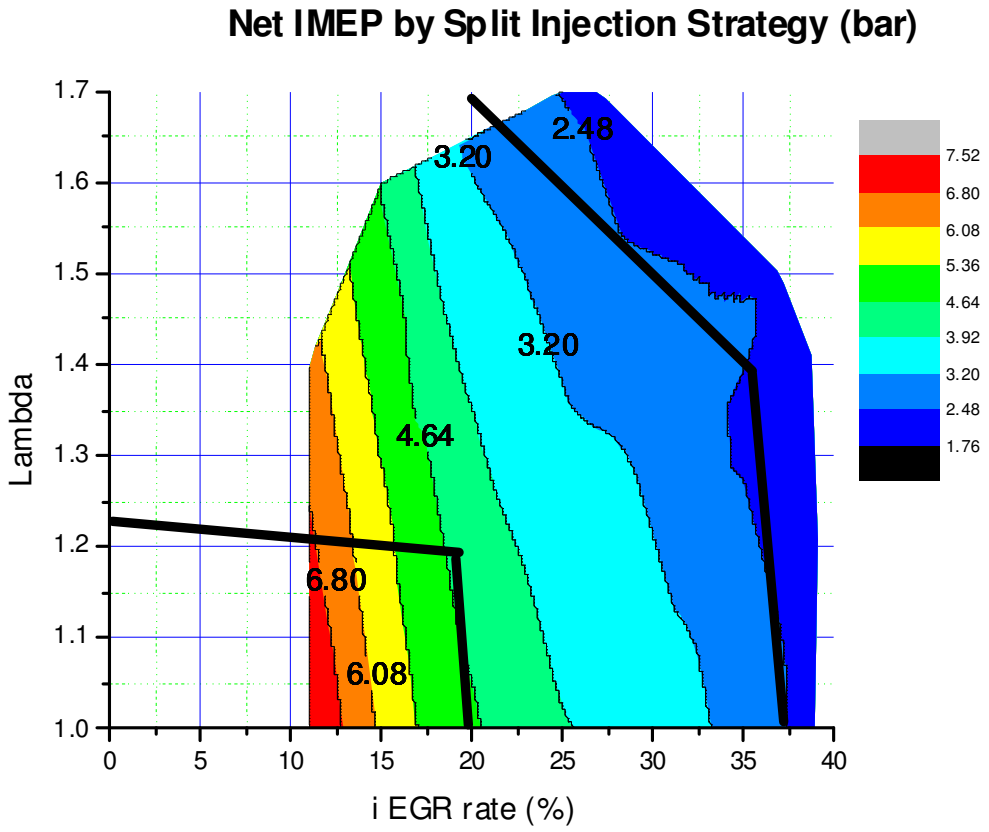

Figure 5.4 Net IMEP Range by Split Injection Strategy

5.3 Extension of CAI Combustion by Different DME Injection Strategies

5.3.1 DME Injection Strategies

In order to extend the IMEP range and avoid the abnormal combustion, three injection strategies were tried and tested as follows.

1) To extend the high load border and avoid knocking, '**Late Single DME Injection Strategy**' in Figure 5.5 is applied when iEGR rate is lower than 13% with the load is higher than 6 bar net IMEP, as well as under condition of λ=1 and λ=1.1 when 13%<iEGR< 18%. The combustion is characterised as fame propagation initiated by the injected DME near TDC.

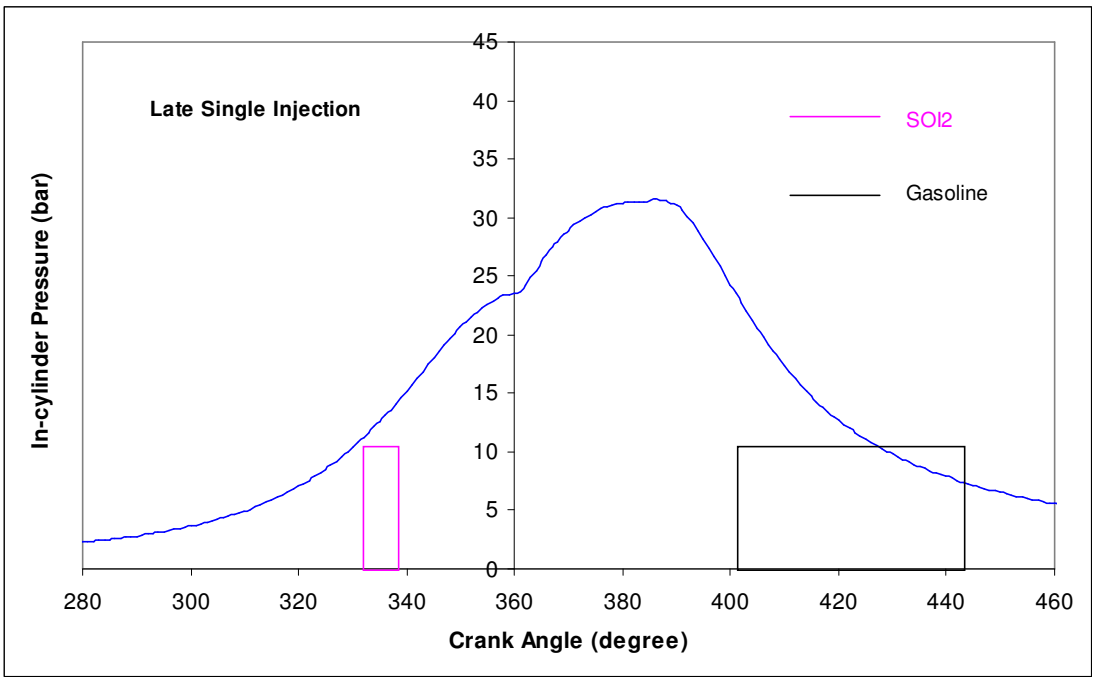

Figure 5.5 Late Single DME Injection Strategy

2) '**Split DME Injection Strategy**' in Figure 5.6 is applied when iEGR is between 13% and 37% with load varying from 6 to 2.5 bar net IMEP as discussed in the previous section. Both SOI1 and SOI2 are applied and hybrid combustion of flame propagation and auto ignition is implemented in this area.

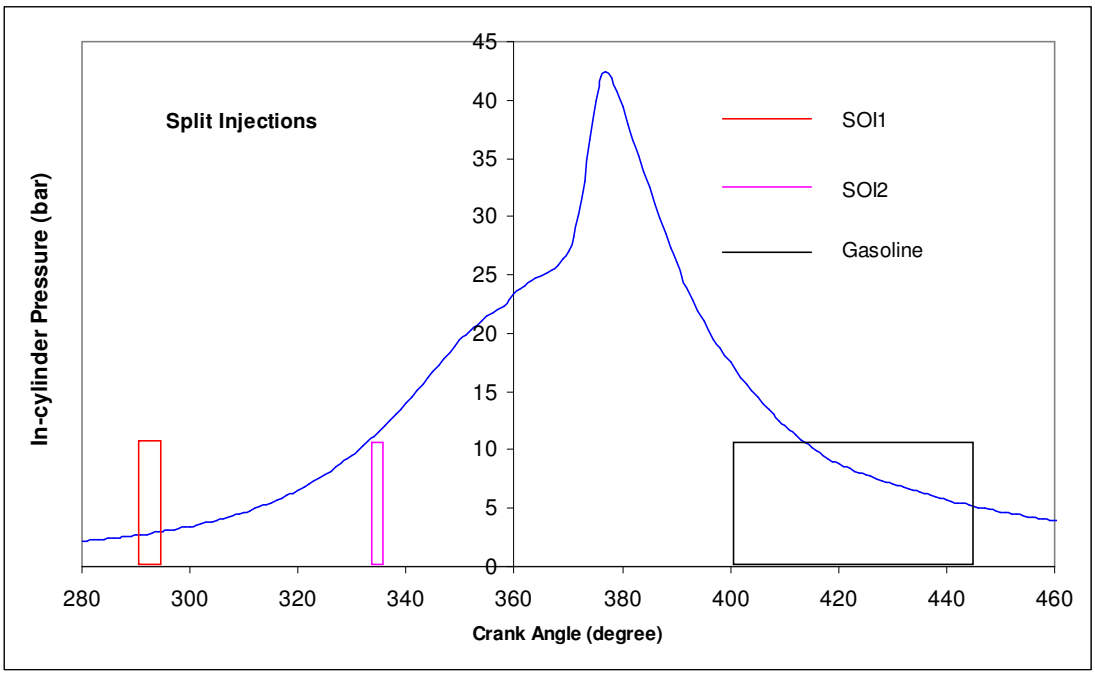

Figure 5.6 Split DME Injection Strategy

3) To extend the lower load border and avoid partial burn and misfire, '**Early Single DME Injection Strategy**' is applied in Figure 5.7 when iEGR is higher than 37% with the load lower than 2.5 bar net IMEP, as well as under leaner mixture when 27%<iEGR< 37%. Auto-ignition combustion is the only heat release mode within this region.

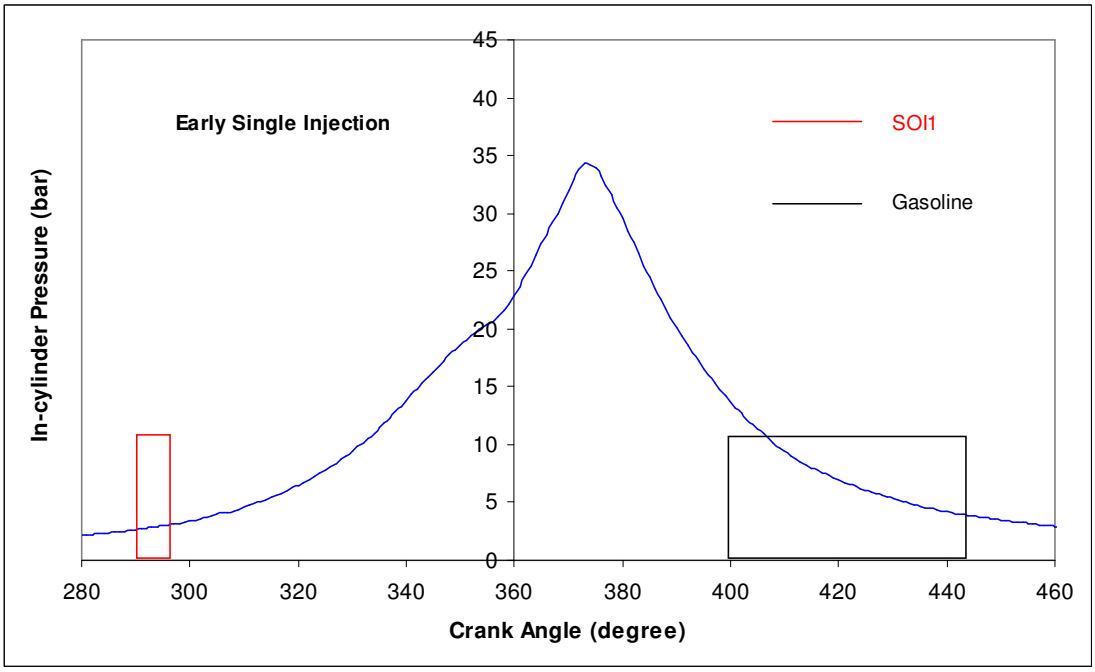

Figure 5.7 Early Single DME Injection Strategy

5.3.2 Characteristics of Three Injection Strategies

Figures 5.8-5.13 show the in-cylinder pressure and heat release characteristics of the above three combustion modes.

The ‘Early Single Injection’ mode is characterised with fast combustion and fast heat release rate. Since higher exhaust back pressure is applied to achieve high iEGR, the in-cylinder pressure is extremely high during the exhaust stroke. The inflexion point (T point) of the MFB graph does not appear due to the entire auto ignition combustion process.

In the ‘Split Injection’ mode, the heat release is shown to take two forms, a slow heat release process and a fast heat release process. In-cylinder pressure suddenly increases in the middle of the combustion resulting in significant peak heat release rate. Hybrid combustion happens in this mode. The T point, as defined in Chapter 3, can indicate the start timing of auto ignition and the fraction of each of combustion process.

In the ‘Late Single Injection’ mode, slow combustion with a long heat release process is shown in the diagrams. Since both of intake and exhaust throttling are minimised in this case, the pumping work is minimum compared to the other modes. The T point is also unable to be identified, which indicates that flame propagation only exists in these combustion processes.

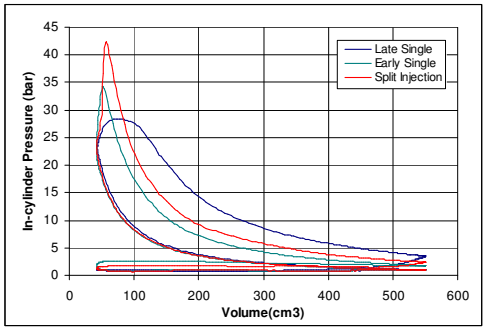

Figure 5.8 Full P-V Diagram of Three Combustion Modes

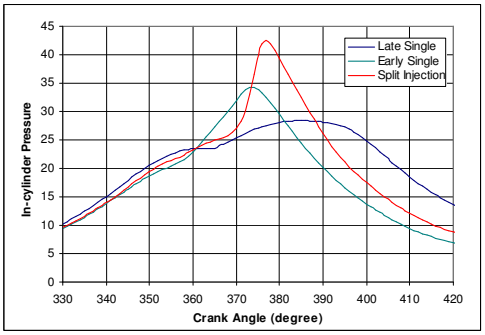

Figure 5.11 Pressure Traces of Three Combustion Modes

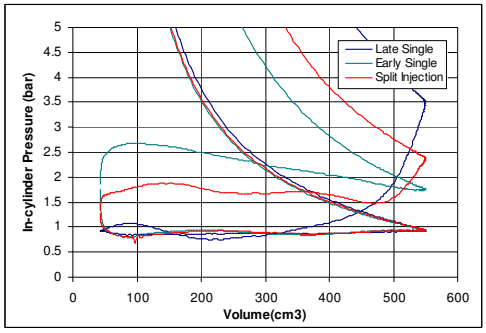

Figure 5.9 Partial P-V Diagram of Three Combustion Modes

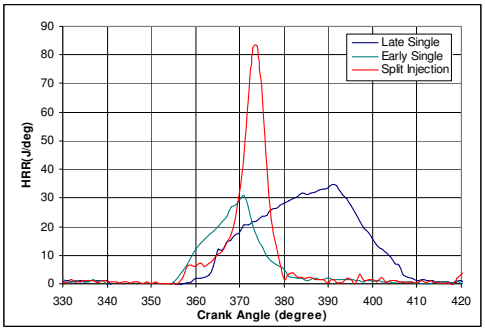

Figure 5.12 Heat Release Rate Diagrams of Three Combustion Modes

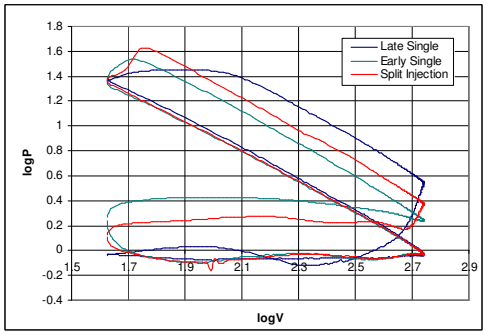

Figure 5.10 logP-logV Diagram of Three Combustion Modes

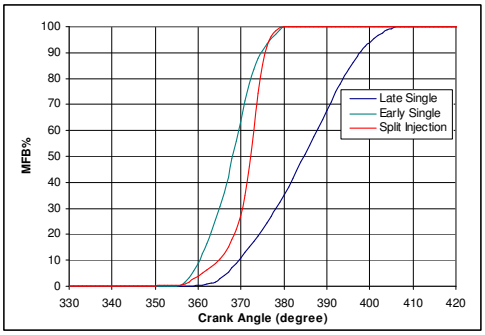

Figure 5.13 MFB Curves of Three Combustion Modes

5.4 Engine Performance over the Extended CAI Operational Range

5.4.1 Net IMEP

Figure 5.14 presents the contours of net IMEP values as a function of iEGR rate and total λ. As the throttle is fully open, the engine outputs are determined by the amount of trapped residual gas and lambda. As expected, the loads are reduced gradually as more iEGR is introduced. Furthermore, for a constant iEGR rate, the net IMEP increases when the lambda value is reduced in most of the operating region. However, at the operating conditions near the border of strategy change between Late Single Injection and Split Injection, the effects of lambda are not evident. This is because the later DME injection can be more advanced with leaner mixture without knocking combustion happening. Thus, the net IMEP is seen to be hardly changed since the mixture goes lean for a constant iEGR rate under this condition. In contrast, as the lambda value decreases and the mixture becomes richer, the single DME injection timing is limited by the occurrence of knocking combustion.

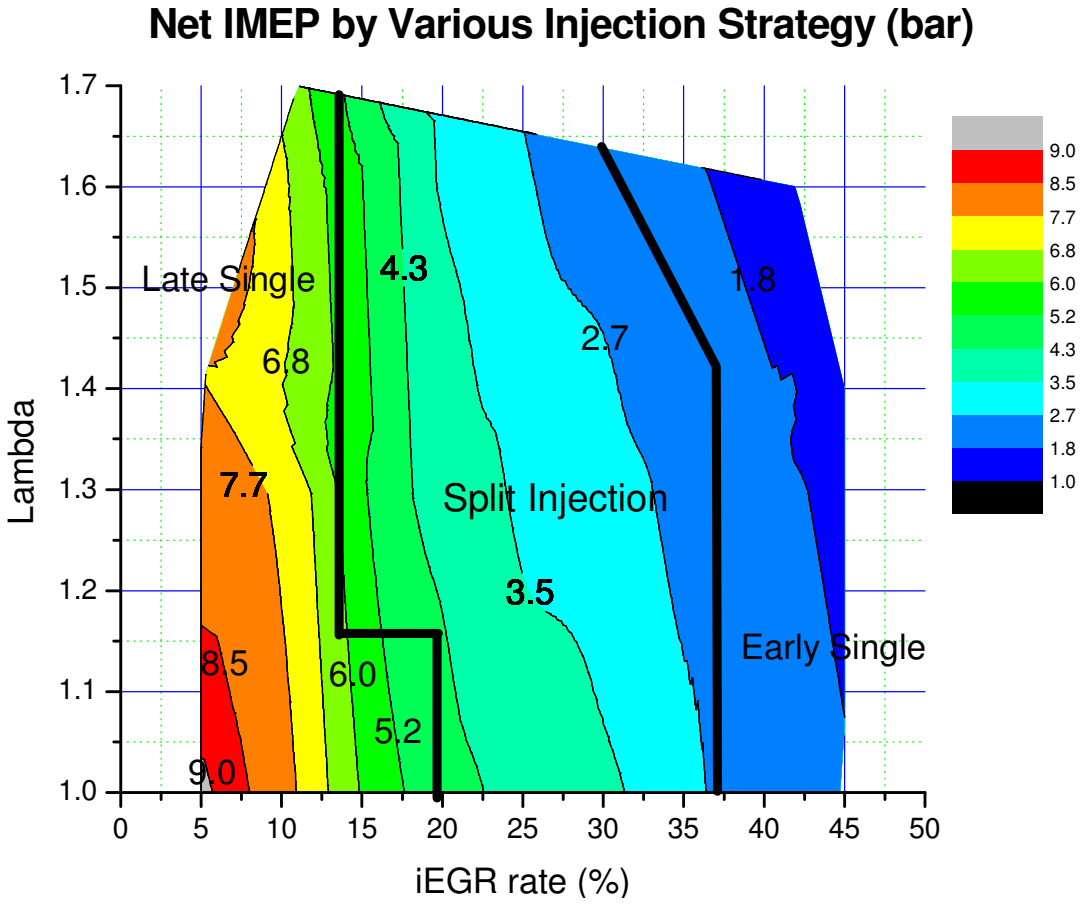

a)

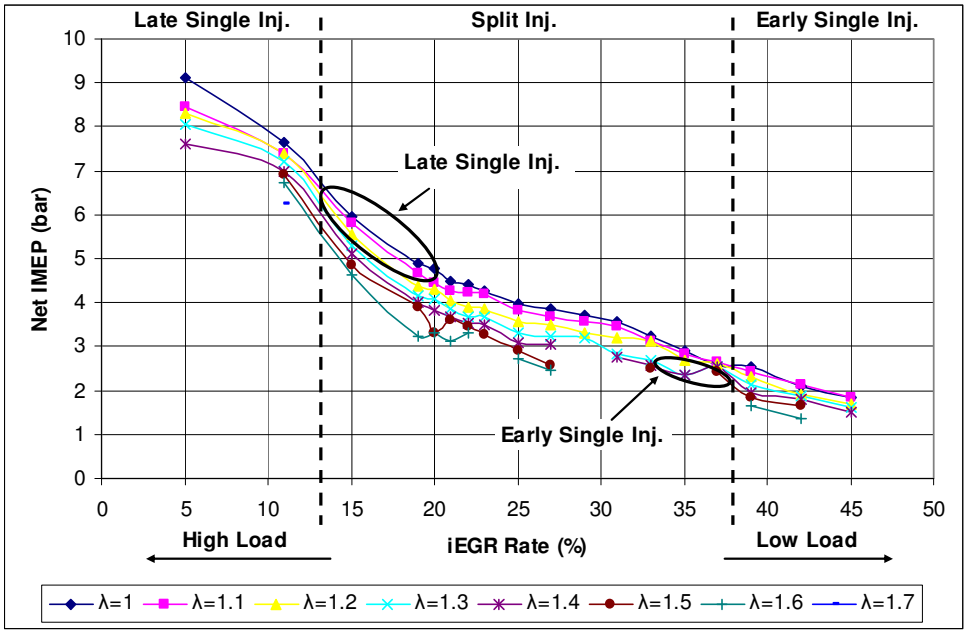

b)

Figure 5.14 Net IMEP as a Function of iEGR Rate and Total Lambda

The maximum IMEP of 9.1 bar is achieved under the stoichiometric condition and at the minimum iEGR rate of 5%. This is almost 2.5 times higher than the maximum load attained by previous studies [98] (3.8 bar) with pure CAI combustion initiated by external EGR and intake air heating. Furthermore, it is also higher than the attainable maximum IMEP of 7.3 bar through SI combustion with WOT. This is because under the condition of CR=13, iEGR rate=5% and WOT in SI combustion, the occurrence of knocking combustion limits the SI timing to TDC or even after TDC. The late ignition timing and combustion phasing would result in low IMEP and sometimes unstable and partial combustion.

Although the combustion modes of both spark ignition and late single DME injection ignition are flame propagation, the 'flame' itself can be significantly different. The previous optical researches on conventional SI combustion and CI (DME) combustion can be used to explain the flame differences.

Under SI combustion, the ignition source is the spark plug. Following spark discharge, the flame starts with a small flame core after a short time of time delay, and continues to grow and propagate across the combustion chamber. In the other word, the flame starts and propagates from a point at a relatively slow speed. Under high load operations, the

unburned mixture ahead of the flame front will have more time to auto-ignite, resulting in knocking combustion.

However, the combustion process of CI (DME) combustion is different. Konno et al. [109] studied spray behaviour and the in-cylinder combustion characteristics of DME using an optical DME CI engine. The direct injected DME evaporates rapidly after injection, and penetrates and spreads across the combustion chamber. The ignition starts in the downstream part of the DME spray rather than the region near the nozzle, shown in Figure 5.15 [109]. (This is because the latent heat of evaporation of DME reduces the temperature near the injector nozzle.) The flame then rapidly propagates across the combustion chamber.

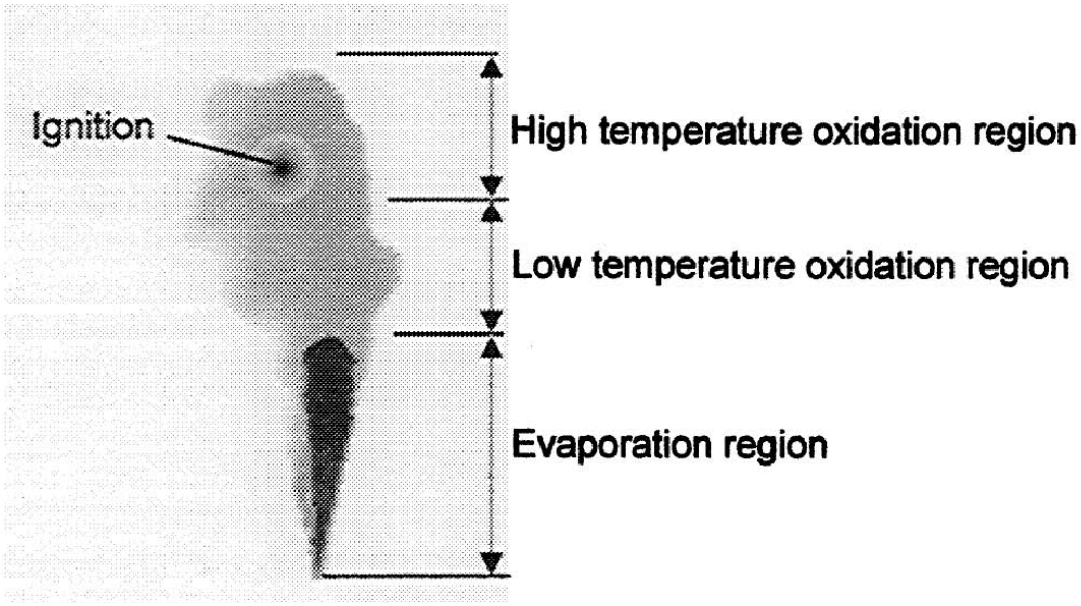

Figure 5.15 Schematic Sketch of DME Spray [109]

Under Late Single DME Injection Strategy of this study, the single injection of DME is the ignition source and injected into the homogeneous air/gasoline mixture. Since the ignition could take place at multiple sites, from which flame propagation would follow, the overall burning rate of the in-cylinder charge would be much faster than that of SI combustion. Hence, there would be less time for the end gas to auto-ignite.

The differences between Late DME Injection and SI can be demonstrated by the heat release rate and MFB curves shown in Figure 5.16 and 5.17 while Table 5.2 states the test conditions and results of higher load operation via these two combustion modes.

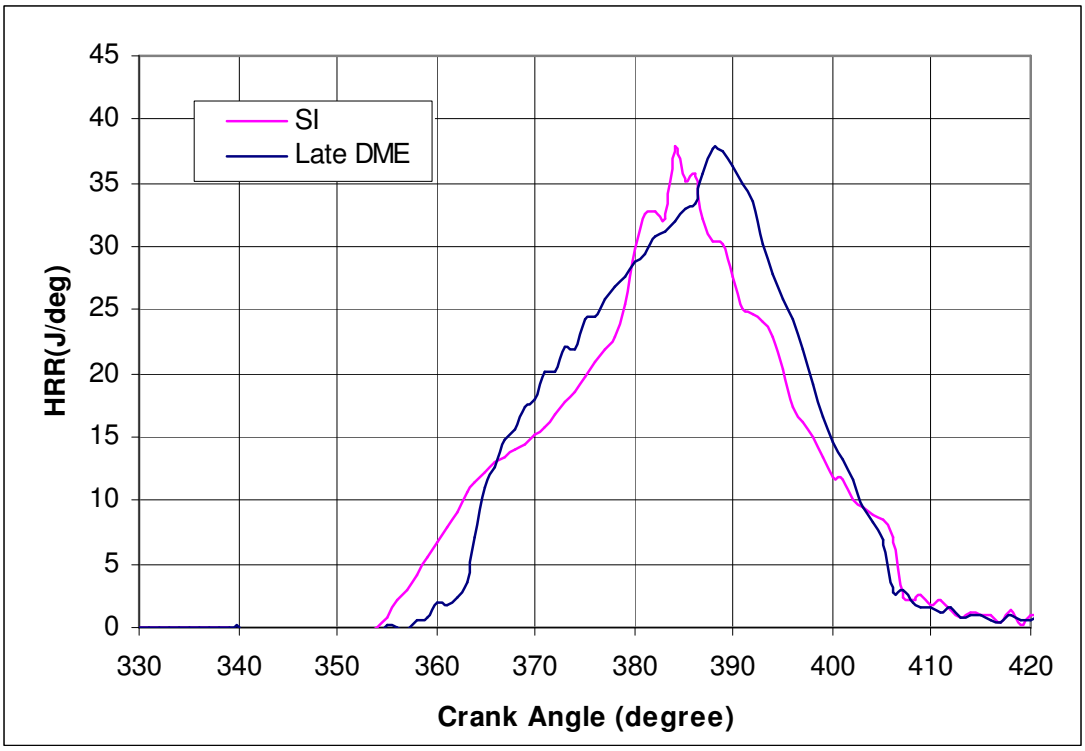

Figure 5.16 Heat Release Rate of SI and Late DME Injection Combustion

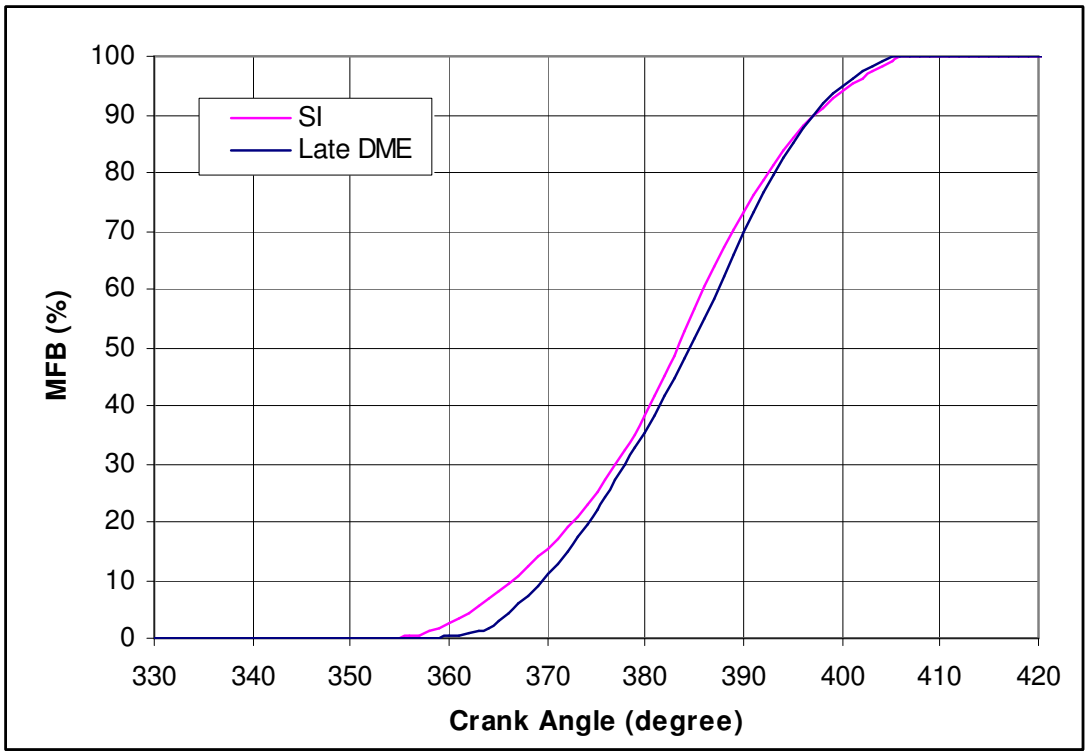

Figure 5.17 Mass Burned Fraction of SI and Late DME Injection Combustion

Table 5.2 Test conditions and Results of Higher Load Operation by SI and Late DME Injection

Parameters	SI	Late DME
Geometric Compression Ratio	13	13
Effective Compression Ratio	12.92	12.92
Lambda	1	1
Intake Throttle Opening (°)	WOT	WOT
SI or SOI2 Timing (CA degree)	**347**	**342**
COVimep (%)	4.59	2.90
Fuel MEP (bar)	27.34	27.7
Gross IMEP (bar)	**7.57**	**7.87**
Net IMEP (bar)	7.28	7.60
Pumping MEP (bar)	0.29	0.27
Combustion Eff (%)	96.37	96.69
Gross Indicated Eff (%)	**27.7**	**28.4**
Net Indicated Eff (%)	26.6	27.43
Thermal Eff (%)	28.74	29.37
CA10 (degree)	**366**	**369**
CA50 (degree)	383	384
CA90 (degree)	397	397
CA10-90 (degree)	**31**	**28**
CO (%)	0.33	0.35
uHC (ppm)	1578	1293
NOx (ppm)	2503	2087

The Single Late DME Injection combustion is characterised with faster heat release rate at the start and end of the combustion process than SI combustion, resulting in shorter CA10-90. As a result, the Late DME Injection combustion performs higher gross output in the same fuelling rate, corresponding to higher gross indicated efficiency. Although the Late DME Injection timing is more advanced than SI timing in these two cases, the Late DME

Injection combustion starts later than SI mode, due to the ignition delay of Late DME Injection.

The CO emissions of these two modes are similar. However, both uHC and NOx emissions of Late DME Injection combustion are lower than SI combustion. This is because the oxygen contained DME performs better combustion quality and lower combustion temperature than SI combustion respectively.

It should be noted that in order to achieve the highest load, the positive valve overlap was changed to 24 °CA in order to minimise the iEGR rate at iEGR=5%. The valve timing is as follows (Table 5.3 and Figure 5.18):

Table 5.3 Valve Timing for Minimum iEGR Rate (24 °CA overlap)

Valve Timing (24 °CA overlap)	IVO	12 BTDC of intake
	IVC	212 ATDC of intake
	EVO	205 BTDC of intake
	EVC	12 ATDC of intake

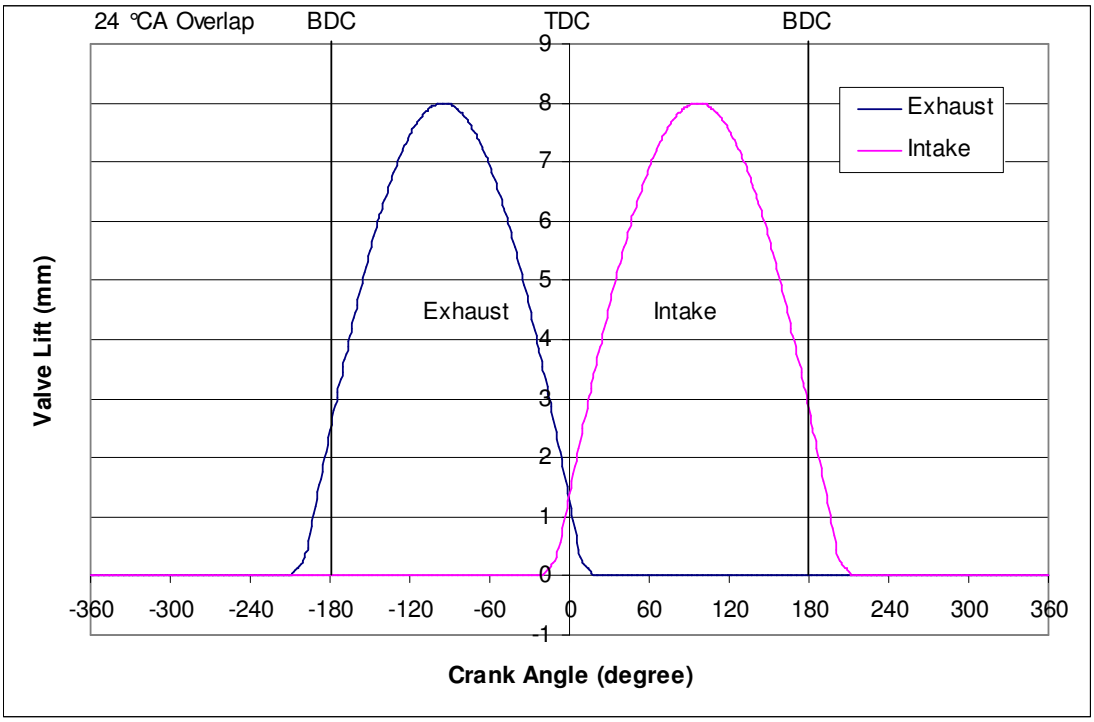

Figure 5.18 Positive Valve Overlap Valve Timing (24 °CA Overlap)

Minimum output is 1.35 bar net IMEP and it occurs when the engine is operated under the condition of maximum iEGR rate and the leanest mixture. This minimum value could be lower if iEGR rate was further increased and DME quantity fraction of total injected fuel was raised. However, as the method to achieve iEGR was PVO combined with exhaust gas throttling, the exhaust back pressure for the maximum iEGR nearly reached 1.1 bar (16 psi) gauge pressure. Due to the concern with the safety operation of the exhaust pipe, no further increase in the exhaust back pressure was made. It is thought that the minimum load border could be further extended if other methods are applied to realise greater amount of iEGR.

5.4.2 Combustion Stability as Measured by COVimep

Figure 5.19 shows the contours of COVimep and hence the combustion stability of the engine. It is obvious that the combustion stability is much improved compared with Split Injection Strategy which is shown in Figure 5.2. Both the misfire boundary and partial burn boundary are significantly extended.

Engine combustion is more stable under high load and near stochiometric mixture than it is under low load and lean mixture. In particular, at values of lambda higher than 1.4, combustion stability is mainly affect by air/fuel ratio. However, when iEGR rate is higher than 30%, the concentration of trapped residual gas becomes the main factor that affects the combustion stability. Even so, the maximum COVimep is lower than 10% in the entire operation region and lower than 5% in the whole Late Single Injection region and most of the Split Injection region, even with an ultra lean mixture. The relatively unstable combustion in the low load condition can be explained with the cyclic variation of iEGR during the combustion. As the load is reduced, the auto-ignition process plays a more important role in the hybrid combustion with higher iEGR rate increasing. When Early Single Injection Strategy is applied, the combustion is dominated by auto-ignition. The iEGR becomes the main factor to provide heat and initiates the auto ignition. The combustion of any cycle is significantly affected by the condition of trapped residual from the previous cycle combustion, which also strongly affects the combustion of the coming cycle. As a result, cyclic variation in combustion occurs due to the mixture distribution, temperature and residual gas composition. It is probable that the COVimep could be reduced under higher iEGR rate if the quantity of DME injection were increased to raise the number of more flammable auto-ignition sites associated with the injected DME.

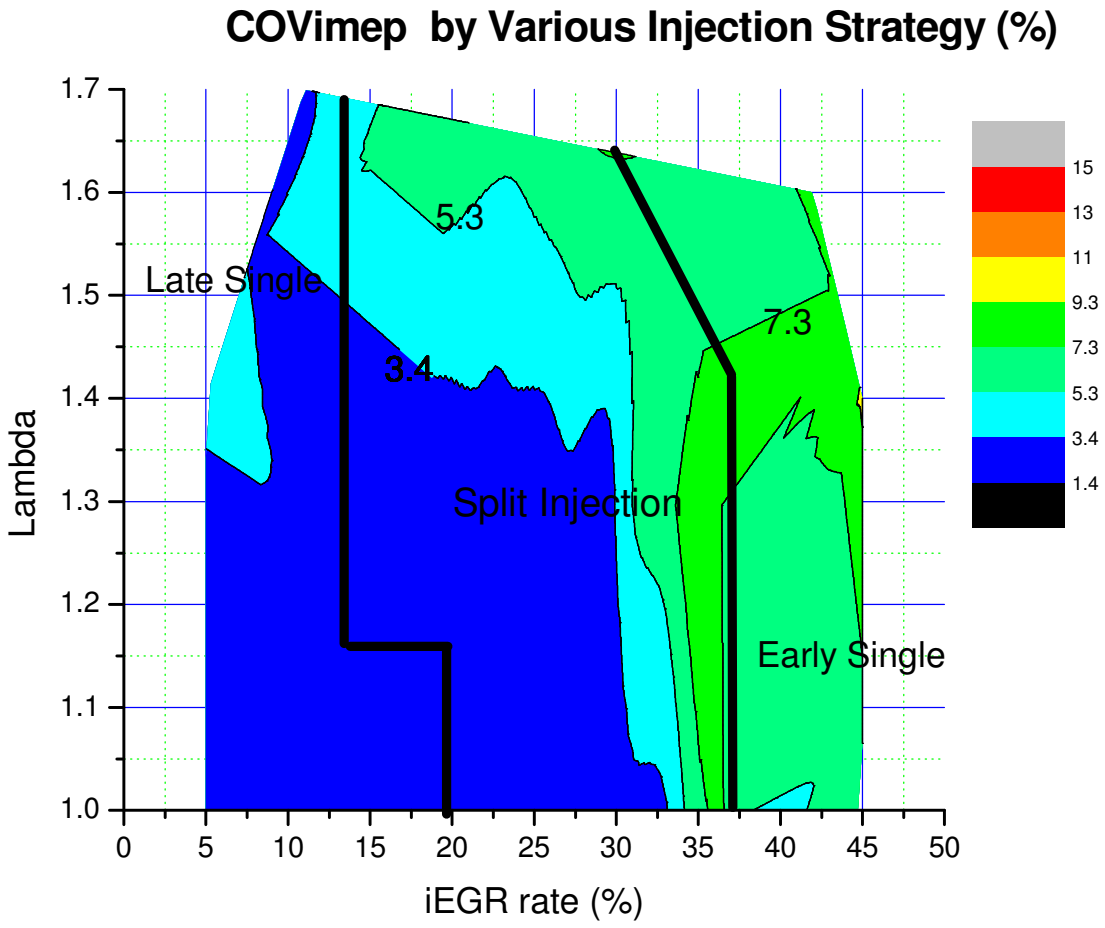

a)

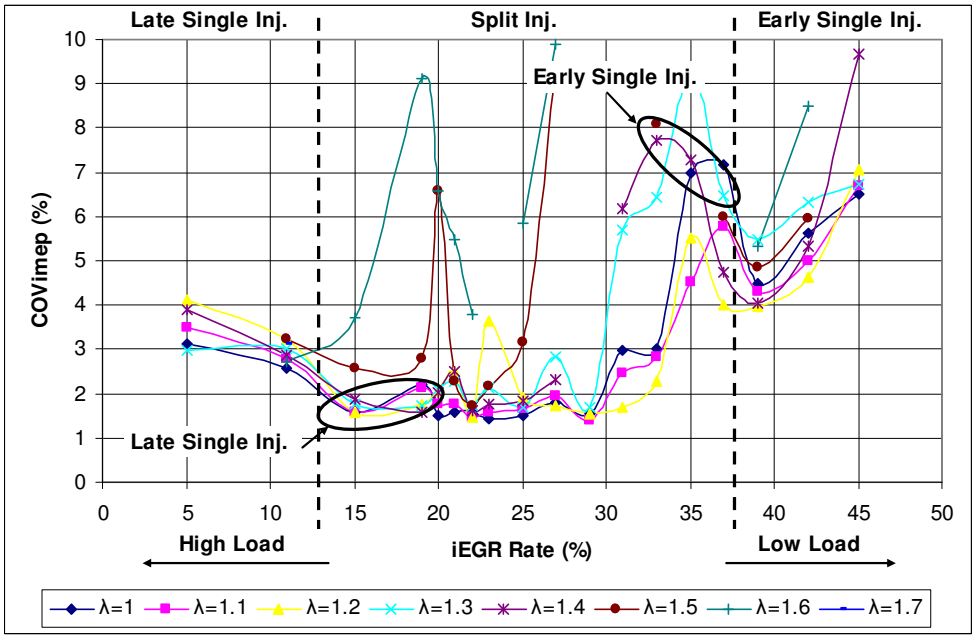

b)

Figure 5.19 COVimep as a Function of iEGR Rate and Total Lambda

5.4.3 Knocking Combustion

The percentage of knocking cycles (max dP/dCA > 5 bar) of 100 cycles is shown in Figure 5.20. It can be seen that the value is lower than 50% in the entire operation region. In particular, knocking combustion is successfully avoided under the high load compared with the results achieved by the Split Injection strategy shown in Figure 5.1. As a result, the high load boundary is extended.

The reason of which Late Single DME Injection combustion is able to achieve higher load than SI combustion has been explained in 5.4.1. The way that Late Single DME Injection combustion can extend the knocking boundary of Split DME Injection combustion can be explained by focusing on the combustion process under the condition of $\lambda=1$ and $\lambda=1.1$ when 13 %<iEGR<18%. With the Split Injection strategy, the end gas mixture contains the pre-mixed DME from the early injection and hence is more prone to auto-ignition than the gasoline/air mixture in the single late DME injection. The auto-ignition of the end gas region due to premixed DME then causes extremely fast combustion and advance combustion phasing.

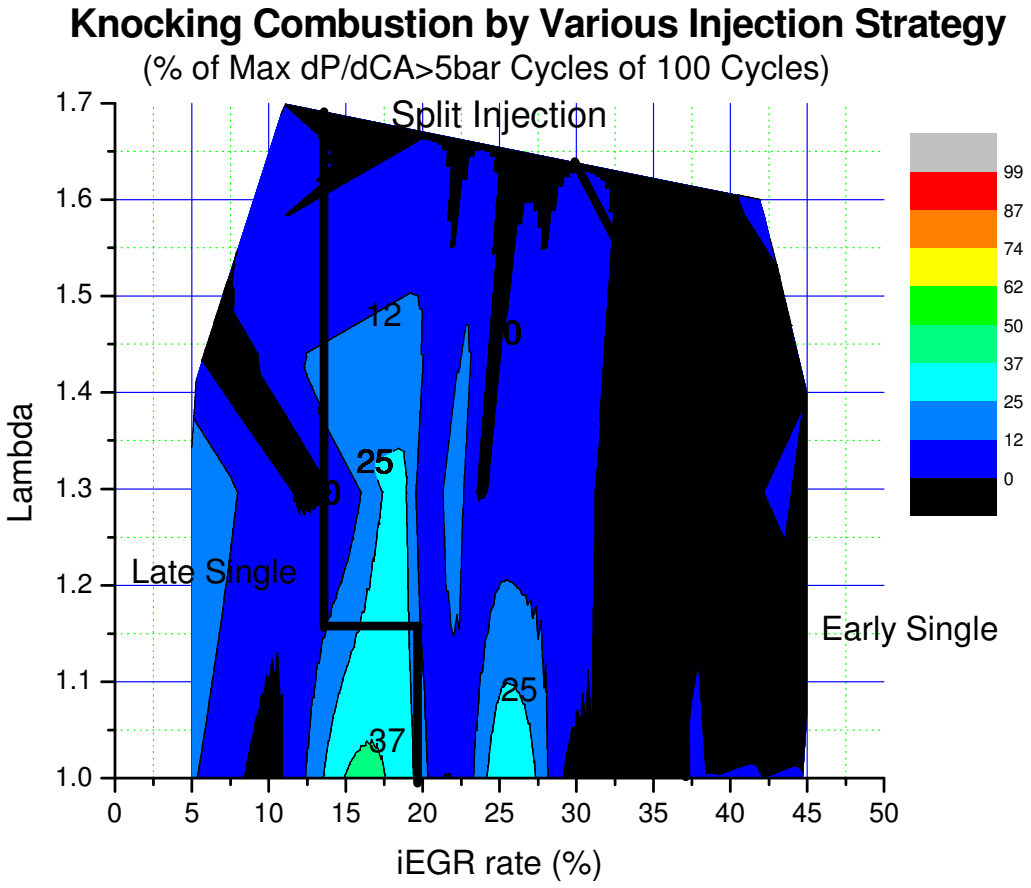

a)

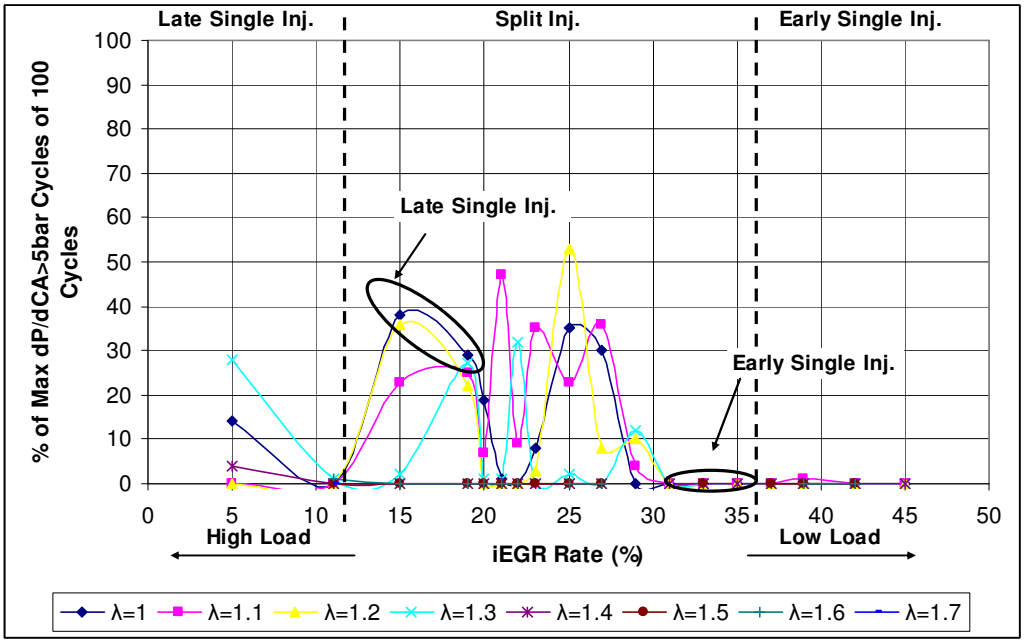

b)

Figure 5.20 Knocking Combustion Determination by Various Injection Strategies

5.5 Engine Exhaust Emissions

5.5.1 CO Emissions

Figure 5.21 shows both the absolute and the indicated specific CO emissions. It is seen that CO emissions increase when more iEGR is introduced. In addition, with a fixed iEGR rate, more CO emissions are detected as the air/fuel mixture gets closer to stoichiometric. This is because the combustion process is likely to deteriorate when more EGR is introduced, which is also indicated by higher COVimep values. A partial rich zone could exist inside the cylinder when combustion starts and it is difficult to further oxide CO with lower combustion temperature. On the other hand, learner mixture provides more air for complete combustion and hence the lower CO emission. The minimum CO emission (3.1 g/kWh) is achieved with minimum iEGR rate and learner mixture and the maximum is 85 g/kWh under maximum EGR rate and stoichiometric mixture.

A similar trend of CO emissions is demonstrated with diesel injection by Akihama et al. [110] and Hanson et al. [58] but opposite to Oakley's results [100], who stated that the CO emissions increase due to partial combustion occuring more at higher air and EGR dilution rate in their studies. The high CO emissions under lean mixture conditions obtained by Oakley are because of the low exhaust temperature due to low load output of the engine. Under this condition, the combustion temperature is too low to fully oxidise the fuel even with high air dilution. As a result, the CO emissions are significant as well as uHC emissions. However, this situation does not occur in this study because under Variable DME Injection combustion, the load is mainly controlled by the iEGR rate. Since flame propagation exists as the main combustion mode under low iEGR rate operation and EGR is recirculated internally, the combustion temperature is kept at high level even at the end of expansion stroke and exhaust stroke. This can be proved by the exhaust temperature data shown in Figure 5.22. The exhaust temperature is seen to be less affected by load or iEGR rate changes, but related to lambda value. Therefore, the CO emissions are reduced as the air dilution increases.

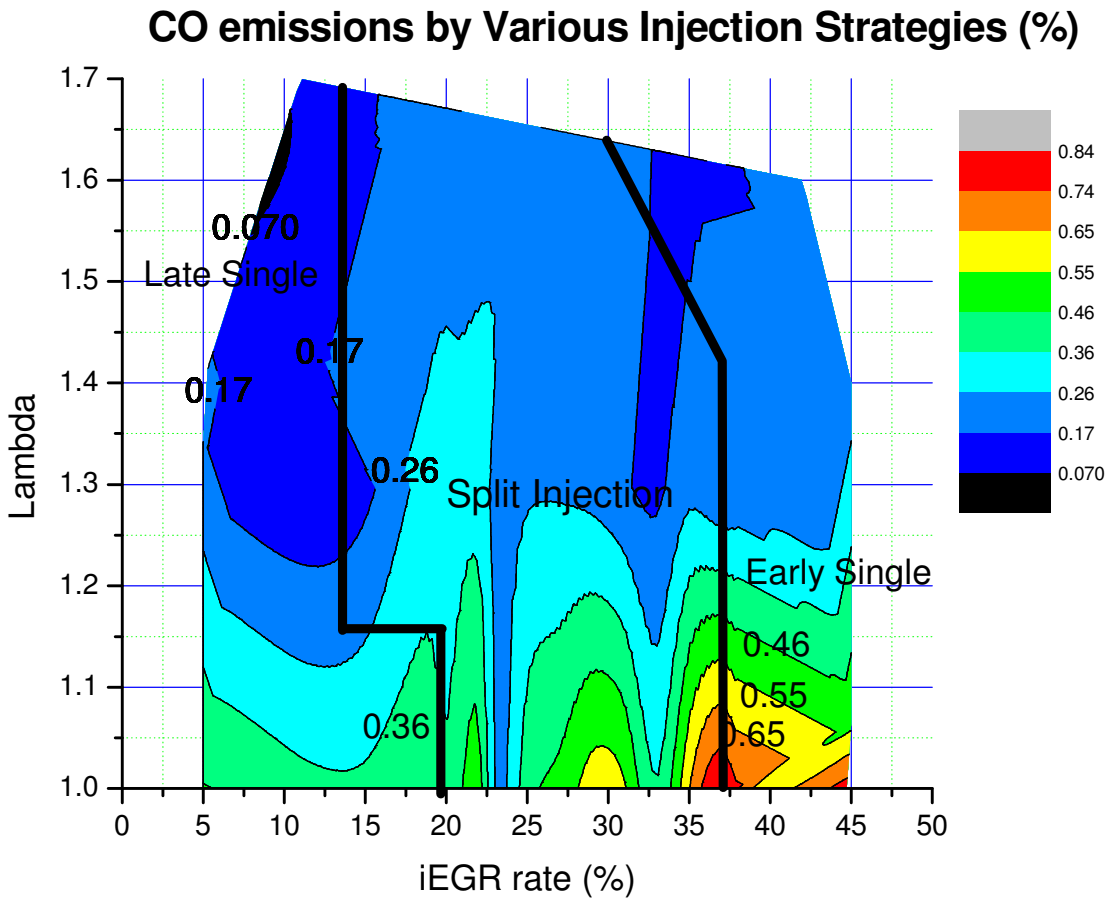

a) Volumetric CO Emissions (%)

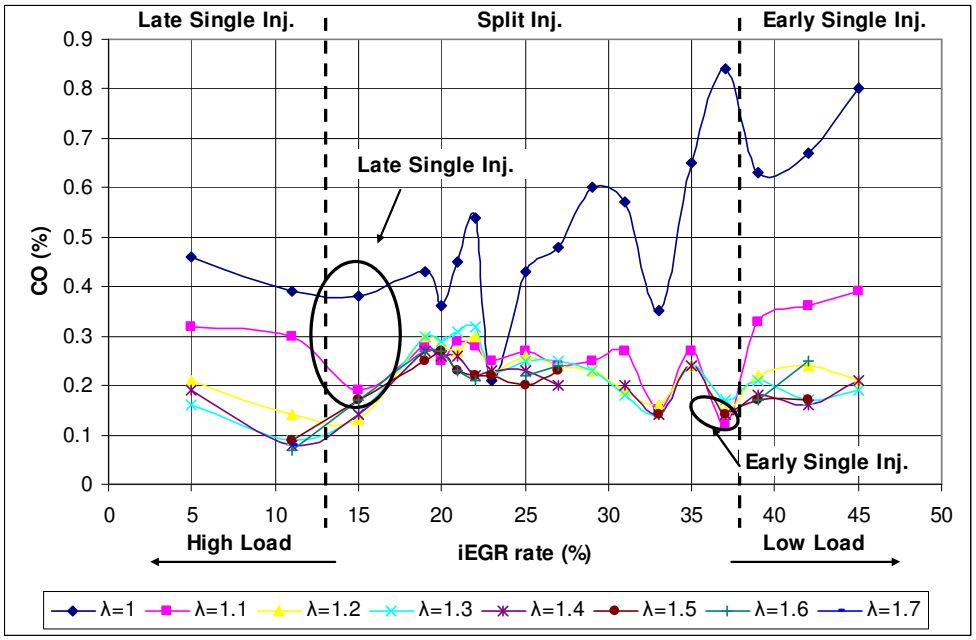

b) Volumetric CO Emissions (%)

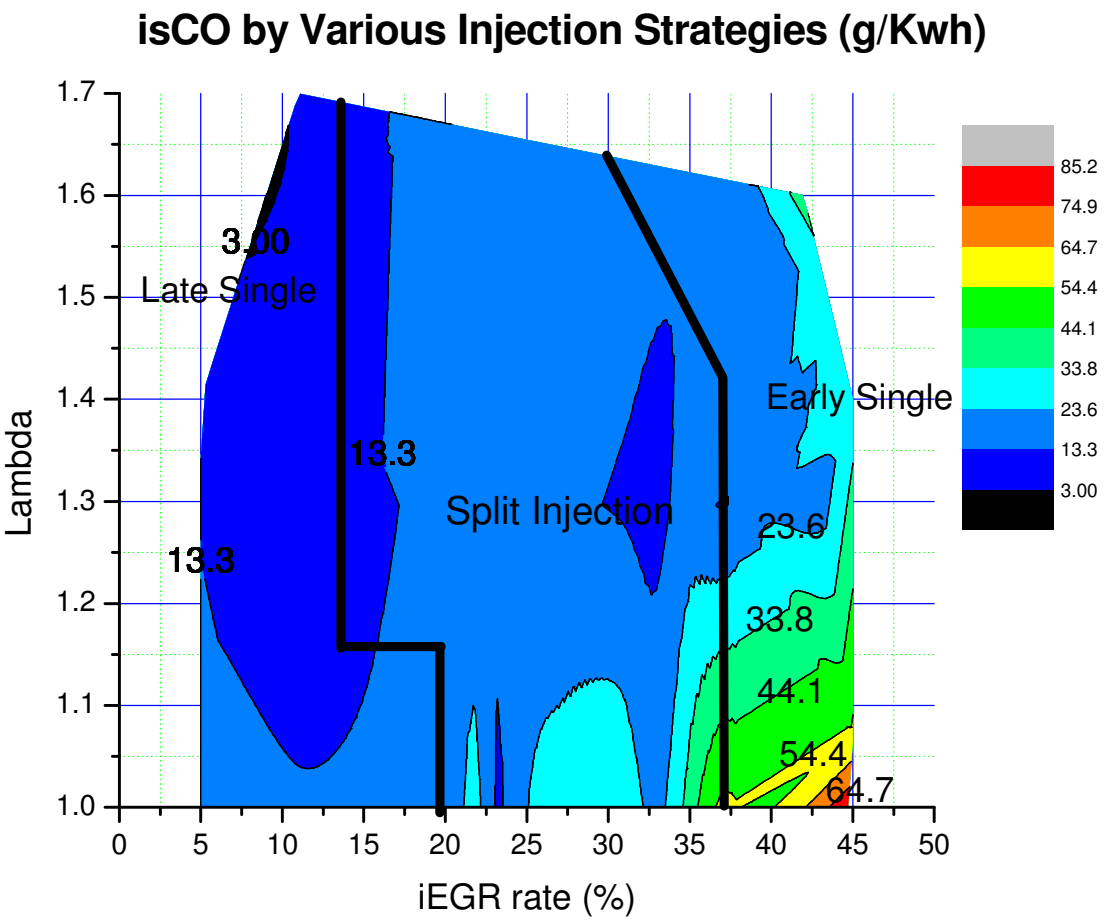

c) Indicated Specific CO Emissions (g/KWh)

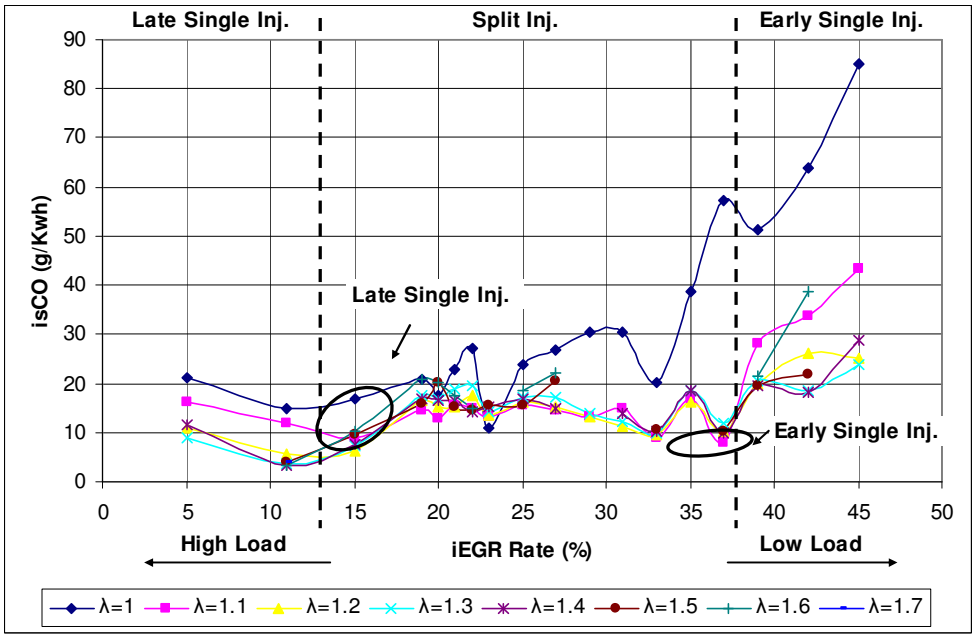

d) Indicated Specific CO Emissions (g/KWh)

Figure 5.21 CO Emissions by Various Injection Strategies

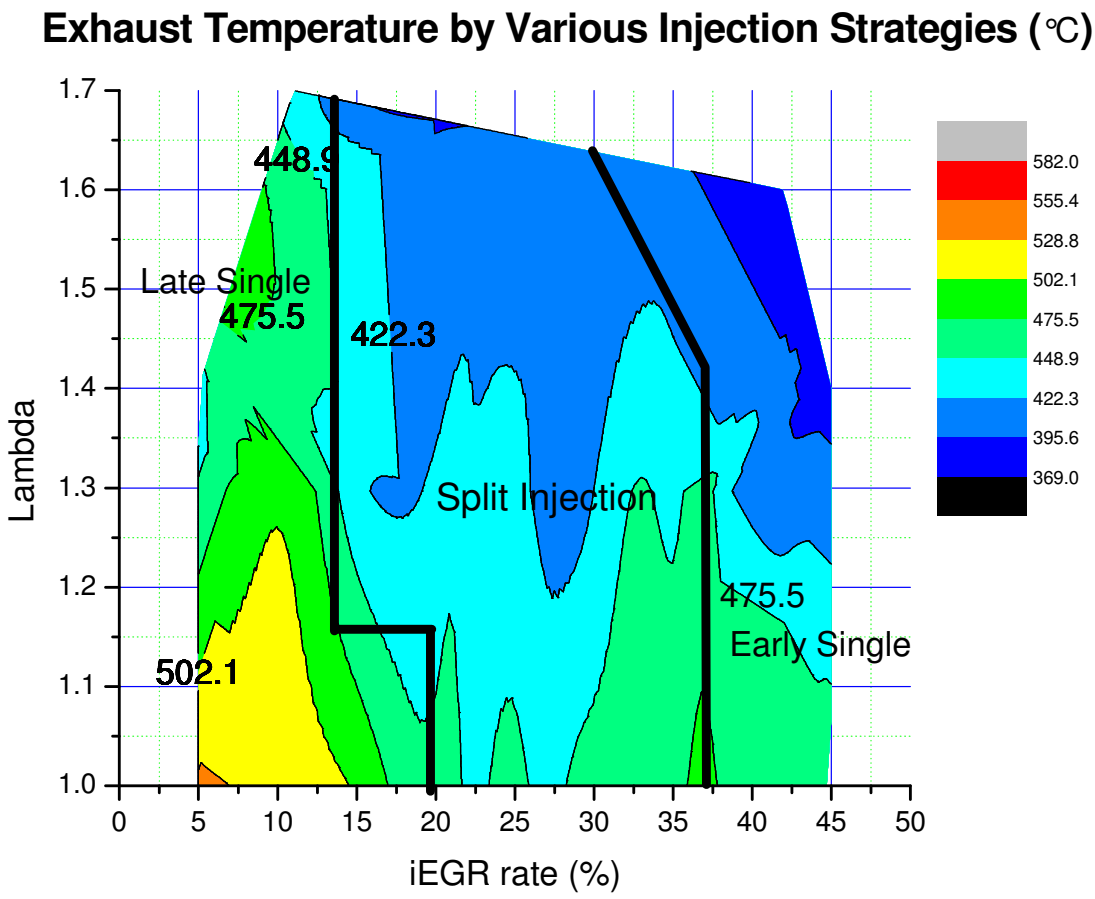

Figure 5.22 Exhaust Temperatures (°C) by Various Injection Strategies

5.5.2 uHC Emissions

Figure 5.23 shows the measured unburned HC emissions. It can be seen that the uHC emissions only depend on the iEGR level and increase with the iEGR rate due to the presence of unstable combustion. The highest uHC emissions are obtained when iEGR is about 30% with the leanest mixture, different from the condition for the maximum CO emission of highest iEGR rate near the stoichiometric mixture. The occasional uHC peaks are caused by the unstable combustion as shown by the higher COVimep values at the same operating conditions. In addition, uHC emissions are found to be related to the exhaust temperature. As the exhaust temperature is higher within the Late Single Injection region, the uHC emissions is significantly reduced.

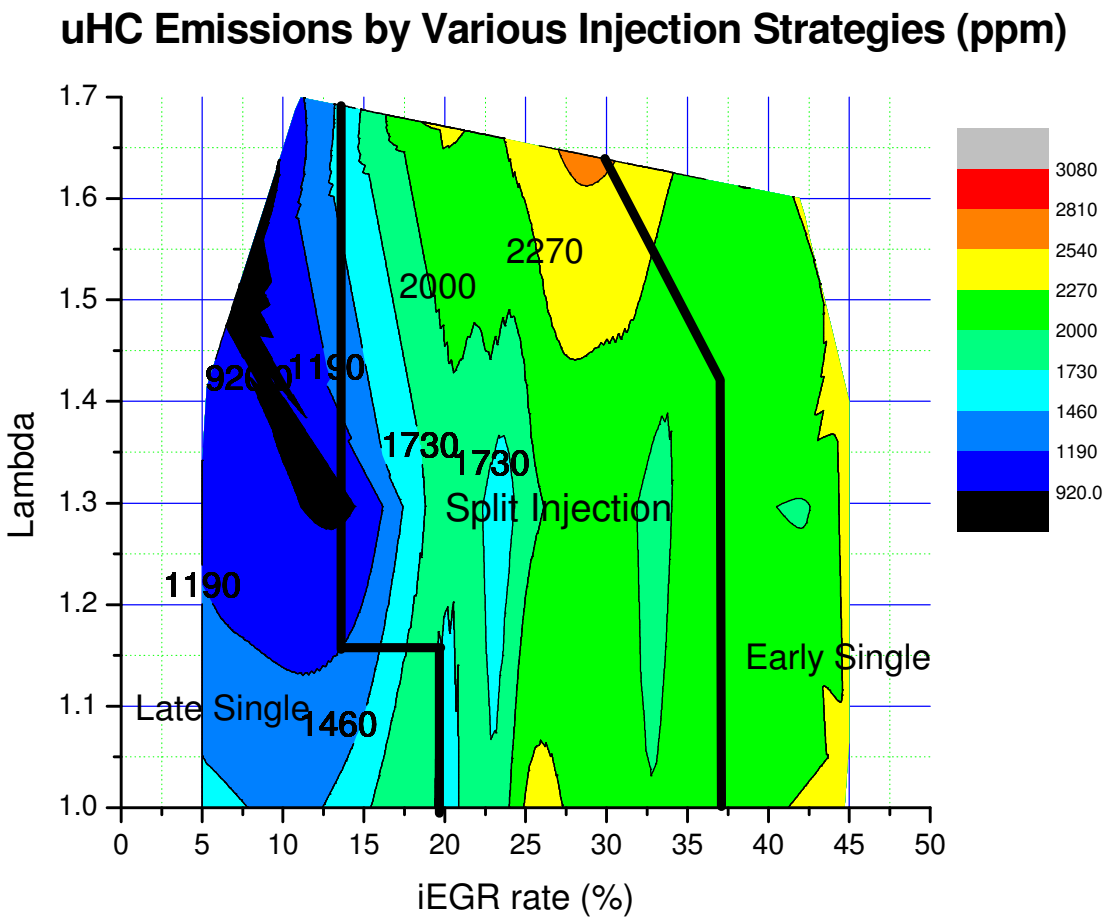

a) Volumetric uHC Emissions (%)

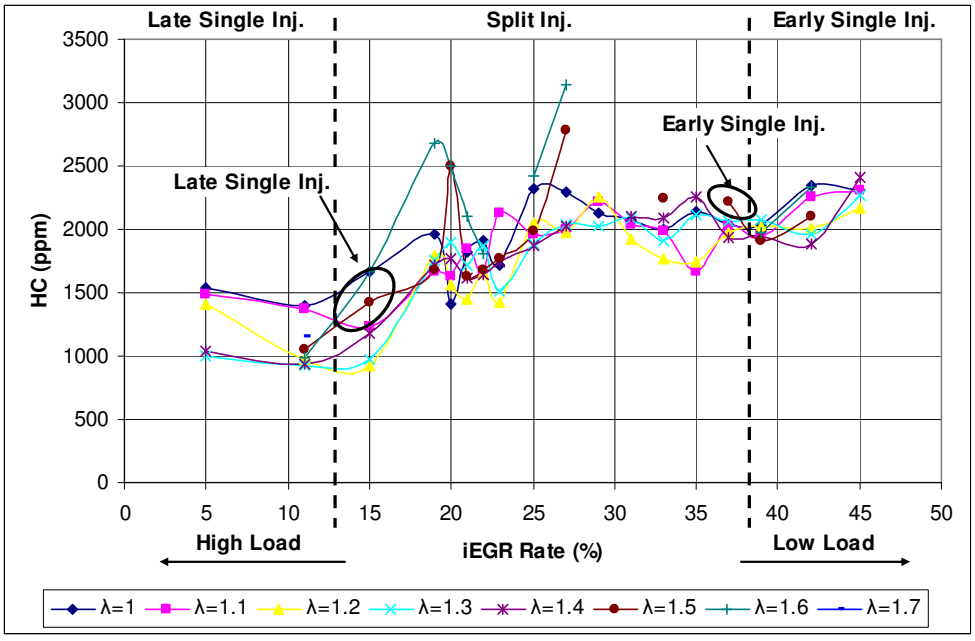

b) Volumetric uHC Emissions (%)

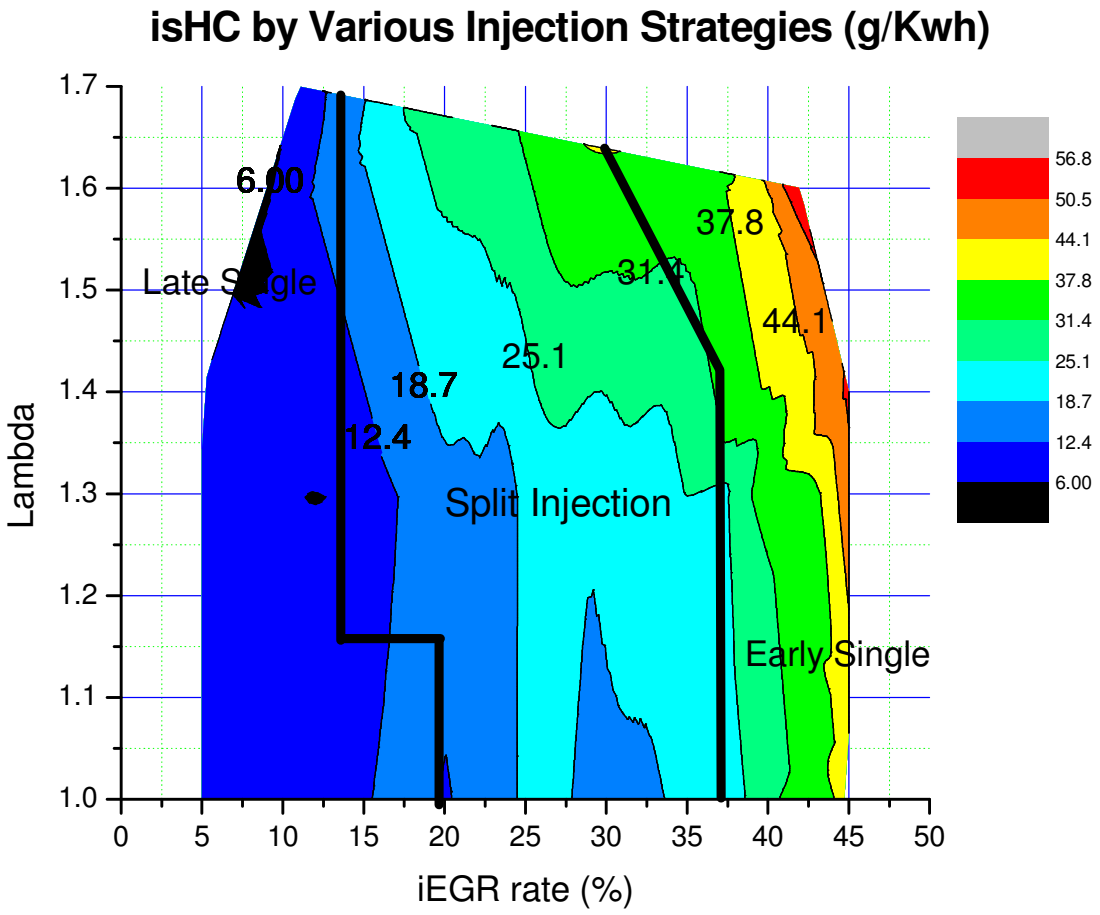

c) Indicated Specific uHC Emissions (g/KWh)

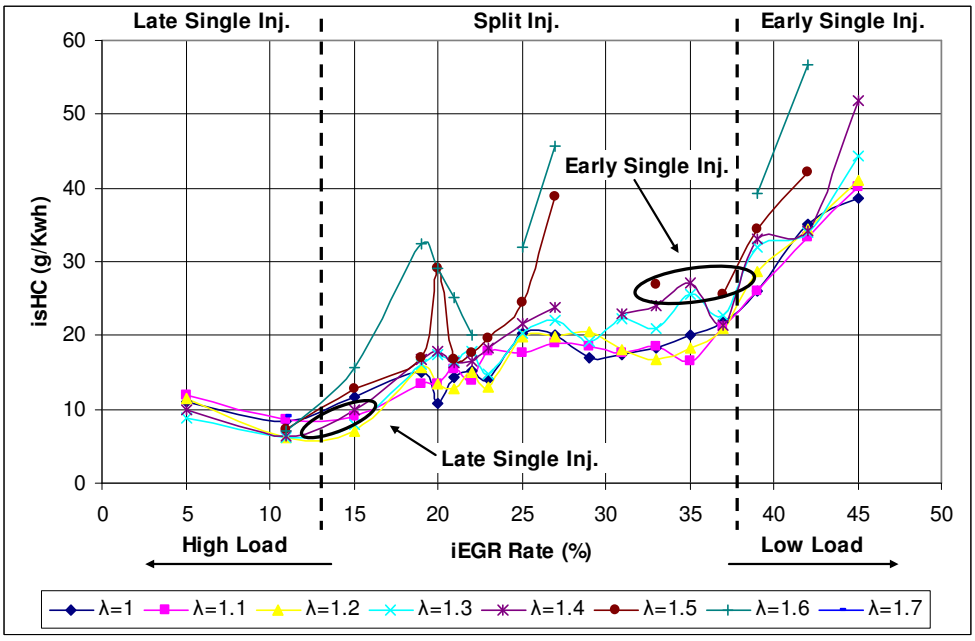

d) Indicated Specific uHC Emissions (g/KWh)

Figure 5.23 uHC Emissions by Various Injection Strategies

5.5.3 NOx Emissions

Figure 5.24 shows the results of NOx emissions as a function of the iEGR rate and lambda value. As expected, NOx emissions are higher as the engine load is increased and peak at the highest load point (iEGR rate 5%, lambda 1.0). When the engine load decreases and more iEGR is introduced, the NOx emissions are dramatically reduced. The average NOx emissions are lower than 70 ppm when the iEGR rate is over 35% and 0.25 g/KWh of isNOx is obtained with iEGR 27% and lambda 1.6.

It is interesting that with lambda of 1.0 and 1.1, the NOx emission rises slightly as the iEGR rate is increased from 10% to 18% and then drops rapidly once the iEGR rate is over 18%. In contrast, at lambda 1.5 and 1.6, the NOx emissions are firstly reduced and then slightly increased between iEGR 35% - 43%. These two regions are the ones in which the combustion mode changes. Therefore, it can be concluded that the NOx emissions are also strongly affected by combustion mode switches. The increasing fraction of auto ignition in any combustion mode can reduce the NOx emissions.

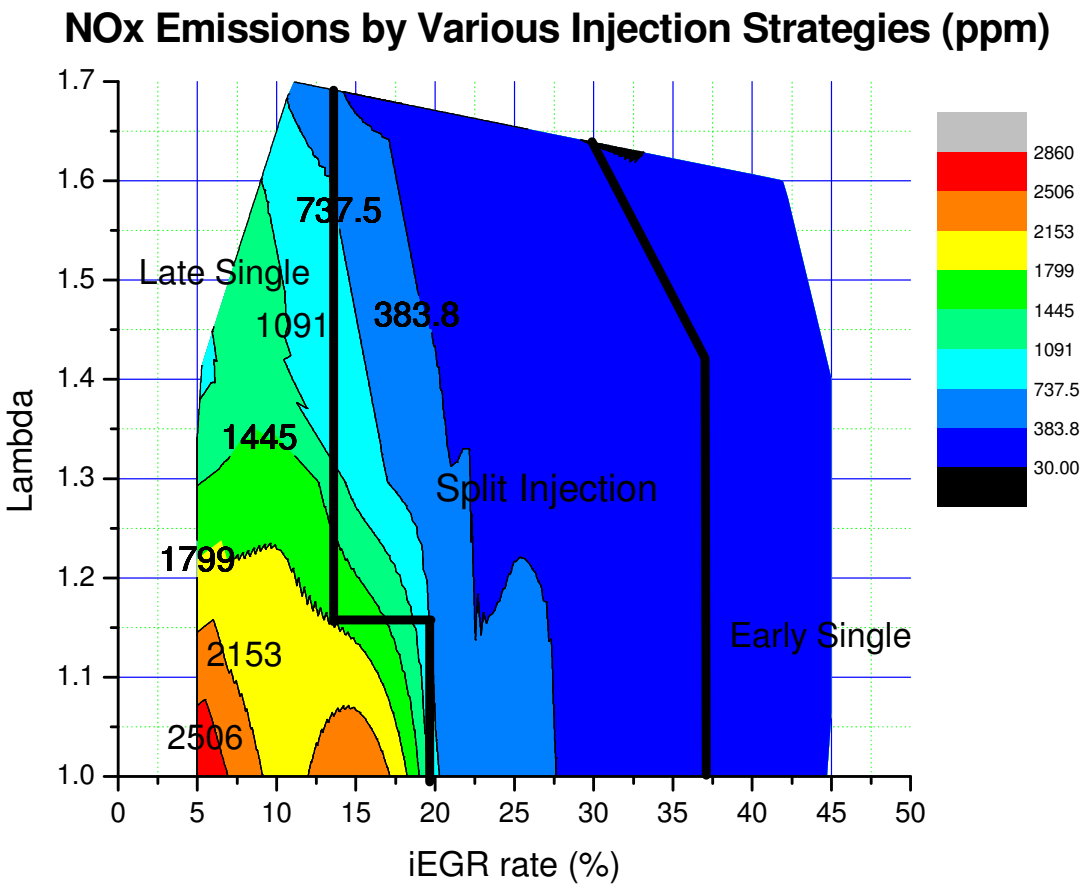

a) Volumetric NOx Emissions (%)

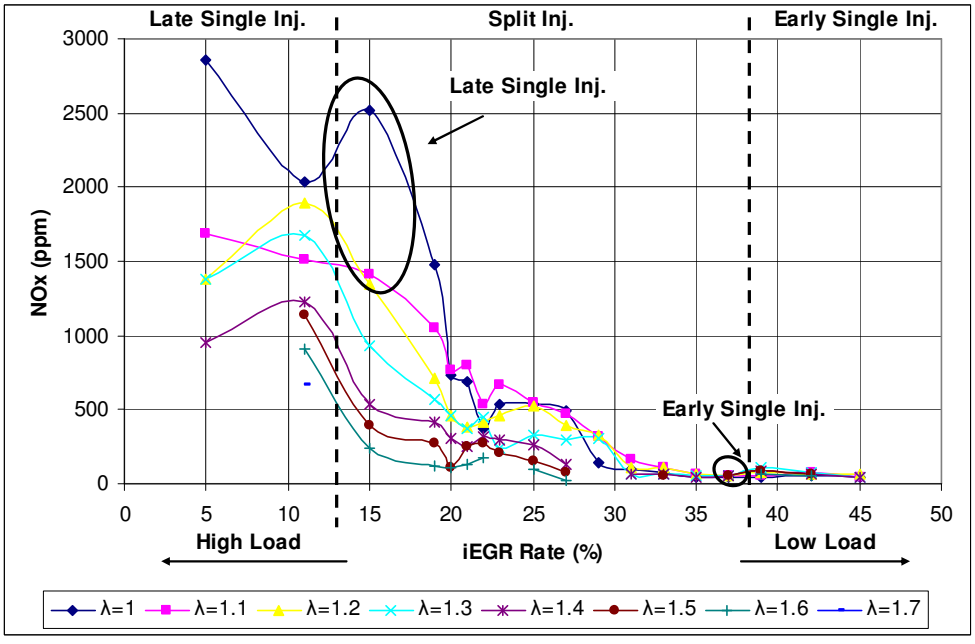

b) Volumetric NOx Emissions (%)

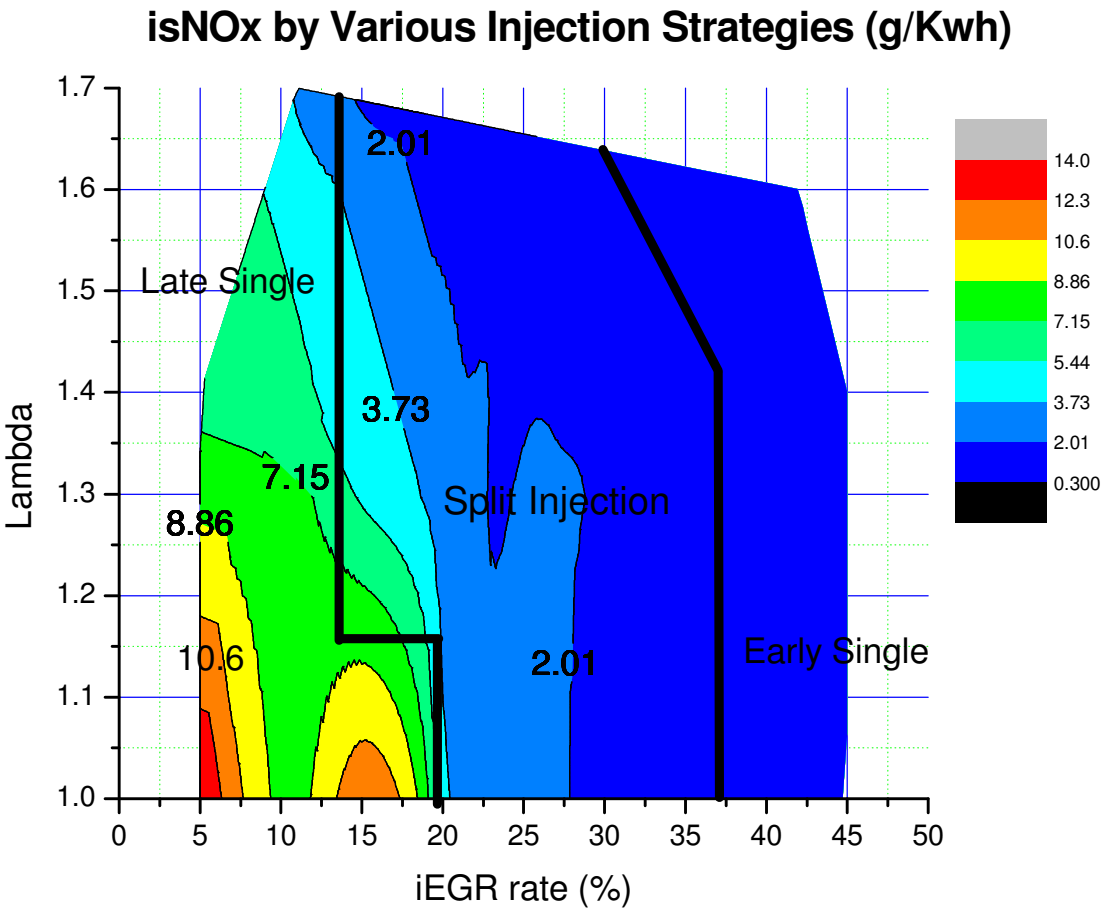

c) Indicated Specific NOx Emissions (g/KWh)

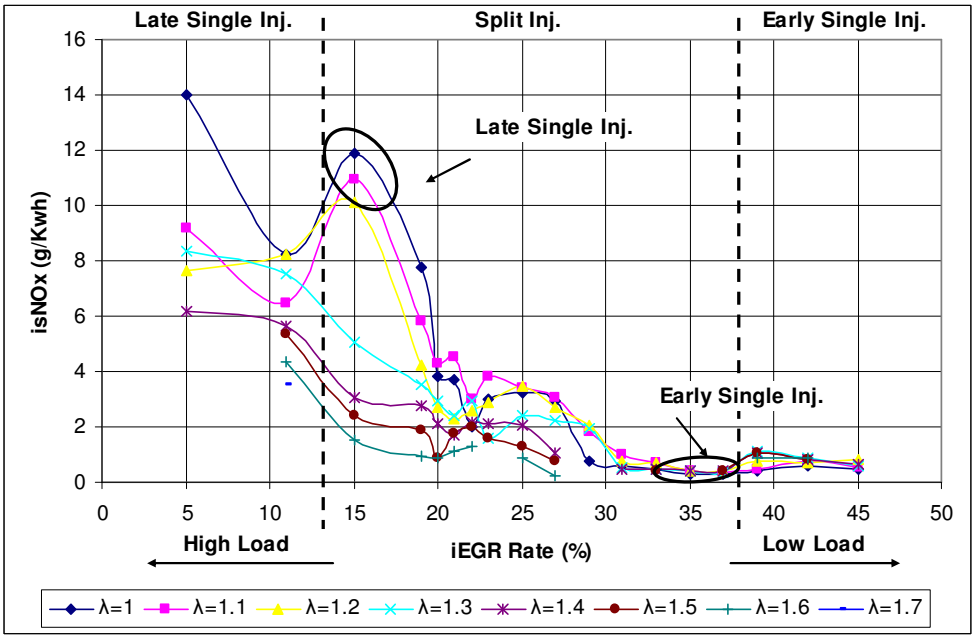

d) Indicated Specific NOx Emissions (g/KWh)

Figure 5.24 NOx Emissions by Various Injection Strategies

5.6 Heat Release Analysis

5.6.1 MBT Injection Timing, Ignition Timing and Ignition Delay

The optimum late injection timing is referred as the Minimum injection advance for Best Torque (MBT) in the operation modes of Late Single Injection and Split Injection. Ignition timing is defined as the crank angle (CA10) where 10% of mass fraction of fuel has been burned. The ignition delay is the period of crank angles between DME SOI2 timing and ignition timing. The MBT timing, ignition timing and ignition delay as a function of the iEGR rate and lambda are shown in Figures 5.25-5.27. It should be noted that in the Early Single Injection Strategy the injection timing is presented for completion.

The MBT timing in the Split Injection region shows a significant dependence on the iEGR rate rather than A/F ratio. The MBT timing becomes more advanced as iEGR rate increases. However, the MBT timing in Late Single region is mainly determined by the lambda value. This is because the advance of SOI2 DME timing is limited by the knocking boundary. Leaner mixture with a fixed iEGR rate in this region can tolerate more advanced SOI2 and hence produce higher net IMEP.

In the Late Single Injection region, the ignition timing exhibits the same trend as the MBT timing and it only depends on the SOI2 DME timing as shown by the constant ignition delay in Figure 5.27. In the Early Single Injection region, the ignition timing strongly depends on the in-cylinder condition such as the air/fuel ratio, iEGR rate, in-cylinder temperature and pressure. In the Split Injection region, as the iEGR rate is increased, the ignition timing is firstly advanced until iEGR rate reaches 30% and then retarded as iEGR rate is further increased even with the advanced SOI2 timing. This can be explained by Zhao's theory [65]. As the iEGR rate increases to 30%, the ignition timing becomes earlier not only because the advanced SOI2 DME timing but also the increasing heating effect on AI timing by a rising EGR rate. However, as the iEGR rate is further increased, the heat capacity effect of the residual gas becomes the main factor for retarding the ignition timing rather than heating effect and earlier SOI2 timing to advance ignition timing.

The ignition delay is a strong function of the iEGR rate for the majority of the results but significantly affected by the A/F ratio in the Early Single region at higher EGR rate. The

reason for this is likely to be related to the increase in CO_2 and H_2O concentration, tending to delay in the reaction time from the SOI2 DME and ignition timing.

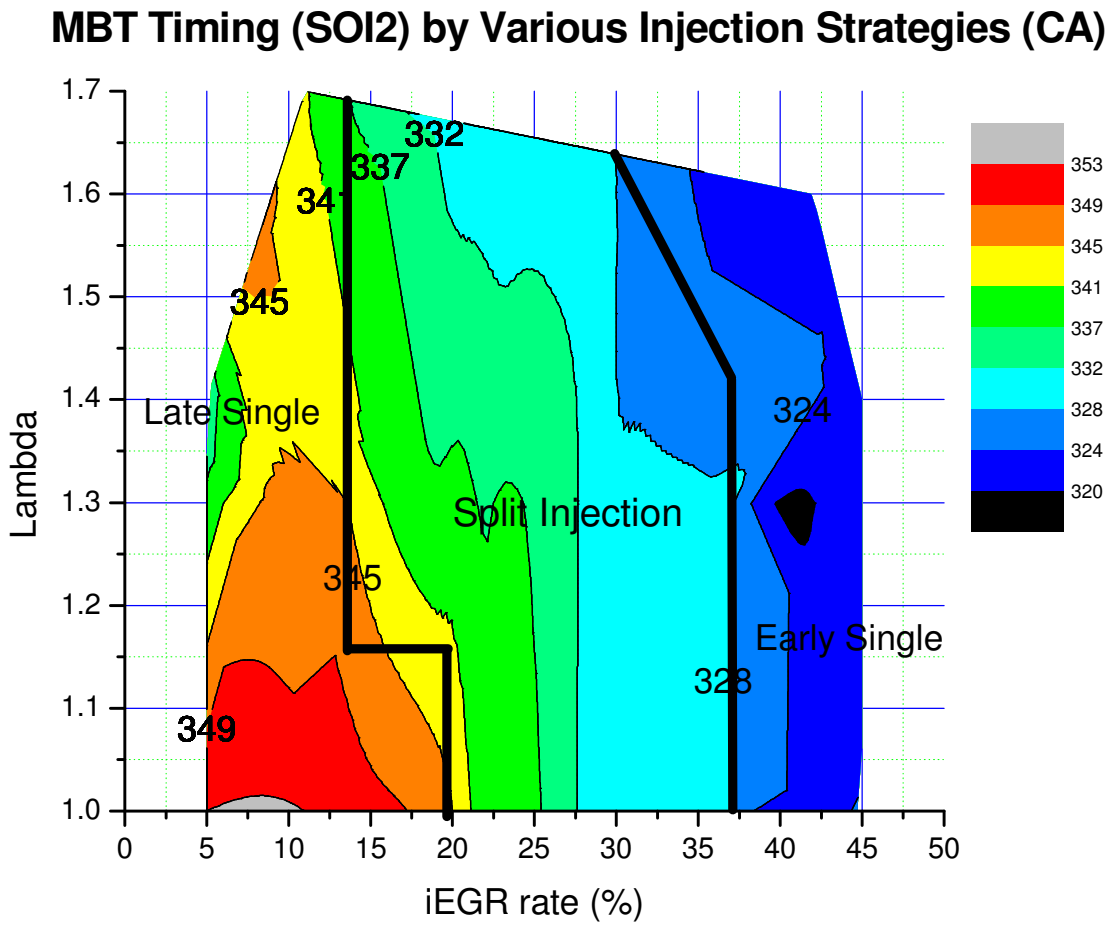

Figure 5.25 MBT Timing by Various Injection Strategies

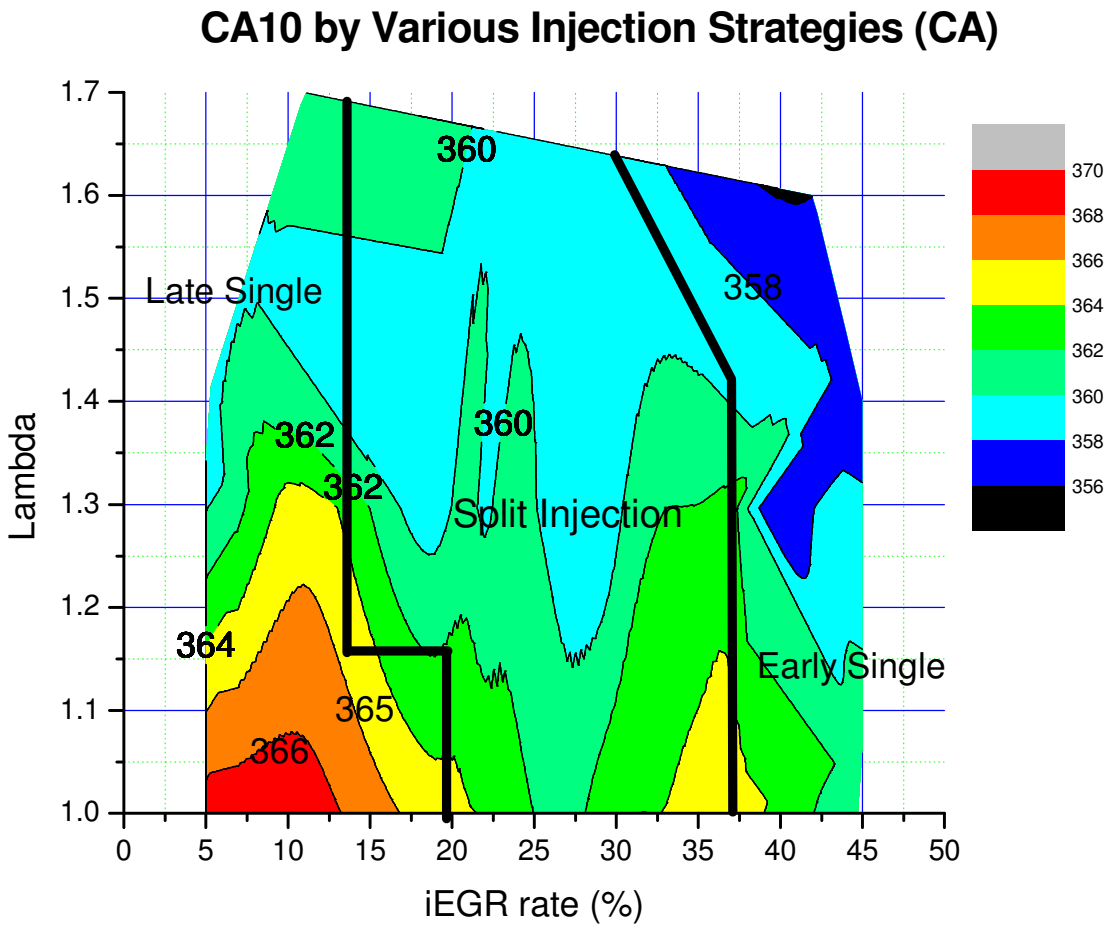

a)

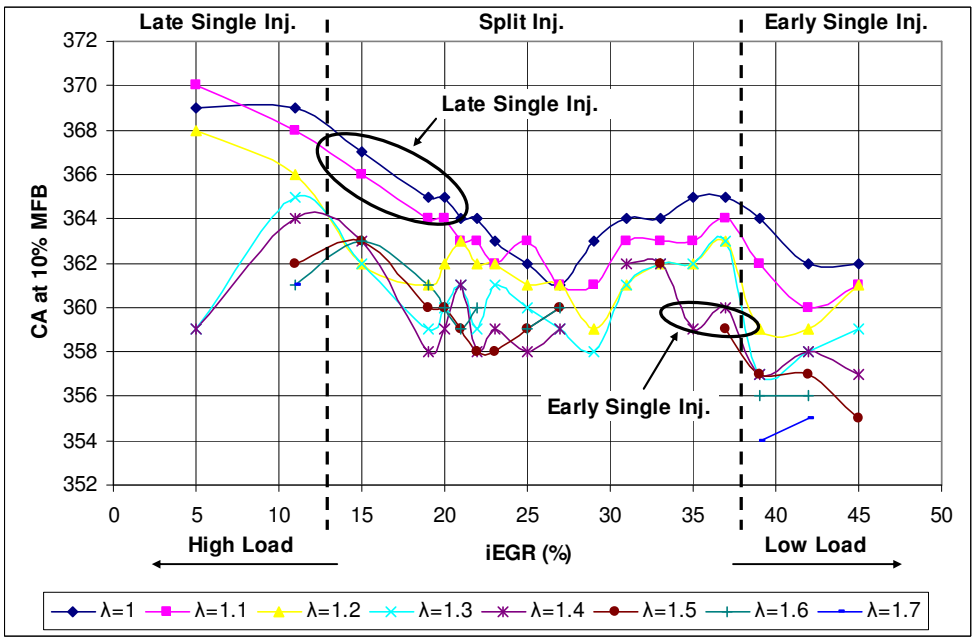

b)

Figure 5.26 Ignition Timing (CA10) by Various Injection Strategies

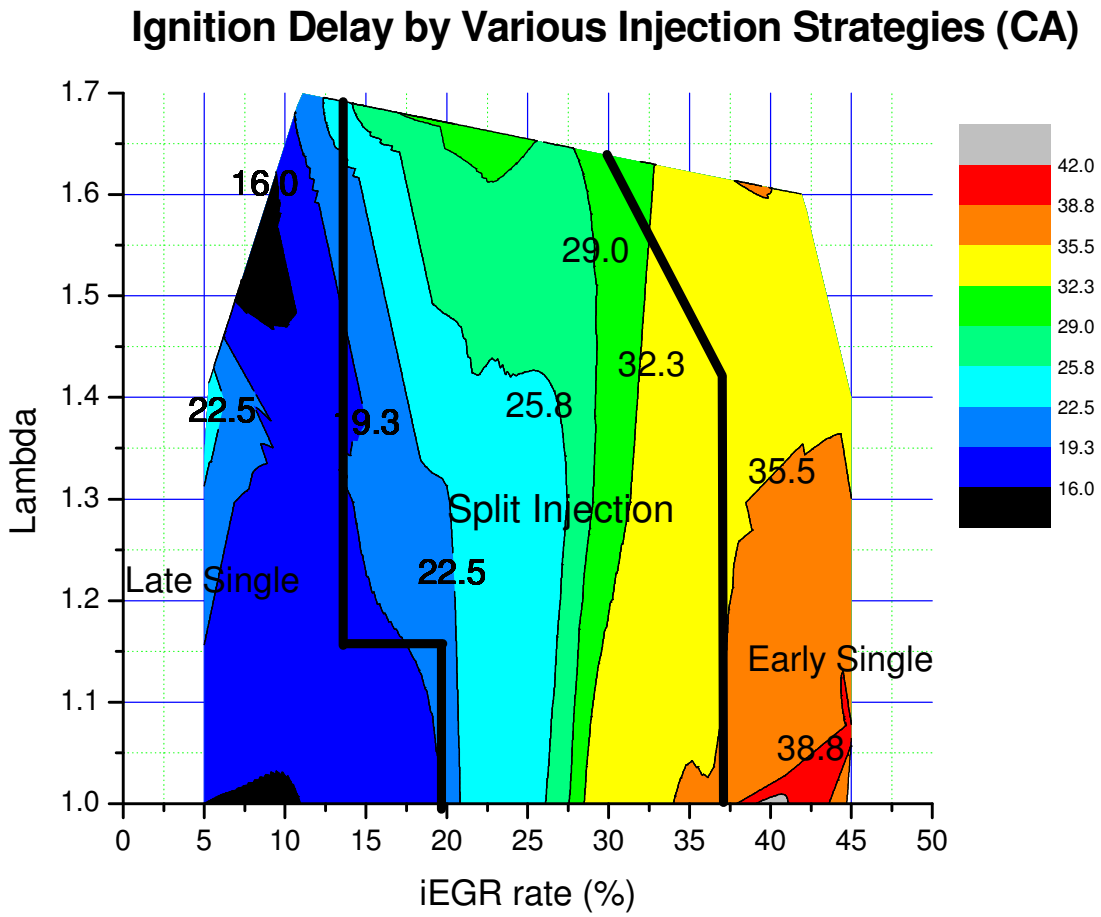

Figure 5.27 Ignition Delay (°CA) by Various Injection Strategies

5.6.2 Combustion Phasing and Combustion Duration

Figure 5.28 and Figure 5.29 shows the combustion phasing and combustion duration results respectively. The combustion phasing is defined by the crank angle position of 50% mass fraction burned and the combustion duration is the crank angle period between 10% and 90% mass fraction burned.

The trends of CA50 are similar to CA10 in most regions. Since MBT timings are applied (except Early Single Injection mode) in these tests, it can be seen that the best combustion phasing in the engine operation map varies with different combustion modes and EGR levels. As discussed above, increased charge heating effect from higher EGR can result in early combustion phasing whilst. The increased heat capacity effect of EGR tends to retard the combustion phasing. The charge heating effect is more dominant at relatively low iEGR concentration with higher burned gas temperature and the heat capacity plays a more dominant role in slowing down combustion at higher EGR concentration. The balance of

these two opposing effects balance at one particular EGR rate, at which the most advanced combustion phasing determines the start and speed of combustion. Results in Figure 5.28 indicate that their dominance is balanced around 28% iEGR where the combustion phasing is delayed with either higher or lower concentration of iEGR.

The combustion duration is determined by the speed of combustion process and will be affected directly by the combustion mode. Long combustion duration is achieved in the Late Single Injection region, where slow flame propagation dominates. The combustion duration shows a strong relationship with the A/F ratio and iEGR rate in the Split Injection region. The long combustion duration in the leaner mixture is caused by the late start of the auto-ignition process in the hybrid combustion mode. The fastest combustion happens around the balanced iEGR rate (28%). As iEGR rate is increased beyond 30% in the Split Injection region, combustion duration becomes almost fully dependant on the EGR rate. This is thought to be because the increased concentration of inert EGR species such as CO_2 and H_2O would hamper the chain propagating and degenerate-branching reactions [98]. Thus, the reaction rates of the auto-ignition process in hybrid combustion are slowed down by increasing EGR.

With the Early Single Injection, the fastest combustion happens in the middle of the region at lambda 1.3 and iEGR 42%, where the earliest CA50 is located. In this case, only auto-ignition combustion takes place. As shown in Figure 5.26 the auto-ignition timing is advanced as the relative air/fuel ratio increases. For a given iEGR ratio, the auto-ignition starts either too early with a leaner mixture or too late with a richer mixture than lambda 1.3 for combustion to take place near TDC.

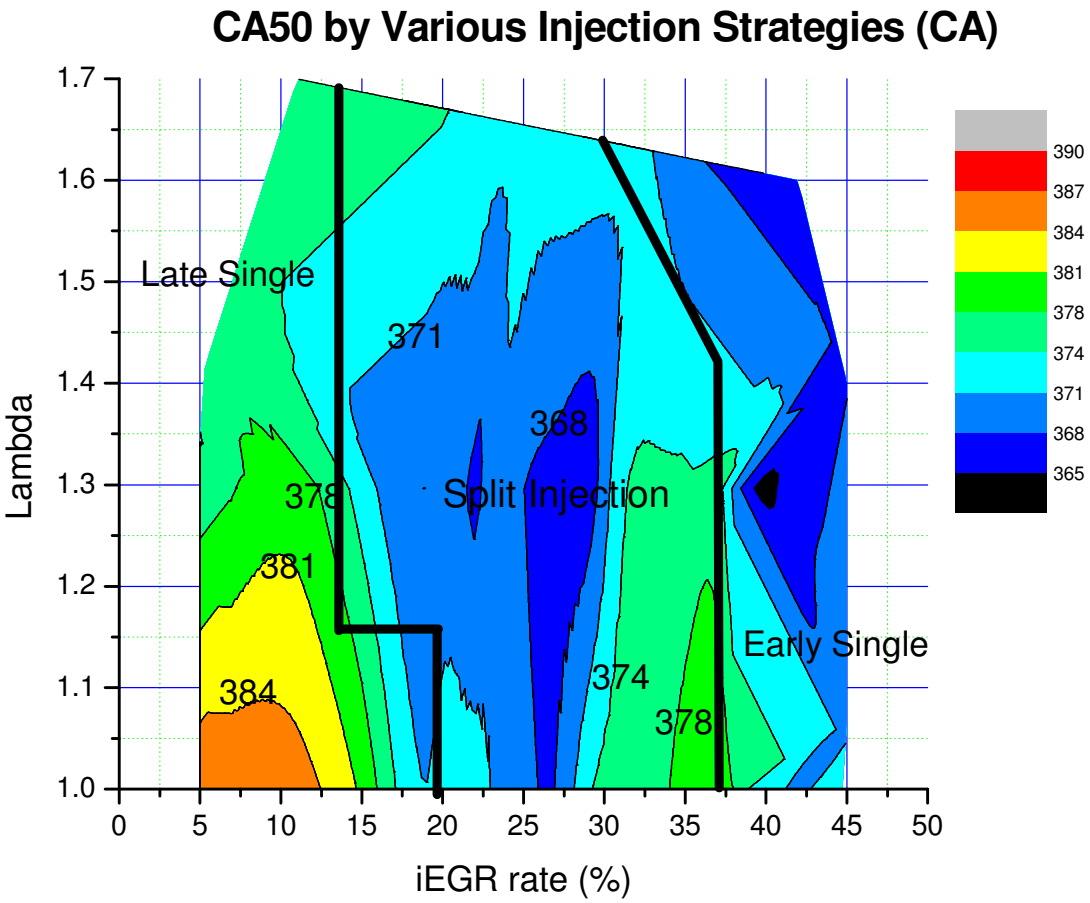

a)

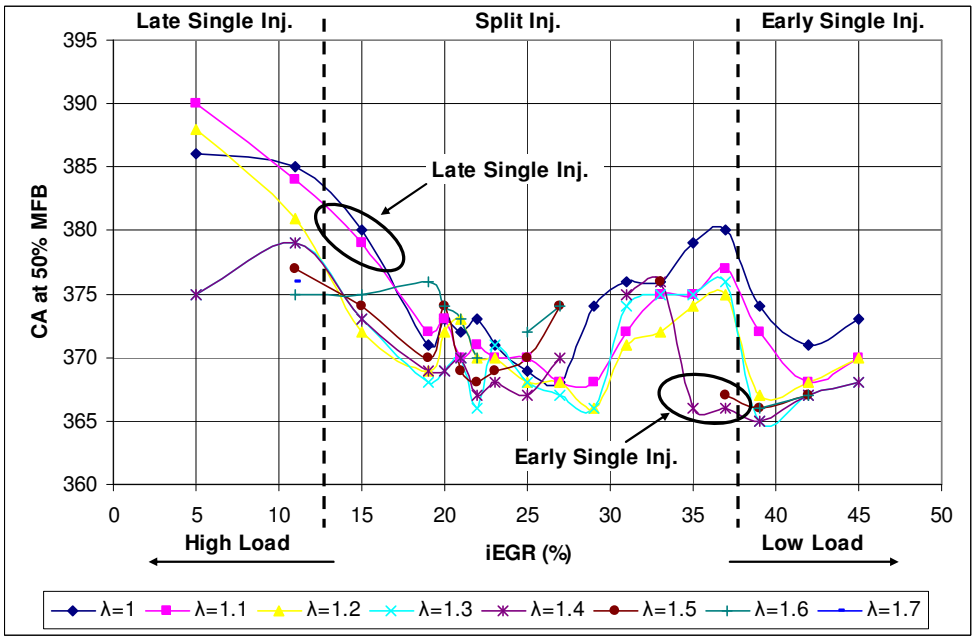

b)

Figure 5.28 Combustion Phasing (CA50) by Various Injection Strategies

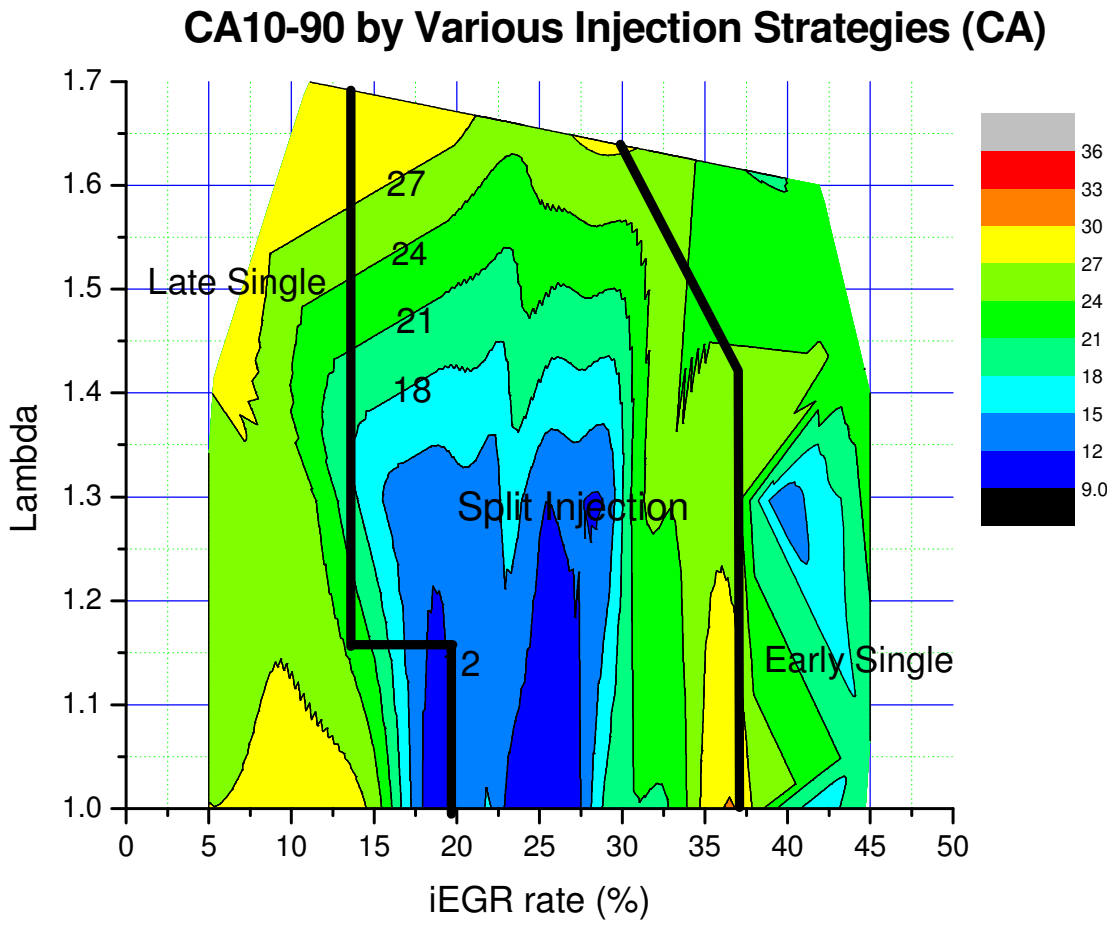

a)

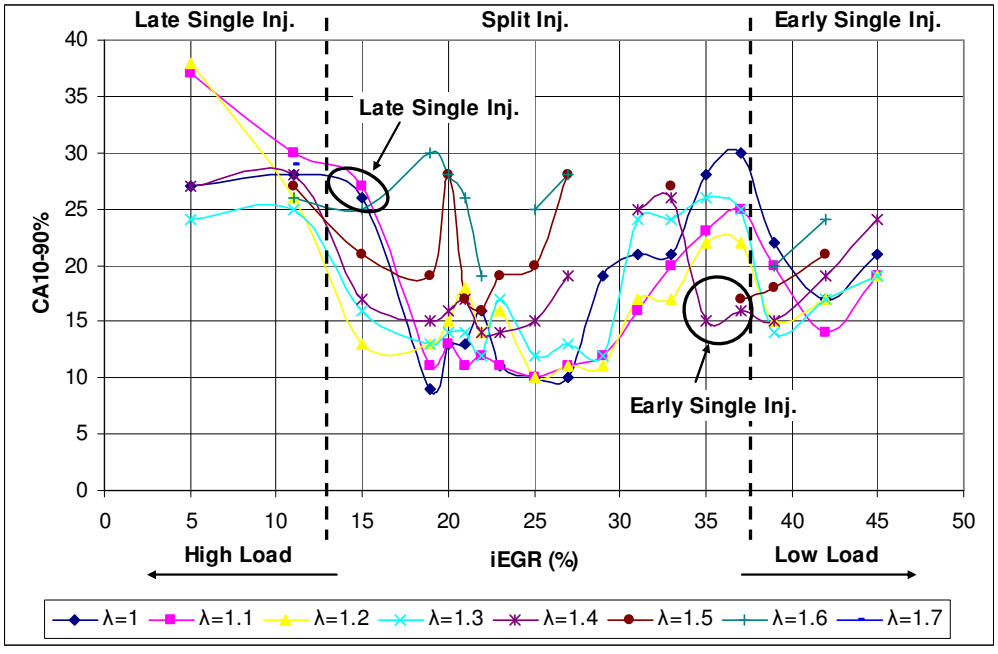

b)

Figure 5.29 Combustion Duration (CA10-90) by Various Injection Strategies

5.7 Efficiencies

Combustion efficiency, gross indicated efficiency and net indicated efficiency as a function of iEGR rate and total lambda are shown in Figure 5.30 - 5.32 respectively.

Combustion efficiency decreases with the increasing concentration of iEGR. As more burned gas is present, the combustion deteriorates resulting in high CO and uHC emissions. The trends and reasons of each emission have been presented and explained in the previous section. The highest combustion efficiency (98%) is achieved in the Late Single Injection region and the lowest value (91.5%) is obtained under maximum EGR rate in a stoichiometric mixture.

Gross indicated efficiency and net indicated efficiency are used to indicate the CO_2 emissions. The definitions are presented in Chapter 3. The gross indicated efficiency does not include the pumping work which is from the gas exchange process and exhaust throttling, however, the net indicated efficiency includes the pumping loss.

Gross indicated efficiency of 34% is as its maximum at the minimum iEGR rate with lambda 1.3 and 1.4. It is not the point that maximum load is achieved but when the most advanced MBT timing is applied. The peak is shifted from bottom to top-left corner in Figure 5.31 a. This is because in the bottom of Late Single Injection region, the combustion phasing was retarded to avoid knocking combustion. Thus, the peak of Gross Indicated Efficiency is achieved under the lean mixture with minimum iEGR rate. At the highest efficiency point, CO and uHC emissions are approximately at their lowest in the entire region. The NOx emissions are higher than most of the operation points but not the highest. It is possible to achieve higher efficiency under one iEGR rate with a leaner mixture. As the iEGR rate increases, the gross indicated efficiency is almost constant until the Early Single Injection strategy is applied. Once the combustion mode is switched to pure CAI, the value is slightly reduced due to relatively lower combustion efficiency.

However, net indicated efficiency is significantly reduced as iEGR rate increases due to a dramatic rise of pumping loss. The engine works at WOT of intake resulting in negligible pumping work. The pumping loss comes from exhaust throttling, which is used to increase the exhaust pressure and then increase the iEGR rate with fixed valve overlap. However, in the Late Single region at lambda 1.0, 1.1 and 1.2, although the iEGR rate is increased, the

net indicated efficiencies of these points are almost constant. This is because the iEGR rate is increased from 5% to 12% by means of increased positive valve overlap (overlap changed from 24 °CA to 63 °CA by both retarding EVC timing and advancing IVO timing), without exhaust throttling. Therefore, it is believed that if other methods are used to realise large iEGR, the increasing pumping work at high iEGR conditions can be avoided. Re-breath strategy is one of such methods which has been selected for further experiments.

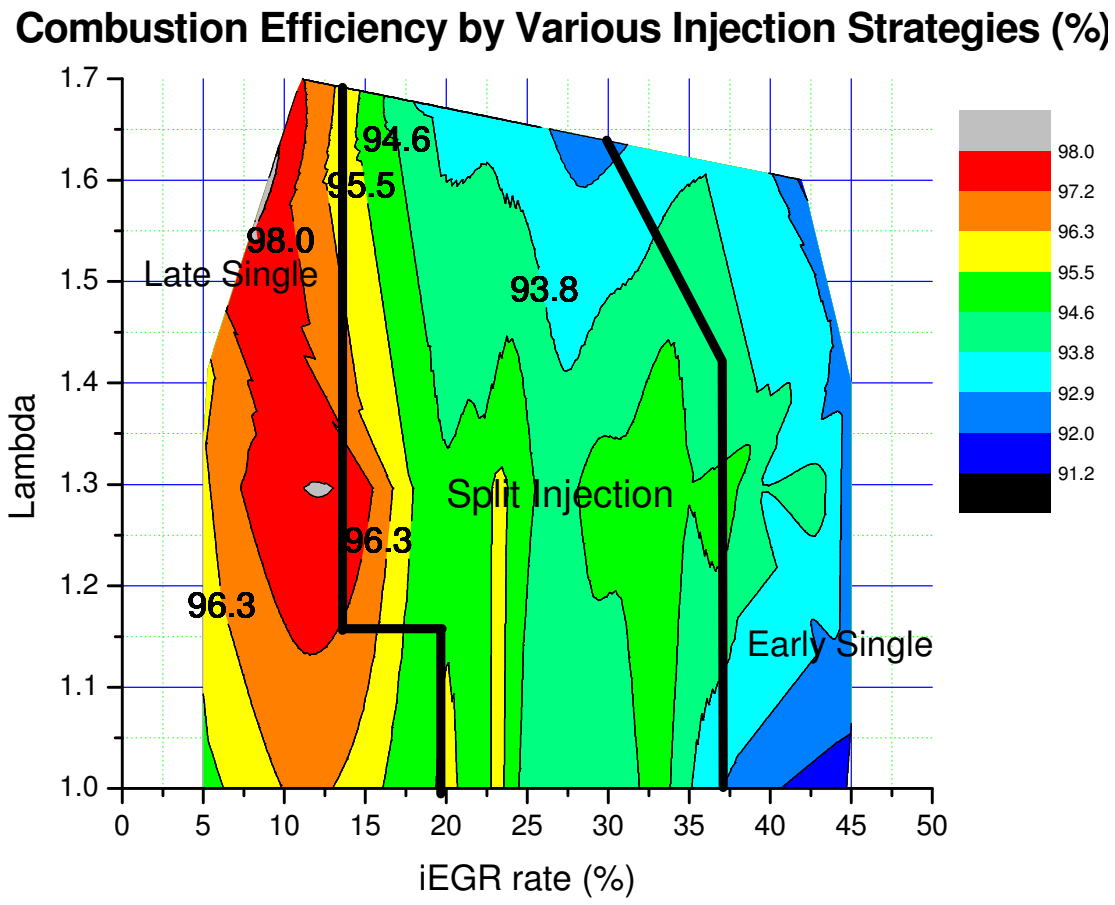

a)

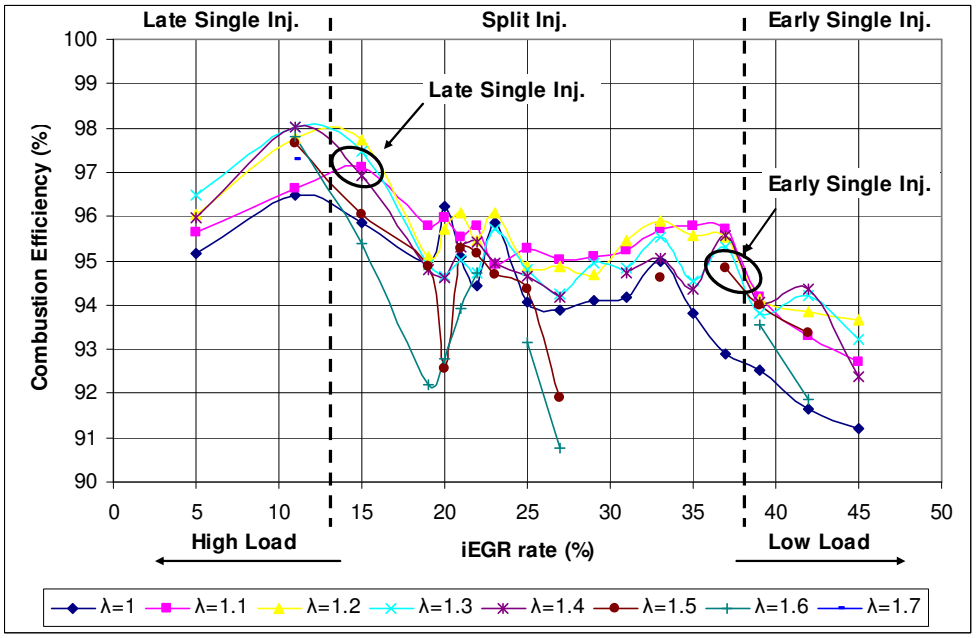

b)

Figure 5.30 Combustion Efficiency by Various Injection Strategies

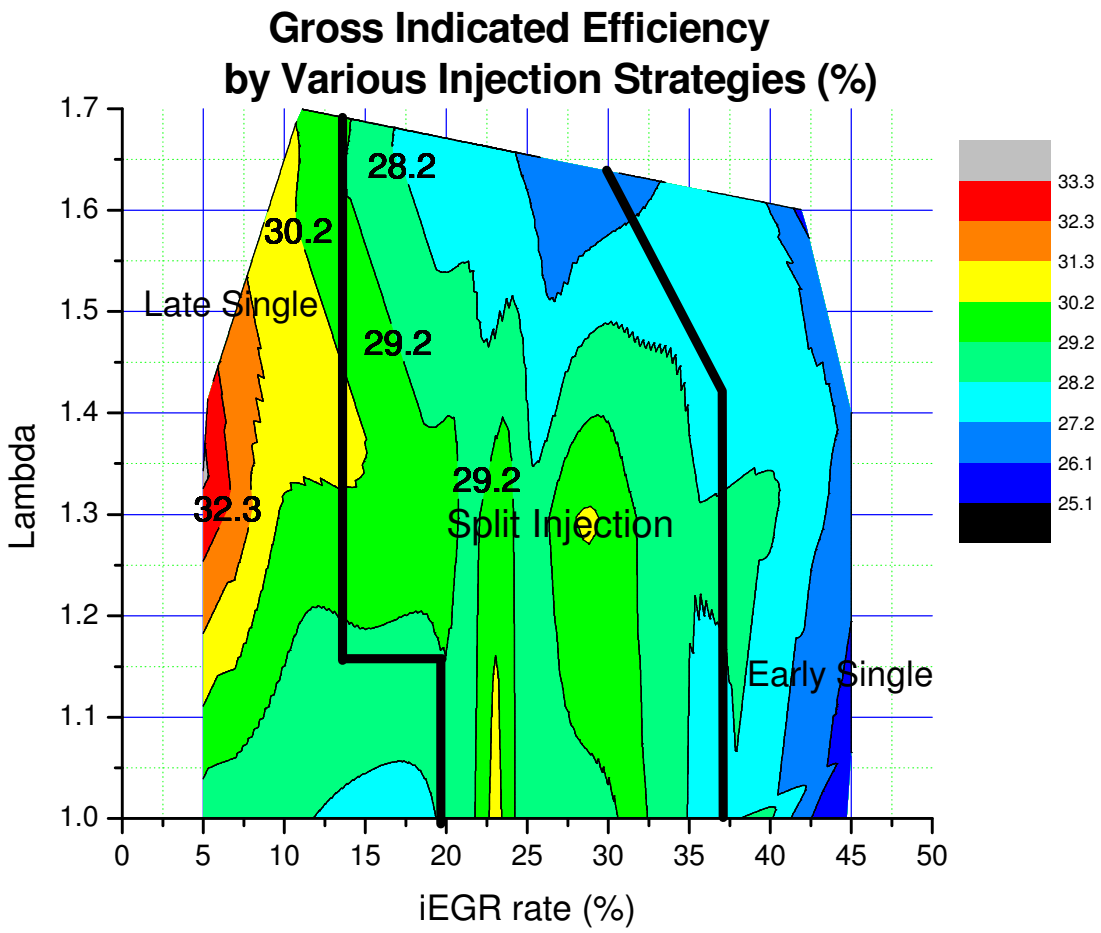

a)

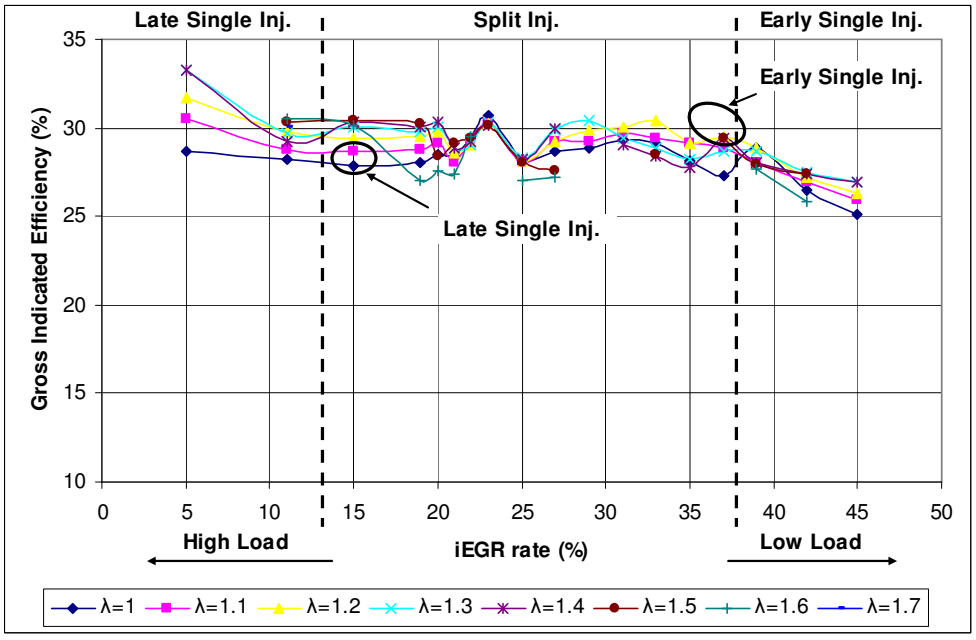

b)

Figure 5.31 Gross Indicated Efficiency by Various Injection Strategies

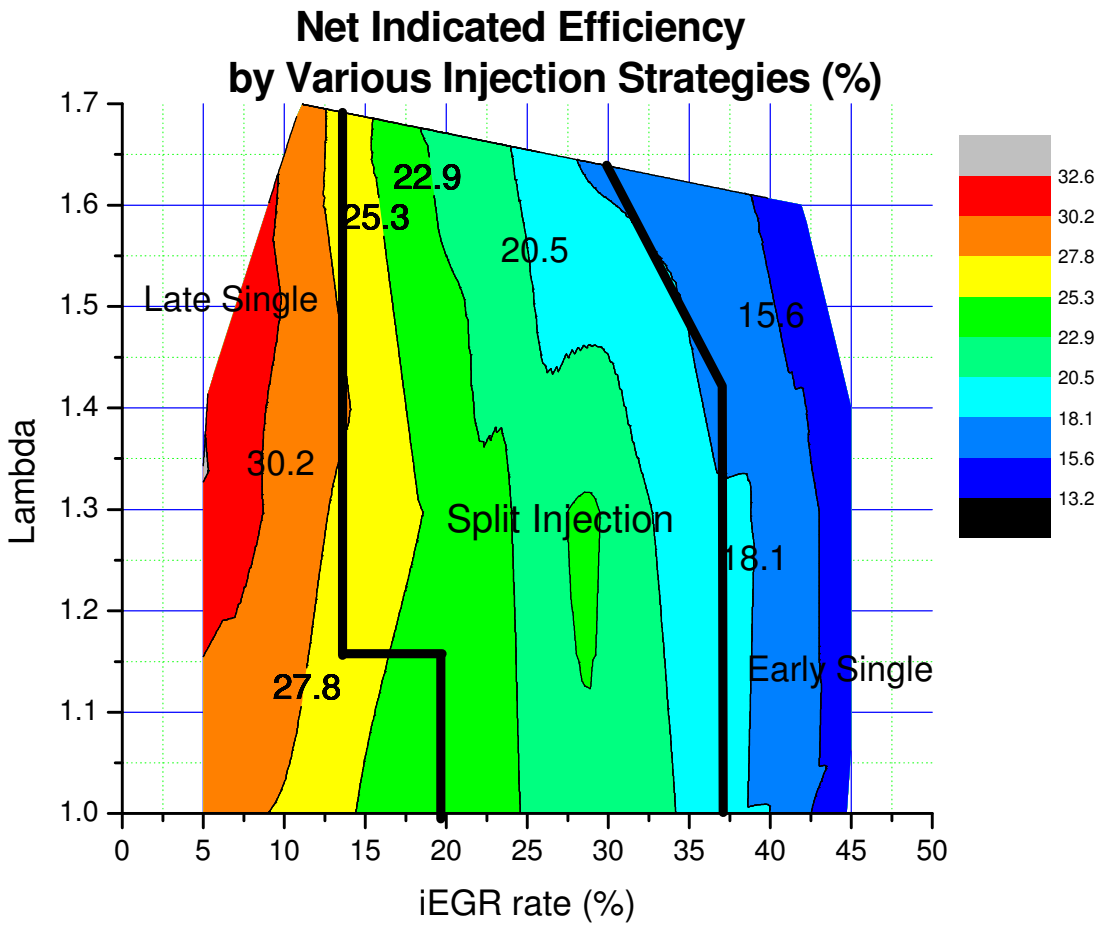

a)

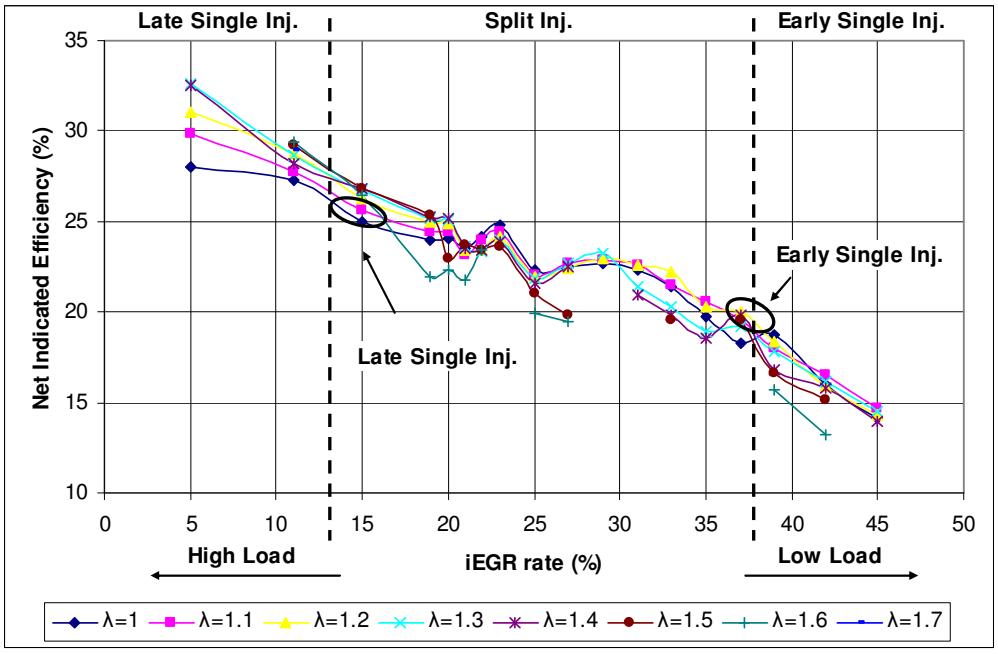

b)

Figure 5.32 Net Indicated Efficiency by Various Injection Strategies

5.8 Comparison of CAI Combustion Using DME Injection with Conventional SI Combustion

5.8.1 Introduction

It is necessary to compare the current results with conventional SI using the same engine. Thus, the advantages and drawbacks of the combustion achieved by Various DME Injection Strategy can be discussed.

The SI test conditions are shown in Table 5.4 and Figure 5.33:

Table 5.4 SI Test Conditions

Parameters		Value	Parameters	Value
Compression Ratio		13	Valve Lift	8 mm
Engine Speed		1500 rpm	Intake Temperature	20~25 °C
Coolant Temperature		80 °C	Gasoline	Unleaded 95 RON
Oil Temperature		55 °C	Gasoline inj. Pressure	2.5 bar
Valve Timing (63 °CA overlap)	IVO	33 BTDC of intake	**Lambda**	**1.1**
	IVC	191 ATDC of intake	DME inj. Pressure	40 bar
	EVO	187 BTDC of intake	EGR	≈13%
	EVC	30 ATDC of intake	**Load Controlled by Throttle**	

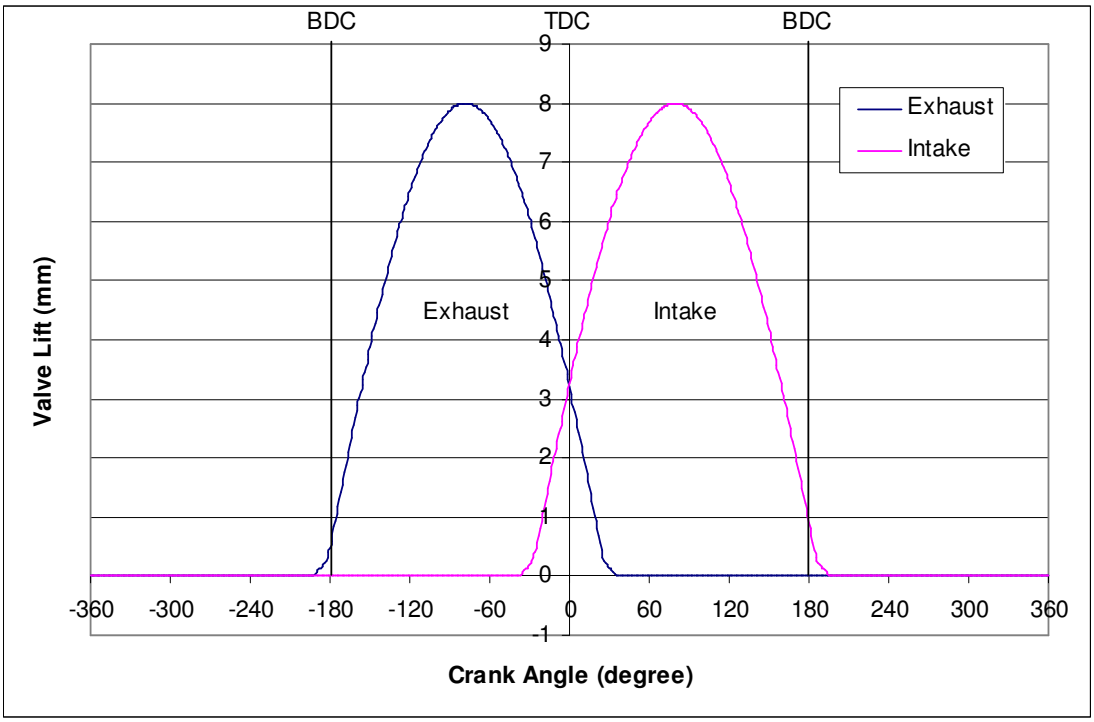

Figure 5.32 Valve Timing of SI Combustion

Although lambda 1 is the most attractive A/F ratio for SI engine, data under lambda 1.1 is selected for the comparison. This is because it is hard to get rid of knocking combustion with CR of 13 under high load, lambda 1 and SI operation on this engine. Both SI and DME pilot combustion are stable under λ= 1.1 and the following results of both modes are achieved at MBT timing. It is noted that the effective compression ratio is 12.4 due to late close of intake valve.

5.8.2 Operation Range and Combustion Stability

The COVimep of both CAI and SI combustions are shown in Figure 5.34. It can be seen that the operation range, either the highest or the lowest load boundary, has been successfully extended by Various DME Injection Strategy. Under CR 13 and lambda 1.1, the highest load of SI combustion is limited by knocking combustion while the lowest load is limited by misfire due to relatively high iEGR. The highest load of Various DME Injection combustion (net IMEP 8.5 bar under lambda 1.1; 9.13 bar under lambda 1.0) is nearly impossible to be achieved with SI combustion under CR 13 without air boosting. The lower border of Various Pilot DME Injection combustion can be further extended, as mentioned if more iEGR is introduced.

Compared with SI mode, more stabile combustion can be achieved with CAI combustion with DME Injection. In addition, since flammable DME is used as the ignition source, the flame starts from multiple injection points of DME rather than a point in SI mode, resulting in better combustion stability.

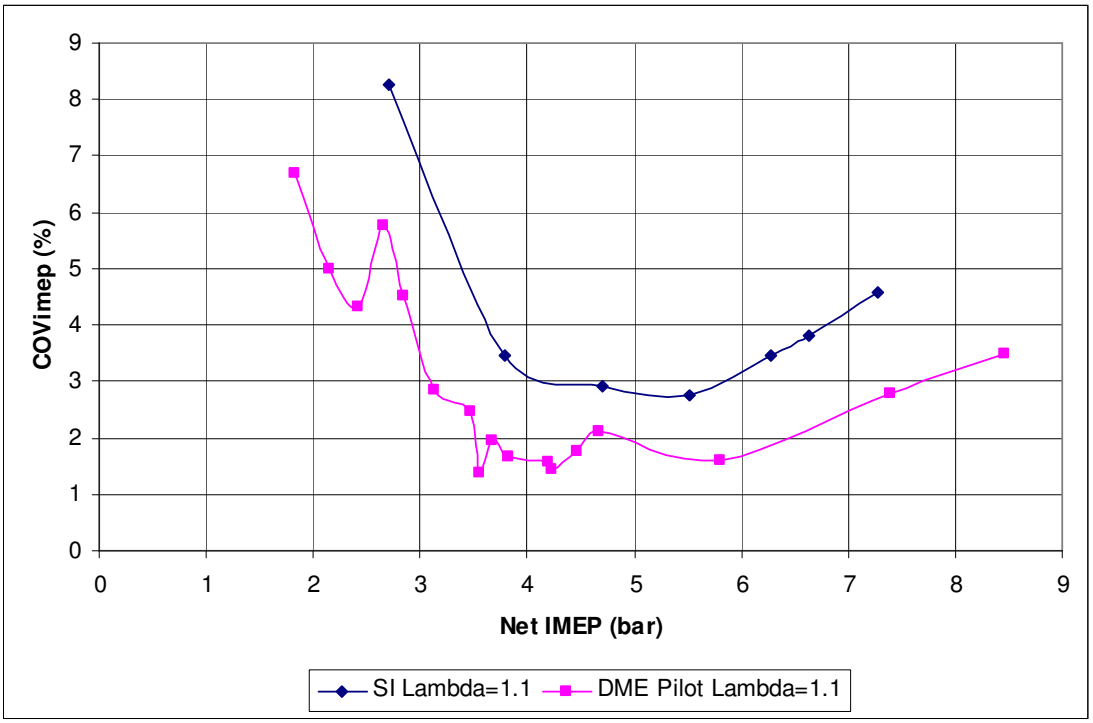

Figure 5.34 COVimep as a Function of Load by SI and DME Pilot combustion

5.8.3 Efficiencies

The trends of gross indicated efficiency and net indicated efficiency are shown in Figure 5.35.

The gross indicated efficiency is generally higher, especially in low load range, in DME split injection combustion mode than it is in conventional SI mode. At higher load range (Net IMEP > 5 bar), the efficiency improvement is insignificant due to the flame propagation of the entire (SI and maximum load DME Split) or main combustion (mid load DME Split) process in both modes. The combustion phasing (CA50) and combustion duration (CA10-90) of DME Pilot mode are slightly earlier and shorter than SI mode as shown in Figure 5.36 and 5.37 respectively, resulting in slightly higher engine output.

However, as the loads decrease (Net IMEP < 5bar), the improvement of gross indicated efficiency is obvious by DME Split injection combustion mode. This is because in low load DME Pilot mode, fast CAI combustion becomes the main combustion process and the benefits of CAI are apparent compared with SI combustion. The earlier and faster combustion of CAI in DME Pilot mode can be apparently observed in CA50 and CA10-90 diagrams.

However, the net indicated efficiencies of DME pilot combustion is lower than SI mode in the entire region except in the maximum load point. The difference between gross and net work is the pumping work. In SI mode, the throttle is used to control the engine load so that the intake pumping loss is increased during part load operation. In DME pilot mode, the engine is operated at WOT to minimise the intake pumping work, however, as the exhaust pipe is throttled to achieve high internal EGR rate, the exhaust pumping work is significantly increased in low load operation. In Figure 5.35, when the load is higher than 6.5 bar net IMEP, the net indicated efficiency of DME Pilot mode is higher than SI mode due to better gross output and the intake pumping work in SI is higher than the exhaust pumping work in DME Pilot. With the load reduced (net IMEP < 6.5 bar), the increased exhaust pumping work in DME pilot combustion is so large that it losses the benefits of both CAI combustion and WOT operation, resulting in low net indicated efficiencies.

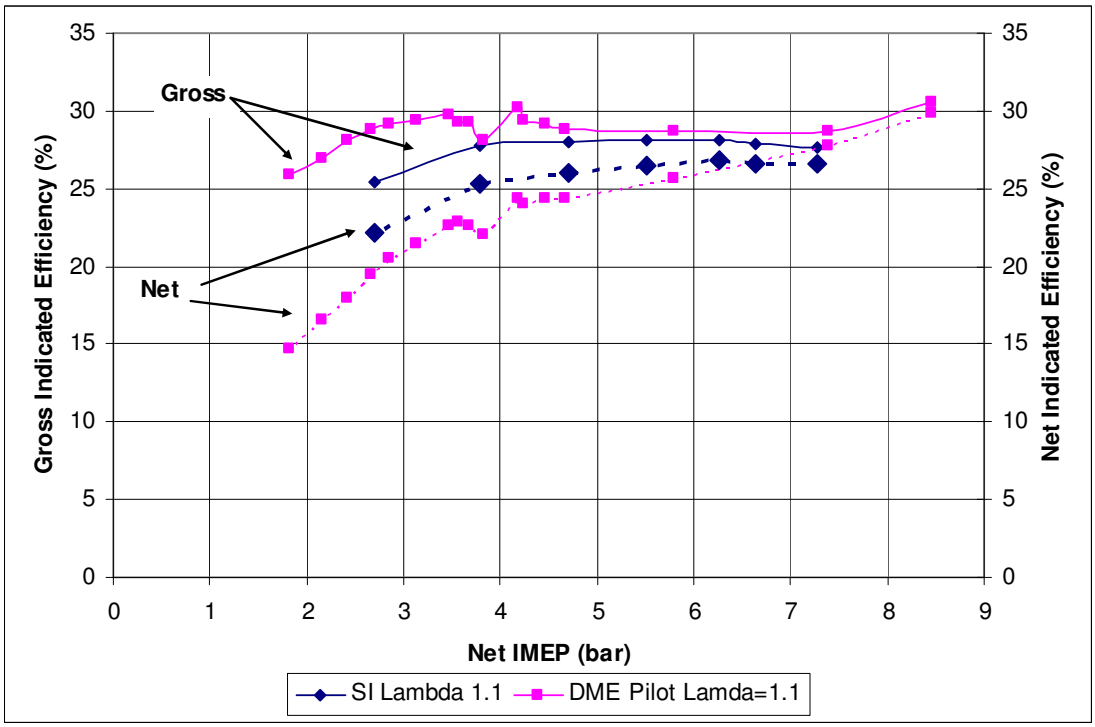

Figure 5.35 Gross and Net Indicated Efficiency (%) as a Function of Load by SI and DME Pilot combustion

5.8.4 Heat Release Analysis and Emissions

Figure 5.36 and Figure 5.37 shows the combustion phasing and combustion duration of both modes respectively. The combustion is advanced as load is reduced in both modes when the IMEP is above 4 bar. The CA50 of CAI combustion with DME injection is more advanced than the SI mode, due to fast auto-ignition combustion.

The combustion durations in both modes are similar at highest loads. In the case of CAI combustion with DME injection, the combustion duration decreases rapidly as the load is reduced and reaches its minimum at 4 bar IMEP, due to the change in combustion modes and the effects of iEGR as explained above. In comparison, the combustion duration in the SI mode stayed fairly constant at high loads and then increases as the load decreases due to slower flame speed at lower pressure and temperature by the throttled intake. At the minimum load (2.7 bar net IMEP) the SI combustion is extremely long even with the most advanced spark timing.

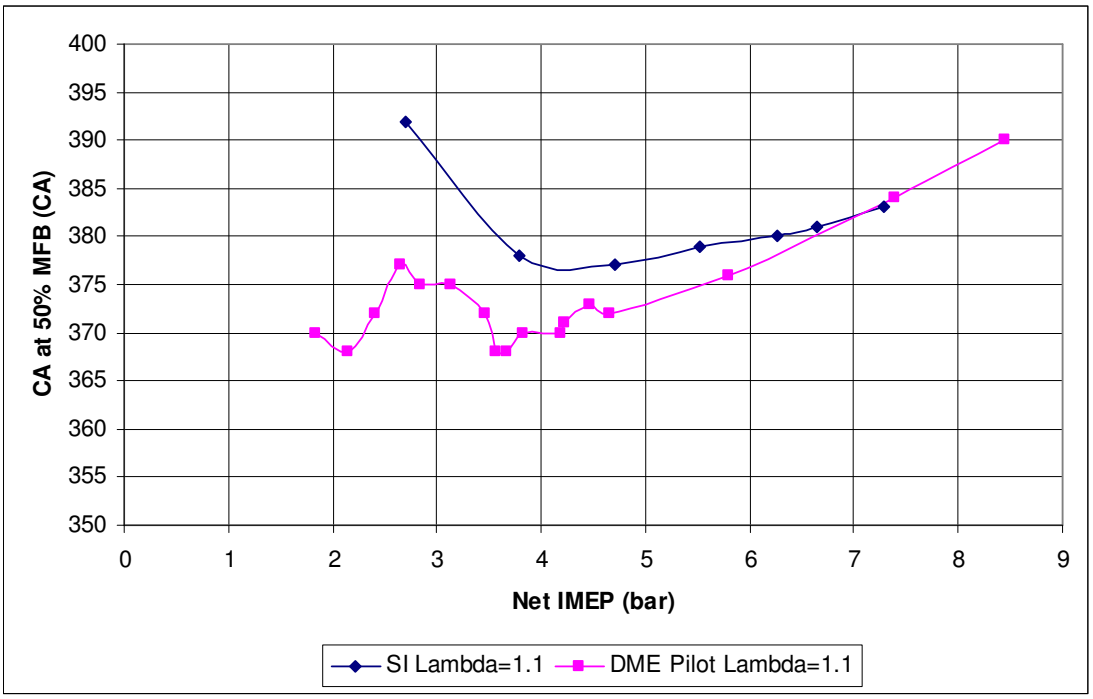

Figure 5.36 CA50 as a Function of Load with SI and DME Pilot Combustion

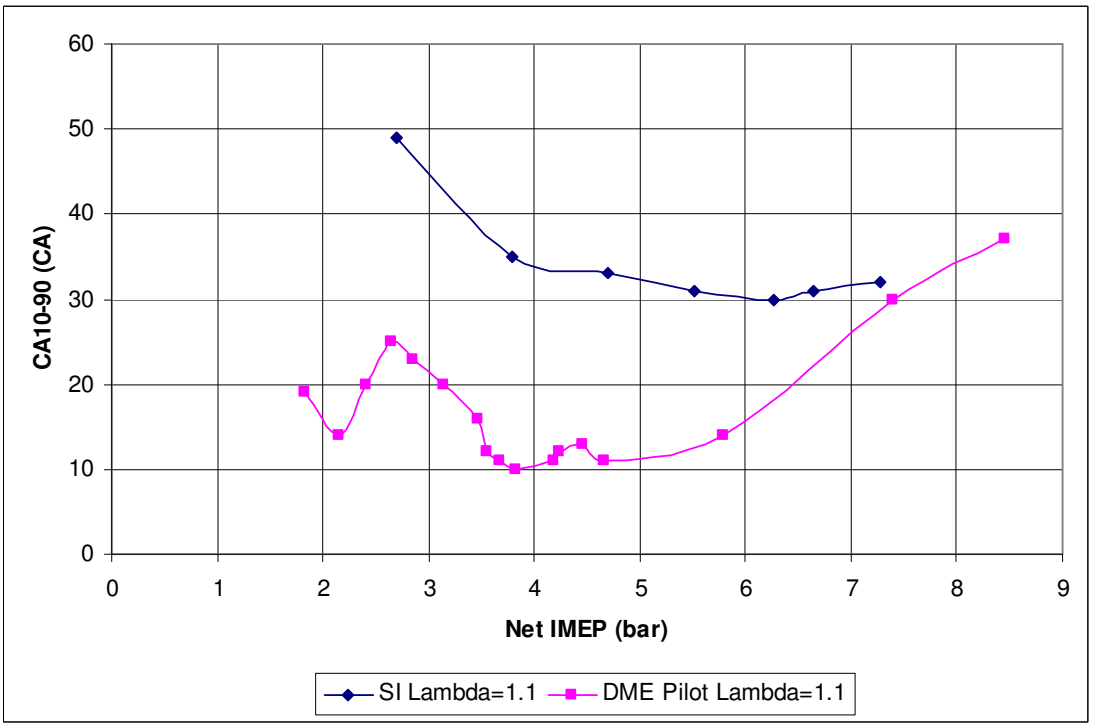

Figure 5.37 CA10-90 as a Function of Load with SI and DME Pilot combustion

CO, uHC and NOx emissions of both modes are presented in Figure 5.38-5.40. It can be seen that CO emissions are similar for both operations. The DME pilot combustion has the

same uHC emissions with SI mode at high load but extremely higher uHC emissions than SI combustion when load reduces. As expected, large reduction of NOx emissions are realised in DME pilot combustion compared to SI combustion.

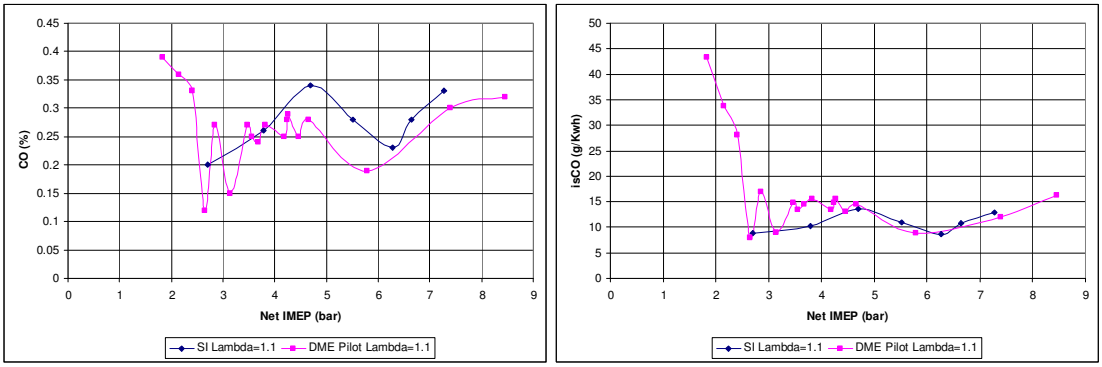

Figure 5.38 CO Emissions as a Function of Load with SI and CAI Controlled by DME Combustion

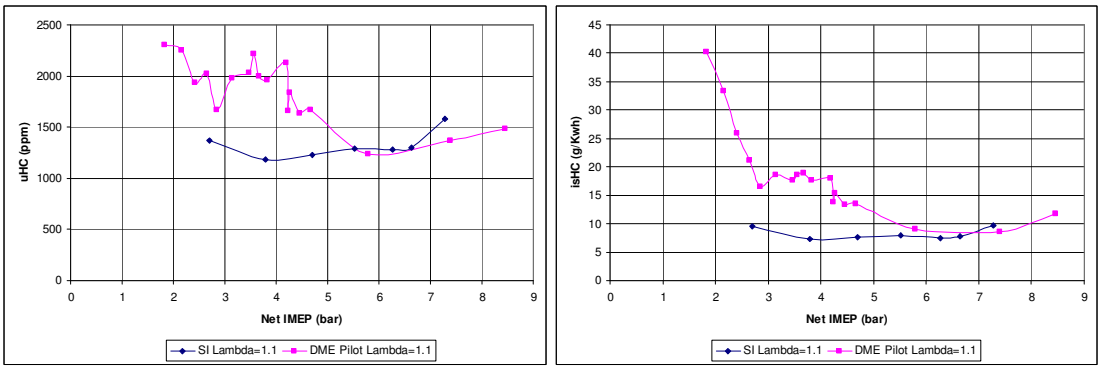

Figure 5.39 uHC Emissions as a Function of Load with SI and CAI Controlled by DME Combustion

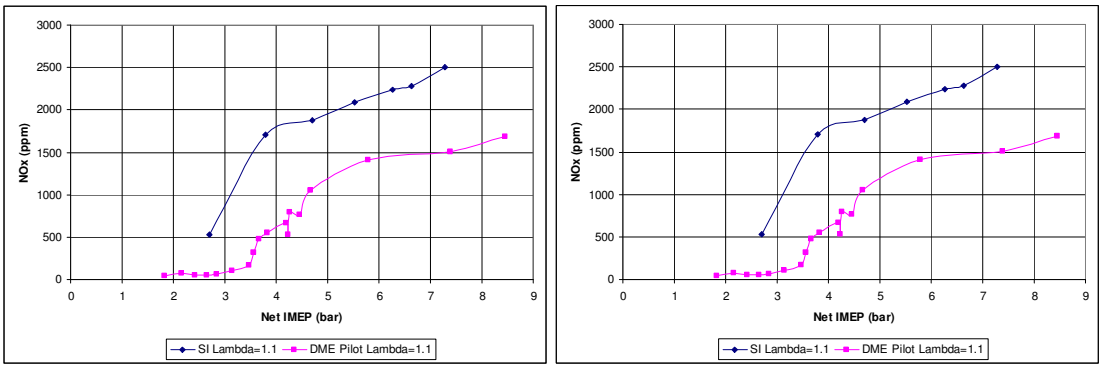

Figure 5.40 NOx Emissions as a Function of Load with SI and CAI Controlled by DME Combustion

In order to further understand both combustion processes, two specific load points with the same fuelling rate are selected and the results are shown in Table 5.5 and Figure 5.41-5.46. The conclusions are as follows:

1) Fast flame propagation and auto-ignition hybrid combustion is successfully achieved with the assistance of DME injection while the conventional SI combustion is characterised as slow flame propagation process.

2) The CAI combustion with DME injection is more close to constant volume combustion than the SI mode and able to achieve higher output and better efficiencies with a same fuelling rate (Figure 5.41).

3) As the SI mode presented here is operated at 63 °CA valve overlap, the intake pressure is higher than nature aspired pressure and the exhaust gas are re-breathed from the exhaust pipe to intake pipe. Thus, iEGR are also included in SI mode and the draw back of intake throttle is not apparent. The exhaust throttling significantly increases the exhaust back pressure, which induces large exhaust pumping work during the exhaust stroke. (Figure 5.42 – 5.43)

4) In CAI combustion mode with DME injection, the peak pressure is always higher than SI due higher peak heat release rate (Figure 5.44).

5) In Figure 5.45, it can be seen that the heat release of SI starts early and last long during the combustion process. However, the CAI combustion with DME injection is

characterised with a hybrid mode of flame propagation and multiple auto-ignition combustion. The transition point, T, between the two combustion modes is at 369 °CA degree and the ratio of flame propagation and auto-ignition is 18.5% / 81.5% (Figure 5.45-5.46).

6) As shown in Table 5.5, the gross indicated efficiency of CAI combustion with DME injection is higher than that of SI mode. But the net indicated efficiency of CAI combustion with DME injection is lower than SI mode because of its greater pumping loss.

7) At the same fuelling rate, CO emissions are similar but uHC emissions from DME pilot mode are as twice as they are in SI mode, resulting in relatively low combustion efficiency. However, over 90% reduction of NOx emissions are achieved in DME pilot mode.

Table 5.5 Operation Conditions and Results of Split Injection Combustion and SI Combustion

Parameters		DME Split		SI	
Geometric Compression Ratio		13		13	
Effective Compression Ratio		12.92		12.46	
Lambda		1.1		1.1	
iEGR (%)		31		6	
Intake Throttle Opening (°)		WOT		8	
SOI2 or SI Timing (CA degree)		347		335	
COVimep (%)		2.12		2.9	
Fuel MEP (bar) *		15.3		14.9**	
Gross IMEP (bar)		4.55		4.15	
Net IMEP (bar)		3.47		3.78	
Pumping MEP (bar)		1.09		0.36	
Combustion Eff (%)		95.24		97.33	
Gross Indicated Eff (%)		29.7		27.74	
Net Indicated Eff (%)		22.6		25.3	
Thermal Eff (%)		31.19		28.5	
CA10 (degree)		363		360	
CA50 (degree)		372		378	
CA90 (degree)		379		395	
CA10-90 (degree)		16		35	
CO (%)	isCO (g/KWh)	0.27	14.8	0.26	10.2
uHC (ppm)	isHC (g/KWh)	2035	17.6	1185	7.36
NOx (ppm)	isNOx(g/KWh)	167	0.98	1702	7.19

* Due to the difference of low heat value between gasoline and DME, the total fuelling rate is evaluated as Fuel MEP, which is equal to $\frac{m_g * LHV_g + m_D * LHV_D}{V_d}$

** The fuelling rates are measured by the injection pulse widths and the actual fuelling rates could vary with different in-cylinder pressure (affect DME) and intake pressure (affect gasoline). The values presented here are calculated from the injection pulse widths.

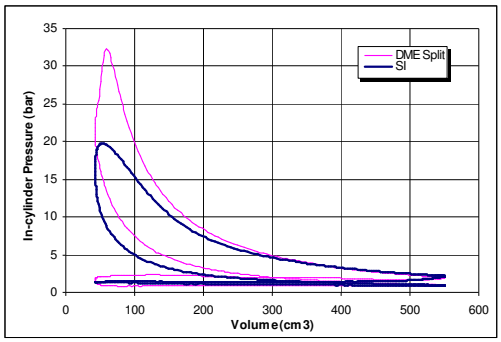

Figure 5.41 Full P-V Diagram at Constant Fuelling Rate

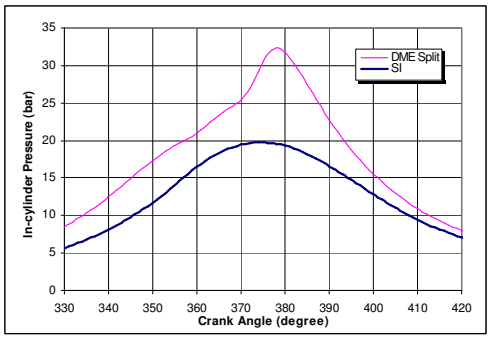

Figure 5.44 Pressure-°CA Diagram at Constant Fuelling Rate

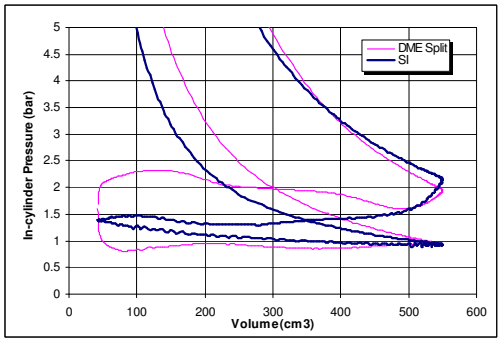

Figure 5.42 Partial P-V Diagram at Constant Fuelling Rate

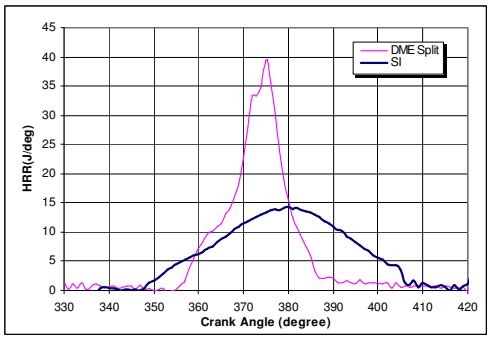

Figure 5.45 HRR-°CA Diagram at Constant Fuelling Rate

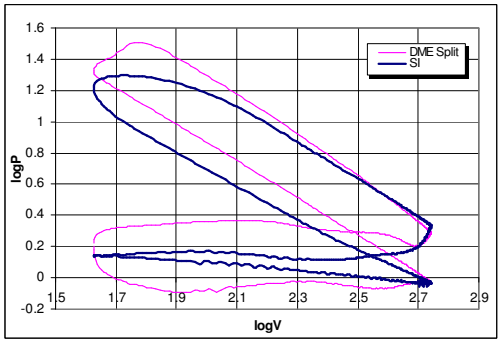

Figure 5.43 logP-logV Diagram at Constant Fuelling Rate

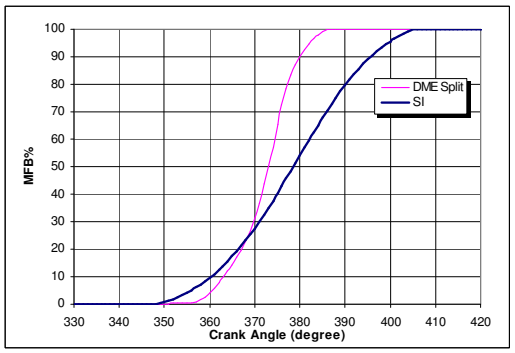

Figure 5.46 MFB-°CA Diagram at Constant Fuelling Rate

Chapter 6

Dual Fuel CAI with iEGR Achieved by Exhaust Re-breathing Strategy

Chapter 6 Dual Fuel CAI with iEGR Achieved by Exhaust Re-breathing Strategy

6.1 Introduction

This chapter presents and discusses the research on DME - Gasoline dual fuel CAI combustion concept with iEGR achieved by the exhaust re-breathing strategy. The exhaust re-breathing method is briefly reviewed following the introduction section. Then the gas exchange processes of five exhaust re-breathing valve profiles are simulated by CFD and the iEGR rates estimated. The experimental results by exhaust re-breathing strategy are presented and compared to the results by PVO & Exhaust Throttling (PVO&ET) strategy under selected test conditions.

6.2 Intake Re-open Re-breathing and Exhaust Re-open Re-breathing

The exhaust re-breathing strategy can be used to provide hot residuals to initiate the CAI combustion. It can be implemented either by exhaust valve being re-opened during the intake stroke or by intake valve being re-opened during the exhaust stroke. Kawasaki et al. [111-112] have compared the effectiveness of each method on the residual gas trapping and their effects on auto ignition combustion in a natural gas engine. Their main findings and others [113-114] are given in Table 6.1. The intake re-open re-breathing method has been chosen because of its mixture uniformity and lack of knocking combustion.

With intake re-open re-breathing strategy, the fresh air fuel mixture and EGR gas are better mixed due to the mixing process begins at the exhaust stroke in the intake port than the exhaust re-open method. As a result, the local high temperature spots are avoided so that knocking combustion is unlikely to happen.

The intake re-open re-breathing strategy is used in this study. The intake valve is pre opened during the exhaust process so that some hot exhaust gases flow into the intake port. The residual is partly mixed with the fresh charge in the intake pipe and then sucked into the cylinder during the main opening of intake valve.

Table 6.1 Comparison of Intake Re-open Re-breathing and Exhaust Re-open Re-breathing

Methods	Intake Re-open	Exhaust Re-open
	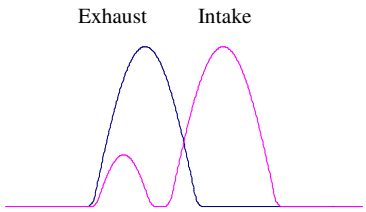	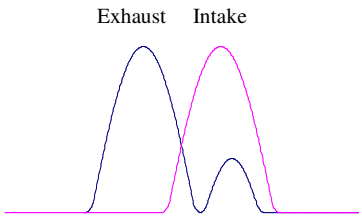
Literatures	[112] [113]	[111] [114]
Exhaust Temperature	Low	High
Average In-cylinder Temperature	High	Low
Working Range	No limitation by knocking combustion	Limited by knocking when iEGR>15%
Gas Uniformity	Well mixed	Not well mixed
Indicated Efficiency	Low	High

6.3 Simulation of Gas Exchange Process and iEGR Rate Prediction

To determine the valve profile and predict the iEGR rate of re-breathing strategy, simple computations were performed to simulate the gas exchange process with the intake re-open re-breathing strategy using Computational Fluid Dynamics software -- ANSYS FLUENT. The standard K-epsilon model is used to imitate gas flow turbulence.

To simplify the simulation, an adiabatic chamber which has a moving bottom boundary (piston) is employed and set as the same dimension of the Ricardo E6 engine as well as the size and position of inlet and outlet ports which are used in this study as shown in Figure

6.1. The movement of the bottom boundary is simulated as the movement of piston and the geometric compression ratio is set as 13 according to the CR used in this study. The intake and exhaust valves are modelled of the same sizes and shapes as the ones used in the experiment. The exhaust valve profile is fixed as well as the main intake valve opening profile. Five intake re-open profiles are simulated in terms of various re-opening timing and re-open valve lift, named as Intake 1- 5, and the Intake 6 is the reference case which is the one without intake re-opening operation, shown in Figure 6.2.

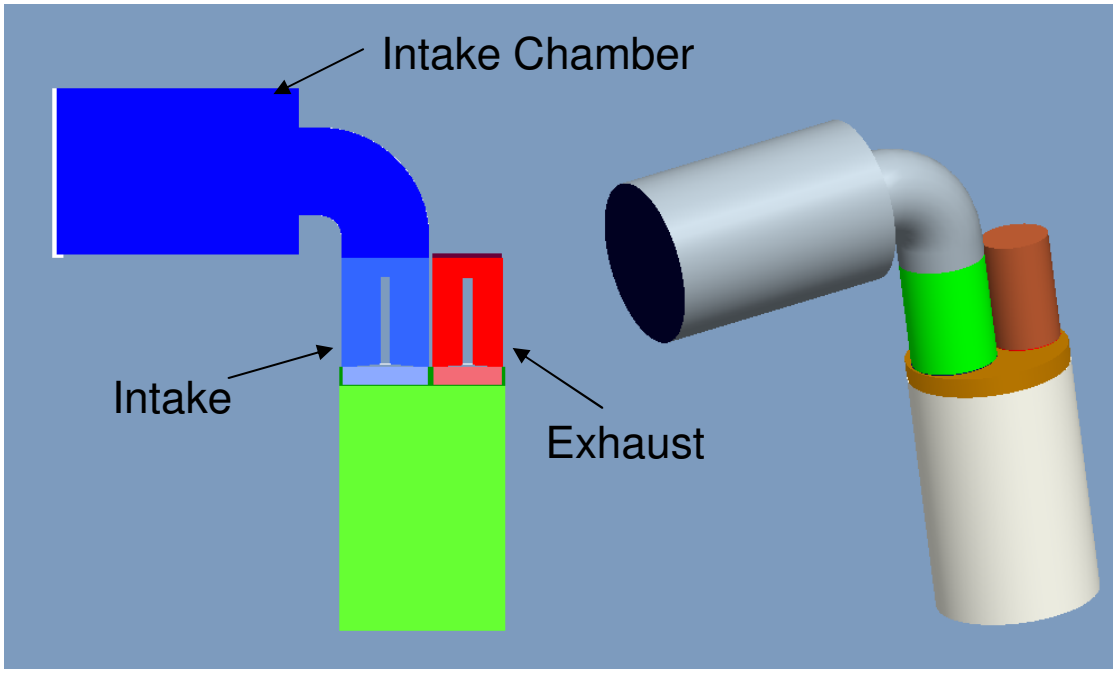

a) 3-D Model of Single Cylinder Engine

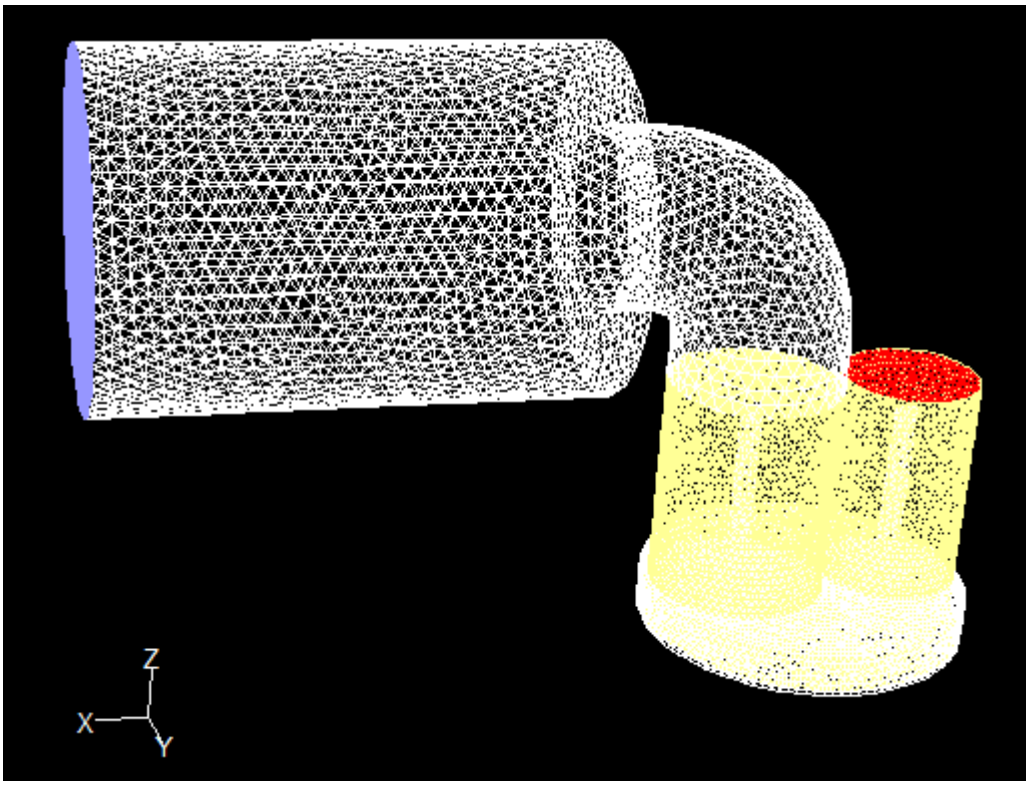

b) Gridded Model of Single Cylinder Engine

Figure 6.1 Simulation Models of Single Cylinder Engine

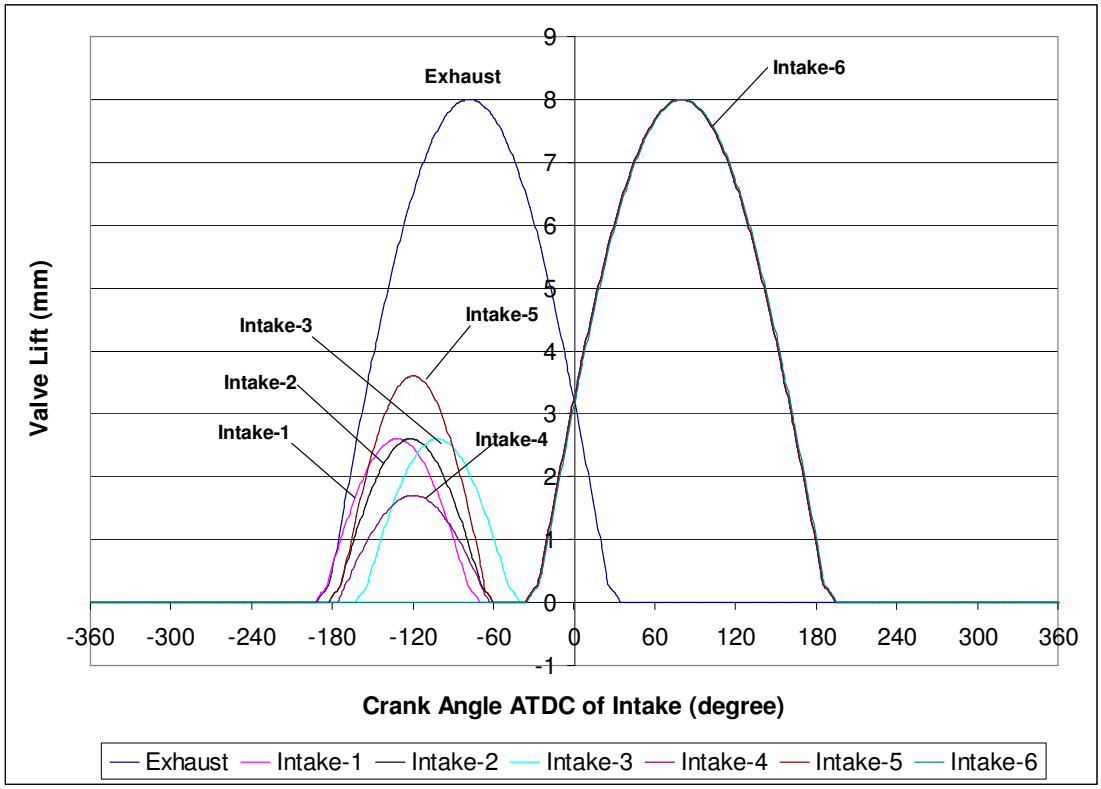

Figure 6.2 Six Intake Valve Profiles Used in the Simulation

Combustion process is not involved in this simulation and the species transport is used as species model (without chemical reactions). Both inlet and outlet port are set as pressure inlet and pressure outlet respectively. In particular, the gases going across the outlet boundary are considered as exhaust gas which is consisted of 20% CO_2 and 80% N_2. In addition, there is an intake chamber with the same size of cylinder chamber attached between inlet boundary and the atmosphere. The intake chamber ensures the entire re-breathed residuals can be trapped and mixed with initial fresh charge (23% O_2 and 77% N_2) within the chamber, and then totally sucked into the combustion chamber. As a result, the boundary between atmosphere and intake chamber can be considered as a pressure boundary that all the gases going across the boundary are fresh charge (23% O_2 and 77% N_2).

During each simulated engine cycle, it starts at the TDC of compression. The initial conditions at TDC are in-cylinder pressure 24 bar, temperature 1500K, and species of 20% CO_2 and 80% N_2. The concentration of CO_2 inside the cylinder is set as 20% to represent the main combustion products (CO_2+H_2O) in order to simply the calculation. The contents of exhaust gas are considered to be constant before exhaust valve opening. Therefore, the

gas exchange process can be modelled and the iEGR rates by the above re-breathing valve timing can be indentified. The iEGR rates by simulations is the actual EGR rate by mass, which is defined as

$$\text{iEGR rate (by mass)} = \frac{\text{Mass of } CO_2 \text{ inside cylinder}}{\text{Mass of } CO_2 \text{ in exhaust}}$$

Where, the mass of CO_2 inside the cylinder is calculated after the intake valve closure.

As shown in Figure 6.3, intake valve lift profile 4 of the smallest opening lift and duration produces the least iEGR. As the valve lift and duration increases from Intake 1, then Intake 2 to Intake 5, more iEGR is obtained. With the same opening duration and lift of Intake 1, Intake 2, and Intake 4, the iEGR rate can be changed from 29.2% to 35% as the intake opening period is shifted towards TDC, demonstrating the potential of controlling iEGR through variable valve timing. Due to the limited time available, the fixed valve timing of Intake 2 is selected for the experimental tests, with a predicted iEGR rate of 31.72%.

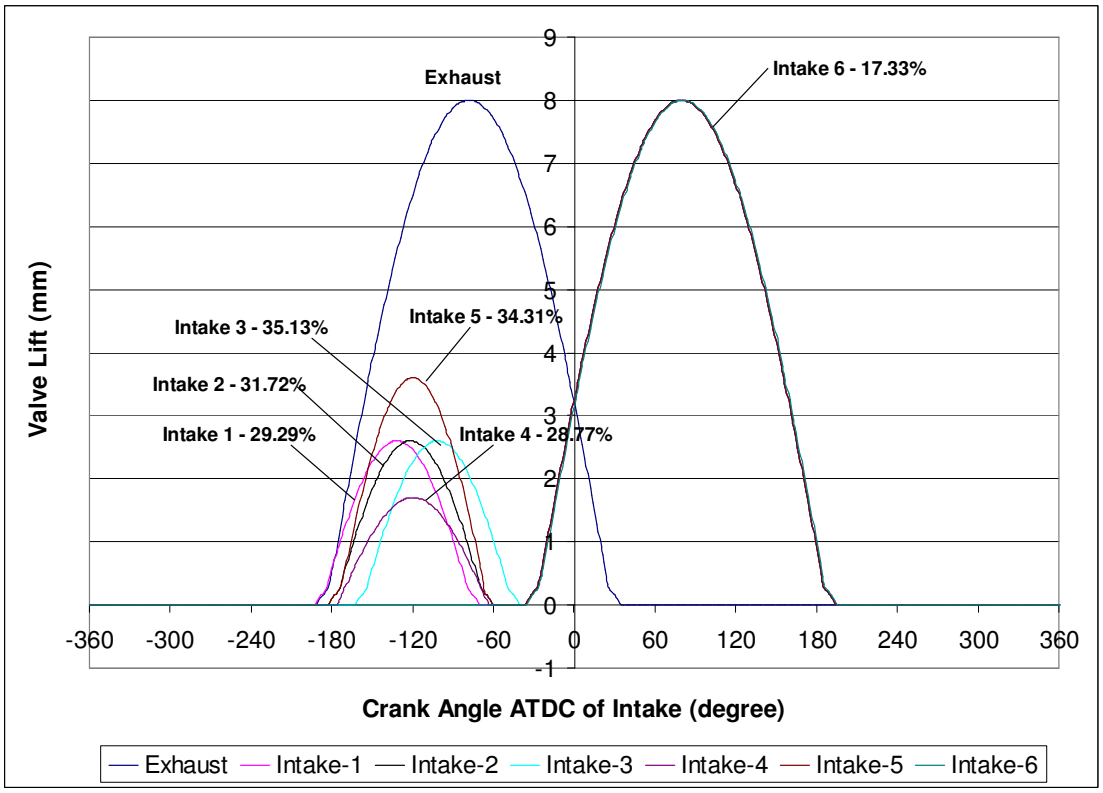

Figure 6.3 Simulation Results of iEGR Rates with Six Intake Valve Profiles

6.4 Cam Lobe Design

Based on the selected valve timing, a new intake cam lobe shown in Figure 6.4 is designed and manufactured in order to implement the intake re-open. The distance between the centre of the hole and the edge corresponding to every degree of the circle are calculated and listed in an Excel file. The 3D drawing of the lobe and the Excel file are given to the factory manufacturing it with the CNC milling machine. The valve timings are shown in Table 6.2 and Figure 6.5. The main open profile of the valve is the same as it is in Chapter 4 and Chapter 5 in order to keep effective compression ratio constant. With this cam lobe, the iEGR rate was measured by the in-cylinder sampling system and it was determined to be 36.5% under the operation condition of lambda 1.

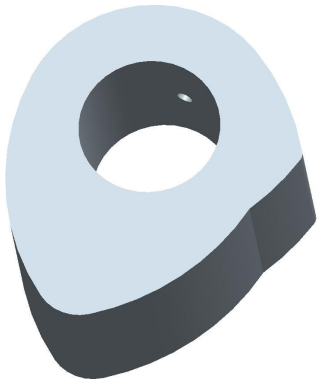

Figure 6.4 Modified Intake Cam Lobe for Intake Re-open Strategy

Table 6.2 Selected Intake Valve Re-open Timing

	Valve Timing (°CA ATDC of Intake)		Valve Lift (mm)
Intake	Re-IVO	-183	2.6
	Re-IVC	-60	
	Main-IVO	-33	8
	Main-IVC	191	
Exhaust	EVO	-187	8
	EVC	30	

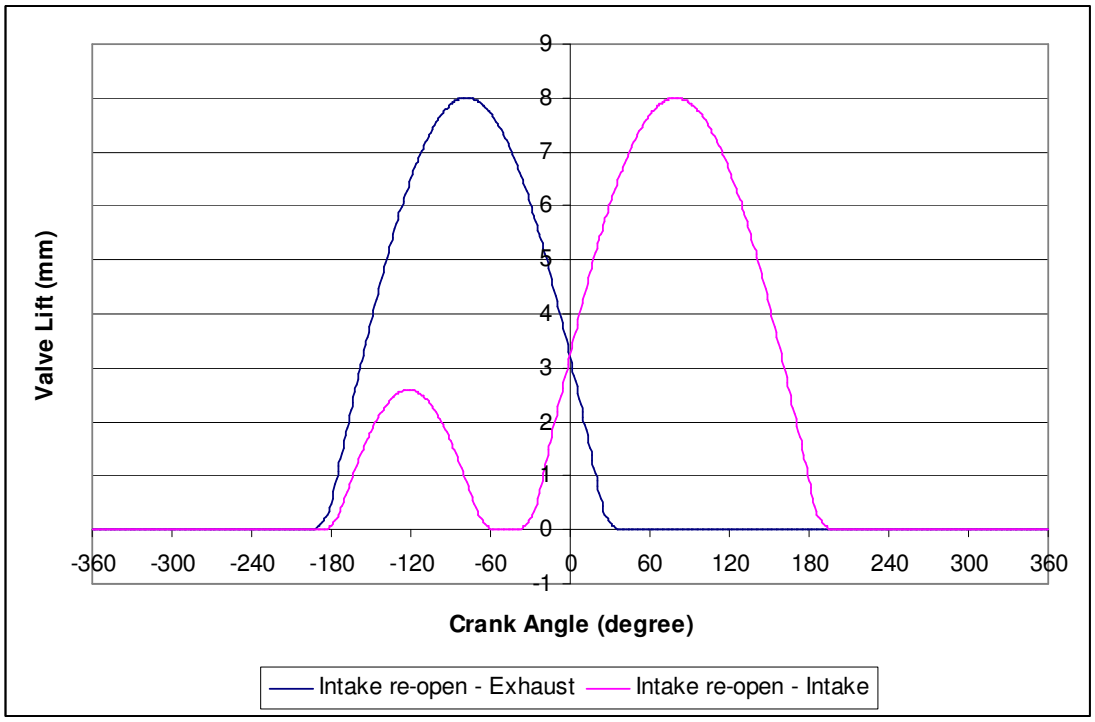

Figure 6.5 Valve Timing Diagrams of Intake Re-open Re-breathing Strategy

6.5 Experimental Test Results and Analysis

6.5.1 DME Split Injection Optimisation

Since the iEGR rate is 36.5%, according to the operating range presented in Chapter 5, DME split injection strategy is applied in the following tests.

The injection timing and quantity of both the first and second DME injections were firstly set as the optimal value as discussed in Chapter 4. However, no stable combustion could be with little heat release which is thought to be low temperature heat release by pilot DME. In order to achieve stable combustion, both DME injection quantities needed to be increased. Thus, under a fixed air fuel ratio, the total percentage of DME of the total fuel was increased as well. Figure 6.6 shows the COVimep as a function of DME fraction for both the re-breathing and PVO & ET methods. The tests are performed under similar mid load condition and the iEGR rate.

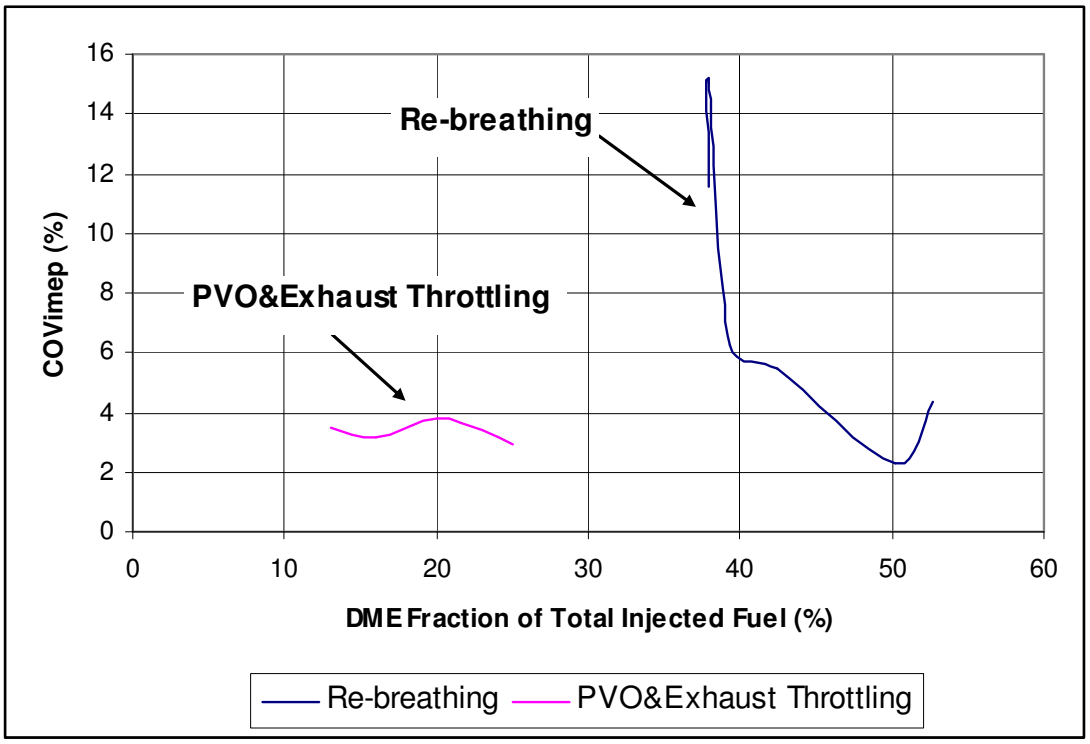

Figure 6.6 COVimep as a Function of DME Fraction by Re-breathing and PVO&ET Methods

Compared to the PVO&ET method, more DME is needed to achieve stable combustion with the re-breathing method under the same iEGR rate. This is because with re-breathing method, some exhaust gas flows into the intake port when the intake valve opens first time, and it is then sucked back into the cylinder during the intake stroke. Due to the heat loss of the re-breathed burned to the intake port, the in-cylinder gas temperature is lower than the burned gas trapping method. In the presence of large recycled burned gas, the flame speed would be too slow to complete the combustion which exhibits large cyclic variation and high HC and CO emission. By increasing the quantity of both DME injections, the greater initial flame forming regions from the late injection and the combustion speed of premixed DME/gasoline/air from the first injection can be increased.

6.5.2 Results and Discussion

After stable combustion was achieved with the re-breathing method, experiments were carried out and compared with the PVO& ET method under three selected conditions. The PVO& ET results with back pressure of 0.69 bar and 0.76 bar were selected for similar engine outputs (IMEP), while the one with back pressure of 0.90 bar was chosen because of the similar rate of iEGR. The test conditions are given in Table 6.3, and the corresponding engine performance and emissions are shown in Figure 6.7-6.12.

Table 6.3 Test Conditions of Comparison Experiments at 1500 rpm

Parameter	**Re-breathing**	**PVO& ET**		
Injection Strategy	Split Injection	Split Injection	Split Injection	Split Injection
Back Pressure (bar/psi)	0/0	0.69/10	0.76/11	0.90/13
iEGR Rate (%)	36.5	31.0	33.2	36.9
λtotal	1- 1.4	1-1.4	1-1.5	1-1.5
DME / Gasoline Fraction	≈ 50 / 50	≈ 20 / 80	≈ 20 / 80	≈ 20 / 80

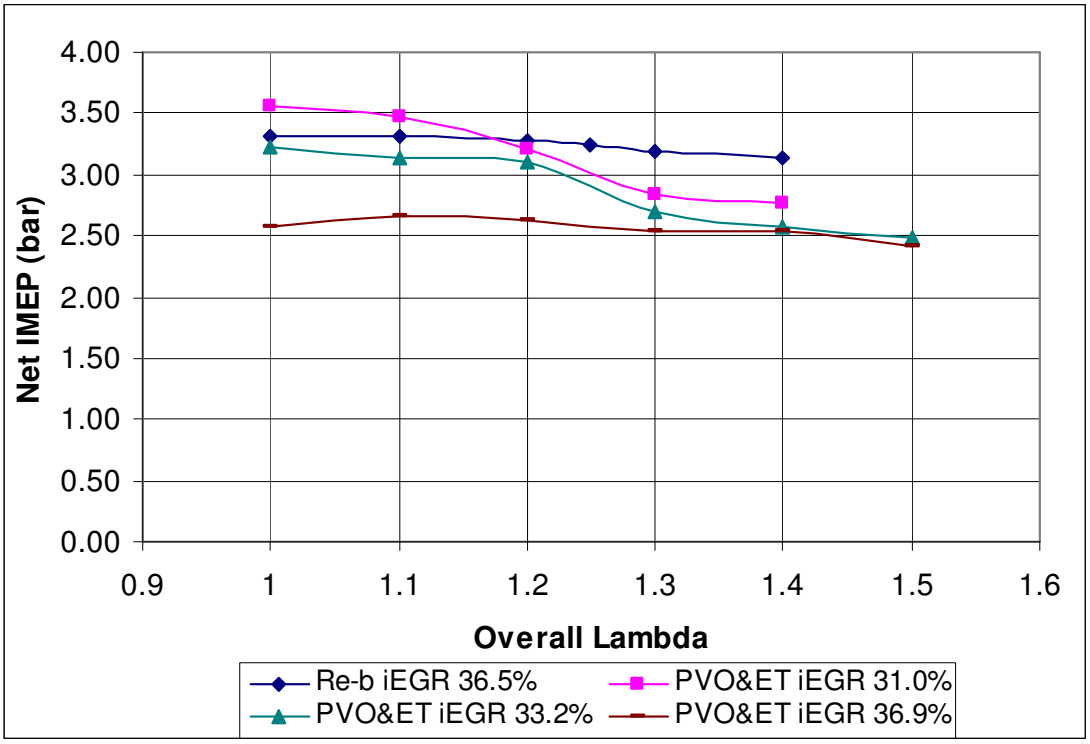

Figure 6.7 Net IMEP as a Function of Overall Lambda

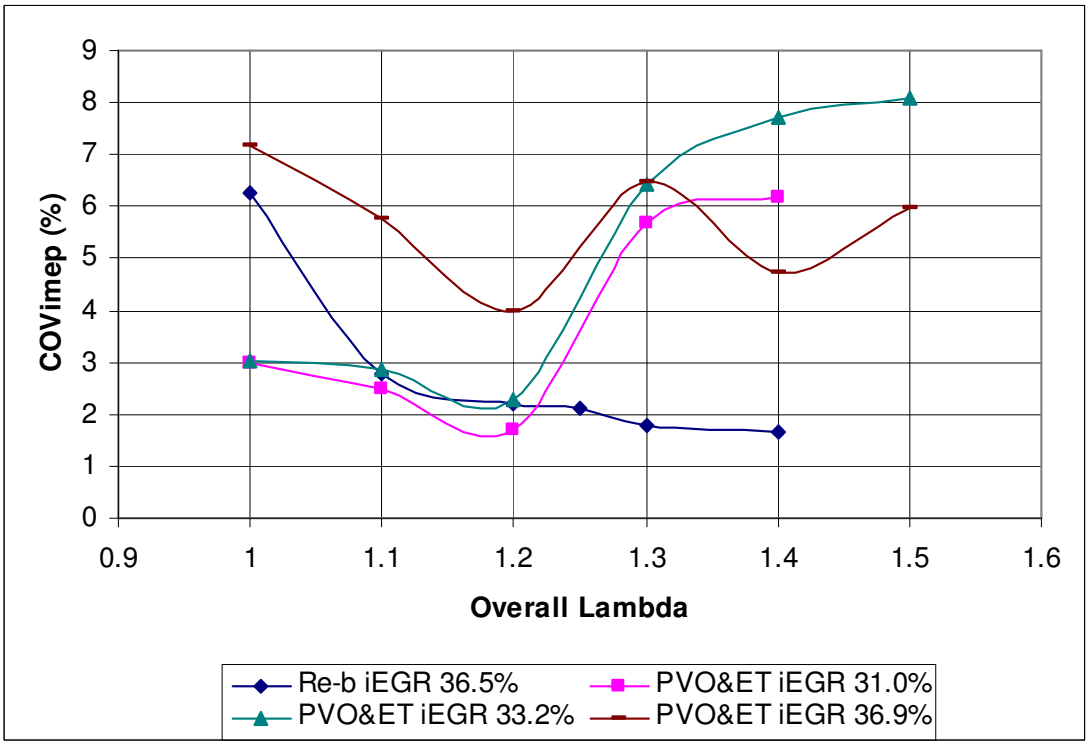

Figure 6.8 COVimep as a Function of Overall Lambda

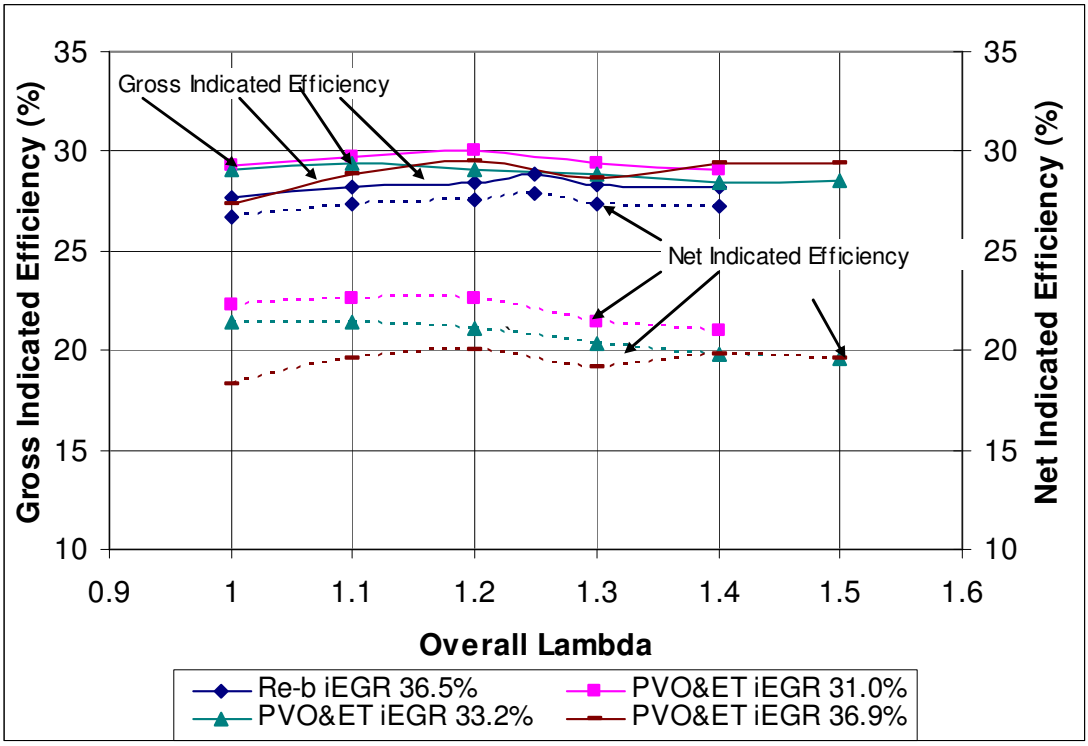

Figure 6.9 Efficiencies as a Function of Overall Lambda

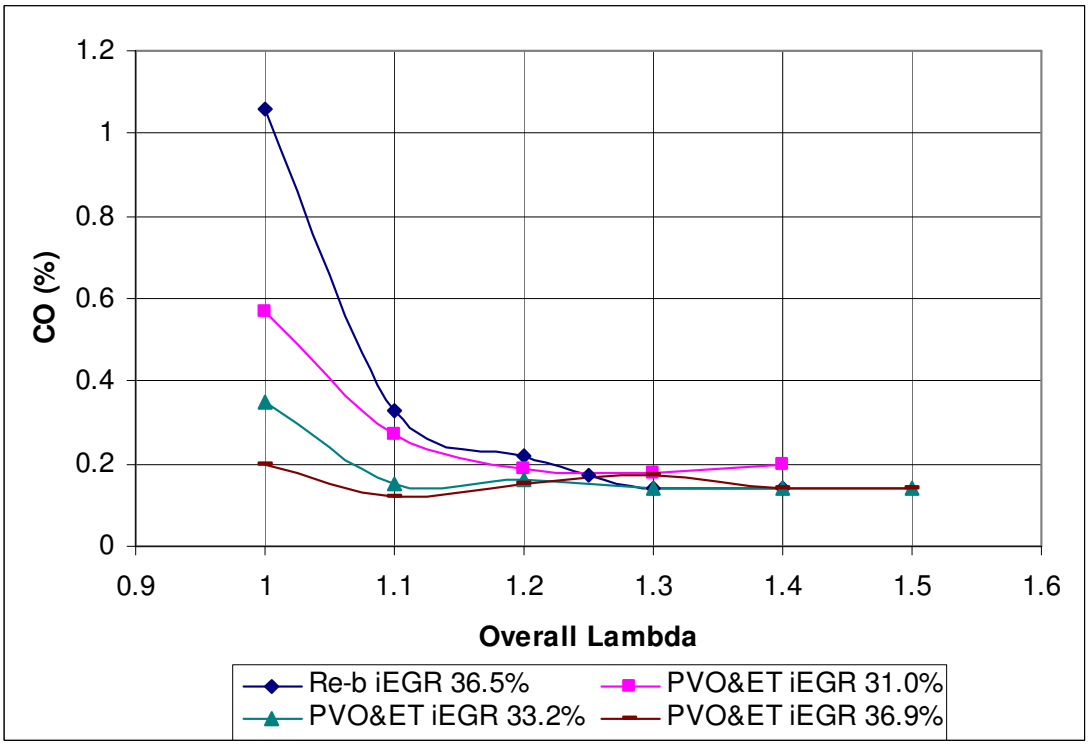

Figure 6.10 CO Emissions as a Function of Overall Lambda

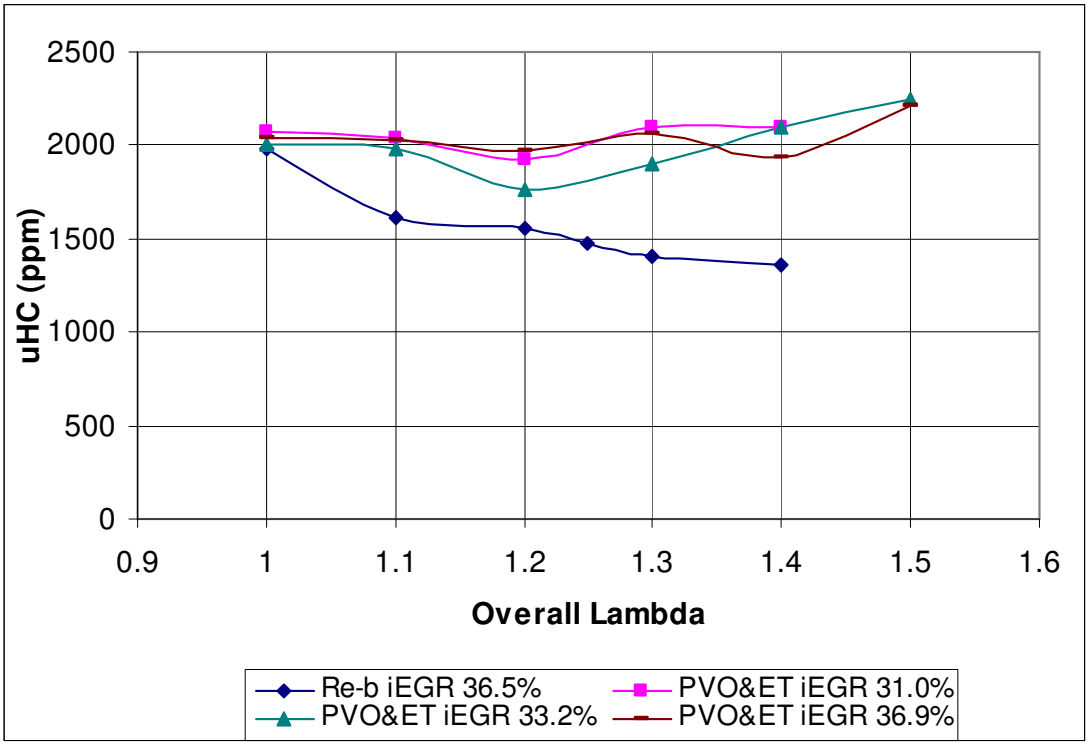

Figure 6.11 uHC Emissions as a Function of Overall Lambda

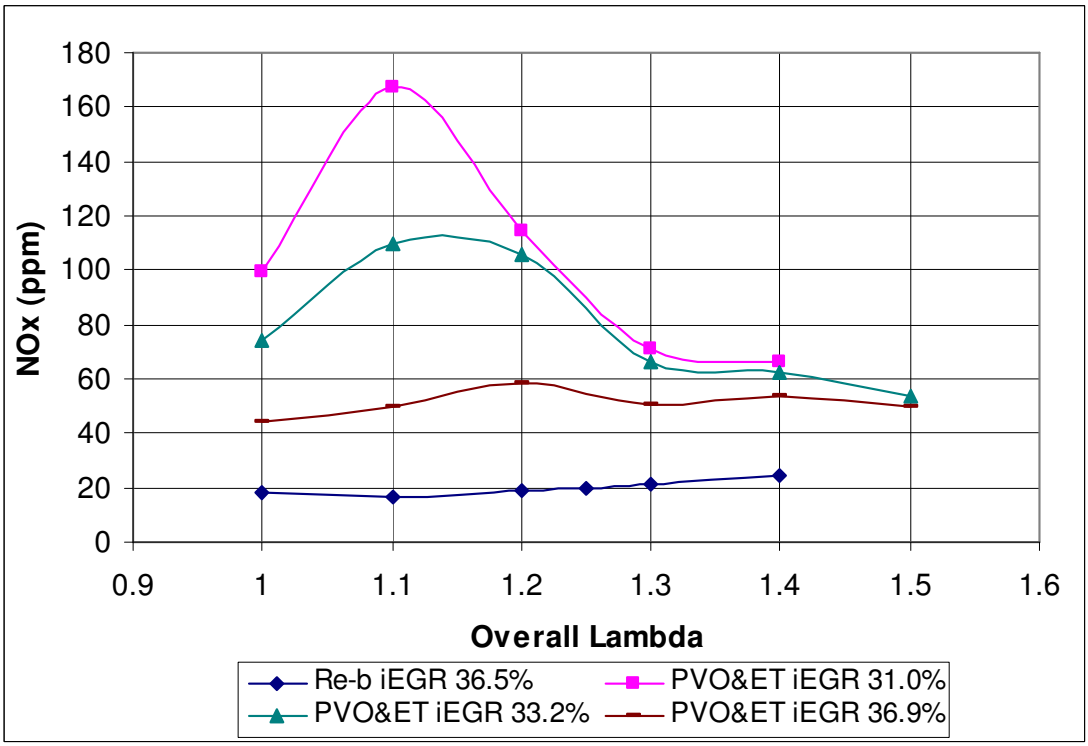

Figure 6.12 NOx Emissions as a Function of Overall Lambda

Figure 6.7 shows that the net IMEP values decrease slightly with the lambda for both re-breathing and PVO&ET at iEGR rate of 36.9%. In comparison, engine outputs of the other two PVO&ET cases are more sensitive to the relative air fuel ratio and start to drop more rapidly at lambda 1.2, when the corresponding cycle variability begins to rise faster as shown in Figure 6.8, as the combustion becomes less stable and the combustion duration becomes longer as shown in Figure 5.27.

Generally, stable combustion is achieved by re-breathing method with COVimep < 3% in the entire lambda sweep as shown in Figure 6.8. The combustion stability in leaner mixture is better than the PVO&ET operations, due to primarily the greater amount of DME injected and hence faster and more stable combustion.

The most significant difference between these two methods is the engine efficiencies shown in Figure 6.9. Engine operations by PVO&ET achieve higher gross indicated efficiencies. However, when pumping work is taken into account, PVO&ET results in much lower net indicated efficiencies than the re-breathing method (see Figures 6.9). The lower gross indicated efficiencies by the re-breathing method could be explained by three reasons. One is the higher heat loss from the gas exchange process as explained above. As a result, less heat of iEGR is utilised and some fuel is needed to be burned to heat up the in-cylinder mixture initiating the combustion. Therefore, less fuel is converted to the work done on the piston and the fuel conversion efficiency is lower. Another reason is the increased compression pumping loss due to the gasification of DME. Liquid DME vaporises as soon as it is injected into cylinder, which increases the in-cylinder pressure during compression stroke. With re-breathing strategy, more DME is injected in order to achieve stable combustion and the DME quantity reaches 50% of the total fuel amount. The compression work is relatively higher resulting in lower gross work compared to PVO&ET method. However, as both intake throttle and exhaust throttle are fully open, little pumping loss is implemented during intake and exhaust stroke. Therefore, the net indicated efficiencies by re-breathing method are quite closed to the gross one, which is one of the objectives in this study. The last reason is the heat capacity when liquid DME vaporises. The vaporisation of DME absorbs heat near the injection spray that reduces local temperature. Thus, the ignition and combustion could be deteriorated resulting in less gross work. Nevertheless, since the brake output of the engine is the power to be utilised, the higher net indicated efficiency is more relevant and it contributes to lower fuel consumption.

In Figure 6.10-6.12, it can be seen that CO emissions by the re-breathing method are generally higher than those with the PVO&ET method, especially near stoichiometric mixture. This could be caused by the presence of more fuel rich regions from the increased amount of DME injected before the start of combustion. The uHC emissions are lower in the entire lambda sweep because of more complete combustion due to increased DME injection quantity. Ultra low NOx emissions are achieved with the re-breathing method and the peak NOx emissions are about 25 ppm in the leanest mixture. This represents an over 98% reduction in NOx emissions compared to SI operation and 30-90% reduction compared to PVO&ET CAI operation under similar conditions shown in Figure 5.22.

In order to illustrate in details the differences between two iEGR trapped methods, the results and heat release analysis curves under specific condition of lambda 1 from above tests are shown in Table 6.4 and Figures 6.13-6.16 respectively, as well as the results of selected SI at part load under the condition of 5° throttle opening and lambda 1.1.

As shown in Figures 6.15-6.16, the heat release is characterised with hybrid combustion process of initial slow flame propagation and then faster multiple auto-ignition in the cases of CAI combustion with DME injection. It is also noted that the CA10 and CA50 of the re-breathing method are earlier due to advanced SOI2 timing. But the combustion duration is no longer than the other three cases of PVO & ET due to lower charge temperature. What's more, the re-breathing strategy resulted in the least amount of heat leased from flame as the transition from flame to auto-ignition heat release occurs at the most advanced crank angle. This is because the auto-ignition process of the premixed air/gasoline/DME mixture becomes more ignitable as more DME is injected during the re-breathing operation, shortening the period of flame propagation.

As shown in Table 6.4, compared to SI combustion, the re-breathing mode operation has a higher thermal efficiency but less combustion efficiency than SI mode due to higher CO and uHC emissions. As a result, the gross indicated efficiency is similar. However, the re-breathing method performs less pumping work than throttled SI combustion. Thus, the net indicated efficiency of re-breathing strategy is higher than the SI case corresponding to 5% better fuel consumption, which is one of the objectives of this study. In addition, 99% reduction of NOx emissions is achieved with re-breathing strategy.

Table 6.4 Operation Conditions and Results of Selected Re-breathing Combustion, PVO & Exhaust Throttling Combustion and SI Comsbution

Parameters	SI	Re-breathing	PVO& Exhaust Throttling		
iEGR (%)	5%	36.5	31.0	33.2	36.9
Geometric Compression Ratio	13	13	13	13	13
Effective Compression Ratio	12.4	12.92	12.92	12.92	12.92
Lambda	1.1	1	1	1	1
Intake Throttle Opening (°)	5°	WOT	WOT	WOT	WOT
SOI2/SI Timing (°CA)	337	323	329	328	327
COVimep (%)	3.45	6.2	2.9	3.02	5.7
Fuel MEP (bar)	14.96	12.4	15.9	15.0	13.5
Gross IMEP (bar)	4.15	3.43	4.67	4.39	3.91
Net IMEP (bar)	3.78	3.31	3.56	3.23	2.65
Pumping MEP (bar)	0.37	0.12	1.11	1.16	1.26
Combustion Eff (%)	97.3	93.05	94.2	95	95.7
Gross Indi Eff (%)	27.7	27.65	29.3	29.1	28.8
Net Indi Eff (%)	25.2	26.72	22.3	21.4	19.5
Thermal Eff (%)	28.5	29.71	31.1	30.6	30.1
CA10 (degree)	360	363	364	364	364
CA50 (degree)	378	373	376	376	377
CA90 (degree)	395	384	385	385	389
CA10-90 (degree)	35	21	21	21	25
CA at T Pisition (degree)	--	370	375	374	374
MFB at T Position (%)	--	30.8	43.2	38.2	35.7
CO (%)	0.26	1.06	0.57	0.35	0.2
uHC (ppm)	1185	1977	2073	2004	2022
NOx (ppm)	1702	12.4	99.3	74.4	49.9

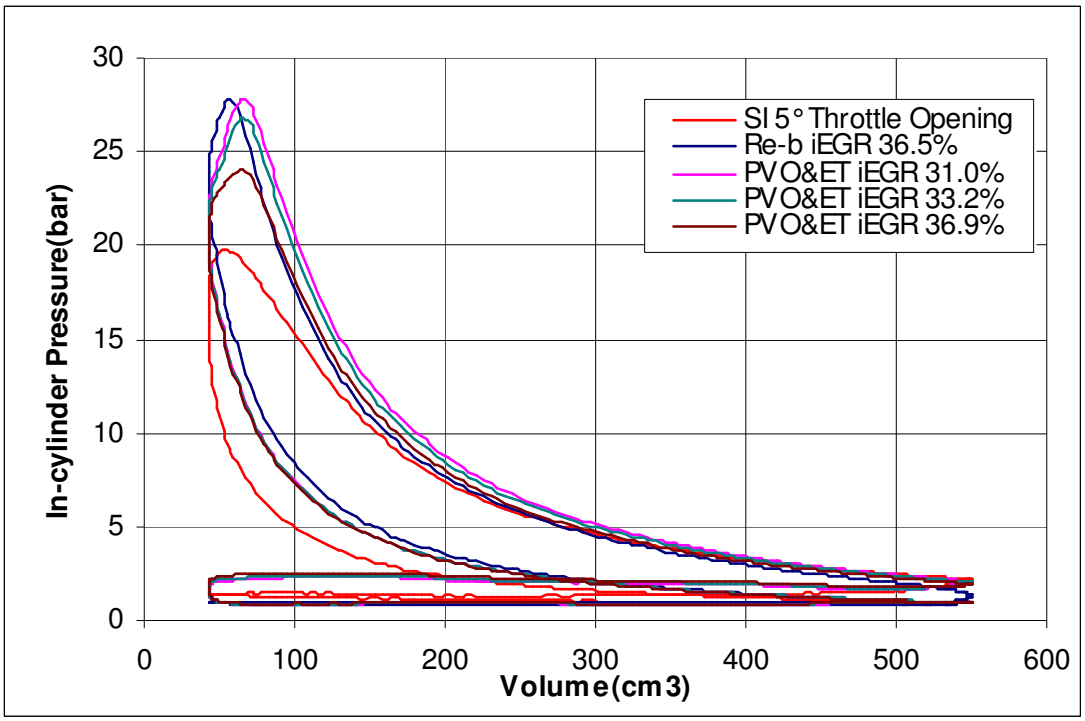

Figure 6.13 Full P-V Diagram

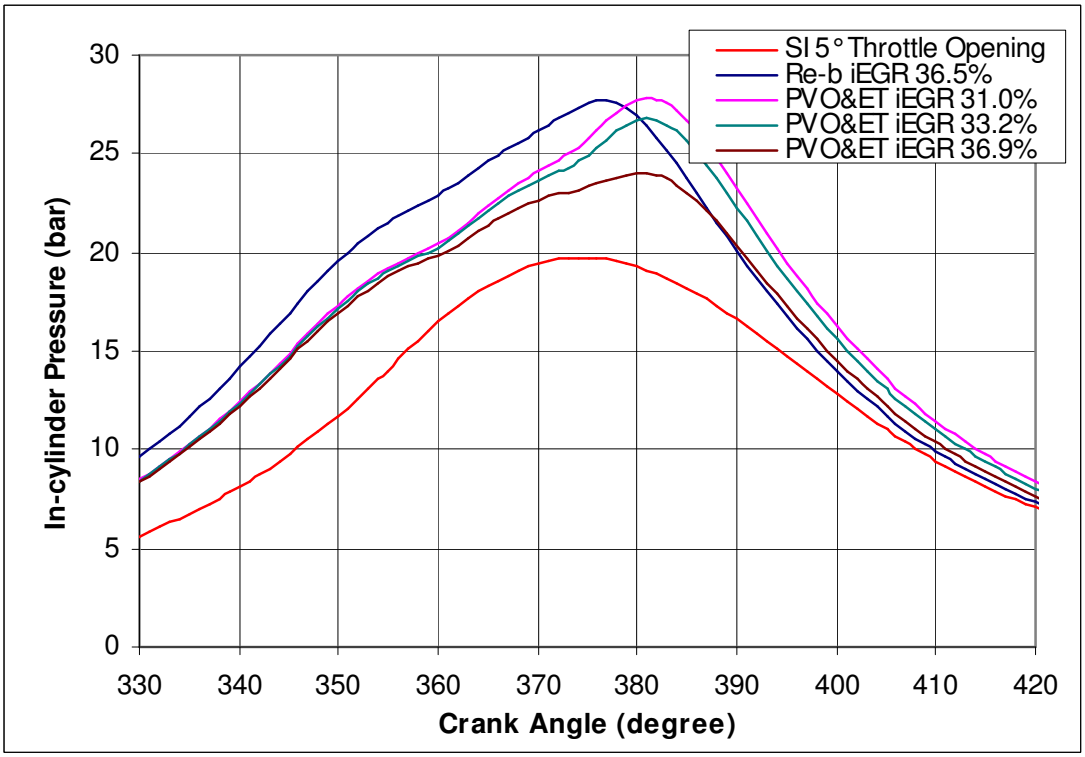

Figure 6.14 Pressure-°CA Diagram

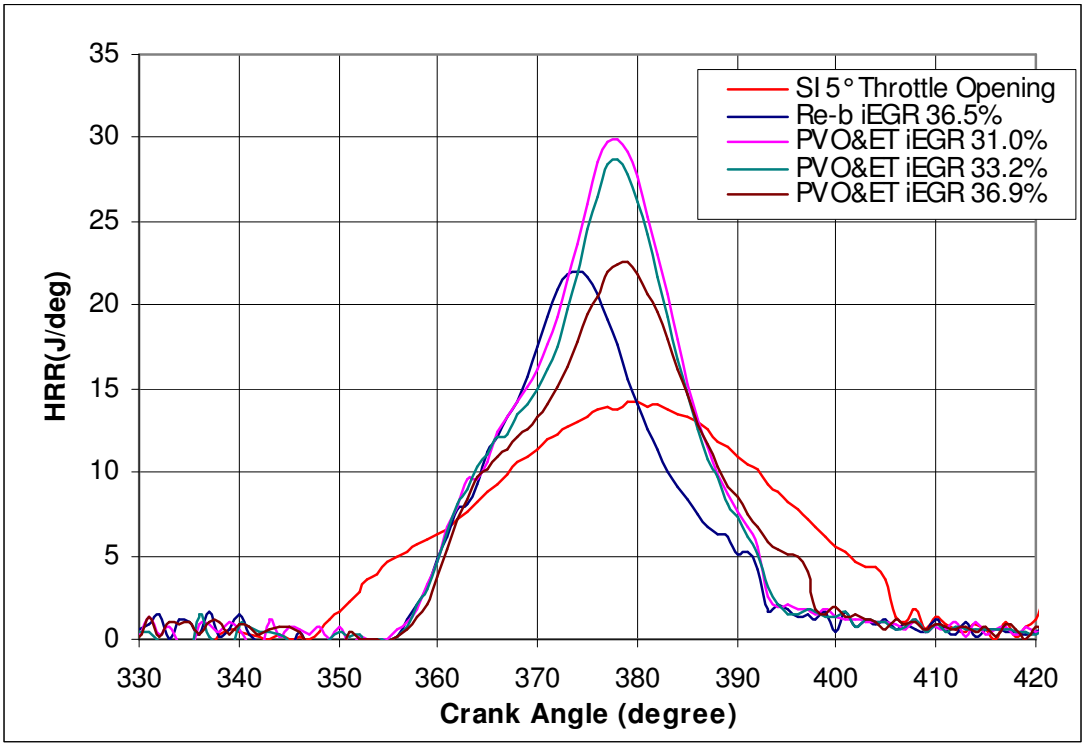

Figure 6.15 HRR-°CA Diagram

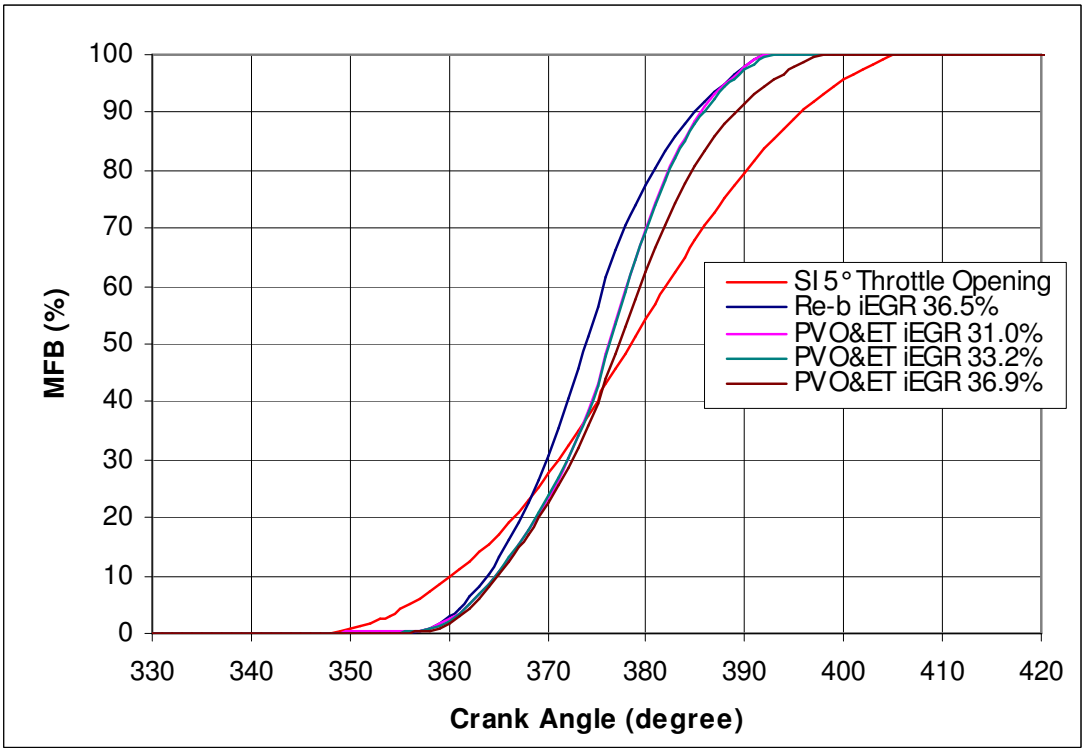

Figure 6.16 MFB-°CA Diagram

Chapter 7

Conclusions and Recommendations for Future Work

Chapter 7 Conclusions and Recommendations for Future Work

7.1 Introduction

Current PFI SI engines suffer from part load inefficiency due to the huge pumping loss when the throttle is used to control engine load. In addition, the knocking combustion limits the utilization of a high compression ratio in the SI engine, which further confines the high efficiency potential of SI engine. On the other hand, CI engines can be operated with higher compression ratio achieving high efficiency engine output. However, the diffusion combustion process generates high temperature reaction zones which form high NOx emission and soot. Alternatively, current CAI applications are basically constrained by lack of effective means of controlling auto-ignition timing and the following combustion speed, which would not only limit the operating range but also lead to an inadequate heat release process, poor emissions and poor driveability.

This thesis presents a new dual fuel CAI concept using the principle of ultra-low emission and high efficiency characteristics of CAI combustion operation. The combustion is organized by taking advantage of the physical and chemical properties of high octane number gasoline and high cetane number DME. Homogeneous air/gasoline mixture is utilized as the main combustible mixture which is formed in the intake port by a PFI injection system. Pressurised DME is directly injected into the cylinder as an ignition promoter by a GDI injector. Various DME injection strategies are applied to realise the control of ignition and combustion. The engine is operated at wide open throttle (WOT) in order to minimize the intake pumping loss. Engine load is controlled by varied amount of trapped residual gases. The residual gases are circulated internally by either Positive Valve Overlap & Exhaust Throttling or Exhaust Re-breathing method, which can effectively utilise the thermal energy of the iEGR to initiate the CAI combustion and then control its heat release rate due to its dilution effect.

7.2 Conclusions

The conclusions of this study are summed up as follows:

(i) Engine operation modes for dual fuel CAI combustion can be arranged according to the engine load as follows.

a. At full load, minimum burned gases are recycled to maximise the power output. DME is injected once near TDC, defined as Late Single Injection Strategy. DME is compression ignited prior to the combustible charge and generates a small core zone of flame kernels, which would develop into an expanding flame front. The flame front propagates from the core zone to the rest of cylinder initiating combustion of the premixed gasoline/air mixture. Combustion timing is mainly controlled by Late Single Injection timing in a similar way to that of spark ignition but with a greater zone of ignition. The combustion process is similar to the conventional SI combustion.

b. At higher part load, as the load decreases to mid load range, the level of EGR increases. Two small DME injections are applied with the compression stroke, defined as Split DME Injections Strategy. The first injected DME is immediately vaporised and premixed with the charge mixture. The second DME injection takes place just before TDC to act as the ignition source. The flame front developed from the auto-ignition sites of DME increase the in-cylinder charge temperature and pressure. The premixed DME vapour begins to auto-ignite leading to the auto-ignition of all the rest combustible mixture independent of flame front. The combustion phasing depends on the second DME injection timing which is also defined as SOI2 timing. It can be concluded from the results that the distribution of DME in the cylinder has large effects on the ignition and combustion. The combustion is characterised as flame propagation and auto-ignition hybrid combustion process as well as spark assistant CAI.

c. At lower part load, as the engine load is further reduced, a larger amount of EGR is introduced into the cylinder and the mixture becomes much diluted. The flame front initiated by the second DME injection can not be developed or sustained because the mixture dilution level beyond its flammability limit. Thus, DME is injected once early in the compression stroke, defined as Early Single Injection Strategy. All DME is premixed with diluted fuel/air mixture. The auto-ignition of DME helps elevate the mixture temperature and pressure to its auto-ignition condition at TDC. No flame propagation is involved and combustion will be dominated by multiple auto-ignition sites. The auto-ignition timing mainly depends on the internal

EGR rate. As a result, both high and low load boundaries of CAI operation range can be extended and controlled auto-ignition can be realised within whole operation regions.

(ii) At part load operation with the split injection strategy, knocking combustion limits the high load operation, and misfire and partial burn define the low load operation boundary. By means of optimised DME injection strategies, the CAI working range are extended from 1.35 bar to 9.2 bar net IMEP.

(iii) Peak CO emissions are detected at highest iEGR rate and with rich air fuel mixtures, while the highest uHC emissions are observed under the condition of the highest iEGR rate and lean mixtures. NOx emissions stay at very low levels when either Split Injection Strategy or Early Single Injection Strategy is applied. However, it significantly increases when Late Single Injection is used under high load operation and peaks with the stoichiometric mixture.

(iv) The engine is operated at WOT and iEGR is used for control the engine load. Exhaust gas is successfully recirculated internally via either positive valve overlap coupled with exhaust gas throttling or exhaust re-breathing strategy. Both of these methods are able to achieve adequate iEGR rate and apply continuous iEGR rate changes. The former method realises the most use of heating effect of trapped residual gas but suffers from large exhaust pumping work. The later method gets rid of exhaust pumping but increase the heat loss of iEGR, resulting in increased injection quantity of DME.

(v) The effects of iEGR for this new combustion concept can be described as follows:

a. The charge heating effects, which increases the combustible mixture temperature prior to combustion, is dominant when the iEGR rate is lower than 30%. The combustion phasing is advanced with faster combustion when iEGR rates rise from 5% to 30%.
b. The dilution and higher heat capacity effects become the main effects when iEGR rate is over 30%, resulting in low temperature combustion and retarded combustion process.

(vi) When compared with conventional SI combustion in the same engine, the new combustion concept produces higher gross indicated efficiency than SI combustion due to the benefits of CAI combustion. The new concept combustion produces similar CO emissions but higher uHC emissions especially in the low load operation than SI mode. However, the NOx emissions are significantly reduced with the new concept due to low temperature combustion and large trapped residual gas. In addition, as the engine is operated at WOT under new concept, intake pumping is negligible during the tests. However, the exhaust pumping of PVO&ET method is significant, resulting in low net indicated efficiency compared to conventional SI combustion. Especially in low load or mid load operation, the exhaust throttling consumes such large pumping work that counteracts the benefits of both CAI combustion and WOT operation.

(vii) However, if iEGR is trapped by the exhaust re-breathing method, both intake and exhaust pumping loss can be avoided. Compared with results by the PVO&ET method, engine with re-breathing iEGR is about 20% more efficient and 25% cleaner in term of net indicated efficiency and uHC emissions respectively. Compared with results by SI combustion, engine with re-breathing iEGR implements 5% better fuel consumption but higher CO and uHC emissions. In addition, dramatically 98% reductions of NOx emissions are achieved compared to conventional SI combustion while 30-90% reductions compared to PVO&ET operation.

7.3 Recommendations for Future Work

7.3.1 Experimental Work

(i) As mentioned in Section 4.5.4.1, the lowest load achieved in this study is 1.35 bar net IMEP due to the concern of damage if the exhaust pressure is further increased. The low load boundary could be extended if more iEGR is introduced by adequate exhaust re-breathing strategy by means of FVVA or hydraulic cam-less valves mechanism.

(ii) The methods to measure and calculate dual fuel air fuel ratio have been presented and discussed in Section 3.4. However, more precise measurement technologies and

methods are recommended to be applied to identify the air flow rate, gasoline injection quantity and DME injection quantity, resulting in more accurate air fuel ratio measurement. What's more, the source of inaccuracy of lambda sensor should also be studied.

(iii) The two border regions of combustion mode transition can be studied in more details in order to optimise the engine performance by means of the applications of different injection strategies.

(iv) As mentioned in Section 4.3.4, the optimal fraction of DME of each injection could be changed according to the engine load.

(v) Compression ratio could be further raised and the tests can be performed in order to increase the engine efficiency.

7.3.2 Simulation Work

Some simulation works are recommended to comprehensively understand the new concept combustion by the use of computing fluid dynamics (CFD) software and the built of adequate engine model and dual fuel combustion model.

(i) The gas exchange process is recommended to be further simulated in the purpose of understanding the iEGR process by different methods.

(ii) Simulation is suggested to be applied on air fuel mixing process and combustion process. The effects on engine performance and emissions of DME spray and distribution within the gasoline air mixture with various injection strategies can be analysed and discussed. A large eddy simulation (LES) base model can be developed and the chemical kinetics of DME and gasoline can be implemented. This could be used to predict the auto ignition and combustion process so as to study the underlying chemical and physical processes involved in the new concept. It also can be used to explain some differences in results between this study (DME as the ignition promoter) and the RCCI research in University of Wisconsin (Diesel as the ignition promoter).

7.3.3 In-cylinder Measurements

It is highly recommended to investigate the in-cylinder DME spray and mixture formation, auto-ignition, and combustion characteristics with premixed air gasoline mixture under the diluted auto-ignition combustion operation in an optical engine using advanced optical diagnostics. The three combustion modes as well as the combustion mode transitions by Various Pilot DME Injection Strategy should be verified and analysed using advanced optical measurements.

7.3.4 Alternative Fuels

Some alternative fuels can be used and applied with this new combustion concept. Some high octane number fuels, such as Compressed Nature Gas (CNG), Liquid Petroleum Gas (LPG) and E85 (85% ethanol and 15% gasoline mixture) can be used to replace gasoline which is premixed with air. On the other hand, the conventional diesel fuel or bio diesel can be instead of DME to initiate and control the auto-ignition.

References

1. Onishi, S., Jo, S., Shoda, K., Jo, P., Kato, S., "Active Thermo-Atmosphere Combustion (ATAC)-A New Combustion Process for Internal Combustion Engines", SAE Paper: 790501, 1979.

2. http://www.whatgreencar.com/caremissions.php

3. "European Union Emission Standards for Cars and Light Trucks", obtained from http://www.dieselnet.com/standards/eu/ld.php , 2011.

4. "The California Low-Emission Vehicle Regulations for Passenger Cars, Light-Duty Trucks and Medium-Duty Vehicles, including all or portions of Sections 1900, 1956.8, 1960.1, 1960.5, 1961, 1961.1, 1962, 1962.1, 1962.2, 1965, 1976, 1978, 2062, and 2101, title 13, California Code of Regulations, as of December 8, 2010", California Environmental Protection Agency Air Resources Board (CARB), September 2010.

5. Heywood, J. B., "Internal Combustion Engine Fundamentals", p.601-619, McGraw-Hill, ISBN 0-07-100499-8, 1988.

6. Heywood, J. B., "Internal Combustion Engine Fundamentals", p.572, McGraw-Hill, ISBN 0-07-100499-8, 1988.

7. Heywood, J. B., "Internal Combustion Engine Fundamentals", p.577, McGraw-Hill, ISBN 0-07-100499-8, 1988.

8. Heywood, J. B., "Internal Combustion Engine Fundamentals", p.582, McGraw-Hill, ISBN 0-07-100499-8, 1988.

9. Heywood, J. B., "Internal Combustion Engine Fundamentals", p.585, McGraw-Hill, ISBN 0-07-100499-8, 1988.

10. "Understanding and responding to Climate Change, Highlight of National Academies Report", 2008 Edition, p 2, 2008.

11. Hansen, J., Sato, Mki., Ruedy, R., Lo, K., Lea, D.W., and Medina-Elizade, M.: "Global Temperature Change", Proc. Natl. Acad. Sci., 103, 14288-14293, doi:10.1073/pnas.0606291103, 2006.

12. "IPCC Fourth Assessment Report: Climate Change 2007", IPCC, obtained from http://www.ipcc.ch/publications_and_data/ar4/wg1/en/ch10s10-es-1-mean-temperature.html, 2007.

13. Russell, R., "The greenhouse effect & Greenhouse Gases", University Corporation for Atmospheric Research Windows to the Universe. Obtained from http://www.windows2universe.org/earth/climate/greenhouse_effect_gases.html, 2007.

14. Rohde, R., Global Warming Art, obtained from http://www.globalwarmingart.com/wiki/File:Greenhouse_Gas_by_Sector_png, 2000.

15. "Reducing Transport Greenhouse Gas Emissions, Trends & Data", International Transport Forum, Leipzig, Germany, 2010.

16. Public Hearing "Reducing CO2 from passenger cars and light-commercial vehicles", obtained from http://ec.europa.eu/clima/events/0005/index_en.htm 2007.

17. "Proposal from the Commission to the European Parliament and Council for a Regulation to Reduce CO2 Emissions from Passenger Cars", Commission of the European Communities, Brussels, 2007.

18. "Progress Report on Implementation of the Community's Integrated Approach to Reduce CO_2 Emissions from Light-duty Vehicles", European Commission, Brussels, obtained from http://eur-lex.europa.eu/LexUriServ/LexUriServ.do?uri=CELEX:52010DC0656:EN:NOT 2010.

19. Tom TheHand, http://en.wikipedia.org/wiki/File:Brent_Spot_monthly.svg#filelinks.

20. "BP Statistical Review of World Energy 2007", June 2007.

21. Wood, J., Long, G., Morehouse, D., "Long-Term World Oil Supply Scenarios-The Future Is Nither as Bleak or Rosy as Some Assert", Energy Information Administration, eia, obtained from www.eia.doe.gov.

22. Helms, H., Pehnt, M., Lambrecht, U., Liebich, A., "Electric Vehicle and Plug-in Hybrid Energy Efficiency and Life Cycle Emissions", 18th International Symposium Transport and Air Pollution, Session 3: Electro and Hybrid Vehicles, 2010.

23. Thomas, C., "Fuel Cell and Battery Electric Vehicles Compared", International Journal of Hydrogen Energy, 34 (2009) 6005-6020, 2009.

24. Plotkin, S., Santini, D., Vyas, A., Anderson, J., Wang, M., He, J., Bharathan, D., "Hybrid Electric Vehicle Technology Assessment: Methodology, Analytical Issues, and Interim Results", Center for Transportation Research, Argonne National Laboratory, ANL/ESD/02-2, 2001.

25. http://www.formula1.com/inside_f1/understanding_the_sport/8763.html

26. Deaton, J., Green, P., "How Hydraulic Hybrids Work", Howstuffworks, obtained from http://auto.howstuffworks.com/hydraulic-hybrid2.htm .

27. "Hydraulic Hybrid Technology- A Proven Approach", Clean Automotive Technology, United States Environmental Protection Agency (EPA), EPA420-F-04-024, 2004.

28. Lee, C-Y., Zhao, H., Ma, T., "Analysis of a Cost Effective Air Hybrid Concept", SAE Paper 2009-01-1111, 2009.

29. Abe, T., Holzwarth, R., May, K., "Hybrid Traction Control System Utilizing an Engine Inertia Brake", SAE Paper 960955, 1996.

30. Huang, Y., Wang, K., "A Hybrid Power Driving System with an Energy Storage Flywheel for Vehicles", SAE Paper 2007-00-4114, 2007.

31. Rizzo, G., Sorrentino, M., and Arsie, I., "Rule-Based Optimization of Intermittent ICE Scheduling on a Hybrid Solar Vehicle", SAE Paper 2009-24-0067, 2009.

32. Searles, R. A., “Emission Catalyst Technology – Challenges and Opportunities in the 21st Century”, Int. Conf. On 21st Century Emissions Technology, IMechE Conference Transactions 2000-2, ISBN 1 86058 322 9, 2000.

33. http://en.wikipedia.org/wiki/Diesel_particulate_filter

34. Theis, J.R., Dearth, M., and McCabe, R., “LNT+SCR Catalyst Systems Optimized for NOx Conversion on Diesel Applications”, SAE Paper 2011-01-0305, 2011.

35. “Engines & Performance”, http://www.volkswagen.co.uk/#/new/golf-vi/which-model/engines, 2011.

36. “FSI engines, More Power”, Less Fuel, http://www.audi.co.uk/audi-innovation/our-technologies/fsi-tfsi-and-tdi.html, 2011.

37. Atkina, M., Koch, C., “A Well-to-Wheel Comparison of Several Powertrain Technologies”, SAE Paper 2003-01-0081, 2003.

38. Hancock, D., Fraser, N., Jeremy, M., Sykes, R., Blaxill, H., “A New 3-Cylinder 1.2l Advanced Downsizing Technology Demonstrator Engine”, SAE Paper 2008-01-0611, 2008.

39. Stephenson, M., “Engine Downsizing – An Analysis Perspective”, SIMULIA Customer Conference, 2009.

40. Hong, H., Parvate-Patil, G., Gordon, B., “Review and Analysis of Variable Valve Timing Strategies - Eight Ways to Approach”, Proc. Instn Mech. Engrs Vol. 218 Part D: J. Automobile Engineering, IMechE, 2004.

41. 2005 Delphi Cylinder Deactivation for Overhead Valve Engines, Delphi, http://delphi.com/manufacturers/auto/powertrain/gas/valvetrain/cydeac/ .

42. Manente, V., Zandar, C-G., Johansson, B., Tunestal, P., “An Advanced Internal Combustion Engine Concept for Low Emissions and High Efficiency From Idle to Max

Load Using Gasoline Partially Premixed Combustion", SAE Paper 2010-01-2198, 2010.

43. "EURO 5 and 6 Emissions Standards for Cars and Vans, Position Paper", European Federation for TRANSPORT and ENVIRONMRNT, September 2006.

44. Najt. P M and Eng. J A, "Gasoline-fuelled HCCI Engines", GM corporation.

45. Hua Zhao (2007), "HCCI and CAI engines for the automotive industry", p11, CRC Press LLC, ISBN 978-1-4200-4459-1, Woodhead Publishing Lt., ISBN 978-1- 84569-128-8.

46. Heywood, J. B., "Internal Combustion Engine Fundamentals", p.169-177, McGraw-Hill, ISBN 0-07-100499-8, 1988.

47. L. M. Pickett, "Soot Formation at Low Flame Temperature Diesel Operating Conditions", 9th International Conference "Present and Future Engines for Automobiles", San Antonio, TX, U.S.A., June, 2005.

48. P. Adomeit et al., "Laser Optical Diagnostics and Numerical Analysis of HSDI Combustion Systems", THIESEL 2004 "Thermo- and Fluid Dynamic Processes in Diesel Engines", Valencia, Spain, 7th–10th September, 2004.

49. Noguchi, M., Tanaka, Y., Tanaka, T., and Takeuchi, Y., "A Study on Gasoline Engine Combustion by Observation of Intermediate Reactive Products during Combustion", SAE Paper 790840, 1979.

50. Thring, R. H., "Homogeneous Charge Compression-Ignition (HCCI) Engines", SAE Paper 892068, 1989.

51. Lavy, J., Dabadie, J., Angelberger, C., Duret, P. (IFP), Willand, J., Juretzka, A., Schaflein, J. (Daimler-Chrysler), Ma, T. (Ford), Lendresse, Y., Satre, A.(PSA Peugeot Citroen), Schulz, C., Kramer, H. (PCI - Heidelberg University), Zhao, H., Damiano (Brunel University), "Innovative Ultra-low NOx Controlled Auto-Ignition Combustion Process for Gasoline Engines : the 4-SPACE Project", SAE Paper 2000-01-1837, 2000.

52. Oakley, A., Zhao, H., Ladommatos, N., “Experimental Studies on Controlled Auto-ignition (CAI) Combustion of Gasoline in a 4-Stroke Engine”, SAE Paper 2001-01-1030, 2001.

53. Hyvonen, J., Wilhelmsson, C., Johansson, B., “The Effect of Displacement on Air-Diluted Multi-Cylinder HCCI Engine Performance”, SAE Paper 2006-01-0205, 2006.

54. Lang, O., Hahn, W.S., Pischinger, S., Hortmann, K., and Bucker, C., “Thermo dynamical and Mechanical Approach towards a Variable Valve Train for the Controlled Auto Ignition Combustion Process”, SAE Paper 2005-01-0762.

55. Kalghatgi G., Risberg P., Angstrom H., “Advantages of Fuels with High Resistance to Auto-ignition in Late-injection, Low-temperature, Compression Ignition Combustion”, SAE Paper 2006-01-3385, 2006.

56. Kalghatgi G., Risberg P., Angstrom H., “Partially Pre-Mixed Auto-Ignition of Gasoline to Attain Low Smoke and Low NOx at High Load in a Compression Ignition Engine and Comparison with a Diesel Fuel”, SAE Paper 2007-01-0006, 2007.

57. Manente, V., Zander, C-G., Johansson, B., Tunestal, P., “ An Advanced Internal Combustion Engine Concept for Low Emission and High Efficiency from Idle to Max Load Using Gasoline Partially Premixed Combustion”, SAE Paper 2010-01-2198, 2010.

58. Hanson R., et al., “Operating a Heavy-Duty Direct-Injection Compression-Ignition Engine with Gasoline for Low Emissions”, SAE Paper 2009-01-1442, 2009.

59. Kalghatgi G., et al., “Some Effects of Fuel Auto-ignition Quality and Volatility in Premixed Compression Ignition Engines”, SAE paper 2010-01-0607, 2010.

60. Manente, V., “Gasoline Partially Premixed Combustion, An Advanced Internal Combustion Engine Concept Aimed to High Efficiency, Low Emissions and Low Acoustic Noise in the Whole Load Range”, PhD thesis, Division of Combustion Engines, Department of Energy Sciences, Lund Institute of Technology, 2010.

61. Hua Zhao (2007), "HCCI and CAI Engines for the Automotive Industry", p345, CRC Press LLC, ISBN 978-1-4200-4459-1, Woodhead Publishing Lt., ISBN 978-1- 84569-128-8.

62. Bessonette, P.W., Schleyer, C.H., Duffy, K.P., Hardy, W.L. et al., "Effects of Fuel Property Changes on Heavy- Duty HCCI Combustion", SAE Paper 2007-01-0191, 2007.

63. Kokjohn, S., Hanson, R., Splitter, D., Reitz, R., "Experiments and Modelling of Dual-Fuel HCCI and PCCI Combustion Using In-Cylinder Fuel Blending", SAE Paper 2009-01-2647, 2009.

64. Hanson R., M., et al., "An Experimental Investigation of Fuel Reactivity Controlled PCCI Combustion in a Heavy-Duty Engine", SAE Paper 2010-01-0864, 2010.

65. Kokjohn, S.L., Hanson, R.M., Splitter, D.A., Reitz, R.D., "Fuel Reactivity Controlled Compression Ignition (RCCI): A Pathway to Controlled High-efficiency Clean Combustion", International Journal of Engine Research 2011 12: 209, DOI: 10.1177/1468087411401548, Institution of Mechanical Engineers, 2011.

66. Yeom, K., Jang, J., Bae, C., "Gasoline HCCI Engine with DME (Di-methyl Ether) as an Ignition Promoter", Proc. 6th International Conference on GDI Engines "Direkteinspritzung im Ottomotor / Gasoline Direct Injection Engines", expert verlag, pp229-239, 2005.

67. Zhao, H., Peng, Z., Williams, J., Ladommatos, N., "Understanding the Effect of Recycled Burned Gases on the Controlled Autoignition (CAI) Combustion in Four-Stroke Gasoline Engines", SAE Paper 2001-01-3607, 2001.

68. Inagaki, K., Fuyuto, T., Nishikawa, K., Nakakita, K. et al., "Dual-Fuel PCI Combustion Controlled by In-Cylinder Stratification of Ignitability", SAE Paper 2006-01-0028, 2006.

69. Li, J., Zhao, H., Ladommatos, N. and Ma, T., “Research and Development of Controlled Auto-ignition Combustion in a Four-stroke Multi-cylinder Gasoline Engine”, SAE paper 2001-01-3608, 2001.

70. Yang, C., Zhao, H., Megaritis, T., “Investigation of CAI Combustion with Positive Valve Overlap and Enlargement of CAI Operating Range”, SAE Paper 2009-01-1104, 2009.

71. Xie H., Yang L., Qin J., et al, “The Effect of Spark Ignition on the CAI Combustion Operation”, SAE Paper 2005-01-3738, 2005.

72. T. Urushihara, K. Yamaguchi, K. Yoshizawa, et al, “A Study of a Gasoline-fueled Compression Ignition Engine ~ Expansion of HCCI Operation Range Using SI combustion as a Trigger of Compression Ignition”, SAE Paper 2005-01-0180, 2005.

73. K. Yoshizawa, A. Teraji, H. Miyakubo, K. Yamaguchi, T. Urushihara, “Study of High Load Operation Limit Expansion for Gasoline Compression Ignition Engines”, Journal of Engineering for Gas Turbines and Power, P.377-387, Vol.128, Apr. 2006.

74. Arcoumanis, C., Bae, C., Crookes, R., Kinoshita, E., “The Potential of Di-methyl Ether (DME) as an Alternative Fuel for Compression-Ignition Engines: A Review”, Fuel 87 (2008) 1014-1030, 2008.

75. Elana M. Chapman, etl “Fuel Technical Report on Di-methyl Ether (DME) –Fueled Shuttle Bus Demonstration Project”, The Energy Institute, The Pennsylvania Transportation Institute, The Pennsylvania State University. 2003.

76. Green Car Congress, “Volvo Introduces DME-Powered Truck”, 2005.

77. Ho Teng, James C M, Jeffrey B Schneyer. “Compression Ignition Delay (Physical + Chemical) of Dimethyl Ether- an Alternative Fuel for Compression-ignition Engines”, SAE Paper 2003-01-0759, Warrendale, PA: SAE Inc. 2003.

78. Jiang. D, Huang, Z, (2007) “The Study of Alternative Fuel for Internal Combustion Engine”, Xi”an Jiaotong University Press, ISBN 978-7-5605-2507-5.

79. “Signal 4000VM Heated Vacuum NOx Analyser Operating Manual”, The Signal Instrument Co. Ltd. P68.

80. Heywood, J. B., “Internal Combustion Engine Fundamentals”, p.231, McGraw-Hill, ISBN 0-07-100499-8, 1988.

81. Zhao, H., Lowry, G., Ladommatos, N., “Time-Resolved Measurements and Analysis on In-cylinder Gases and Particulates in Compression-Ignition Engines”, SAE Paper 961168, 1996.

82. Ladommatos, N., Balian, R., Horrocks, R., Cooper, L., “The Effect of Exhaust Gas Recirculation on Combustion and NOx Emissions in a High-Speed Direct-Injection Diesel Engine”, SAE Paper960840, 1996.

83. Ladommatos, N., Balian, R., Horrocks, R., Cooper, L., “The Effect of Exhaust Gas Recirculation on Soot Formation in a High-Speed Direct-Injection Diesel Engine”, SAE Paper 960841, 1996.

84. Kajitani, S., Chen, Z., Konno, M., Rhee, K., “Engine Performance and Exhaust Characteristics of Direct-injection Diesel Engine Operated with DME”, SAE Paper 972973, 1997.

85. Sorenson, S., Mikkelsen, S., “Performance and Emissions of a 0.273 Liter Direct Injection Diesel Engine Fuelled with Neat Dimethyl Ether”, SAE Paper 950064, 1995.

86. Yu, J., Zhang, Y., Elkelawy, M., Qiu, K., “Spray and Combustion Characteristics of HCCI Engine Using DME/Diesel Blended Fuel by Port-Injection”, SAE Paper 2010-01-1485, 2010.

87. Kim, M., Yoon, S., Ryu, B., Lee, Chang., “Combustion and Emission Characteristics of DME as an Alternative Fuel for Compression Ignition Engines with a High Pressure Injection System”, Fuel 87 (2008) 2779-2786,2008.

88. McCandless, J., Teng, H., Schneyer, J., "Development of a Liquid-DME Fuel tank~A Two-Fluid Thermodynamic Pump", SAE Paper 2001-01-0652, 2001.

89. Zhou, L., Wang, H., Jiang, D., Huang, Z., "Study of Performance and Combustion Characteristics of a DME- Fueled, Light-Duty, Direct-Injection Diesel Engine", SAE Paper 1999-01-3669, 1999.

90. Lee, D., Cho, S., Lee, B., Park, C,. Maeng, S., Choi, Jiho., "Optimaize of Piston Cavity in a DME Engine", The 13th International Pacific Conference on Automotive Engineering.

91. Song, J., Huang, Z., Qiao X., Wang, W,. "Performance of a Controllable premixed Combustion Engine Fuelled with Dimethyl Ether", Energy Conversion and Management 45 (2004) 2223-2232, 2004.

92. "How the Wide Band Sensor Works", Precision Wideband Controller by Bowling and Grippo Group, obtained from http://www.megamanual.com/PWC/LSU4.htm, 2004.

93. "Oxygen Percentage and Lambda", by Edge Pty. Ltd, obtained by http://www.wbo2.com/sw/percent-o2.htm, 2011.

94. Snyder, D., Washington, E., Indrajuana, A., Shaver, G., "Steady-State Biodiesel Blend Estimation via a Wideband Oxygen Sensor", 2008 American Control Conference, 2008.

95. Elting, L., "Fuel Air Ratio and Distribution from Exhaust Gas Composition", SAE Transactions, Vol. 77, 1968, Paper 680114.

96. Spindt, R. S., "Air Fuel Ratios from Exhaust Gas Analysis", SAE Paper 650507, Society of Automotive Engineers, 1965.

97. Brettschneider, Johannes, "Berechung des Luftverhaeltnisses λ von Luft-Kraftstoff-Gemsichen und des Einflusses on Messfehlern auf λ", Bosch Technische Berichte, Band 6, Heft 4, Seite 177-186, Stuttgat, 1979.

98. Silvis, W., “An Algorithm for Calculation the Air/Fuel Ratio Exhaust Emissions”, SAE Paper 970514, 1997.

99. Heywood, J. B., “Internal Combustion Engine Fundamentals”, p.148, p 153, McGraw-Hill, ISBN 0-07-100499-8, 1988.

100. Oakley, A., “Experimental Investigations on Controlled Auto-ignition Combustion in a Four Stroke Gasoline Engine”, PhD Thesis, Brunel University, 2001.

101. Heywood, J. B., “Internal Combustion Engine Fundamentals”, p.384, McGraw-Hill, ISBN 0-07-100499-8, 1988.

102. Zhao, H., Ladommatos, N., “Engine Combustion instrument and Diagnostics”, p.77, SAE, ISBN0-7680-0665-1.

103. Zhang, Y., Zhao, H., Xie, H., Hou, S., Yang, C., “Characterization and Heat Release Model Development of SI-CAI Hybrid Combustion and Its Application to a 4-Stroke Gasoline Engine Operating with Highly Diluted Mixtures”, IC engine and Gas Turbine Combustion, 2010.

104. Eng, J.A., “Characterization of Pressure Wave Oscillations in HCCI Combustion”, SAE Paper 2002-01-2859, 2002.

105. Cairns, A., Blaxill, H., “The Effects of Combined Internal and External Exhaust Gas Recirculation on Gasoline Controlled Auto-ignition”, SAE Paper 2005-01-0133, 2005.

106. Fuerhaper, A., Piock, W.F., Fraidl, G.K., “CAI - Controlled Auto Ignition - The Best Solution for the Fuel Consumption – versus Emission Trade-off?”, SAE Paper 2003-01-0754, 2003.

107. Milovanovic, N., Blundell, D., Pearson, R., Turner, J., Chen, R., “ Enlarge the Operational Range of a Gasoline HCCI Engine by Controlling the Coolant Temperature”, SAE Paper 2005-01-0157, 2005.

108. Andreae, M.M., Cheng, W.K., Kenney, T., Yang, J., “On HCCI Engine Knock”, SAE Paper 2007-01-1858, 2007.

109. Konno, M., Kajitani, S., Chen, Z., Yoneda, K., Matsui, H., Goto, S., “Investigation of the Combustion Process of a DI CI Engine Fueled with Dimethyl Ether”, SAE Paper 2001-01-3504.

110. Akihama, K., Takatori, Y., Inagaki, K., Sasaki, S. and Dean, A., “Mechanism of the Smokeless Rich Diesel Combustion by Reducing Temperature”, SAE Paper 2001-01-0655, 2001.

111. Kawasaki, K., Hirota, K., Nagata, S., Yamane, K., Ohtsubo, H., Nakazono, T., “ Improvement of Natural-gas HCCI Combustion by Internal EGR by Means of Exhaust Valve Re-opening”, SAE Paper 2009-32-0079, 2009.

112. Kawasaki, K., Takegoshi, A., Yamane, K., Ohtsubo, H., Nakazono, T., Yamauchi, K., “Combustion Improvement and Control for a Natural Gas HCCI Engine by the Internal EGR by Means of Intake-valve Pilot-opening”, SAE Paper 2006-01-0208, 2006.

113. Benajes, J., Reyes, E., and Lujan, J.M., “Intake Pre-lift Effect on the Performance of a Turbocharged Diesel Engine”, SAE Paper 960950, 1996.

114. Chang, K., Babajimopoulos, A., Lavoie, G.A., Filipi, Z.S., and Assanis, D.N., “ Analysis of Load and Speed Transitions in An HCCI Engine Using 1-D Cycle Simulation and Thermal Networks”, SAE Paper 2006-01-1087, 2006.

Appendix A. Adjustable Valve Timing Camshaft for Ricardo E6 Engine

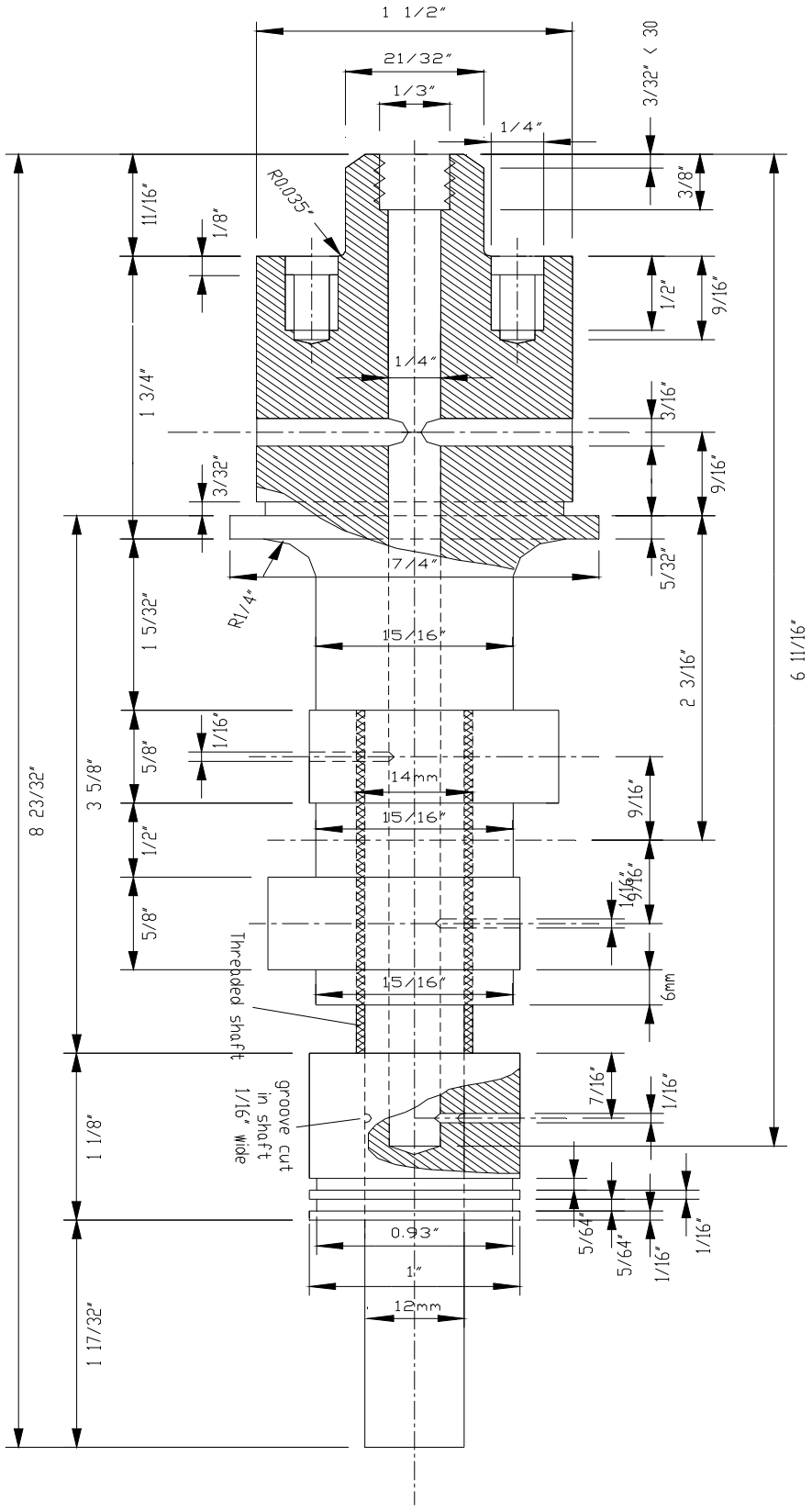

Designed and modified by Dr. Kayiu Mann and Dr. Changho Yang. Brunel University, February 2008.

Appendix B. Drive Current for DME DI Injector

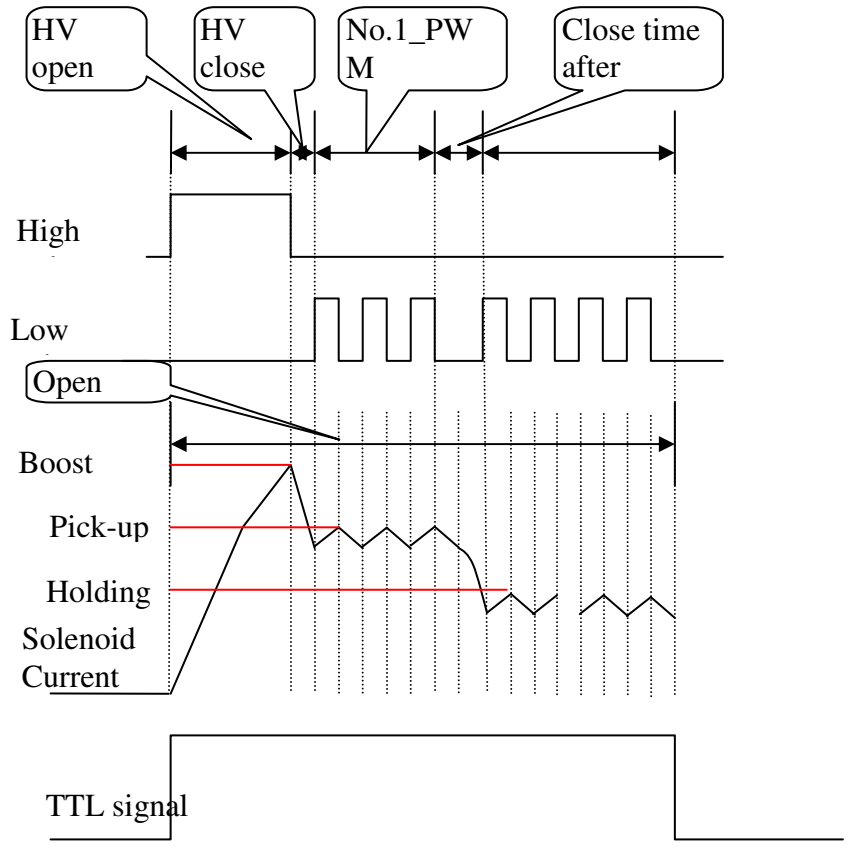

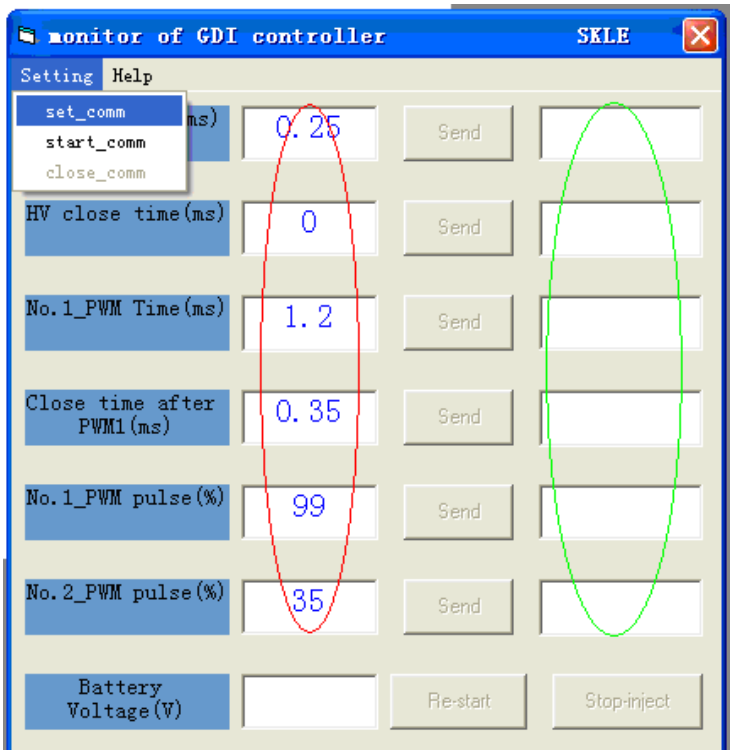

Appendix C. Instructions for the Use of Portable Air Flow Testing Set

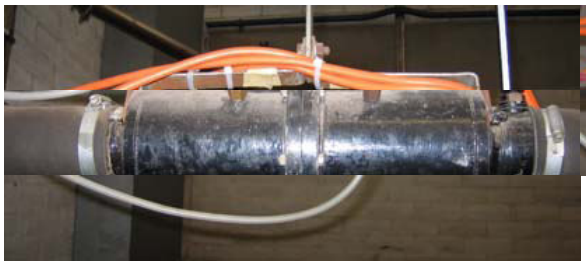

Combined Calibration with Multislope Manometer (all figure are for volume in ubic feet per minute)

Vertical Position Volume = 2.840 * Manometer Reading
Top Inclined = 1.420 * Manometer Reading
2nd = 0.580 * Manometer Reading
3rd = 0.284 * Manometer Reading
Bottom = 0.143 * Manometer Reading

Appendix D. Gasoline Injector Calibration and DME Injector Calibration